Seakeeping Experiment of Two Side-by-Side Floating Bodies

by

©Doug Smith

A thesis submitted to the School of Graduate Studies in partial fulfillment of the requirements for the degree of

Master of Engineering

Faculty of Engineering and Applied Science

Memorial University of Newfoundland

May 2014

St. John's Newfoundland

Abstract

After determining a need to further investigate the hydrodynamic behavior of the side-by-side floating bodies at a close proximity, model scale experiments were conducted. This experiment changed parameters such as the gap width and wave heading to examine the effects of hydrodynamic interaction. Two initial gap widths, 300 and 450 mm, and four wave headings, 90°, 60°, 30° and 0°, were examined. Each experimental setup was examined over a range of wave frequencies, while free surface elevation and vessel motion responses were monitored and recorded. Analysis of the data showed the narrow gap resonance phenomena. However, the experiment did show little variation of the frequency where gap resonance occurred. Beam seas cases showed one peak frequency where values were significantly amplified compared to surrounding frequencies, while other wave headings showed two peak frequencies. There was little variation of the frequency where resonance occurred for each case. However, the magnitude of amplification did show significant variation over each case. The vessel motion response showed significant amplification over quite broad frequency bands. Beam seas cases showed very little pitch motion but head seas cases showed significant roll motion.

Acknowledgements

I would like to thank my supervisor, Dr. Wei Qiu, for his support over the course of my master's program. His technical, professional and financial support is greatly appreciated. This work could not have been completed with out his support. I would like to thank Trevor Clark for his assistance in lab testing. The experimental set up was very labour intensive and often required two people to complete the job. I would like to thank Jordan Hull for his assistance in laboratory work while I was recovering from a separated shoulder. I would like to thank Oceanic Consulting Corporation for assistance with the mooring design for the model tests. I would like to thank my family for their continued support in every way. I would like to thank my colleagues in the Advanced Marine Hydrodynamics Lab for their support and dialogue over the course of this project.

Table of Contents

List of Tables

List of Figures

Chapter 1

Introduction

The increasing complexity of offshore operations often require that multiple vessels be operating in the same vicinity and working together to complete a given task. The close proximity of the working vessels require that more intricate procedures be put in place to carry out the task. Procedures must consider the safety of all vessels from collision while still ensuring the usual safety requirements for any vessel on a solo mission. Also, the presence of multi-bodies at close proximity require that additional care be taken in analyzing the fluid behavior. Radiated and diffracted waves from neighboring bodies can interact, causing unique fluid behavior in the water column between the floating bodies. Multi-body operations are being seen more and more in offshore activities in recent years, such as offshore fuel transfers, supply/crew transfer or very large floating structures (VLFS).

Naval vessels preform refueling and supply transfer operations at sea which are often essential to their mission requirements. It is important that analysis be performed prior to transfer at sea operations to ensure a safe transfer. Accurate predictions are essential in determining operational limits to prevent spills and ensure crew safety. Fueling lines and connections should not be overloaded to prevent me-

chanical failure and protect from environmental damage. Also, modeling the vessels station-keeping performance is paramount for close proximity operations such as supply transfers. Accurate modeling of two ships at close proximity is essential to the success of these operations.

Very large floating structures (VLFS) are being investigated as alternatives to on-land infrastructure in cities with low land availability, such as airports. These structure can have length scales in kilometers thus making it very difficult to be constructed as one continuous body. They are typically assembled as a series of modules that are connected with narrow gaps between them. Accurately predicting the fluid behavior between the modules is essential to the design of the connecting mechanisms which is crucial to the design of the VLFS.

The analysis of side-by-side floating bodies is a specialized hydrodynamic area that offers challenges that are not seen in traditional hydrodynamic problems. Computational or experimental analysis may be used as with single body cases but special care must be taken for the side-by-side case. This can be seen in greater detail in chapter 2.

1.1 Computational Approach

Numerical models can be developed based on computational fluid dynamics (CFD) or potential flow methods. These two distinct types of models are based on different assumptions and special care should be taken when implementing a model. The characteristics of each type of model should be appropriate for the problem being modeled.

The CFD model is based on the continuity equation and the conservation of momentum equations also known as the Navier-Stokes equations. Equation 1.1 show

the Navier-Stokes equation where U_i is the velocity vector, p is the pressure, τ_{ij} is the stress tensor and F_i is the body force vector. This method requires that entire fluid domain be discretized to compute the velocity and pressure terms. In cases where turbulent flow is present the grid for the fluid domain must be small enough to capture the smallest eddies present in the domain. A larger grid may be used but the user must adopt Reynolds-Averaged Navier-Stokes (RANS) equations and a turbulence model which adds more equations and unknowns to the problem. Due to the typically large number of grid points, large system of equations, iterative nature and temporal sensitivity, the CFD model can be quite computationally expensive.

$$\rho\left(\frac{\partial U_i}{\partial t} + U_i \cdot \nabla U_i\right) = -\nabla p + \nabla \cdot \tau_{ij} + F_i \tag{1.1}$$

Potential Flow models are developed to satisfy the Laplace equation, seen in equation 1.2, where ϕ is the velocity potential. A velocity potential implies the following assumptions; that the fluid is inviscid, incompressible and irrotational. This model may be solved using the panel method which requires that only the boundary of the body be discretized, thus decreasing the mesh size significantly. This much smaller domain attributes to the panel method being a much more computational efficient method than RANS equations. In applications where the potential flow assumptions are considered valid the panel method is typically the desired model for numerical simulations. However, the convergent nature of numerical models lead to uncertainty in the computed results until a model is validated against full scale or model scale data.

$$\nabla\phi = 0 \tag{1.2}$$

1.2 Experimental Approach

Full scale ship data is not always available or practical, in such a case a model scale experiment should be performed. A model scale experiment could also be performed to explore an application with very little previous work conducted. The model scale test should be conducted in a controlled environment such as a tank testing facility. The scale of the experiment should be such that data measurements can be made practically and similitude is achieved for all parameters, including those that do not scale linearly.

Model scale experiments are a safe way of determining the operational limits of a vessel or critical parameters for vessel designs. These experiments can be expensive and time consuming but it is a proven approach for collecting important hydrodynamic data. They are also critical to numerical modeling as a validation tool. Good agreement in numerical and experimental results improve the confidence level for the numerical model, thus improving the confidence in numerical design work.

Chapter 2

Literature Review

For many years multi-body interaction has been an important research topic in marine hydrodynamics. Although many of the same techniques can be applied in multi body and single cases, special care must be taken due to unique phenomena in multi body cases. Fluid interaction between multiple floating bodies cause additional forces to be applied by the fluid and add to the complexity of the problem. Diffracted and radiated waves from neighboring floating bodies can influence the forces on floating bodies and effect the fluid behavior in the region. This research is intended to explore the two ship interaction problem and much of the background literature comes directly from this field. However, some closely related applications such as multi-hull vessels and moonpool dynamics also provided insight to the problem.

Kodan (1984) showed that an interaction effect is present between two adjacent floating bodies. The wave force and vessel motions showed significant differences from the adjacent body case to the single body case. This analysis was performed theoretically by the strip theory analysis of slender bodies. Model tests were then performed and showed good agreement with the theoretical predictions. Both model tests and strip theory predictions showed evidence of significant interaction effects.

Miao et al. (2001) provided a theoretical formulation and numerical evaluation of twin large caissons with a small gap between. This study was performed using potential theory by considering only the incident wave potential and diffracted wave potential since the caissons were fixed to the bottom there was no need for radiation potential. Simulations were carried out on twin rectangular caissons and then twin cylindrical caissons. The body forces on each caisson were examined as single bodies and as twin bodies to improve the understanding of the interaction effect of two caissons at a close proximity. The Twin body case showed showed similar body forces to the single body case except for sharp peak forces at certain frequencies. These frequencies were said to produce a force up to 10 times greater than the single body case due to the narrow open channel resonance phenomena. It was noted that the the resonance phenomena was more pronounced in the rectangular case than the cylindrical case. The resonant frequencies were said to be around $kL \approx n\pi(n = 1, 2, 3, 4, ..., \infty)$, where k is the wave number and L is the gap length.

Molin (2001) presented a theoretical approach for predicting fluid resonance in moonpools. This potential flow model was solved in 2 and 3 dimensions. Predictions for moonpool resonance were given for piston and sloshing modes. The piston mode assumed that the fluid would oscillate vertically as a solid block while the sloshing mode would allow the fluid to move freely inside the moonpool. Quasi-analytical expressions were derived for predicting moonpool resonance and it was noted that the natural frequency would increase as the width and draft of the moonpool decrease.

Molin et al. (2002), while conducting model test on a narrow channel between a captive barge and a wall, made a modification to the expression derived for gap natural frequency presented in Molin (2001). It was found that the boundary condition for the longitudinal ends should be changed from the Neumann condition to the Dirichlet condition. An updated derivation was given for the natural frequency using the new

boundary conditions.

McTaggart et al. (2003) conducted a set of semi-captive experiments on a frigate and a supply ship at a close proximity. The models were restrained in surge, sway and yaw by connection to a tow carriage. The test program included runs at zero and nonzero speeds, head seas and oblique seas, single body and double body and longitudinal aligned and not aligned all with the same gap width (for double body cases). These tests were desirable because of the lack of validation material for two body numerical predictions. The numerical code was then updated to include restraining forces and found to be in good agreement with the experimental results. Numerical predictions and experimental results both showed the larger ship to be not significantly affected by the presence of the smaller ship while the smaller ship was significantly affected by the presence of the larger ship.

Chen (2005) produced numerical results for two side-by-side barges and a barge adjacent to a Wigley hull, then compared the results to measured values. The numerical model was based on the linear potential theory with the addition of a damping term to the free surface boundary conditions in the gap region. the boundary condition is given in equation (2.1) where ϕ is the fluid potential, $k' = \omega/g$ and ϵ is the damping coefficient. Numerical simulations were conducted with $\epsilon = 0$ and $\epsilon = 0.016$. In the case of the twin barges the predicted wave height was compared to measured values. It was found that that the both values of ϵ showed good agreement with with most frequencies except near the resonant frequency. In the resonance band wave heights were overpredicted using $\epsilon = 0$ while good agreement with measured values was achieved with $\epsilon = 0.016$. In the case of the barge and Wigley hull the drift force was examined. Similarly, both numerical cases showed good agreement for non-resonant frequencies and drift force in the resonance band was over predicted using

$\epsilon = 0$ while better agreement to measured data was achieved with $\epsilon = 0.016$.

$$\phi_z - k'\phi - i\epsilon k'\phi = 0 \tag{2.1}$$

Cheetham et al. (2007) presented a numerical validation using AQWA software for side by side ship hydrodynamics. AQWA is a potential theory code for frequency-domain and time-domain analysis. A linearized damping lid boundary condition was used in the gap region and can be seen in equation (2.2), where ω_e is the encounter frequency and α is the damping factor. Simulations were performed for a ship and barge case where it was determined that a value of $\alpha = 0.01$ was the most appropriate. A trimaran case was then evaluated and it was found that $\alpha = 0.01$ showed a good fit for most frequencies. $\alpha = 0.1$ showed a better fit through the resonant band but it was found that the hydrodynamic coefficients were overdamped outside the resonant band.

$$\omega_e^2(\alpha - i)^2\phi + g\frac{\partial\phi}{\partial z} = 0, \ (z = 0) \tag{2.2}$$

Pauw et al. (2007) performed a comparison of measured data and numerical analysis of two side by side LNG carriers. The numerical analysis was again performed with a panel method code using a flexible damping lid in the gap region. A variety of gap widths were used in head seas in an attempt to obtain rationale for predicting suitable damping factors. It was concluded that no unique value for the damping factor could fully cover all the measured cases. It was noted that the damping factor should be tuned via the second-order drift force and not first-order quantities, such as wave height. The damping factor was said to have the greatest effect on the second-order drift force.

Zhu et al. (2008) presented a time domain solution for two floating side by side structures using potential flow. Two side by side box like hulls with a narrow gap

between were fixed and the body forces due to the incoming waves and diffracted waves were computed. This time domain analysis showed good agreement for the narrow gap resonant phenomena with the frequency domain analysis. The resonant frequencies were again said to be around $kL \approx n\pi(n = 1, 2, 3, 4, ..., \infty)$.

Bunnick et al. (2009) performed a numerical simulation using the damping lid method, as described in Chen (2005), to compare to model tests conducted for two side by side LNG carriers in head seas. The damping lid also extended inside the body of the vessel and not just the free surface gap. There was a reasonable agreement between numerical analysis and measured results. A damping factor of $\epsilon = 0.03$ was was deemed adequate for this case.

Molin et al. (2009) used the software package, DIODORE, to analyze two side by side fixed barges. The software is based on linear potential flow to solve the problem. A set of massless plates were added to the gap between the barges and a quadratic damping force was applied to the plates. The results from the software was then compared to model test of two rectangular barges in irregular waves. Measured results were obtained for two sea states, two gap widths and two wave headings. A drag coefficient, $C_D = 0.5$, for determining the quadratic damping force showed good agreement with measured data. It was recommended that an investigation of freely floating ships be performed in the future.

Kawabe et al. (2010) examined water surface response in a moonpool for a freely floating vessel. There was a comparison of numerical results with a damped moon pool free surface and measured data. This investigation showed a damping factor of $\epsilon = 0.05$ resulted in a good agreement between numerical and measured results.

Lu et al. (2010a) performed numerical simulations on two identical bodies and three identical bodies at a close proximity. Numerical work was performed with an undamped potential flow model and a viscous flow model. The viscous flow model was

solved using Navier-Stokes equations and the CLEAR-VOF method to capture the free surface in the gap region. Experimental results were used to assess the performance of each model. Both numerical models perform equally as well for frequencies outside the resonance band, while the potential flow model overpredicts the wave height around resonant frequencies. The viscous flow model showed good agreement with measured values for all frequencies. Both models were said to accurately predict the values of resonant frequencies based on experimental data.

Lu et al. (2010b) extended the previous work to include a potential flow numerical model that included artificial damping of the free surface. Here a damping term was introduced into the momentum equation as shown in equation (2.3). The results were presented for experimental data, a viscous model and potential flow model with $\mu = 0$, $\mu = 0.3$, $\mu = 0.4$ and $\mu = 0.5$. The viscous flow model and experimental results showed good agreement over all wave frequencies and cases presented. The potential flow model with $\mu = 0.4$ showed good agreement with the viscous flow and measured values for two body cases and for both gaps in three body cases. There is uncertainty regarding the use of $\mu = 0.4$ for differing geometric cases and further investigation is encouraged.

$$f = -\mu(x)\nabla\phi \tag{2.3}$$

Lu et al. (2011) examined the effects of changing gap width, body draft, body width and number of bodies of multi-bodies at close proximity. A viscous model and potential flow model (damped and undamped) were used in all cases and experimental data was examined when available. It was noted that as the gap width increases the resonant frequency decreases, although the maximum wave height is found at a distinct frequency. Increasing the draft of the bodies results in lower resonant frequencies, while resonant wave heights become larger. A reduction in beam of the downstream body was found to increase the resonant frequency and decrease

the resonant wave height. The addition of an identical body (i.e. three instead of two) produces two resonant frequencies. The fundamental frequency is lower than resonant frequencies for two bodies and the second frequency is greater than the two body resonant frequency. The resonant wave heights for three bodies were found to be lower than two body cases. Also, the wave height of fundamental frequency is generally larger than the wave height for the second resonant frequency for both gaps. By using various damping factors in the damped potential flow model it was determined that $\mu \in [0.4, 0.5]$ produced results in good agreement with the viscous model and experimental data when applicable. The geometry of the bodies and the spatial arrangement was said to have no effect on the value of μ.

Lu & Chen (2012) examined the rate of dissipation around resonant frequencies for a two body case using a viscous model. The dissipation was said to be relatively constant over frequencies near the resonant frequency. The dissipation rate was examined over various zones that include the gap free surface (zone 1) then extend to the seabed (zone 2) and then include the areas under the bodies (zone 3). The total dissipation rate needs to include zone 3 to produce accurate results while the rate of dissipation density is much greater in zone 1. It was also estimated using the dissipation rate that an acceptable value for the damping factor is $\mu = 0.4$.

It has been seen through previous work that there is a significant interaction effect present for two and three bodies at a close proximity in waves. Work has been conducted to examine the narrow gap resonance phenomena present for multi-body interaction cases. Methods have be developed to deal with this phenomena and successfully applied to a number of cases. Generally, the preferred method is the damped potential flow model, however there is much uncertainty in determining an appropriate damping factor to apply. Many cases can be explored using the damped potential flow model however novel numerical models must be validated by experiments or full

scale tests. The amount of experimental data that is available on side-by-side floating body cases is scarce and hinders the progress of numerical work. The majority of the experimental work conducted has been performed using captive models. Captive model tests can be performed easier than free-motion tests but do not consider the motion effects of the floating bodies, thus neglecting the radiated wave effects.

A semi-captive side-by-side model experiment would be a very valuable addition to this research field. There is a significant gap in hydrodynamic knowledge of non-captive multi-body interaction problems. Performing such an experiment would fill this gap and simulate a more realistic offshore environment than the captive tests.

Chapter 3

Model Tests

A set of experiments were conducted to further the amount of available data in hydrodynamic interaction of two floating bodies at close proximity. This data is necessary to extend the reliability of numerical predictions for two body interaction seakeeping problems. The past success in using the "LID" method is promising for numerical predictions of multi-body hydrodynamic problems. It has been proven that the narrow gap resonance phenomena in potential flow models can be dealt with using this method. The method uses an artificial damping factor to suppress the free surface in the gap region for resonant frequencies. Due to the lack of experimental data available it is difficult to verify appropriate damping factors for a wide range of body geometries and spatial arrangements.

While a wide range body geometries could be encountered in side by side applications, given the variety of ship types available, this factor would be held constant for all tests. The effects of gap width and wave heading would be examined in these experiments. Due to the set-up time and availability of tank facilities only the two afore mentioned factors could be examined. Important responses were the wave height in the gap region and body responses for each model.

These experiments were conducted at the Ocean Engineering Research Center (OERC) at Memorial University during March and April of 2013. The OERC has a 58 m long tow tank with a width of 4.5 m and depth of 3.04 m. The tow tank is also equipt with tow carriage and a hydraulically actuated wave board. The towing facility can be seen in Figure 3.1.

Figure 3.1: OERC Tow Tank Facility

3.1 Model Test Plan

The model tests were performed over a wide range of frequencies for each case to examine the nonlinearities involved in narrow gap resonance. In order to control the gap width between the models, a horizontal spread mooring would be used to restrain non-restoring modes of motion. The bodies would remain essentially free to heave,

pitch and roll. Another important factor to examine is the wave heading. This was achieved by designing an apparatus that could be rotated to different wave headings and keep the same relative geometric and spatial arrangement. See Figure 3.2 for experimental setup.

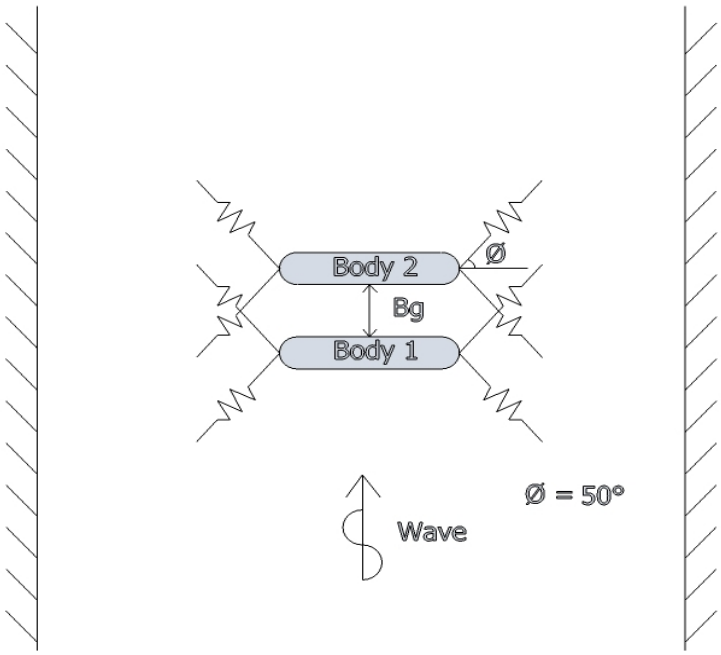

Figure 3.2: Sketch of Experimental Setup

The definition of the ship local coordinate system can be seen in Figure 3.3. The local coordinate system of the ship was placed at the center of gravity and body motions were referenced from there.

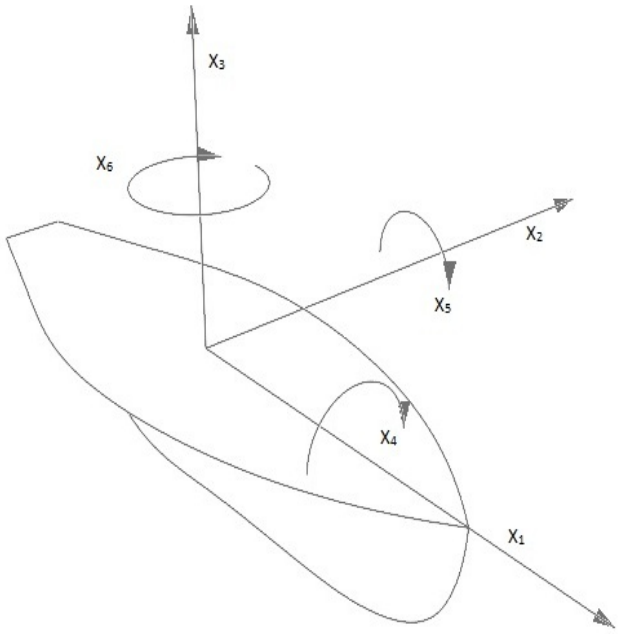

Figure 3.3: Ship Coordinate Convention

3.2 Model Test Matrix

The model test consisted of two gap widths, 4 wave headings and 21 wave periods ranging from 1.00 s to 1.40 s. This frequency range was chosen to examine the problem around resonance frequencies. Resonant frequency estimation can be found in section 3.5 and the test matrix can be seen in Table 3.2.

Run	Gap Width (mm)	Heading (deg)	Period (s)
1	300	90	1.00

Run	Gap Width (mm)	Heading (deg)	Period (s)
2	300	90	1.02
3	300	90	1.07
4	300	90	1.13
5	300	90	1.15
6	300	90	1.18
7	300	90	1.20
8	300	90	1.21
9	300	90	1.22
10	300	90	1.23
11	300	90	1.25
12	300	90	1.26
13	300	90	1.27
14	300	90	1.28
15	300	90	1.30
16	300	90	1.32
17	300	90	1.35
18	300	90	1.37
19	300	90	1.40
20	300	60	1.00
21	300	60	1.02
22	300	60	1.07
23	300	60	1.10
24	300	60	1.13

Run	Gap Width (mm)	Heading (deg)	Period (s)
25	300	60	1.15
26	300	60	1.18
27	300	60	1.22
28	300	60	1.23
29	300	60	1.25
30	300	60	1.27
31	300	60	1.30
32	300	60	1.32
33	300	60	1.35
34	300	60	1.37
35	300	60	1.40
36	300	30	1.00
37	300	30	1.02
38	300	30	1.07
39	300	30	1.10
40	300	30	1.13
41	300	30	1.15
42	300	30	1.18
43	300	30	1.20
44	300	30	1.21
45	300	30	1.22
46	300	30	1.23
47	300	30	1.25

Run	Gap Width (mm)	Heading (deg)	Period (s)
48	300	30	1.26
49	300	30	1.27
50	300	30	1.28
51	300	30	1.30
52	300	30	1.32
53	300	30	1.35
54	300	30	1.37
55	300	30	1.40
56	300	0	1.00
57	300	0	1.02
58	300	0	1.07
59	300	0	1.10
60	300	0	1.13
61	300	0	1.15
62	300	0	1.18
63	300	0	1.20
64	300	0	1.21
65	300	0	1.22
66	300	0	1.23
67	300	0	1.25
68	300	0	1.26
69	300	0	1.27
70	300	0	1.28

Run	Gap Width (mm)	Heading (deg)	Period (s)
71	300	0	1.30
72	300	0	1.32
73	300	0	1.35
74	300	0	1.37
75	300	0	1.40
76	450	90	1.00
77	450	90	1.02
78	450	90	1.07
79	450	90	1.10
80	450	90	1.13
81	450	90	1.15
82	450	90	1.18
83	450	90	1.20
84	450	90	1.21
85	450	90	1.22
86	450	90	1.23
87	450	90	1.25
88	450	90	1.26
89	450	90	1.27
90	450	90	1.28
91	450	90	1.30
92	450	90	1.32
93	450	90	1.35

Run	Gap Width (mm)	Heading (deg)	Period (s)
94	450	90	1.37
95	450	90	1.40
96	450	60	1.00
97	450	60	1.02
98	450	60	1.07
99	450	60	1.10
100	450	60	1.13
101	450	60	1.15
102	450	60	1.18
103	450	60	1.20
104	450	60	1.21
105	450	60	1.22
106	450	60	1.23
107	450	60	1.25
108	450	60	1.26
109	450	60	1.27
110	450	60	1.28
111	450	60	1.30
112	450	60	1.32
113	450	60	1.35
114	450	60	1.37
115	450	60	1.40
116	450	30	1.00

Run	Gap Width (mm)	Heading (deg)	Period (s)
117	450	30	1.02
118	450	30	1.07
119	450	30	1.10
120	450	30	1.13
121	450	30	1.15
122	450	30	1.18
123	450	30	1.20
124	450	30	1.21
125	450	30	1.22
126	450	30	1.23
127	450	30	1.25
128	450	30	1.26
129	450	30	1.27
130	450	30	1.28
131	450	30	1.30
132	450	30	1.32
133	450	30	1.35
134	450	30	1.37
135	450	30	1.40
136	450	0	1.00
137	450	0	1.02
138	450	0	1.07
139	450	0	1.10

Run	Gap Width (mm)	Heading (deg)	Period (s)
140	450	0	1.13
141	450	0	1.15
142	450	0	1.18
143	450	0	1.20
144	450	0	1.21
145	450	0	1.22
146	450	0	1.23
147	450	0	1.25
148	450	0	1.26
149	450	0	1.27
150	450	0	1.28
151	450	0	1.30
152	450	0	1.32
153	450	0	1.35
154	450	0	1.37
155	450	0	1.40

3.3 Models

Two models were constructed of simple geometry for these experiments. The hulls were "box-like" with rounded bow and stern and rounded bilges. The rounded edges allow for more stable numerical simulations to be preformed. The ratio of the principal dimensions were similar to that of a tanker or FPSO hull. A drawing of a model hull can be seen in Figure 3.4.

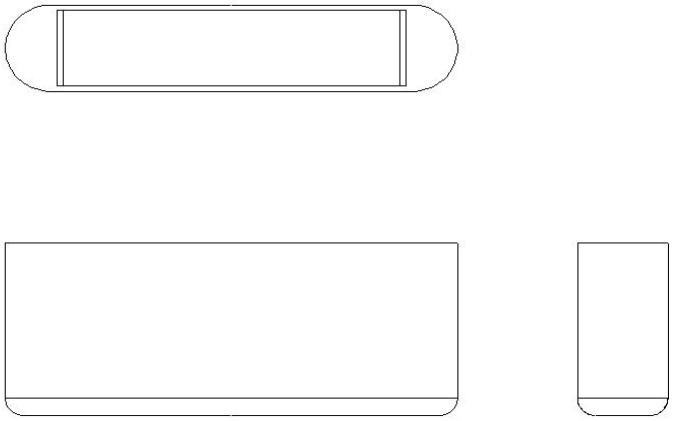

Figure 3.4: Drawing of Model

Table 3.1 shows general geometric parameters for the model hulls.

Table 3.1: Model Parameters

Property	Value
Length (m)	1.25
Beam (m)	0.25
Height (m)	0.50
Draft (m)	0.35
Displacement (kg)	103.2
Bow/Stern Radius (m)	0.125
Bilge Radius (m)	0.05

The models were constructed by Technical Services at Memorial University. The models were constructed of pure pine and bonded together with epoxy. The surface was smoothed and painted in a flat black paint. The model was then delivered to the client and draft marks and station lines were added.

Ballast weight was used from the available supply in the OERC and care was taken to ensure similar weight distributions were used for each model. The mass properties of each model are given in table 3.2.

Table 3.2: Mass Parameters

Property	Body 1	Body 2
Mass (kg)	103.77	104.41
LCG (m)	0.000	-0.001
TCG (m)	0.000	-0.001
VCG (m)	0.161	0.161
I_{xx} (kg·m^2)	1.44	1.50
I_{yy} (kg·m^2)	11.66	12.74
I_{zz} (kg·m^2)	11.19	12.33

3.4 Mooring

A horizontal spread mooring was used to restrain the non-restoring modes of motion of the floating bodies. The mooring system needed to be "stiff" enough to control the gap between the bodies but have a minimal effect on self restoring forces. Figure 3.5 shows the general configuration for a single line of the spread mooring system. The maximum wave period used in the testing matrix was used to determine the minimum period of the mooring system. A factor of 2 was applied to the maximum wave period and then the mooring system was designed such that the natural period of the system was greater than the target design period.

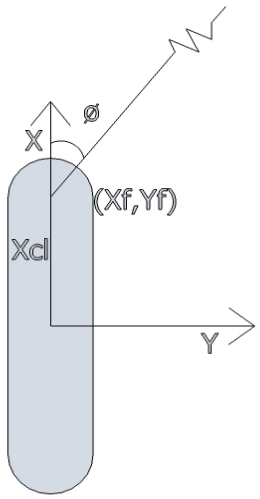

Figure 3.5: Spread Mooring Configuration

The required stiffness was then computed from the target period using equation 3.1.

$$k_{req,i} = (M + M_{A,i}) \left(\frac{2\pi}{T_{req}} \right)^2 \tag{3.1}$$

where M is the model mass, $M_{A,i}$ is the added mass in the given direction and T_{req} is the required period.

The stiffness of the mooring system was then computed using equation 3.2.

$$k_i = 4 \left(\frac{F_0}{L} \sin^2 \phi_i + k_s \cos^2 \phi_i \right) \tag{3.2}$$

where F_0 is the pre-tension, L is the line length, k_s is the spring stiffness and ϕ_i is the angle for the given direction.

Parameters were chosen to compute k_i such that it was greater than $k_{reg,i}$ in each direction. The parameters used are shown in Table 3.3.

Table 3.3: Mooring System Design

Property	Value	Comments
T_{req} (s)	2.8	2x1.4
M (kg)	103.2	Model Displacement
$C_{A,1}$ (-)	0.1	Added Mass Coefficient - Surge
$C_{A,2}$ (-)	0.9	Added Mass Coefficient - Sway
$M + M_{A,1}$ (kg)	114	Mass + Added Mass - Surge
$M + M_{A,2}$ (kg)	196	Mass + Added Mass - Sway
$k_{req,1}$ (N/m)	572	Required Stiffness - Surge
$k_{req,2}$ (N/m)	987	Required Stiffness - Sway
F_0 (N)	53.5	Pre-Tension
ϕ_1 (°)	50	Line Angle -Surge
ϕ_2 (°)	40	Line Angle - Sway
L (m)	1	Line Length
k_s (N/m)	415	Individual Spring Stiffness
k_1 (N/m)	811.5	Mooring Stiffness - Surge
k_2 (N/m)	1062.5	Mooring Stiffness - Sway
X_{fair} (m)	0.7	Long. Position of Fairlead
Y_{fair} (m)	0.0	Lat. Position of Fairlead
X_{cl} (m)	0.7	Moment arm - Yaw
k_3 (Nm/°)	9.1	Mooring Stiffness - Yaw

3.5 Resonace Predictions

In order to estimate where gap resonance may occur, a method presented in Molin et al. (2009) was used. Equation 3.3 was derived for predicting moonpool resonance but has been used to predict gap resonance of two captive models as well.

$$\omega_n^2 \simeq g\lambda_n \frac{1 + J_n \tanh \lambda_n h}{J_n + \tanh \lambda_n h} \tag{3.3}$$

where

$$J_n(r) = \frac{2}{n\pi^2 r}\Bigg\{ \int_0^1 \frac{r^2}{u^2\sqrt{u^2+r^2}} \Big[1 + 2u + (u-1)\cos(n\pi u) - \ \sin(n\pi u)\Big]\, du \\ -\frac{1}{\sin\theta_0} + 1 + 2r \ln \frac{1+\cos\theta_0}{1-\cos\theta_0}\Bigg\}$$

where n is the resonance mode, $u = x' - x$ given that x is the longitudinal dimension within the global domain and x' is the longitudinal position within the moonpool or sub-domain, $\lambda_n = n\pi/l_g$, $r = b_g/l_g$ and $\tan\theta_0 = r^{-1}$, l_g is the gap length, b_g is the gap width and h is the draft. J_n can be solved numerically for each gap geometry and then ω_n can be computed easily. See Table 3.4 for predictions for the two gap widths.

Table 3.4: ω_n predictions

Gap Width (mm)	ω_n (rad/s)
300	5.1675
450	5.061

3.6 Data Acquisition

Data was recorded for free surface analysis and vessel dynamics of the two side by side model setup. The free surface elevations were measured using 5 Akamina wave probe heads and 5 Akamina AWP-24 wave probe gauges. The configuration of the wave probes in the experimental setup can be seen in Figure 3.6. The vessel dynamics were measured using a Qualysis optical tracking system. The system consists of 3 Osus 100 cameras positioned around the setup where cameras have good visibility of passive markers placed on the models as seen in Figure 3.7.

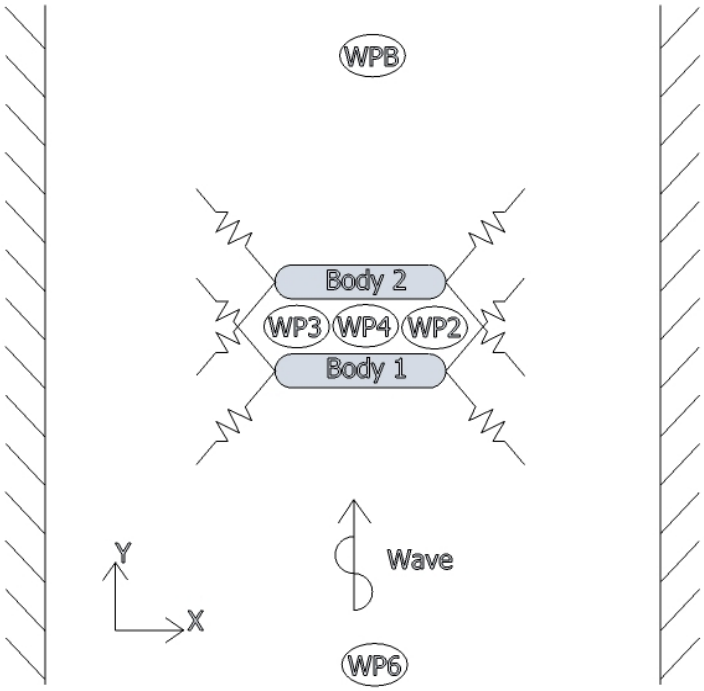

Figure 3.6: Wave Probe Configuration

Figure 3.7: One Camera View

The wave probes were located 2.5 m upstream and downstream of the gap centerline and 3 were located on the gap centerline with one placed in-line with model midships and two 0.5 m forward and aft. The upstream and downstream wave probes were mounted to lockable walkways positioned upstream and downstream of the test area, respectively. The three wave probes in the gap region were mounted to a piece of angle steel suspended above the free surface. See Figure 3.8 for a picture of the wave probe setup during the experiments. Table 3.5 displays the locations of each wave probe with the origin located at the center of the gap. These positions are for the beams seas case only. For other wave heading the wave probes in the gap are rotated with the models and the upstream and downstream wave probes remain in the original positions. See Figure 3.9 and Figure 3.10 for additional pictures of test

configurations.

Table 3.5: Wave Probe Locations

Wave Probe	X (m)	Y(m)
WP6	0	-2.5
WP3	-0.5	0
WP4	0	0
WP2	0.5	0
WPB	2.5	0

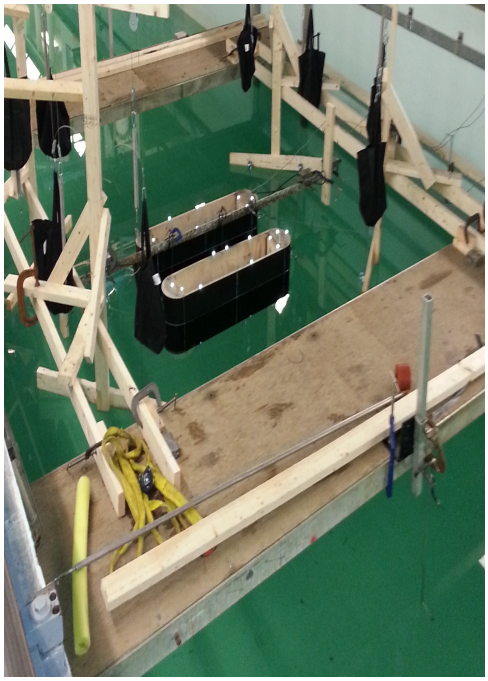

Figure 3.8: Wave Probe Setup

Figure 3.9: Test in Beam Seas

Figure 3.10: Test in Oblique Seas

Chapter 4

Model Test Results

The free surface elevations and vessel motions were of particular interest for this set of experiments. The time signals were recorded for free surface elevation at 5 different locations in the testing field and the rigid body motions of each floating body. The time signals were then imported to Matlab for data processing. The following section presents the experimental results and the methodology for the analysis.

4.1 Data Processing

The time histories of the recorded data were processed to obtain significant parameters of the signal. Some parameters can be difficult to obtain in the time domain and need to be converted to frequency domain. This process can be performed using a fast Fourier transform (FFT). The fast Fourier transform is a numerical method and was used to transform the discretely sampled time history to frequency domain. This numerical approximation is useful for data processing but care must be taken to minimize numerical errors. Numerical errors can be presented because of the discrete nature of the FFT while major assumptions of the Fourier transform is that the function is continuous and perfectly periodic.

Scalloping or the so called "picket fence effect" can cause poor estimates of amplitude. This occurs when the frequency of a signal lies between two neighboring frequency bins of the FFT. In this case the energy of the signal is actually spreads across the two adjacent frequency bins and the amplitude is lower than it should be.

Spectral leakage can also cause poor estimates of signal amplitude. This is when the energy for a given frequency is spread across neighboring frequencies but it is because of the assumption that the data is continuous where in fact the data is truncated at the ends. Also, when the bins are very close to each other the computation is susceptible to spectral leakage.

To obtain accurate estimates for the signal amplitude some data was resampled to generate frequency bins such that the bin would fall closely to the signal frequency and be spaced sufficiently far apart so that energy would not leak to neighboring frequency bins. The frequency of the signal was estimated by sampling at a higher rate than the amplitude. The neighboring bins would be used to estimate the frequency by using a weighted average of the power distribution around an apparent peak. Equation 4.1 (Cerna & Harvey, 2000) shows how the frequency was estimated.

$$f_{estimate} = \frac{\sum_{i=j-3}^{j+3} A_i \cdot i \cdot \Delta f}{\sum_{i=j-3}^{j+3} A_i} \tag{4.1}$$

where j is the index of the apparent peak, A_i is the bin amplitude and Δf is the frequency spacing.

An example of the data processing algorithm is displayed in the following figures. Figure 4.1 shows an original time signal record. Figure 4.2 shows an example of the discrete Fourier transform (DFT) when the original sampling frequency was inappropriate for the case presented. Figure 4.3 shows the DFT of resampled data that can

correctly recover the frequency components for the given case. The amplitude recovered by the original DFT is much lower than that of the original time signal and the energy appears to be spread to neighboring bins. The resampled DFT shows a much improved approximation of the original time signal amplitude. However, The original DFT may be more appropriate for approximating the frequency using equation 4.1.

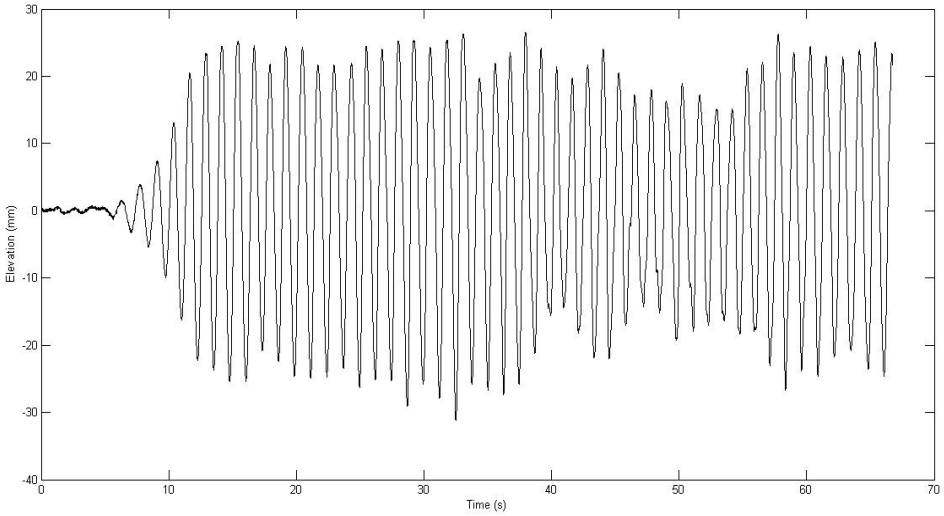

Figure 4.1: Original Time Signal Example

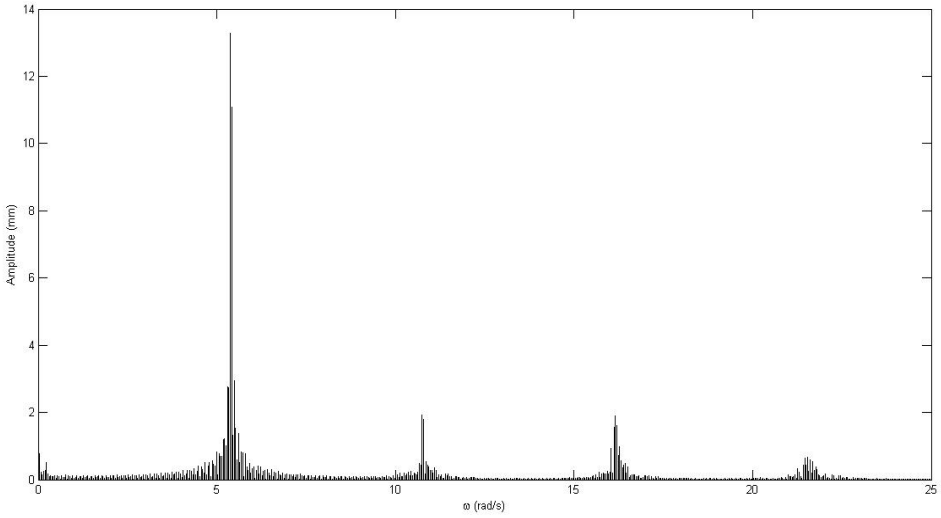

Figure 4.2: Discrete Fourier Transform Example

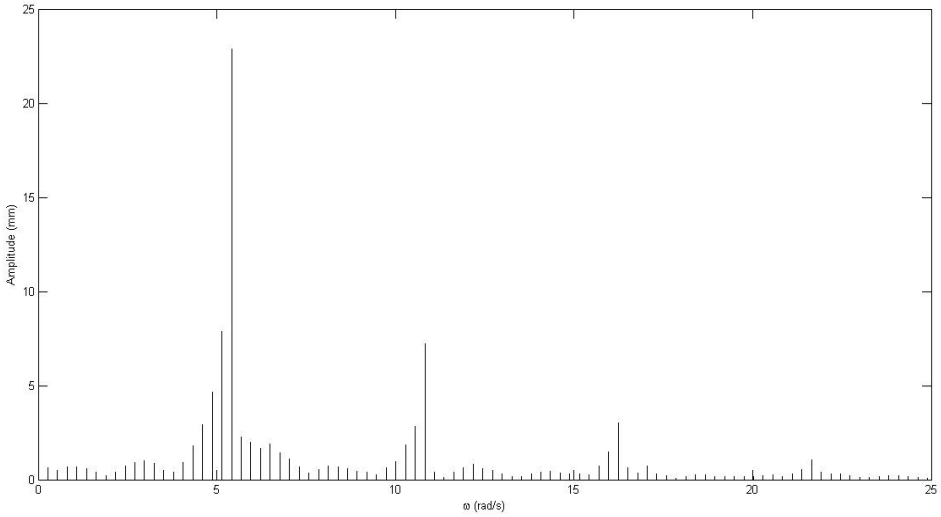

Figure 4.3: Resampled Discrete Fourier Transform Example

4.2 Free Surface

The free surface elevations for this experiment have been recorded at 5 positions in the tow tank. Refer to Figure 3.6 for the positions of each wave probe. All the time histories for the wave elevations can be found in appendix A. There were discrepancies between the desired frequency and the actual frequency produced by the wave board in some cases.The same signal was sent to the wave board for a given frequency for each case, however in some runs the desired frequency was not recovered by WP6. In these cases the measured frequency was used in the analysis even though it may not be listed in the test plan. The computed wave frequency from WP6 was used to represent each case. Also, there were cases where there were signal drop offs in wave probes. The signal drop offs were from a combination of defective instrumentation and intermittent drop offs. In these cases the probe that was not producing a measurement was omitted from figures in appendix A. When there were issues due to defective instrumentation one of the off center wave probes in the gap was omitted and only two cases had issues with the center gap probe.

Determining gap resonance for this experiment can done by plotting the ratio of the first order gap wave height, H_g to the first order incoming wave height, H_i, against the non-dimensional wave number kL, where k is the wave number using the deep water approximation $\omega^2 = gk$ and L is the model length. The first order wave height is referred to as the component of the free surface elevation having the dominate frequency, usually the frequency of the incoming wave. The plots for 8 configurations of wave headings and gap width can be seen in Figures 4.4 - 4.11 and the values are presented in Tables 4.1 - 4.4.

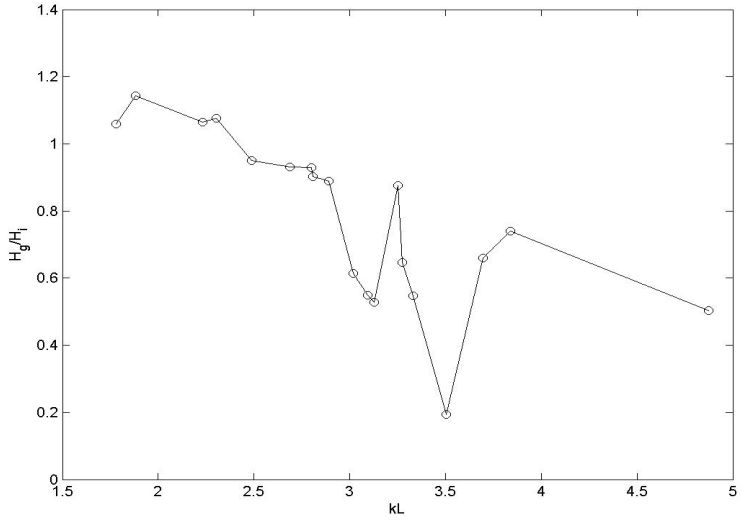

Figure 4.4: First Order Wave Height in Gap for Wave Heading 90° and 300 mm Gap

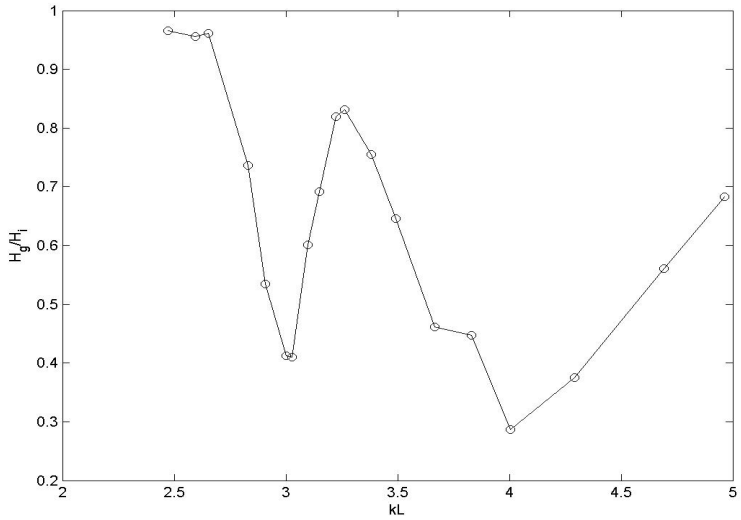

Figure 4.5: First Order Wave Height in Gap for Wave Heading 90° and 450 mm Gap

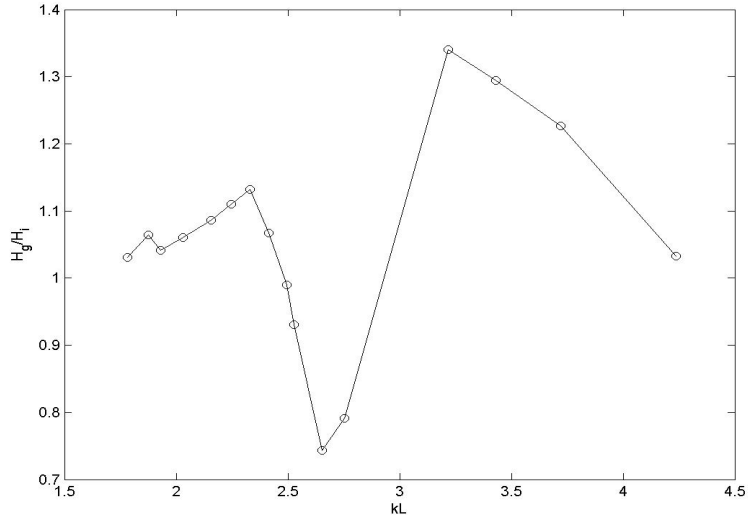

Figure 4.6: First Order Wave Height in Gap for Wave Heading 60° and 300 mm Gap

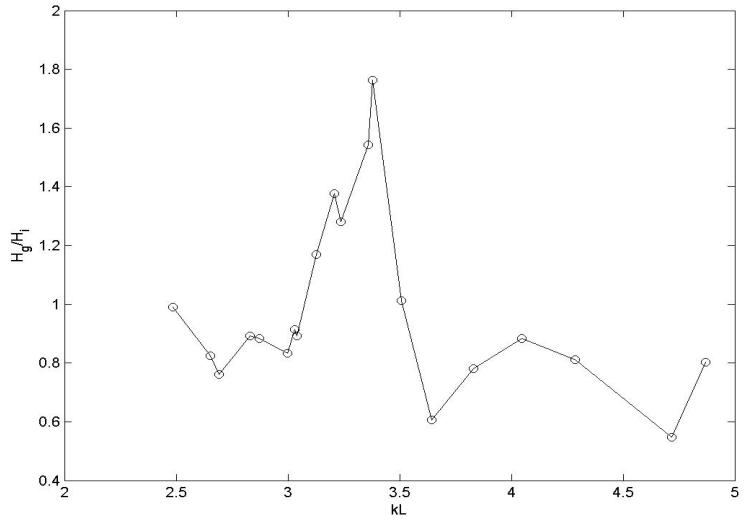

Figure 4.7: First Order Wave Height in Gap for Wave Heading 60° and 450 mm Gap

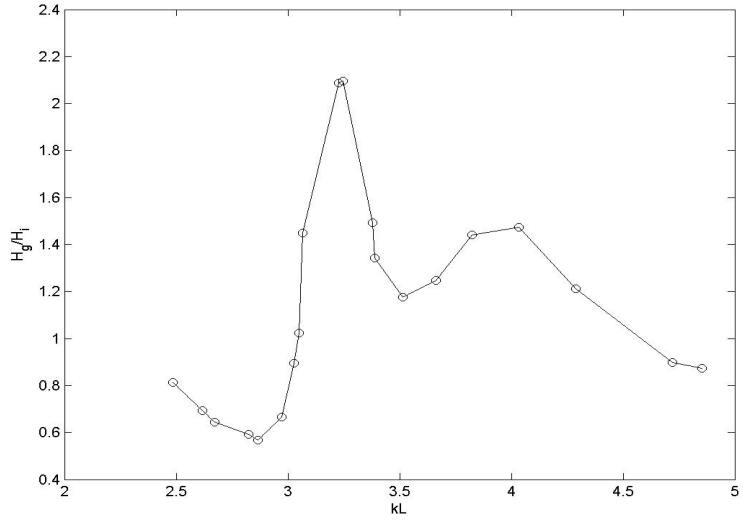

Figure 4.8: First Order Wave Height in Gap for Wave Heading 30° and 300 mm Gap

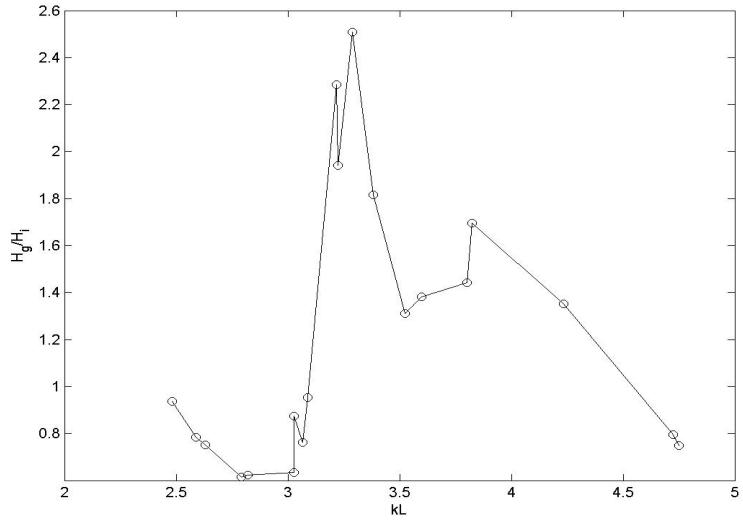

Figure 4.9: First Order Wave Height in Gap for Wave Heading 30° and 450 mm Gap

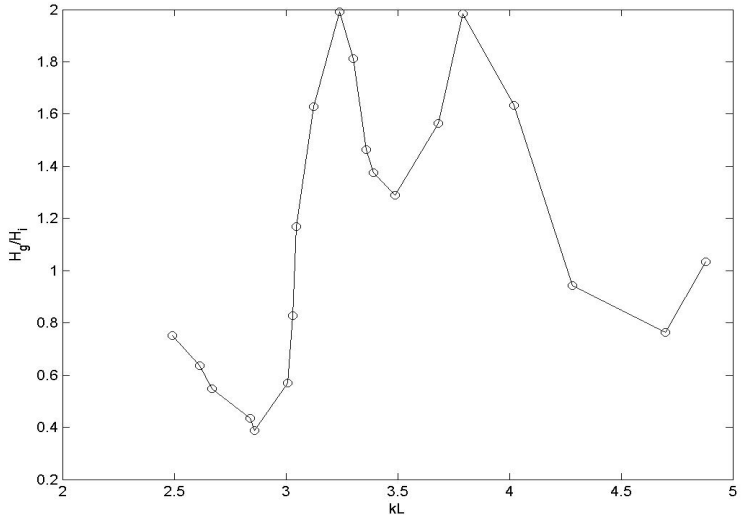

Figure 4.10: First Order Wave Height in Gap for Wave Heading 0° and 300 mm Gap

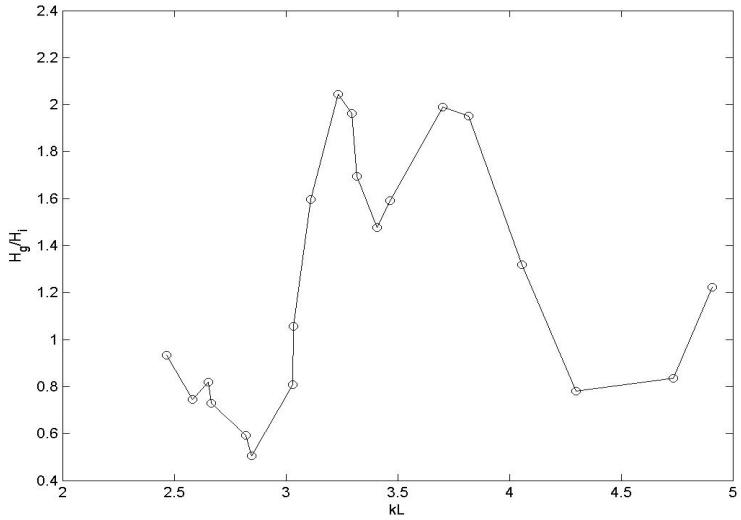

Figure 4.11: First Order Wave Height in Gap for Wave Heading 0° and 450 mm Gap

Second-order analysis of the gap region using data from WP6 showed the presence of second-order wave elevations. Second order wave elevation is the component of

the free surface elevation that has a frequency of twice the dominate or fundamental frequency. This refers to the second-harmonic of the fundamental frequency which usually becomes significant due to non-linearity in the problem. The significance of the second harmonic gives an indication of the non linearity of the set up. Figures 4.12 - 4.19 and Tables 4.1 - 4.4 show the ratio of second-order wave amplitude to first-order wave amplitude present in the wave probe signal.

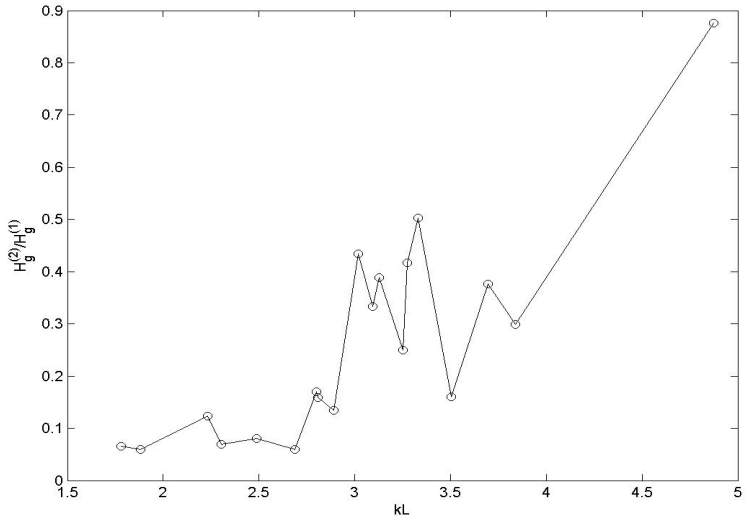

Figure 4.12: Second Order Wave Height in Gap for Wave Heading 90° and 300 mm Gap

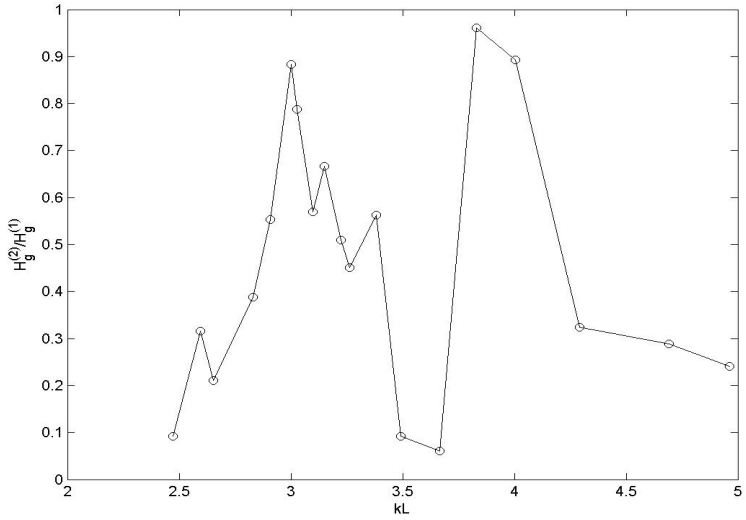

Figure 4.13: Second Order Wave Height in Gap for Wave Heading 90° and 450 mm Gap

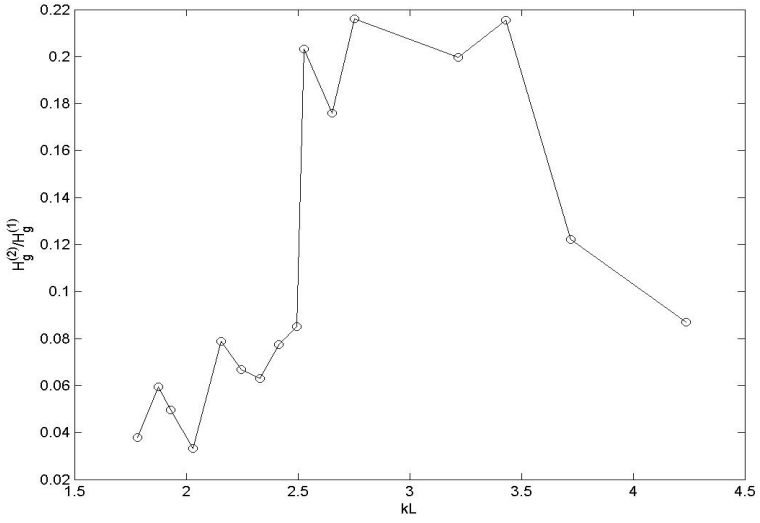

Figure 4.14: Second Order Wave Height in Gap for Wave Heading 60° and 300 mm Gap

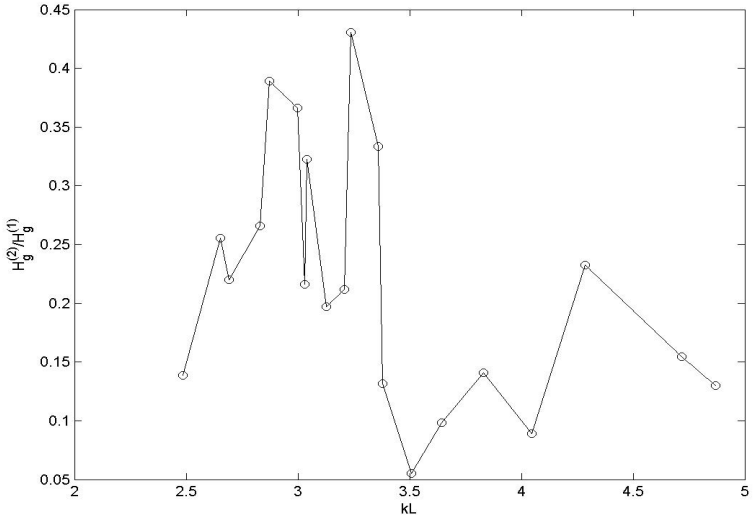

Figure 4.15: Second Order Wave Height in Gap for Wave Heading 60° and 450 mm Gap

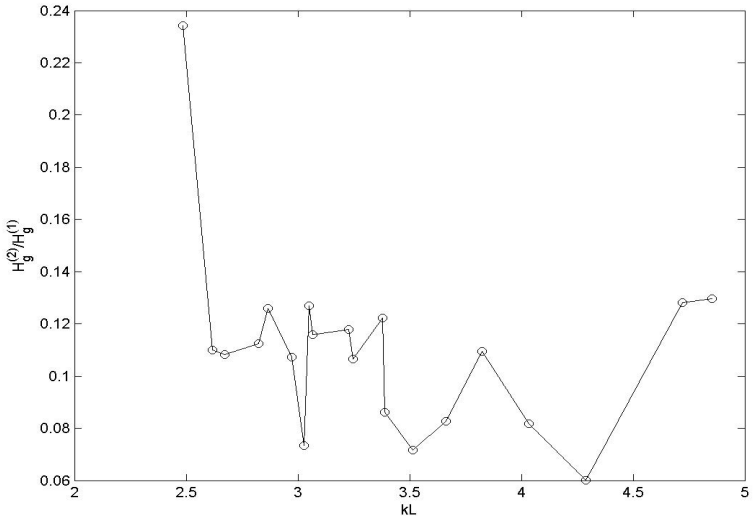

Figure 4.16: Second Order Wave Height in Gap for Wave Heading 30° and 300 mm Gap

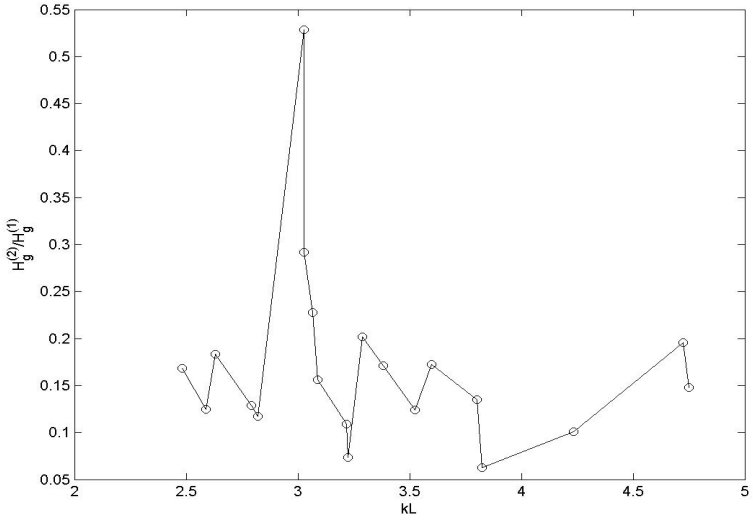

Figure 4.17: Second Order Wave Height in Gap for Wave Heading 30° and 450 mm Gap

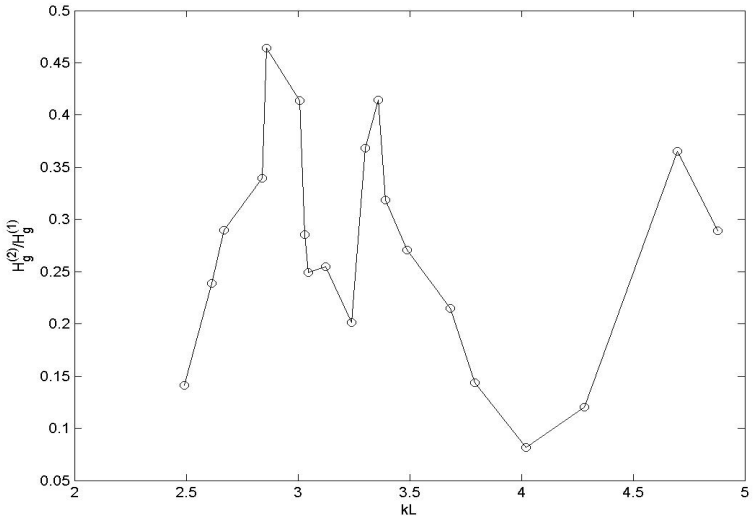

Figure 4.18: Second Order Wave Height in Gap for Wave Heading 0° and 300 mm Gap

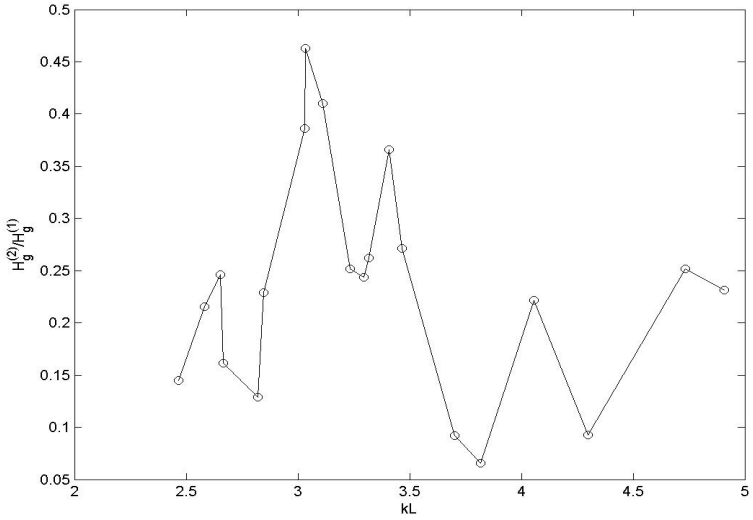

Figure 4.19: Second Order Wave Height in Gap for Wave Heading 0° and 450 mm Gap

Table 4.1: Gap Wave Height for Wave Heading 90°

300 mm			450 mm		
kL	H_g/H_i	$H_g^{(2)}/H_g^{(1)}$	kL	H_g/H_i	$H_g^{(2)}/H_g^{(1)}$
1.78	1.06	0.07	2.47	0.97	0.09
1.88	1.14	0.06	2.60	0.96	0.32
2.23	1.06	0.12	2.65	0.96	0.21
2.30	1.08	0.07	2.83	0.74	0.39
2.49	0.95	0.08	2.91	0.53	0.55
2.69	0.93	0.06	3.00	0.41	0.88
2.80	0.93	0.17	3.03	0.41	0.79
2.81	0.90	0.16	3.10	0.60	0.57
2.89	0.89	0.13	3.15	0.69	0.67
3.02	0.61	0.43	3.22	0.82	0.51
3.09	0.55	0.33	3.26	0.83	0.45
3.13	0.53	0.39	3.38	0.75	0.56
3.25	0.88	0.25	3.49	0.65	0.09
3.27	0.65	0.42	3.66	0.46	0.06
3.33	0.55	0.50	3.83	0.45	0.96
3.50	0.19	0.16	4.00	0.29	0.89
3.69	0.66	0.38	4.29	0.38	0.32
3.84	0.74	0.30	4.69	0.56	0.29
4.88	0.50	0.88	4.96	0.68	0.24

Table 4.2: Gap Wave Height for Wave Heading 60°

300 mm			450 mm		
kL	H_g/H_i	$H_g^{(2)}/H_g^{(1)}$	kL	H_g/H_i	$H_g^{(2)}/H_g^{(1)}$
1.78	1.03	0.04	3.24	1.28	0.43
1.88	1.06	0.06	2.48	0.99	0.14
1.93	1.04	0.05	2.65	0.82	0.26
2.03	1.06	0.03	2.69	0.76	0.22
2.16	1.09	0.08	2.83	0.89	0.27
2.25	1.11	0.07	2.87	0.88	0.39
2.33	1.13	0.06	3.00	0.83	0.37
2.41	1.07	0.08	3.03	0.91	0.22
2.49	0.99	0.09	3.04	0.89	0.32
2.53	0.93	0.20	3.13	1.17	0.20
2.65	0.74	0.18	3.21	1.38	0.21
2.75	0.79	0.22	3.36	1.54	0.33
3.22	1.34	0.20	3.38	1.76	0.13
3.43	1.29	0.22	3.51	1.01	0.06
3.72	1.23	0.12	3.64	0.61	0.10
4.24	1.03	0.09	3.83	0.78	0.14
			4.05	0.88	0.09
			4.29	0.81	0.23
			4.72	0.55	0.15
			4.87	0.80	0.13

Table 4.3: Gap Wave Height for Wave Heading 30°

300 mm			450 mm		
kL	H_g/H_i	$H_g^{(2)}/H_g^{(1)}$	kL	H_g/H_i	$H_g^{(2)}/H_g^{(1)}$
2.49	0.81	0.23	2.48	0.94	0.17
2.62	0.69	0.11	2.59	0.78	0.12
2.67	0.64	0.11	2.63	0.75	0.18
2.83	0.59	0.11	2.79	0.62	0.13
2.86	0.57	0.13	2.82	0.62	0.12
2.97	0.67	0.11	3.03	0.63	0.53
3.03	0.90	0.07	3.03	0.87	0.29
3.05	1.02	0.13	3.07	0.76	0.23
3.07	1.45	0.12	3.09	0.95	0.16
3.23	2.09	0.12	3.22	2.28	0.11
3.25	2.09	0.11	3.23	1.94	0.07
3.38	1.49	0.12	3.29	2.51	0.20
3.39	1.34	0.09	3.38	1.81	0.17
3.52	1.18	0.07	3.52	1.31	0.12
3.66	1.25	0.08	3.60	1.38	0.17
3.82	1.44	0.11	3.80	1.44	0.13
4.03	1.47	0.08	3.83	1.70	0.06
4.29	1.21	0.06	4.23	1.35	0.10
4.72	0.90	0.13	4.72	0.80	0.20
4.85	0.87	0.13	4.75	0.75	0.15

Table 4.4: Gap Wave Height for Wave Heading 0°

300 mm			450 mm		
kL	H_g/H_i	$H_g^{(2)}/H_g^{(1)}$	kL	H_g/H_i	$H_g^{(2)}/H_g^{(1)}$
2.49	0.75	0.14	2.47	0.93	0.14
2.62	0.64	0.24	2.58	0.75	0.22
2.67	0.55	0.29	2.65	0.82	0.25
2.84	0.43	0.34	2.67	0.73	0.16
2.86	0.39	0.46	2.82	0.59	0.13
3.01	0.57	0.41	2.85	0.50	0.23
3.03	0.83	0.29	3.03	0.81	0.39
3.05	1.17	0.25	3.04	1.05	0.46
3.12	1.63	0.25	3.11	1.60	0.41
3.24	1.99	0.20	3.23	2.04	0.25
3.30	1.81	0.37	3.30	1.96	0.24
3.36	1.46	0.41	3.32	1.69	0.26
3.39	1.37	0.32	3.41	1.48	0.37
3.49	1.29	0.27	3.47	1.59	0.27
3.68	1.56	0.21	3.70	1.99	0.09
3.79	1.98	0.14	3.82	1.95	0.07
4.02	1.63	0.08	4.06	1.32	0.22
4.28	0.94	0.12	4.30	0.78	0.09
4.70	0.76	0.37	4.73	0.84	0.25
4.88	1.03	0.29	4.91	1.22	0.23

4.3 Vessel Dynamics

The motions of each model were restrained by a horizontal spread mooring in surge, sway and yaw. Heave, roll and pitch were relatively free to move as the mooring system restraining force would be minimal for these modes of motion. Therefore, only heave, roll and pitch will be analyzed in this section. The time histories for the motions of each body can be seen in Appendix B. The ship local coordinate system can be recalled from Figure 3.3.The response amplitude operators (RAO) for heave, roll and pitch are presented in Figures 4.20 - 4.35 and Tables 4.5 - 4.12. The definitions for the heave, roll and pitch RAOs are given in equations 4.2 - 4.4, where k is the wave number and η is the first order wave amplitude.

$$RAO_3 = \frac{X_3}{\eta} \tag{4.2}$$

$$RAO_4 = \frac{X_4}{k\eta} \tag{4.3}$$

$$RAO_5 = \frac{X_5}{k\eta} \tag{4.4}$$

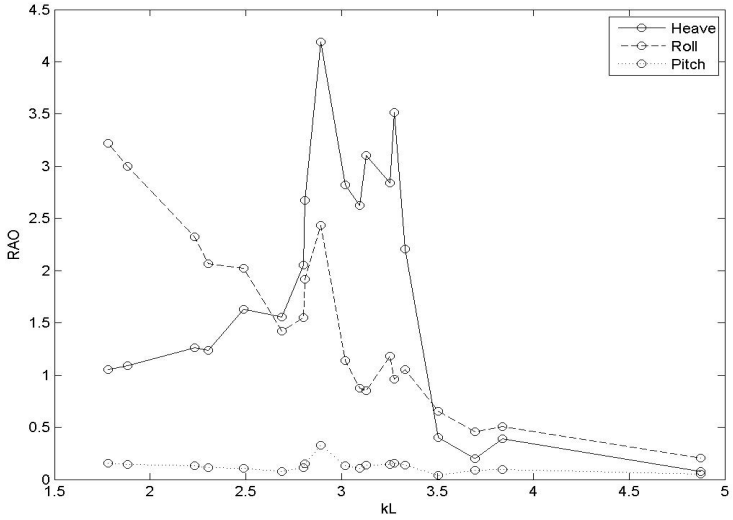

Figure 4.20: RAO for Body 2 for Wave Heading 90° and 300 mm Gap

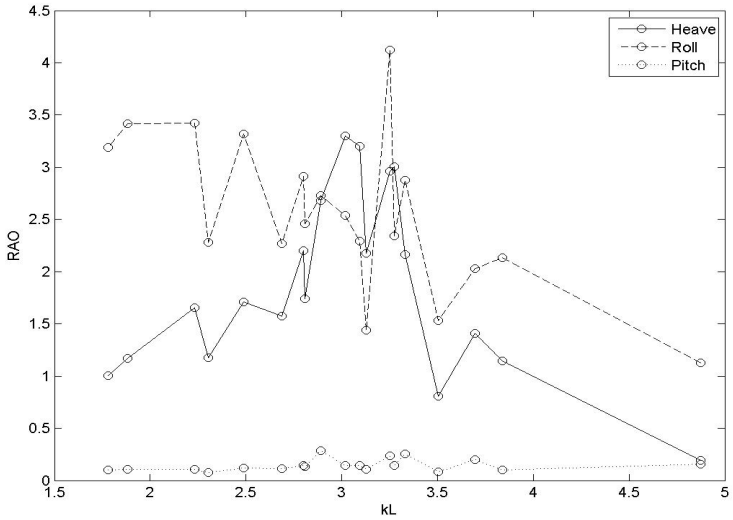

Figure 4.21: RAO for Body 1 for Wave Heading 90° and 300 mm Gap

Table 4.5: Body Motions for Wave Heading 90° and 300 mm Gap

Body 2				Body 1			
kL	RAO_3	RAO_4	RAO_5	kL	RAO_3	RAO_4	RAO_5
1.78	1.00	3.19	0.10	1.78	1.05	3.22	0.16
1.88	1.17	3.42	0.11	1.88	1.09	3.00	0.14
2.23	1.65	3.42	0.11	2.23	1.26	2.32	0.13
2.30	1.18	2.28	0.08	2.30	1.24	2.06	0.12
2.49	1.71	3.32	0.12	2.49	1.63	2.02	0.10
2.69	1.58	2.27	0.11	2.69	1.56	1.42	0.08
2.80	2.20	2.91	0.15	2.80	2.06	1.55	0.11
2.81	1.74	2.46	0.13	2.81	2.67	1.92	0.15
2.89	2.68	2.73	0.29	2.89	4.19	2.43	0.33
3.02	3.30	2.54	0.14	3.02	2.82	1.14	0.13
3.09	3.20	2.29	0.14	3.09	2.63	0.88	0.11
3.13	2.17	1.44	0.11	3.13	3.10	0.85	0.14
3.25	2.96	4.12	0.24	3.25	2.84	1.18	0.14
3.27	3.01	2.34	0.14	3.27	3.52	0.96	0.15
3.33	2.16	2.88	0.26	3.33	2.20	1.05	0.14
3.50	0.81	1.53	0.08	3.50	0.40	0.65	0.04
3.69	1.41	2.03	0.20	3.69	0.20	0.45	0.09
3.84	1.14	2.14	0.10	3.84	0.39	0.50	0.10
4.88	0.19	1.13	0.16	4.88	0.08	0.20	0.05

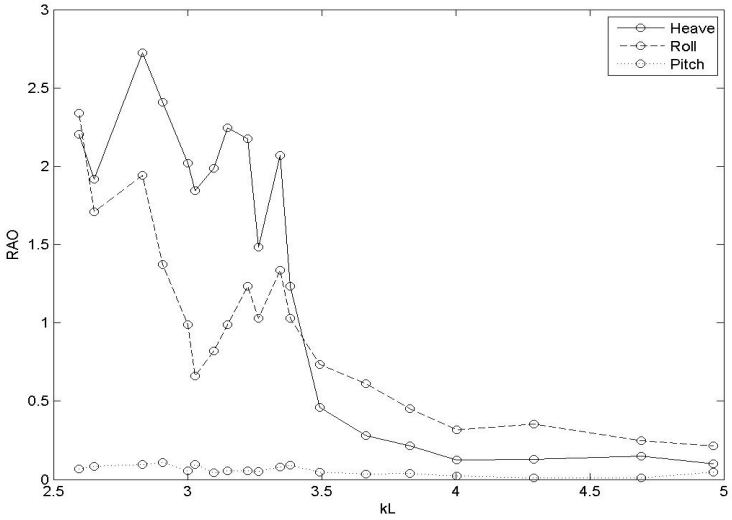

Figure 4.22: RAO for Body 2 for Wave Heading 90° and 450 mm Gap

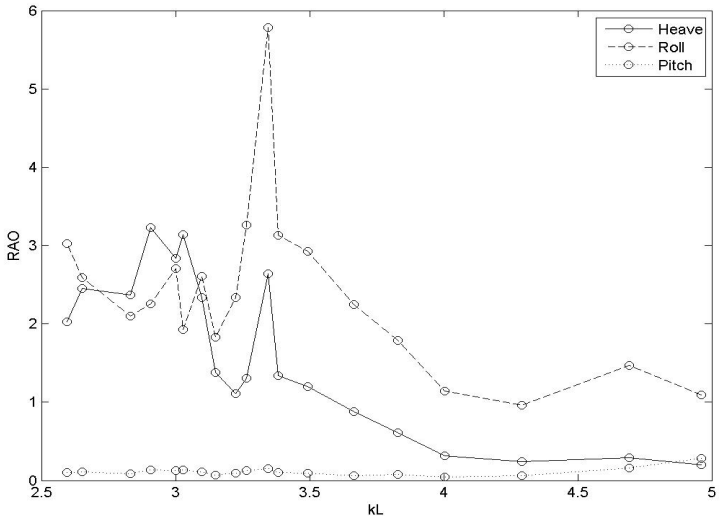

Figure 4.23: RAO for Body 1 for Wave Heading 90° and 450 mm Gap

Table 4.6: Body Motions for Wave Heading 90° and 450 mm Gap

Body 2				Body 1			
kL	RAO_3	RAO_4	RAO_5	kL	RAO_3	RAO_4	RAO_5
2.60	2.02	3.03	0.10	2.60	2.20	2.34	0.07
2.65	2.45	2.59	0.11	2.65	1.92	1.71	0.09
2.83	2.37	2.10	0.08	2.83	2.73	1.94	0.09
2.91	3.23	2.25	0.14	2.91	2.41	1.37	0.11
3.00	2.84	2.71	0.12	3.00	2.02	0.99	0.06
3.03	3.14	1.93	0.14	3.03	1.84	0.66	0.10
3.10	2.34	2.61	0.11	3.10	1.99	0.82	0.05
3.15	1.38	1.83	0.07	3.15	2.24	0.99	0.06
3.22	1.11	2.34	0.09	3.22	2.17	1.24	0.06
3.26	1.30	3.26	0.12	3.26	1.48	1.03	0.05
3.35	2.64	5.78	0.15	3.35	2.07	1.34	0.08
3.38	1.34	3.13	0.10	3.38	1.23	1.03	0.09
3.49	1.20	2.93	0.10	3.49	0.46	0.73	0.05
3.66	0.88	2.25	0.06	3.66	0.28	0.61	0.04
3.83	0.61	1.79	0.07	3.83	0.22	0.45	0.04
4.00	0.32	1.14	0.04	4.00	0.13	0.32	0.02
4.29	0.24	0.96	0.06	4.29	0.13	0.35	0.01
4.69	0.29	1.47	0.16	4.69	0.15	0.25	0.01
4.96	0.20	1.09	0.28	4.96	0.10	0.22	0.05

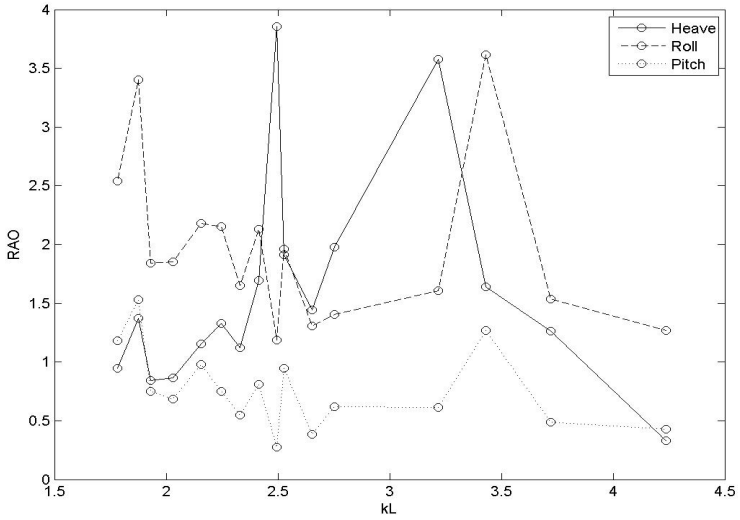

Figure 4.24: RAO for Body 2 for Wave Heading 60° and 300 mm Gap

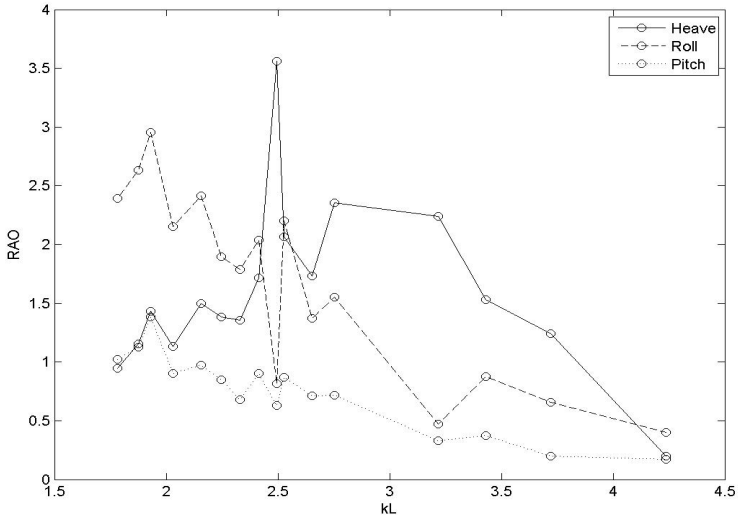

Figure 4.25: RAO for Body 1 for Wave Heading 60° and 300 mm Gap

Table 4.7: Body Motions for Wave Heading 60° and 300 mm Gap

Body 2				Body 1			
kL	RAO_3	RAO_4	RAO_5	kL	RAO_3	RAO_4	RAO_5
1.78	0.95	2.40	1.02	1.78	0.95	2.54	1.18
1.88	1.15	2.64	1.12	1.88	1.37	3.40	1.53
1.93	1.43	2.96	1.39	1.93	0.84	1.84	0.75
2.03	1.13	2.16	0.90	2.03	0.86	1.85	0.68
2.16	1.50	2.41	0.97	2.16	1.16	2.18	0.98
2.25	1.38	1.90	0.85	2.25	1.33	2.15	0.75
2.33	1.35	1.79	0.68	2.33	1.12	1.65	0.55
2.41	1.72	2.04	0.90	2.41	1.69	2.13	0.81
2.49	3.56	0.82	0.63	2.49	3.86	1.18	0.28
2.53	2.07	2.20	0.87	2.53	1.91	1.96	0.94
2.65	1.73	1.37	0.71	2.65	1.44	1.31	0.39
2.75	2.36	1.55	0.72	2.75	1.98	1.41	0.62
3.22	2.24	0.47	0.33	3.22	3.58	1.61	0.61
3.43	1.53	0.88	0.38	3.43	1.64	3.62	1.27
3.72	1.24	0.66	0.20	3.72	1.27	1.54	0.49
4.24	0.20	0.40	0.17	4.24	0.33	1.27	0.43

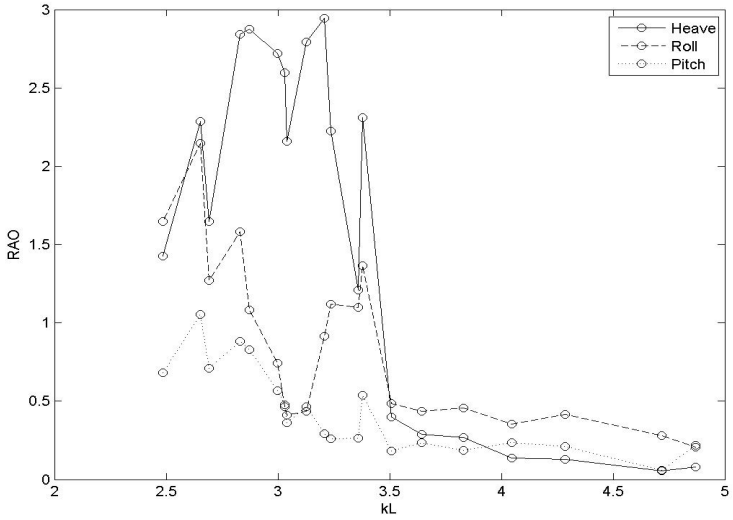

Figure 4.26: RAO for Body 2 for Wave Heading 60° and 450 mm Gap

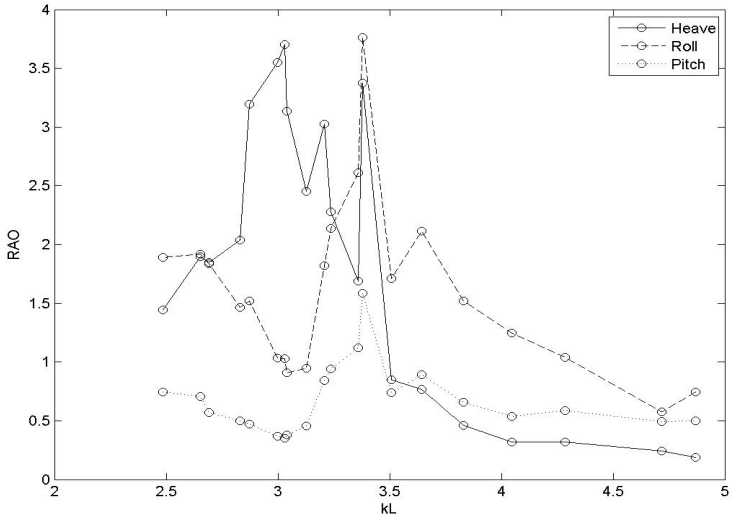

Figure 4.27: RAO for Body 1 for Wave Heading 60° and 450 mm Gap

Table 4.8: Body Motions for Wave Heading 60° and 450 mm Gap

Body 2				Body 1			
kL	RAO_3	RAO_4	RAO_5	kL	RAO_3	RAO_4	RAO_5
2.48	1.45	1.89	0.74	2.48	1.43	1.65	0.68
2.65	1.90	1.92	0.71	2.65	2.28	2.15	1.06
2.69	1.85	1.83	0.57	2.69	1.65	1.27	0.71
2.83	2.04	1.46	0.50	2.83	2.84	1.58	0.88
2.87	3.20	1.52	0.47	2.87	2.87	1.08	0.83
3.00	3.55	1.03	0.37	3.00	2.72	0.74	0.57
3.03	3.70	1.03	0.35	3.03	2.60	0.47	0.48
3.04	3.14	0.91	0.38	3.04	2.16	0.41	0.36
3.13	2.46	0.95	0.45	3.13	2.79	0.43	0.46
3.21	3.03	1.82	0.84	3.21	2.94	0.92	0.29
3.24	2.28	2.13	0.94	3.24	2.23	1.12	0.26
3.36	1.69	2.61	1.12	3.36	1.21	1.10	0.26
3.38	3.38	3.77	1.58	3.38	2.31	1.36	0.54
3.51	0.85	1.71	0.74	3.51	0.40	0.48	0.18
3.64	0.77	2.12	0.89	3.64	0.29	0.44	0.24
3.83	0.46	1.52	0.66	3.83	0.27	0.46	0.19
4.05	0.32	1.25	0.54	4.05	0.14	0.35	0.23
4.29	0.32	1.04	0.59	4.29	0.13	0.42	0.21
4.72	0.25	0.58	0.50	4.72	0.06	0.28	0.06
4.87	0.19	0.75	0.50	4.87	0.08	0.21	0.22

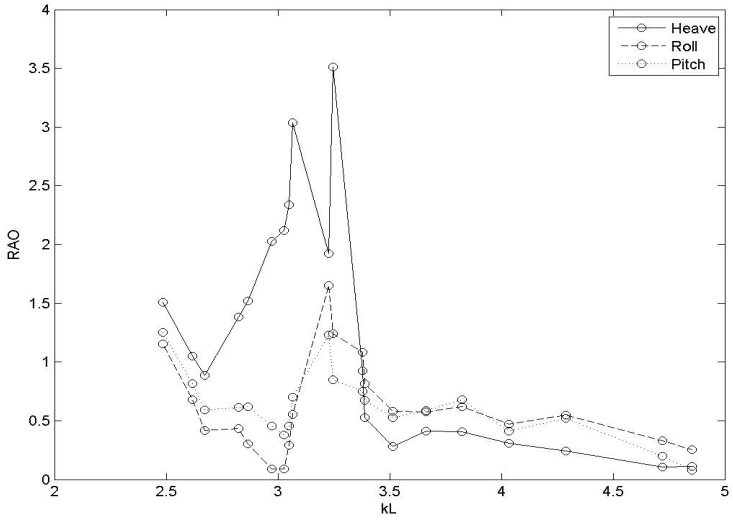

Figure 4.28: RAO for Body 2 for Wave Heading 30° and 300 mm Gap

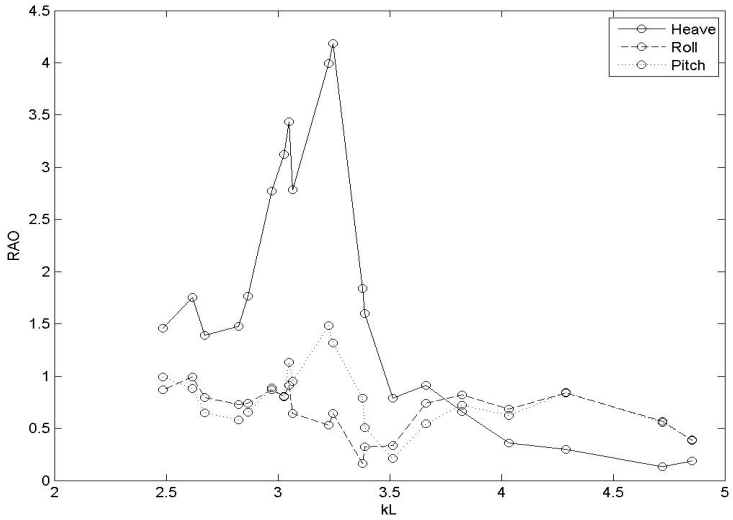

Figure 4.29: RAO for Body 1 for Wave Heading 30° and 300 mm Gap

Table 4.9: Body Motions for Wave Heading 30° and 300 mm Gap

Body 2				Body 1			
kL	RAO_3	RAO_4	RAO_5	kL	RAO_3	RAO_4	RAO_5
2.49	1.46	0.87	0.99	2.49	1.51	1.15	1.25
2.62	1.75	0.99	0.88	2.62	1.05	0.68	0.82
2.67	1.39	0.79	0.65	2.67	0.89	0.42	0.59
2.83	1.48	0.73	0.58	2.83	1.38	0.43	0.61
2.86	1.76	0.74	0.65	2.86	1.52	0.30	0.62
2.97	2.77	0.87	0.88	2.97	2.03	0.09	0.46
3.03	3.12	0.81	0.80	3.03	2.12	0.09	0.38
3.05	3.44	0.91	1.14	3.05	2.34	0.29	0.45
3.07	2.79	0.64	0.95	3.07	3.04	0.55	0.70
3.23	3.99	0.53	1.48	3.23	1.92	1.65	1.23
3.25	4.18	0.64	1.32	3.25	3.51	1.24	0.85
3.38	1.84	0.16	0.79	3.38	0.93	1.08	0.75
3.39	1.60	0.32	0.50	3.39	0.53	0.82	0.68
3.52	0.79	0.33	0.21	3.52	0.28	0.58	0.53
3.66	0.91	0.74	0.54	3.66	0.41	0.57	0.59
3.82	0.66	0.82	0.72	3.82	0.40	0.62	0.68
4.03	0.36	0.68	0.62	4.03	0.31	0.47	0.41
4.29	0.30	0.84	0.84	4.29	0.24	0.55	0.52
4.72	0.13	0.57	0.55	4.72	0.11	0.33	0.20
4.85	0.19	0.38	0.39	4.85	0.11	0.25	0.08

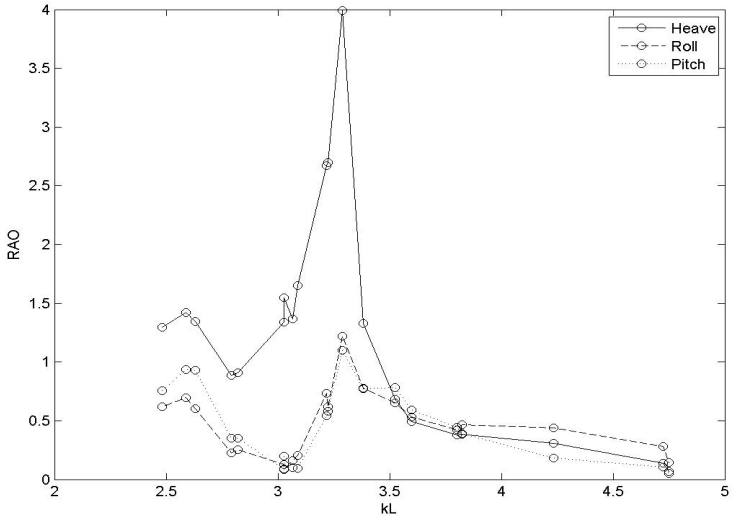

Figure 4.30: RAO for Body 2 for Wave Heading 30° and 450 mm Gap

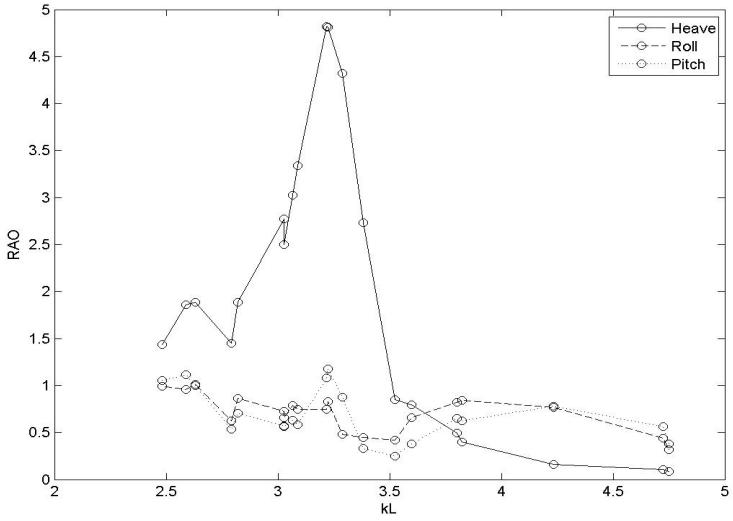

Figure 4.31: RAO for Body 1 for Wave Heading 30° and 450 mm Gap

Table 4.10: Body Motions for Wave Heading 30° and 450 mm Gap

Body 2				Body 1			
kL	RAO_3	RAO_4	RAO_5	kL	RAO_3	RAO_4	RAO_5
2.48	1.44	0.99	1.06	2.48	1.30	0.62	0.76
2.59	1.86	0.96	1.11	2.59	1.42	0.70	0.94
2.63	1.89	1.01	1.00	2.63	1.35	0.60	0.93
2.79	1.45	0.62	0.54	2.79	0.89	0.23	0.35
2.82	1.89	0.86	0.70	2.82	0.91	0.25	0.35
3.03	2.77	0.73	0.57	3.03	1.34	0.13	0.08
3.03	2.50	0.66	0.56	3.03	1.55	0.09	0.20
3.07	3.02	0.78	0.63	3.07	1.37	0.16	0.10
3.09	3.34	0.75	0.58	3.09	1.65	0.20	0.10
3.22	4.82	0.75	1.08	3.22	2.67	0.74	0.54
3.23	4.81	0.83	1.17	3.23	2.70	0.62	0.58
3.29	4.32	0.48	0.88	3.29	3.99	1.22	1.10
3.38	2.73	0.45	0.33	3.38	1.33	0.78	0.77
3.52	0.85	0.42	0.25	3.52	0.68	0.65	0.78
3.60	0.80	0.66	0.38	3.60	0.50	0.53	0.59
3.80	0.49	0.82	0.65	3.80	0.38	0.42	0.44
3.83	0.40	0.84	0.62	3.83	0.39	0.47	0.39
4.23	0.16	0.77	0.78	4.23	0.31	0.44	0.18
4.72	0.11	0.44	0.57	4.72	0.14	0.28	0.11
4.75	0.09	0.32	0.38	4.75	0.07	0.14	0.05

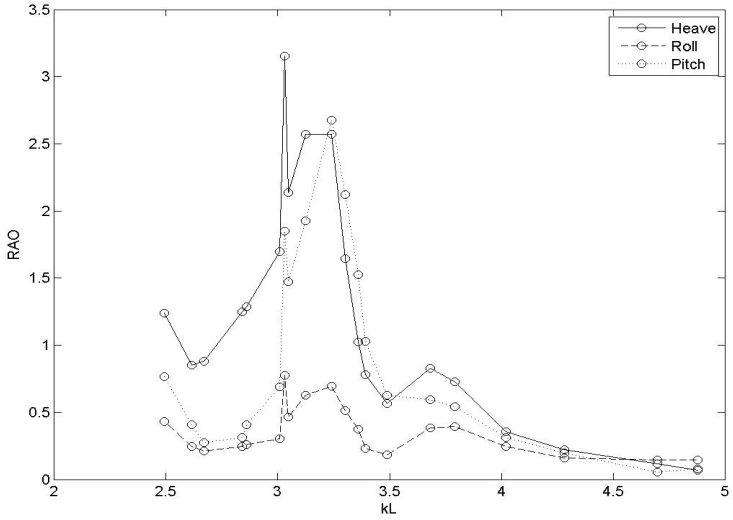

Figure 4.32: RAO for Body 2 for Wave Heading 0° and 300 mm Gap

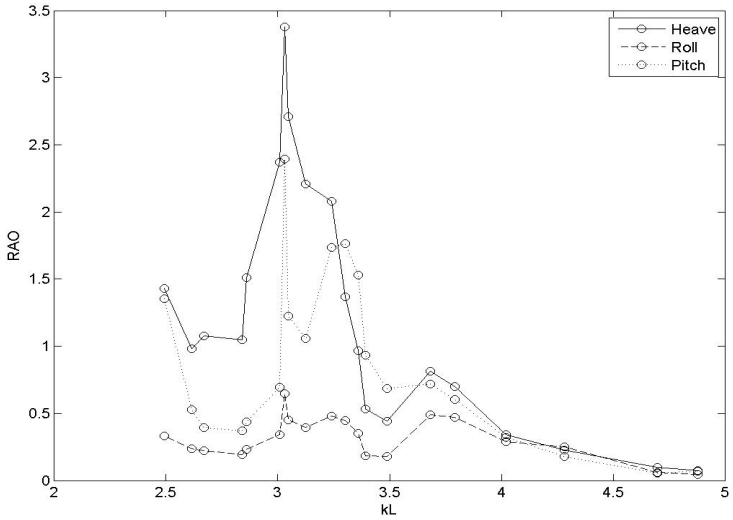

Figure 4.33: RAO for Body 1 for Wave Heading 0° and 300 mm Gap

Table 4.11: Body Motions for Wave Heading 0° and 300 mm Gap

Body 2				Body 1			
kL	RAO_3	RAO_4	RAO_5	kL	RAO_3	RAO_4	RAO_5
2.49	1.43	0.33	1.35	2.49	1.24	0.43	0.77
2.62	0.98	0.24	0.53	2.62	0.85	0.24	0.41
2.67	1.08	0.22	0.39	2.67	0.88	0.21	0.28
2.84	1.05	0.19	0.37	2.84	1.25	0.24	0.31
2.86	1.51	0.23	0.44	2.86	1.29	0.26	0.41
3.01	2.37	0.34	0.69	3.01	1.70	0.30	0.69
3.03	3.38	0.65	2.40	3.03	3.15	0.77	1.85
3.05	2.71	0.45	1.23	3.05	2.14	0.47	1.47
3.12	2.21	0.39	1.06	3.12	2.57	0.63	1.93
3.24	2.08	0.48	1.73	3.24	2.57	0.69	2.68
3.30	1.37	0.45	1.76	3.30	1.65	0.51	2.12
3.36	0.97	0.35	1.53	3.36	1.03	0.37	1.53
3.39	0.53	0.18	0.94	3.39	0.78	0.23	1.03
3.49	0.44	0.18	0.69	3.49	0.57	0.19	0.63
3.68	0.81	0.49	0.72	3.68	0.83	0.38	0.59
3.79	0.70	0.47	0.60	3.79	0.73	0.39	0.54
4.02	0.34	0.29	0.32	4.02	0.36	0.24	0.31
4.28	0.23	0.25	0.18	4.28	0.22	0.16	0.20
4.70	0.10	0.06	0.05	4.70	0.12	0.15	0.06
4.88	0.07	0.05	0.07	4.88	0.07	0.15	0.08

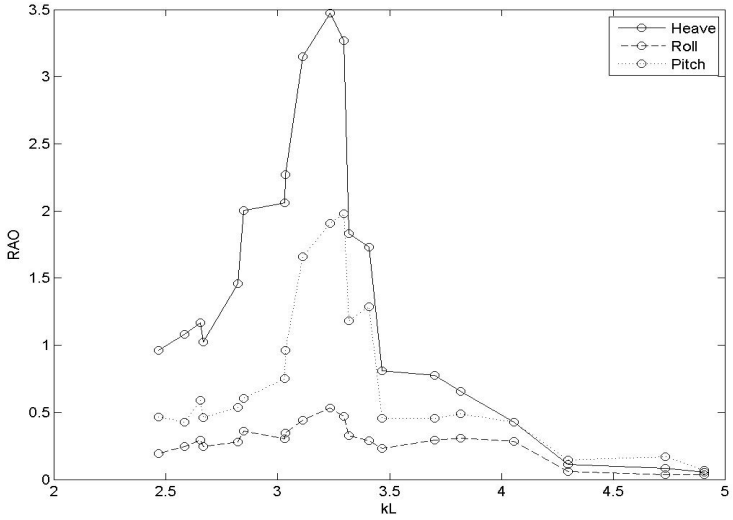

Figure 4.34: RAO for Body 2 for Wave Heading 0° and 450 mm Gap

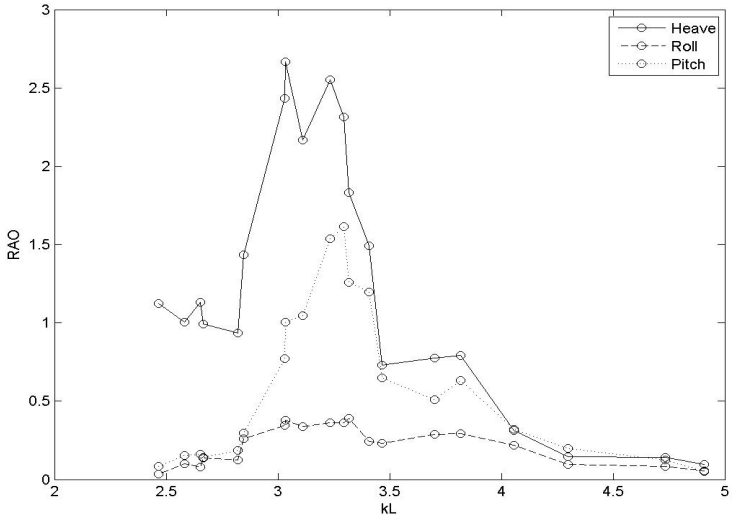

Figure 4.35: RAO for Body 1 for Wave Heading 0° and 450 mm Gap

Table 4.12: Body Motions for Wave Heading 0° and 450 mm Gap

Body 2				Body 1			
kL	RAO_3	RAO_4	RAO_5	kL	RAO_3	RAO_4	RAO_5
2.47	1.12	0.03	0.08	2.47	0.96	0.19	0.46
2.58	1.01	0.10	0.15	2.58	1.08	0.25	0.43
2.65	1.13	0.08	0.16	2.65	1.17	0.29	0.59
2.67	0.99	0.14	0.14	2.67	1.02	0.24	0.46
2.82	0.93	0.12	0.19	2.82	1.46	0.28	0.54
2.85	1.44	0.26	0.30	2.85	2.00	0.36	0.60
3.03	2.43	0.34	0.77	3.03	2.06	0.30	0.75
3.04	2.66	0.38	1.00	3.04	2.27	0.34	0.96
3.11	2.17	0.34	1.04	3.11	3.15	0.44	1.66
3.23	2.55	0.36	1.54	3.23	3.47	0.53	1.91
3.30	2.31	0.36	1.62	3.30	3.27	0.47	1.98
3.32	1.83	0.39	1.26	3.32	1.83	0.33	1.18
3.41	1.49	0.24	1.20	3.41	1.73	0.29	1.29
3.47	0.73	0.23	0.65	3.47	0.81	0.23	0.45
3.70	0.78	0.29	0.51	3.70	0.78	0.29	0.46
3.82	0.79	0.29	0.63	3.82	0.66	0.31	0.49
4.06	0.31	0.22	0.32	4.06	0.43	0.28	0.43
4.30	0.14	0.10	0.20	4.30	0.11	0.06	0.15
4.73	0.14	0.08	0.13	4.73	0.08	0.04	0.17
4.91	0.09	0.05	0.05	4.91	0.05	0.03	0.07

The results from the experimental testing showed many characteristics of the

two body side by side seakeeping case. The results provided information about both the free surface and vessel dynamics. This information can be used to provide insight into determining appropriate assumptions for numerical models.

The effects of narrow gap resonance can be seen in all cases. The amplification of the wave height in the gap indicates resonant behavior and peak values for each case are determined to represent resonance. The peak values are determined by locating the highest point in a frequency band. It was seen in Figures 4.4 to 4.11 that the cases with 0° wave heading have one peak value that appears to be less than one for both gap widths. The cases with 90° wave heading appear to have two distinct peaks with similar magnitudes, where the oblique wave heading cases appear to have two peak values with one being of higher magnitude than the other.

Determining resonant frequencies and values of resonant wave heights are areas of high interest for two body seakeeping cases. Figures 4.36 and 4.37 show the frequencies of the peak values and the magnitude of the peak values for each case, respectively. The primary peak is selected as the largest peak and secondary peak is the lower peak, when applicable. It can be seen that there was little change in the frequency of the primary peak for each case. Head seas also showed both primary and secondary peaks that were of similar magnitude. The magnitude of the primary peak was similar for both gap widths for head and beam seas. However, the oblique seas cases showed the magnitude increasing with gap width for each wave heading. The resonant behavior for these semi-captive test of this study was quite different from that of the fixed body case and moonpool case reported in the literature.

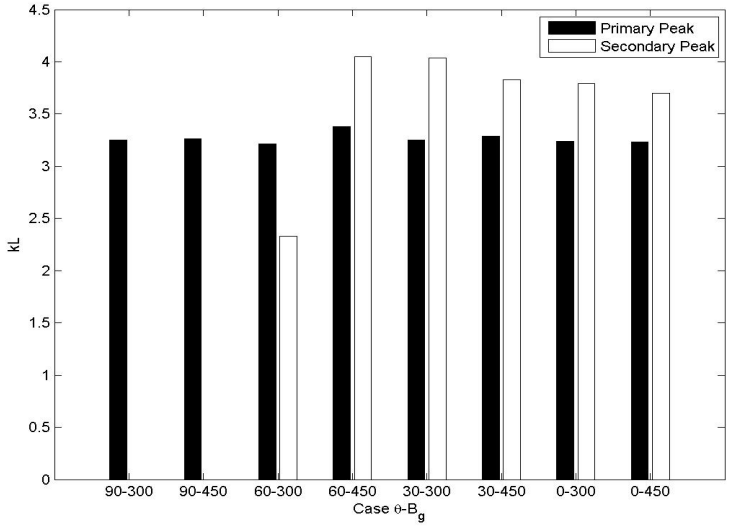

Figure 4.36: Peak Frequencies for Gap Resonance

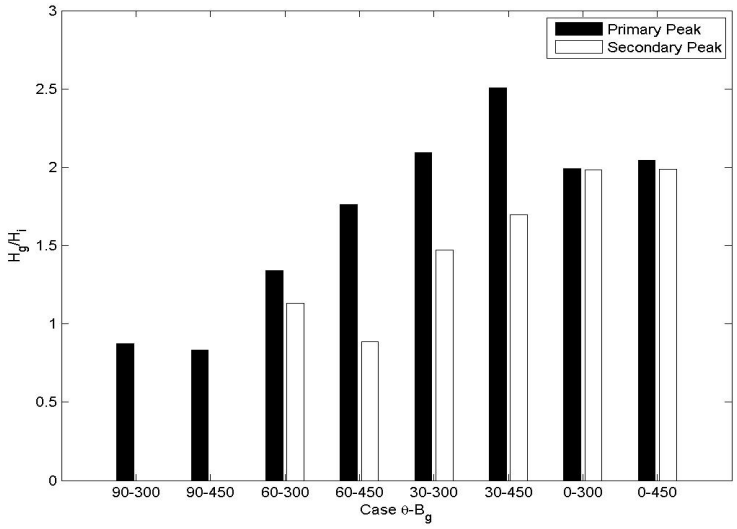

Figure 4.37: Peak Amplitudes for Gap Resonance

Another result seen in the experiment was the non-linearity of the free surface for all cases. Figures 4.12 to 4.19 show the significance of the second order wave

height compared to the first order wave height. It can be seen that the second order wave height ranges from approximately 2% to 90%. No trend can be determined for significance of second order wave height. However, the number of significant second order wave heights show the non linearity of the side by side seakeeping case.

The body motions can be seen in Figures 4.20 to 4.35 by way of the RAOs for heave, roll and pitch for both bodies. The experimental data shows a lot of motion amplification even away from peak values. There are a number of points away from peak values that show RAO values greater than 1. Beam seas cases showed that the body 1 had significantly more roll motion than body 2 which may be caused by sheltering effects. However, both bodies showed relatively similar heave motions and both showed very little pitch. Oblique sea cases showed motion response that was largely dominated by heave motion. Wave heading of 60° showed roll motion to be more significant than pitch, where as wave heading of 30° showed roll and pitch to be very similar over most frequencies. Head sea cases were dominated by heave motion and followed closely by pitch. Roll motion was less but still significant when considering the wave is traveling parallel with roll axis. The wave reflections from the diffracted wave in the gap region seem to cause significant roll motions.

Chapter 5

Conclusions

After reviewing available literature it was determined that there was a lack of experimental data available for two body seakeeping cases. It was determined that a two body seakeeping experiment should be conducted to further the amount of data available and improve the understanding of the side by side seakeeping problem. Two identical ship hulls were used while the gap width and wave heading were varied over the experimental runs. Data was collected about the free surface at five locations using wave probes and the vessel motions were recorded using Qualysis motion capture system.

The test consisted of 155 runs that varied wave heading from 0° to 90°, the gap width from 300 mm to 450 mm over wave frequencies ranging from 4.488 rad/s to 2π rad/s. The test was performed relatively well with a couple exceptions.There were a few incorrect frequencies produced by the wave board leading to frequencies that fell outside the desired frequency range. However, there was enough frequencies available to determine the trend of the data.

This experiment can offer insight into set up for a semi-captive model test experiment and the general behavior of changing geometric parameters in the side by

side seakeeping case. It was seen that the primary peak frequency for each case was relatively unchanged with $3.22 < kL < 3.38$. This result is quite different from the fixed body case and moonpool case. The beam seas cases showed one peak frequency while head seas cases showed two peak frequencies at similar magnitudes. The oblique seas cases showed two peak values with one peak of larger magnitude. While the frequency of the the primary peak values where relatively constant the magnitude of the peak values showed variation. The second order analysis of the gap showed significant nonlinearity of the free surface in the gap region. The motion analysis of the vessels showed significant amplification of the motions over a broad frequency band. Beam seas case showed very little pitch motion which was expected but head seas case showed significant roll motion. Some sheltering effects were seen where the forward model had greater motion responses than the downstream model. However, there were frequencies at which the heave motion for the downstream model exceeded the upstream model.

Validations of numerical models may be performed using this data. Numerical models may be developed to confirm the trend of this data. In order to increase the confidence of this data repetition is required to determine the statistical variation involved with experimental results. Conducting an experiment with repetition would allow for an uncertainty analysis to be performed thus increasing the confidence level.

This experiment showed resonant frequency does not vary significantly with spatial arrangement or orientation. Oblique and head seas cases show two peaks where as beam sea cases show one peak. There is significant non-linearity in the gap region of the free surface. The motion response of two semi-captive identical bodies show significant motion amplification over relatively broad frequency bands.

5.1 Recommendations and Future Work

It is recommended that frequency analysis of incoming waves be performed at the time of testing. This will allow the experimenter to determine if the desired wave frequency is actually being produced by the wave board. There was a couple of runs where the desired wave frequency was not produced and could not be checked until after due to software limitations. The same signal was sent to the wave board for a given frequency at each case but the wave board did not produce the desired frequency for some cases.

It is difficult to determine the level of confidence in the experimental results because of no repetition. Time constraints and tank availability did not allow for repetition of experimental runs. Completing repetitions of will allow the variance of the experiment to be quantified and increase the confidence in measured values. Repetitions can be done in the future to assess this or further investigation my be continued with lower confidence.

Future work from these experiments should be done numerically. Numerical models should be developed in both potential flow and CFD. The CFD model should be able to quantify the significance of fluid viscosity which is missing from the potential flow model. The potential flow model can be applied to two body seakeeping problem using artificial damping in the gap region (LID method). Data from this experiment and the CFD model can be used as a validation source for determining appropriate damping factors for for the damped potential flow model.

Bibliography

Bunnick, T., Pauw, W., & Voogt, A. (2009). Hydrodynamic analysis for side-by-side offloading. In *Proceedings of the 19th International Offshore and Polar Engineering Conference* (pp. 648–653).

Cerna, M. & Harvey, A. (2000). The fundamentals of fft-based signal analysis and measurement. *Application Note 041 National Instruments*.

Cheetham, P., Du, S., May, R., & Smith, S. (2007). Hydrodynamic analysis of ships side by side in waves. In *International Aerospace CFD Conference*.

Chen, X. (2005). Hydrodynamic analysis for offshore lng terminals. In *2nd International Workshop on Applied Offshore Hydrodynamics*.

Kawabe, H., Kwak, H. U., Park, J., & Ha, M. (2010). The numerical and experimental study on moonpool water surface response of a ship inwave condition. In *Proceedings of the 20th International Offshore and Polar Engineering Conference* (pp. 469–474).

Kodan, N. (1984). The motions of adjacent floating structures in oblique waves. *Journal of Energy Resources Technology*, 106, 199–205.

Lu, L. & Chen, X. (2012). Dissipation in the gap resonance between two bodies. In *27th International Workshop on Water Waves and Floating Bodies*.

Lu, L., Cheng, L., Teng, B., & Sun, L. (2010a). Comparison of potential flow and viscous fluid models in gap resonance. In *25th International Workshop on Water Waves and Floating Bodies*.

Lu, L., Cheng, L., Teng, B., & Sun, L. (2010b). Numerical simulation and comparison of potential flow and viscous fluid models in near trapping of narrow gaps. *Journal of Hydrodynamics*, 22, 120–125.

Lu, L., Teng, B., Cheng, L., Sun, L., & Chen, X. (2011). Modelling of multi-bodies in close proximity under water waves - fluid resonance in narrow gaps. *SCIENCE CHINA Physics, Mechanics & Astronomy*, 54, 16–25.

McTaggart, K., Cumming, D., Hsiung, C., & Li, L. (2003). Seakeeping of two ships in close proximity. *Ocean Engineering*, 30, 1051–1063.

Miao, G., Saitoh, T., & Ishida, H. (2001). Water wave interaction of twin large scale caissons with a small gap between. *Coastal Engineering Journal*, 43, 39–58.

Molin, B. (2001). On the piston and sloshing modes in moonpools. *Journal of Fluid Mechanics*, 430, 27–50.

Molin, B., Remy, F., Camhi, A., & Ledoux, A. (2009). Experimental and numerical study of the gap resonances in-between two rectangular barges. In *13th Congress of International Maritime Association of Mediterranean*.

Molin, B., Remy, F., Kimmoun, O., & Stassen, Y. (2002). Experimental study of the wave propagation and decay in a channel through a rigid ice sheet. *Applied Ocean Research*, 24, 247–260.

Pauw, W. H., H.M.Huijsmans, R., & Voogt, A. (2007). Advances in the hydrody-

namics of side-by-side moored vessels. In *Proceedings of the 26th International Conference on Offshore Mechanics and Arctic Engineering*.

Zhu, H., Zhu, R., & Miao, G. (2008). A time domain investigation on the hydrodynamic resonance phenomena of 3-d multiple floating structures. *Journal of Hydrodynamics*, 20, 611–616.

Appendix A

Wave Probe Time History

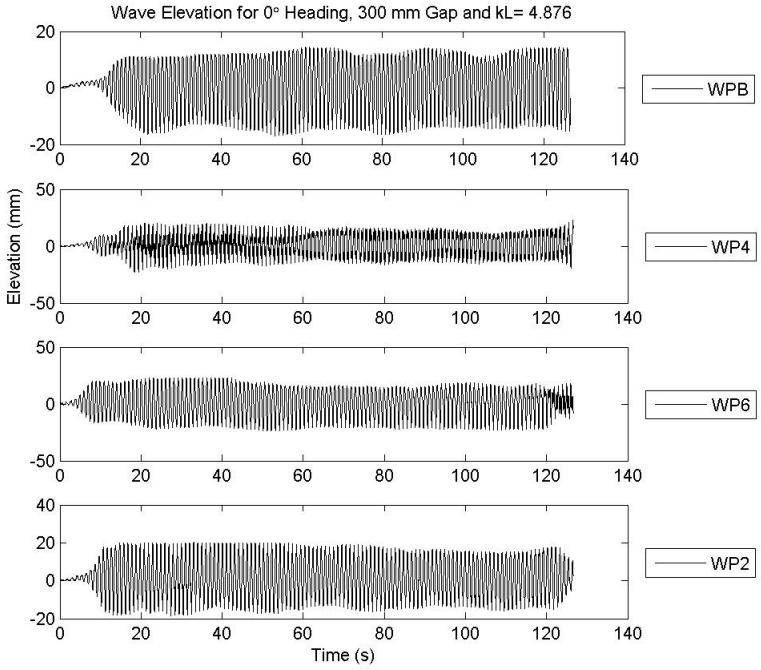

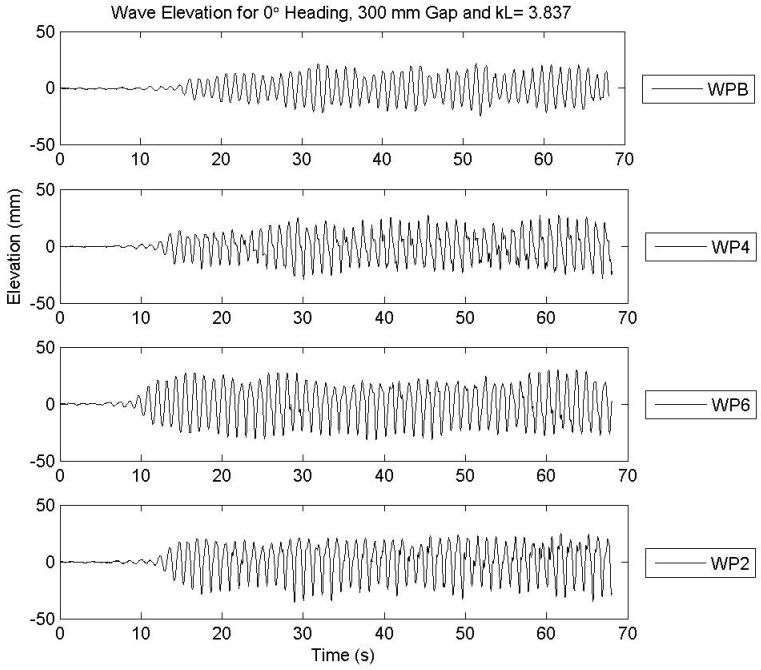
Wave Elevation for 0° Heading, 300 mm Gap and kL= 3.837
Elevation (mm)
Time (s)
WPB
WP4
WP6
WP2

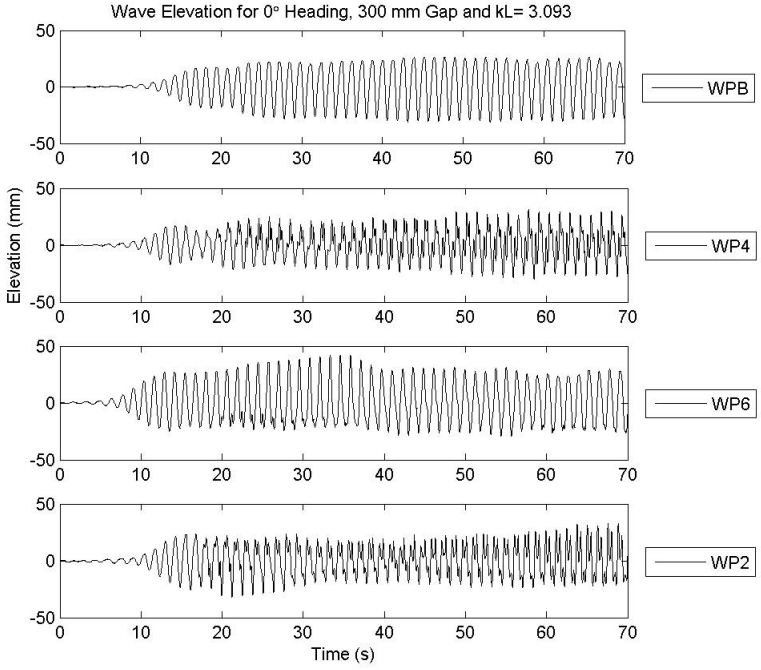
Wave Elevation for 0° Heading, 300 mm Gap and kL= 3.093
Elevation (mm)
Time (s)
WPB
WP4
WP6
WP2

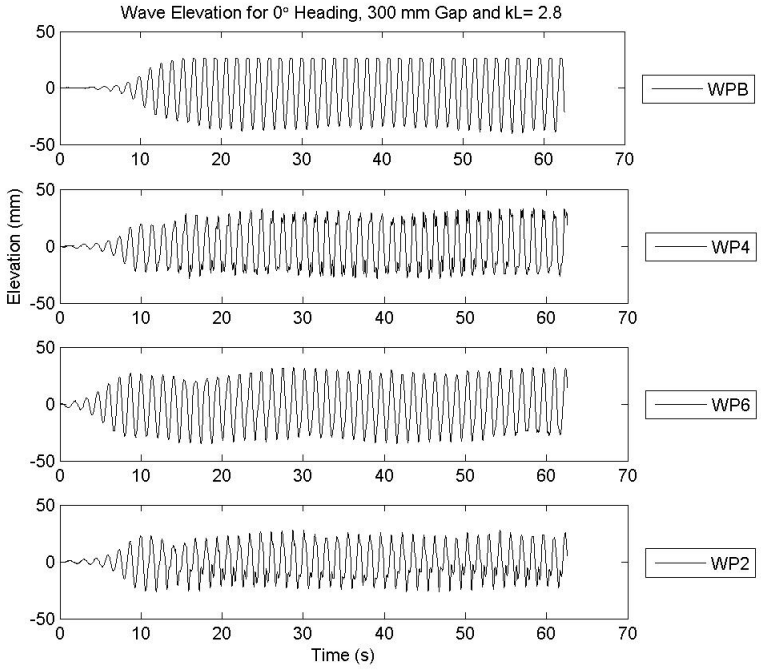
Wave Elevation for 0° Heading, 300 mm Gap and kL= 2.8
Elevation (mm)
Time (s)
WPB
WP4
WP6
WP2

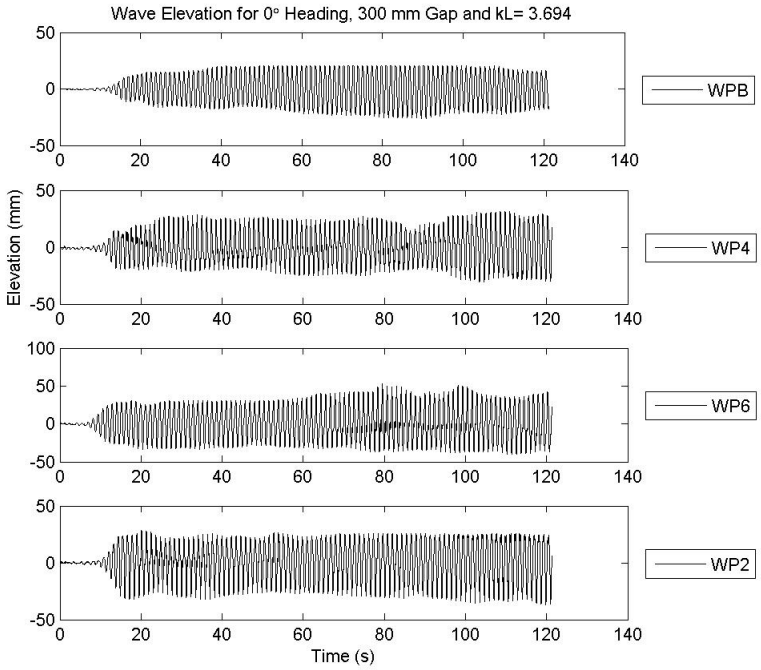
Wave Elevation for 0° Heading, 300 mm Gap and kL= 3.694
Elevation (mm)
Time (s)
WPB
WP4
WP6
WP2

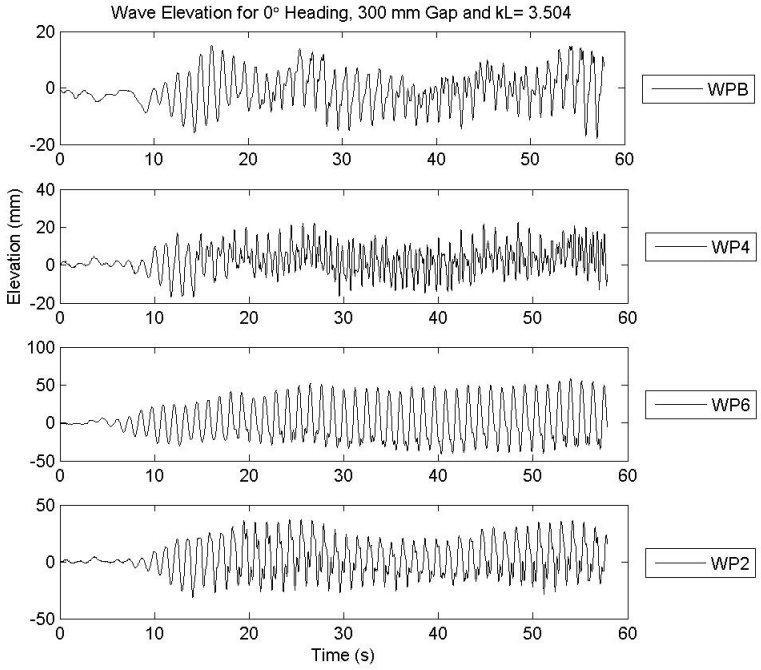
Wave Elevation for 0° Heading, 300 mm Gap and kL= 3.504
Elevation (mm)
Time (s)
WPB
WP4
WP6
WP2

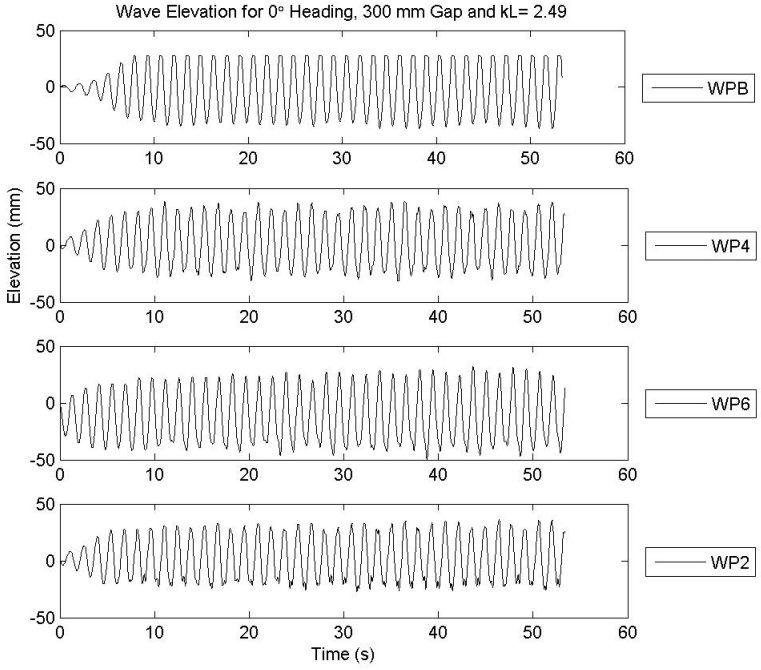
Wave Elevation for 0° Heading, 300 mm Gap and kL= 2.49
Elevation (mm)
Time (s)
WPB
WP4
WP6
WP2

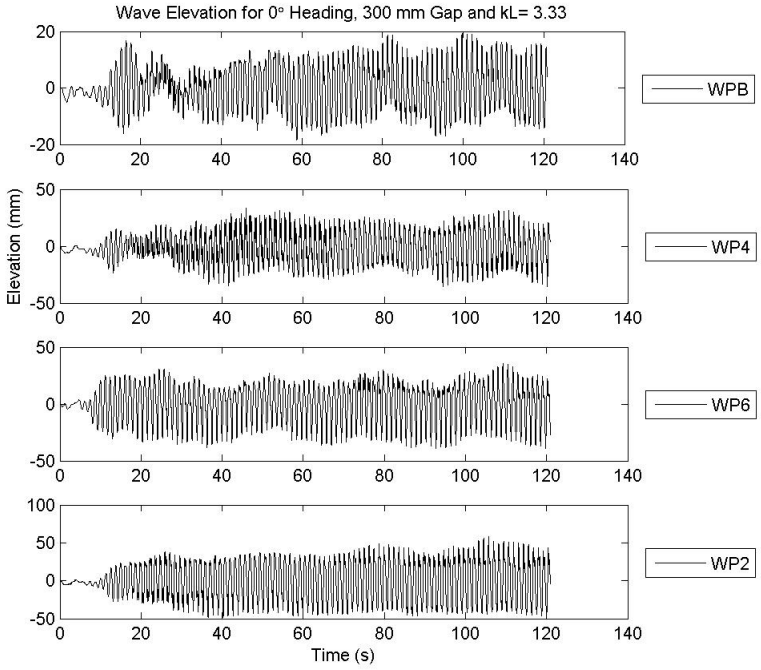
Wave Elevation for 0° Heading, 300 mm Gap and kL= 3.33
WPB
WP4
WP6
WP2
Elevation (mm)
Time (s)

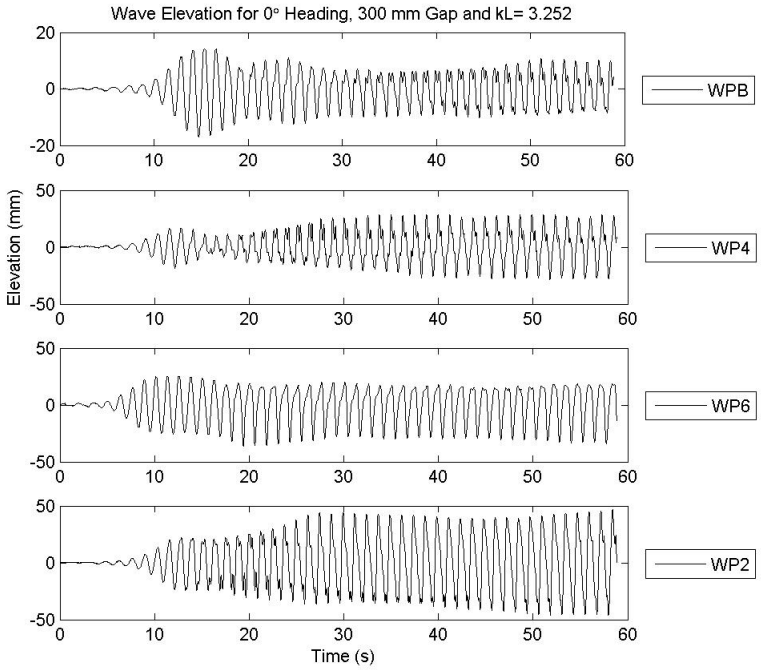
Wave Elevation for 0° Heading, 300 mm Gap and kL= 3.252
WPB
WP4
WP6
WP2
Elevation (mm)
Time (s)

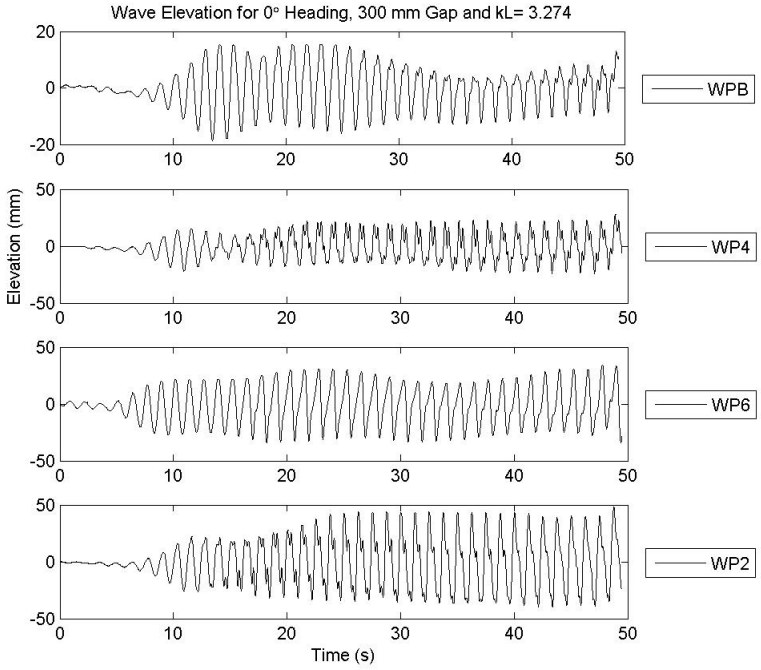
Wave Elevation for 0° Heading, 300 mm Gap and kL= 3.274
Elevation (mm)
Time (s)
WPB
WP4
WP6
WP2

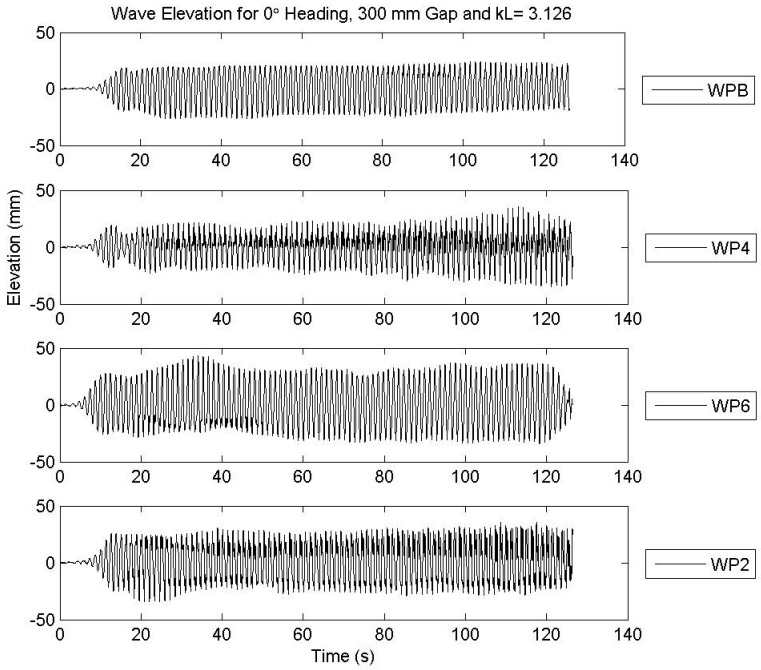
Wave Elevation for 0° Heading, 300 mm Gap and kL= 3.126
Elevation (mm)
Time (s)
WPB
WP4
WP6
WP2

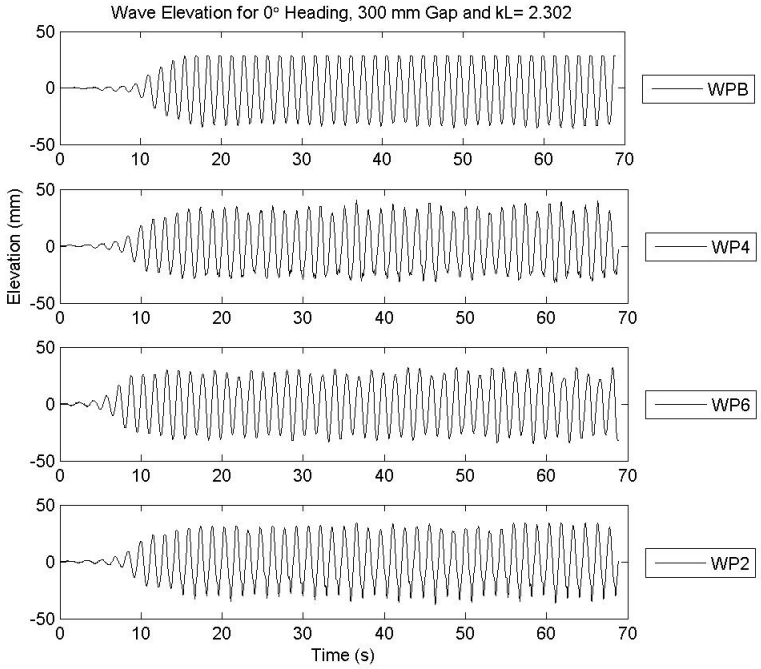
Wave Elevation for 0° Heading, 300 mm Gap and kL= 2.302
Elevation (mm)
Time (s)
WPB
WP4
WP6
WP2

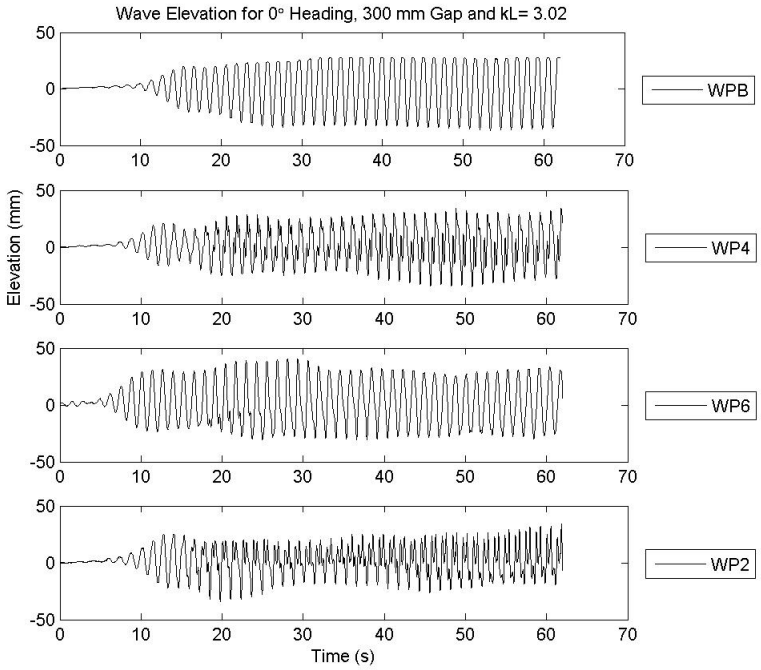
Wave Elevation for 0° Heading, 300 mm Gap and kL= 3.02
Elevation (mm)
Time (s)
WPB
WP4
WP6
WP2

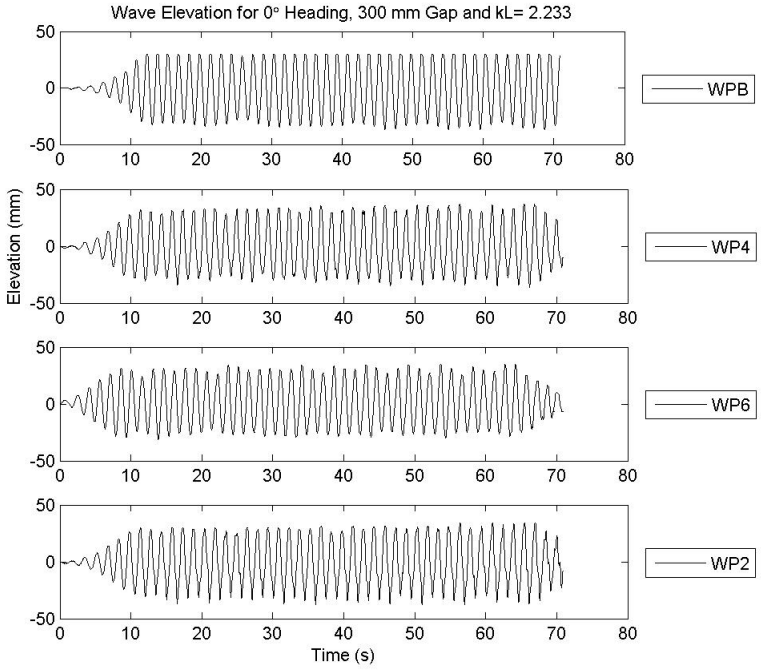
Wave Elevation for 0° Heading, 300 mm Gap and kL= 2.233
Elevation (mm)
Time (s)
WPB
WP4
WP6
WP2

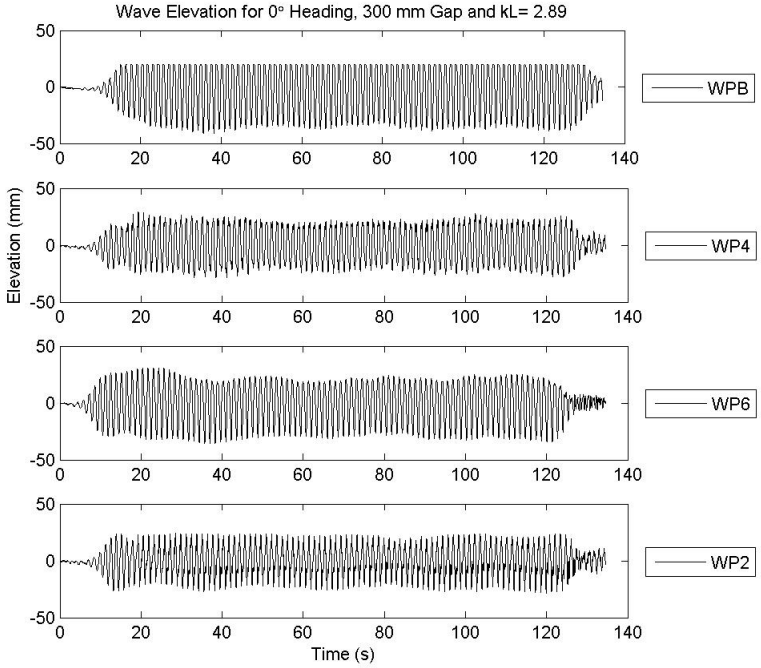
Wave Elevation for 0° Heading, 300 mm Gap and kL= 2.89
Elevation (mm)
Time (s)
WPB
WP4
WP6
WP2

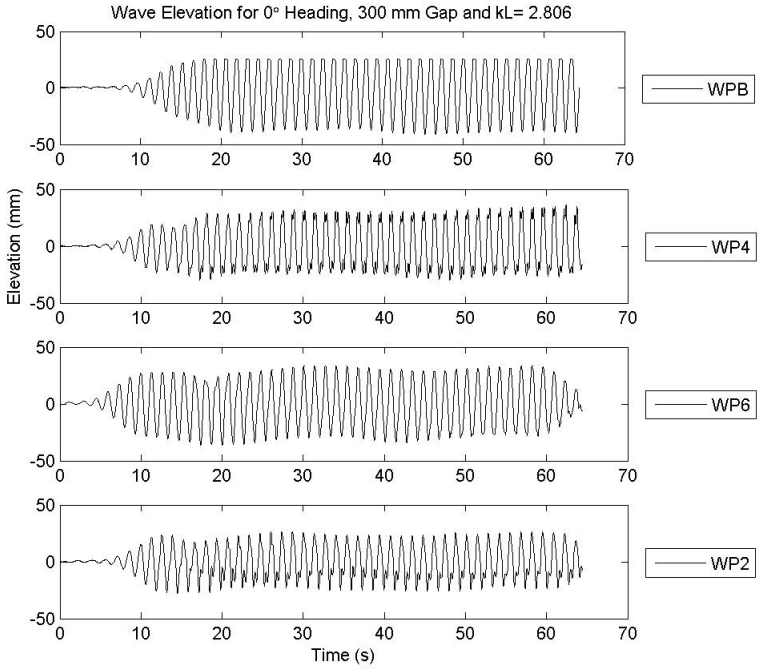
Wave Elevation for 0° Heading, 300 mm Gap and kL= 2.806
Elevation (mm)
Time (s)
WPB
WP4
WP6
WP2

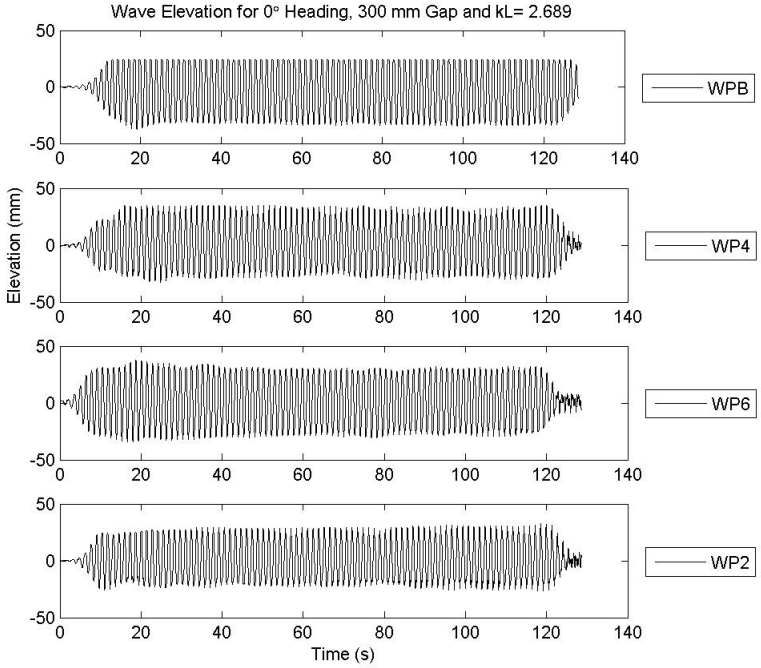
Wave Elevation for 0° Heading, 300 mm Gap and kL= 2.689
Elevation (mm)
Time (s)
WPB
WP4
WP6
WP2

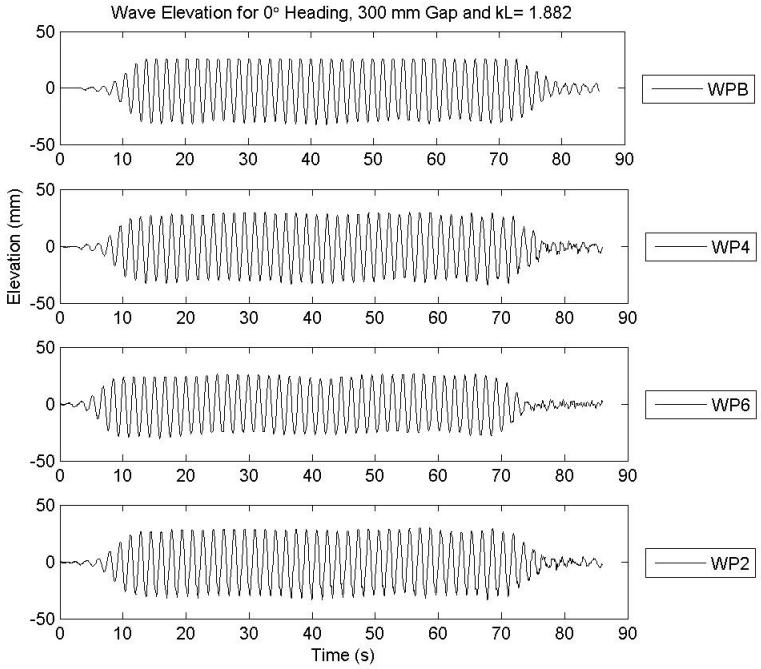
Wave Elevation for 0° Heading, 300 mm Gap and kL= 1.882
Elevation (mm)
Time (s)
WPB
WP4
WP6
WP2

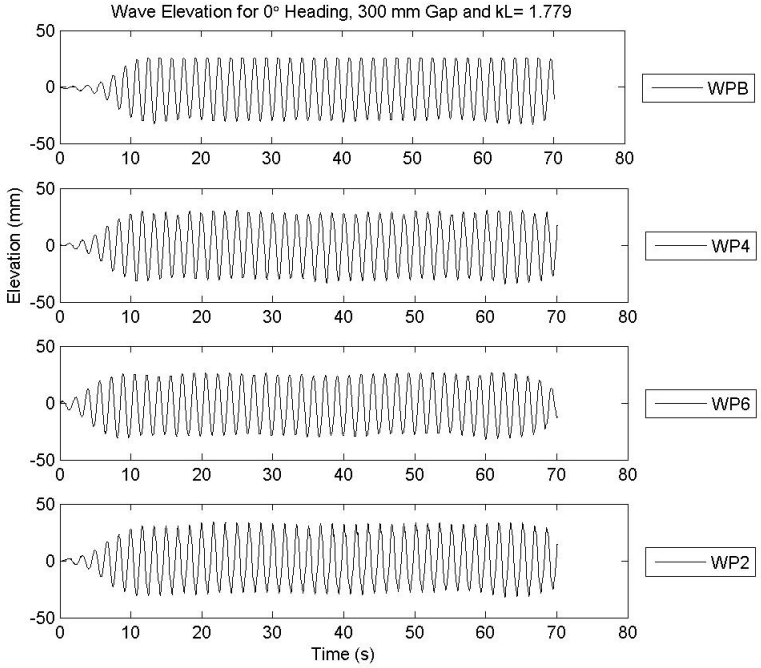
Wave Elevation for 0° Heading, 300 mm Gap and kL= 1.779
Elevation (mm)
Time (s)
WPB
WP4
WP6
WP2

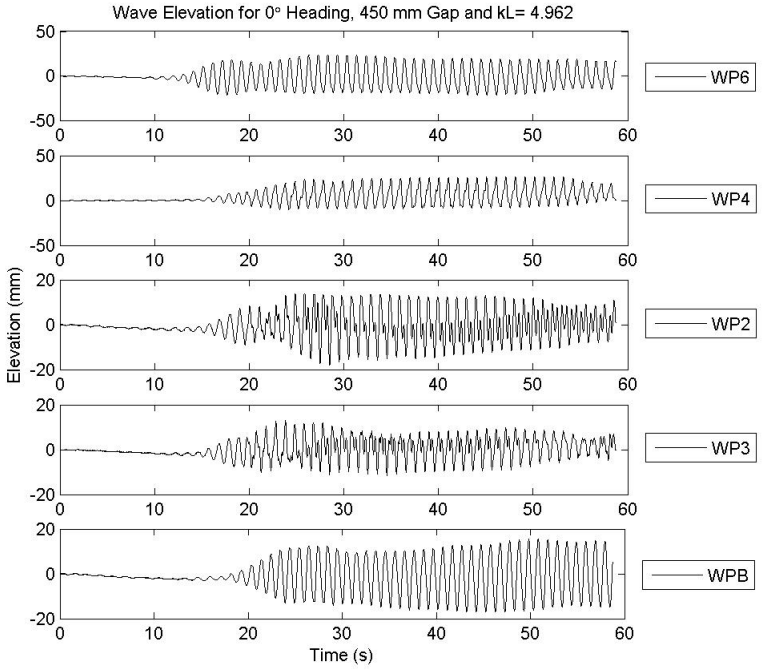
Wave Elevation for 0° Heading, 450 mm Gap and kL= 4.962
WP6
WP4
WP2
WP3
WPB
Elevation (mm)
Time (s)

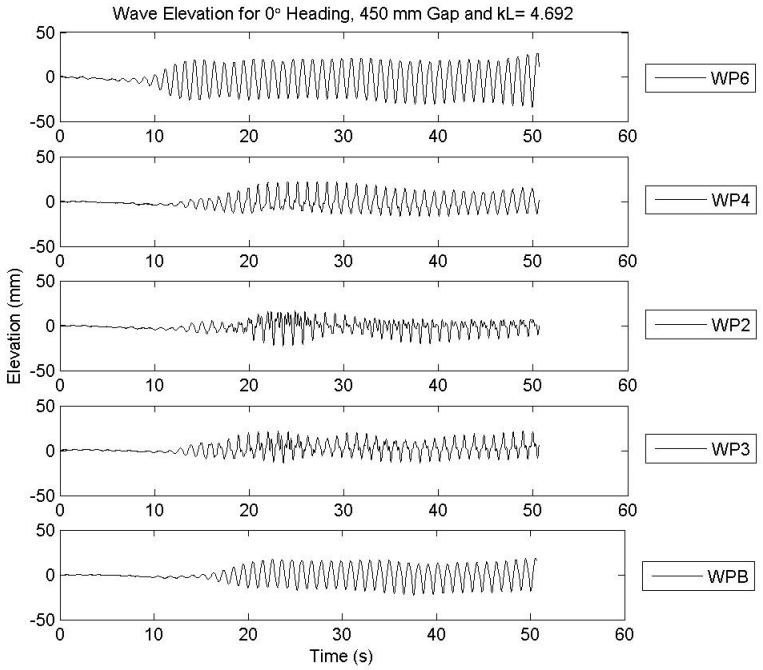
Wave Elevation for 0° Heading, 450 mm Gap and kL= 4.692
WP6
WP4
WP2
WP3
WPB
Elevation (mm)
Time (s)

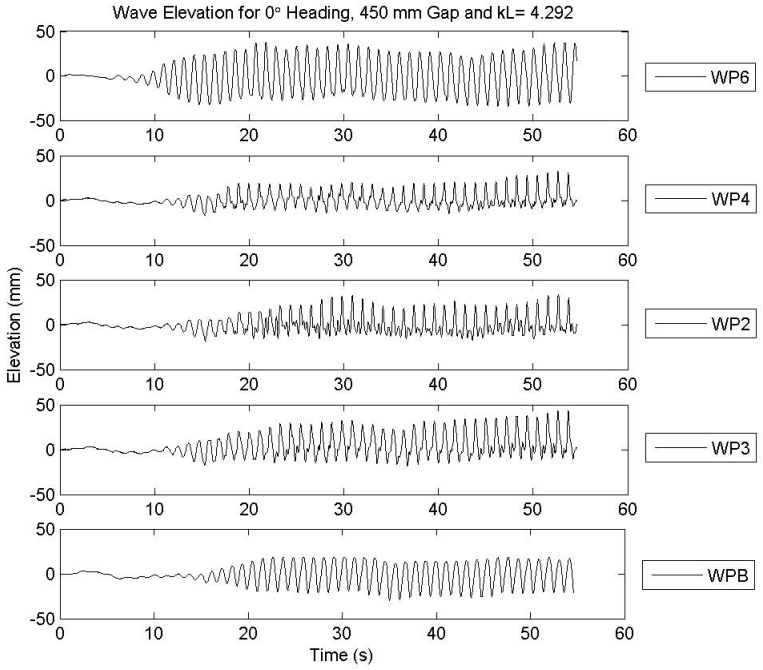
Wave Elevation for 0° Heading, 450 mm Gap and kL= 4.292
WP6
WP4
WP2
WP3
WPB
Elevation (mm)
Time (s)

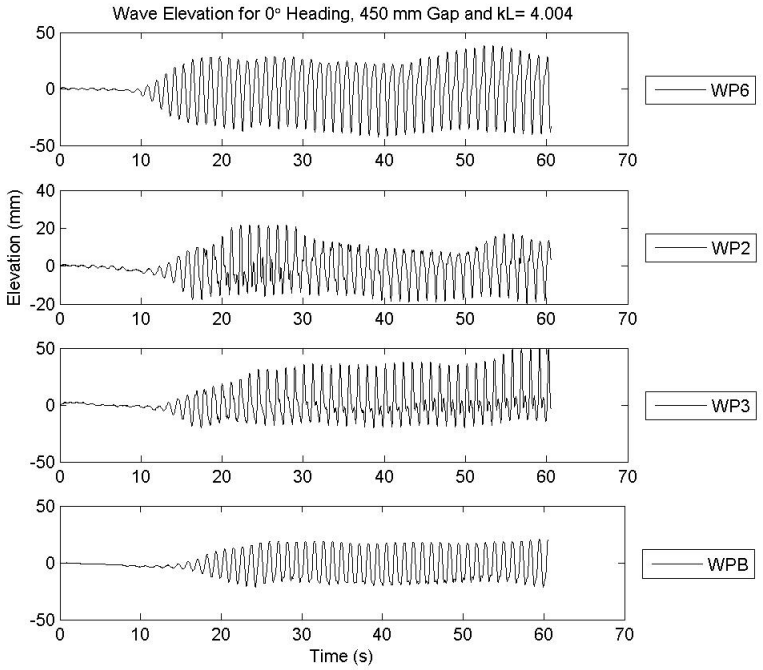
Wave Elevation for 0° Heading, 450 mm Gap and kL= 4.004
WP6
WP2
WP3
WPB
Elevation (mm)
Time (s)

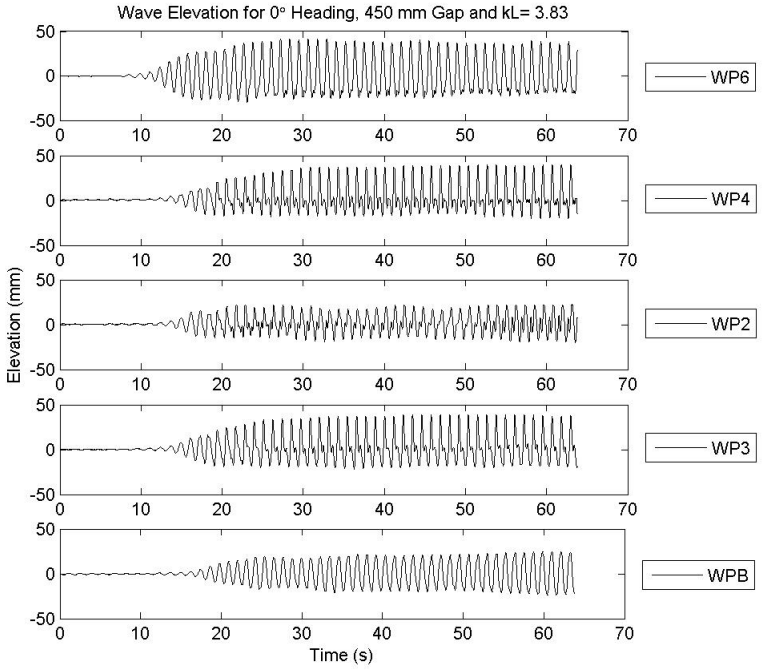
Wave Elevation for 0° Heading, 450 mm Gap and kL= 3.83
WP6
WP4
WP2
WP3
WPB
Elevation (mm)
Time (s)

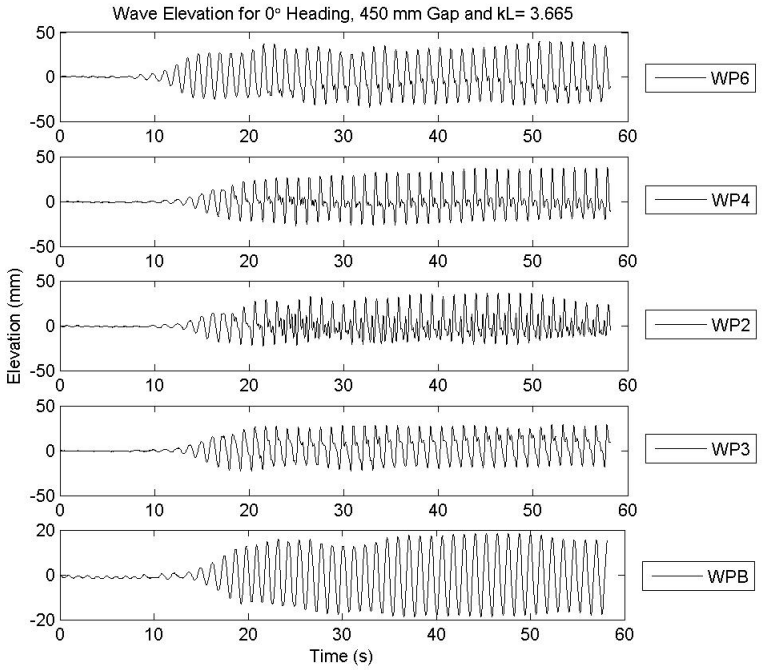
Wave Elevation for 0° Heading, 450 mm Gap and kL= 3.665
WP6
WP4
WP2
WP3
WPB
Elevation (mm)
Time (s)

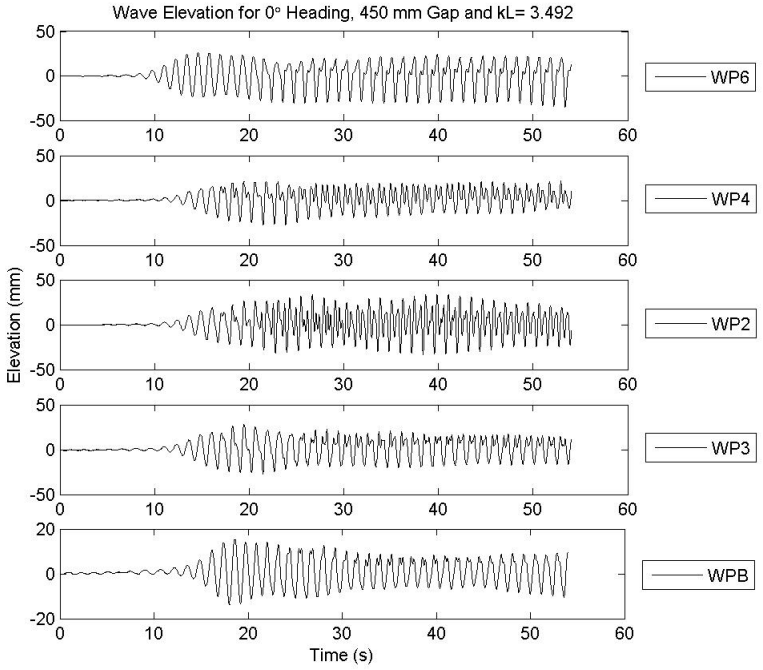
Wave Elevation for 0° Heading, 450 mm Gap and kL= 3.492
WP6
WP4
WP2
WP3
WPB
Elevation (mm)
Time (s)

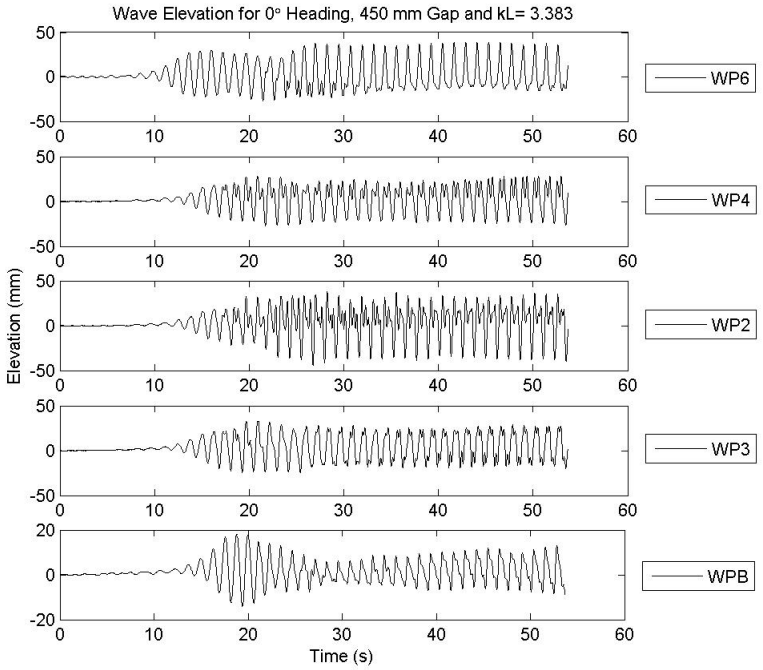
Wave Elevation for 0° Heading, 450 mm Gap and kL= 3.383
WP6
WP4
WP2
WP3
WPB
Elevation (mm)
Time (s)

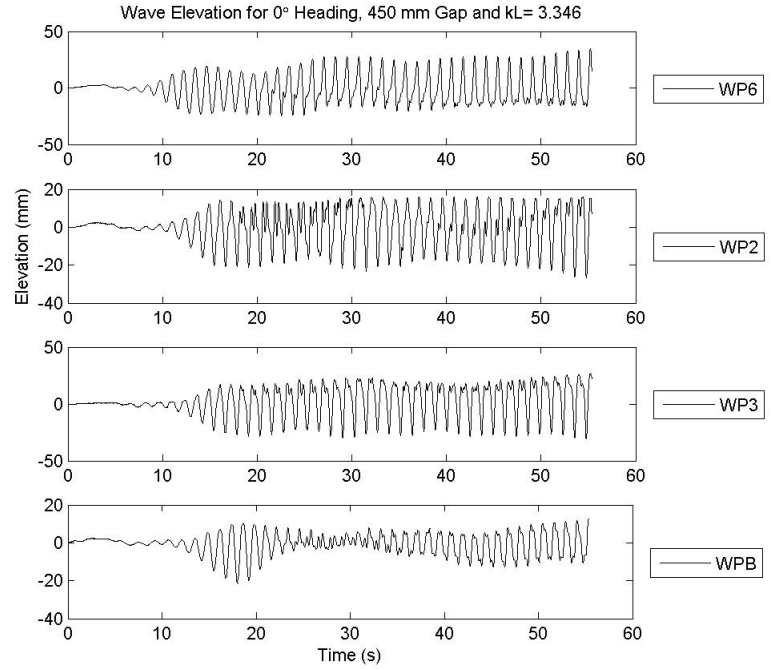
Wave Elevation for 0° Heading, 450 mm Gap and kL= 3.346
Elevation (mm)
Time (s)
WP6
WP2
WP3
WPB

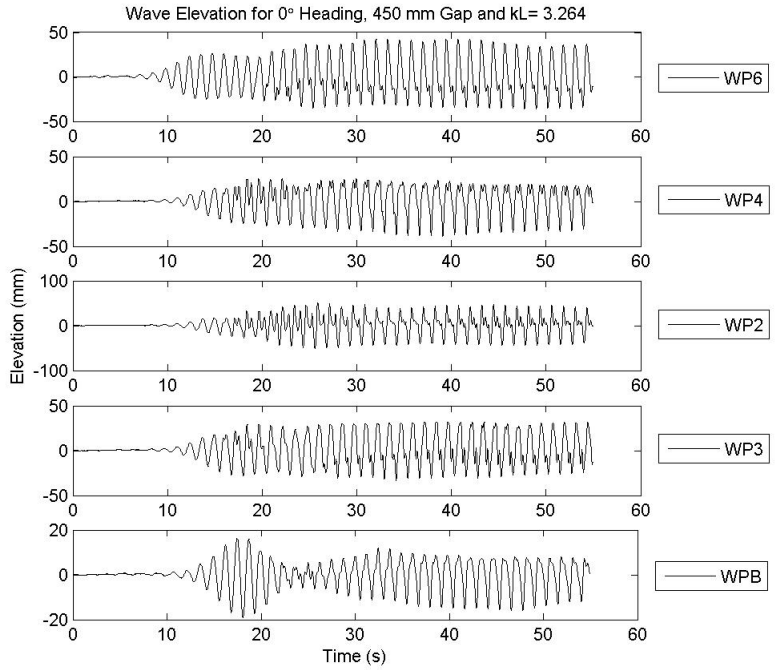
Wave Elevation for 0° Heading, 450 mm Gap and kL= 3.264
Elevation (mm)
Time (s)
WP6
WP4
WP2
WP3
WPB

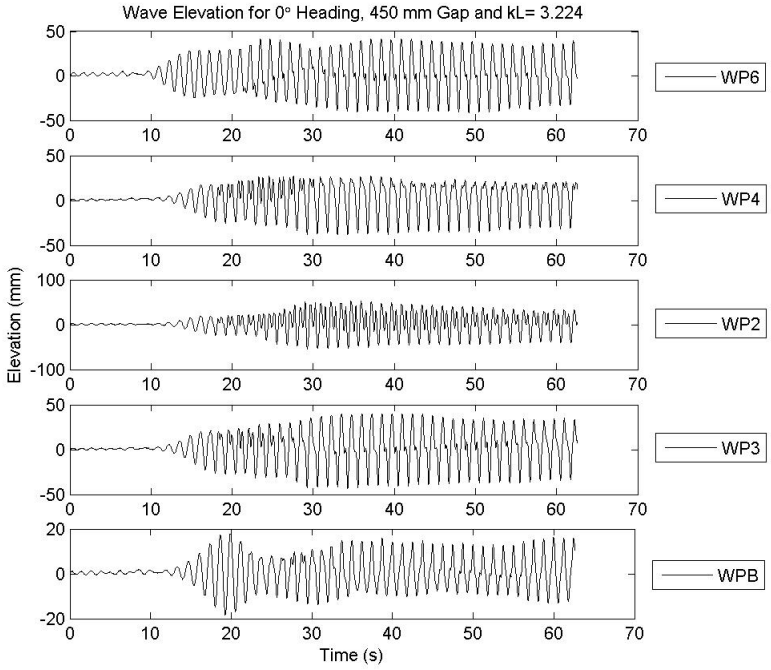
Wave Elevation for 0° Heading, 450 mm Gap and kL= 3.224
Elevation (mm)
Time (s)
WP6
WP4
WP2
WP3
WPB

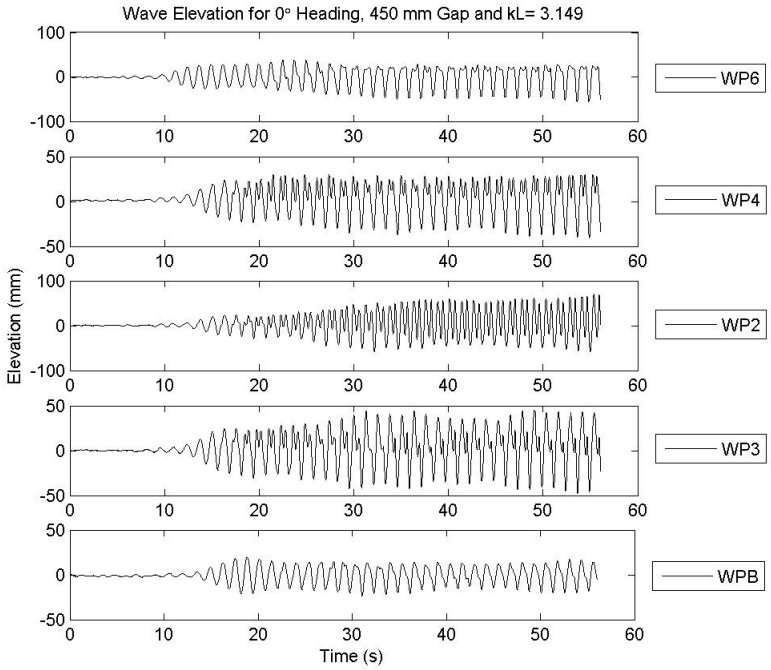
Wave Elevation for 0° Heading, 450 mm Gap and kL= 3.149
Elevation (mm)
Time (s)
WP6
WP4
WP2
WP3
WPB

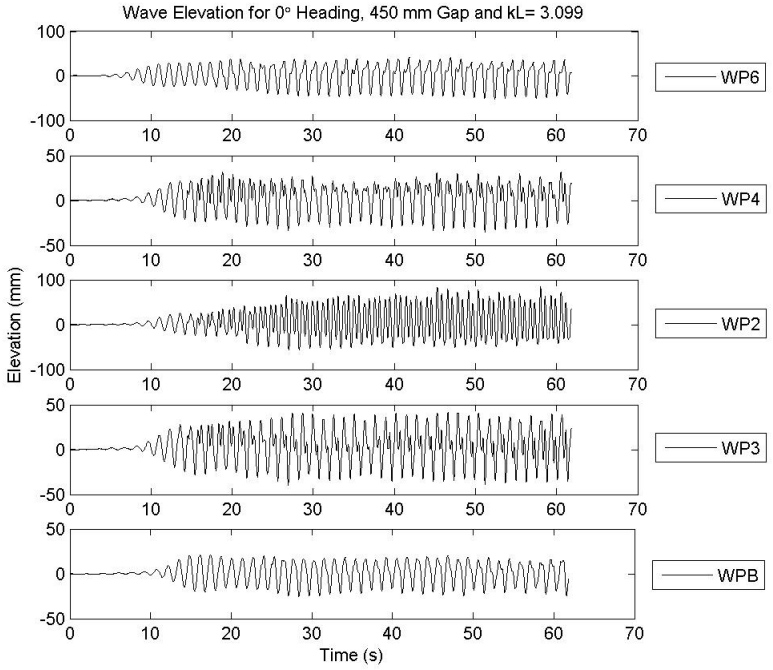
Wave Elevation for 0° Heading, 450 mm Gap and kL= 3.099
Elevation (mm)
Time (s)
WP6
WP4
WP2
WP3
WPB

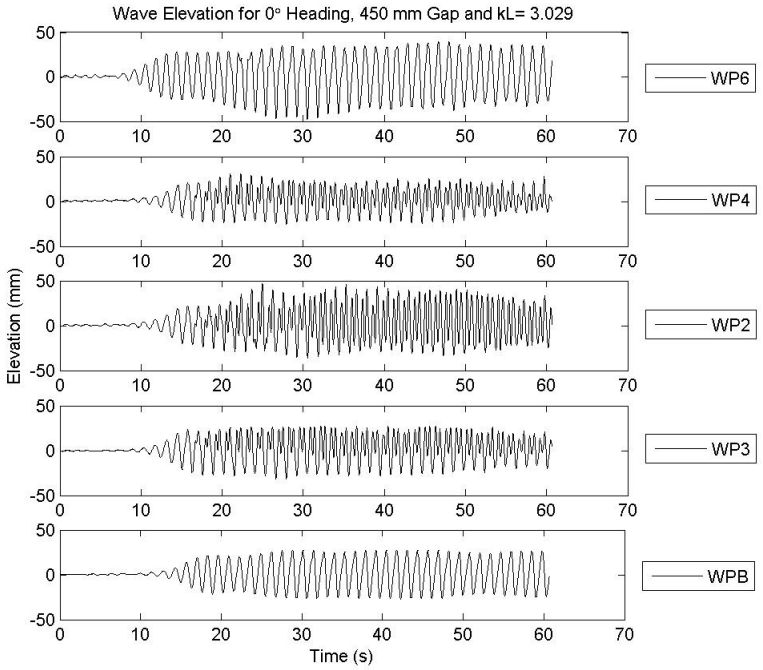
Wave Elevation for 0° Heading, 450 mm Gap and kL= 3.029
Elevation (mm)
Time (s)
WP6
WP4
WP2
WP3
WPB

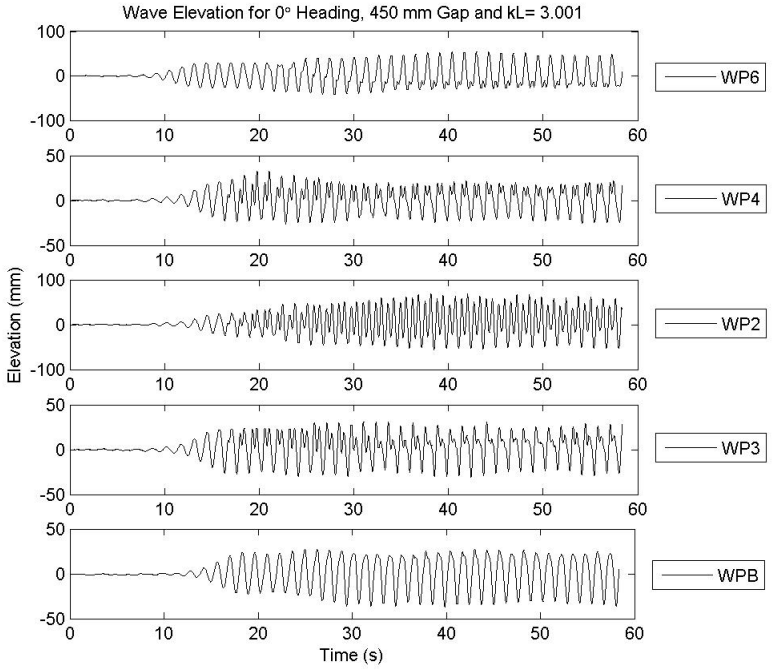
Wave Elevation for 0° Heading, 450 mm Gap and kL= 3.001
Elevation (mm)
Time (s)
WP6
WP4
WP2
WP3
WPB

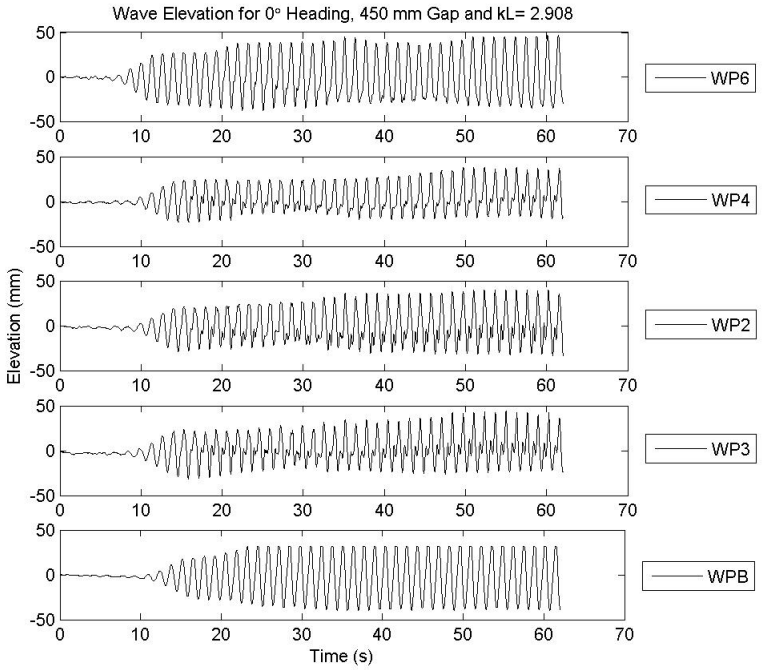
Wave Elevation for 0° Heading, 450 mm Gap and kL= 2.908
Elevation (mm)
Time (s)
WP6
WP4
WP2
WP3
WPB

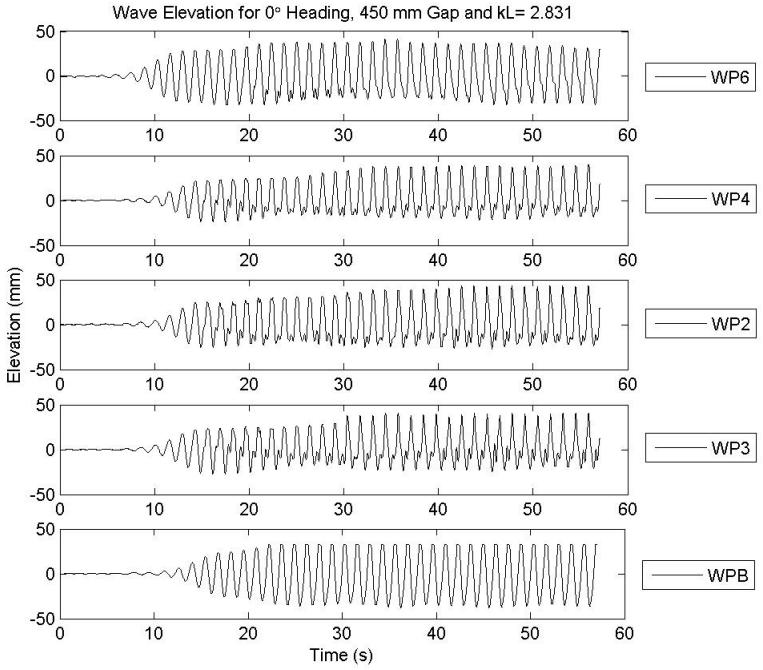
Wave Elevation for 0° Heading, 450 mm Gap and kL= 2.831
Elevation (mm)
Time (s)
WP6
WP4
WP2
WP3
WPB

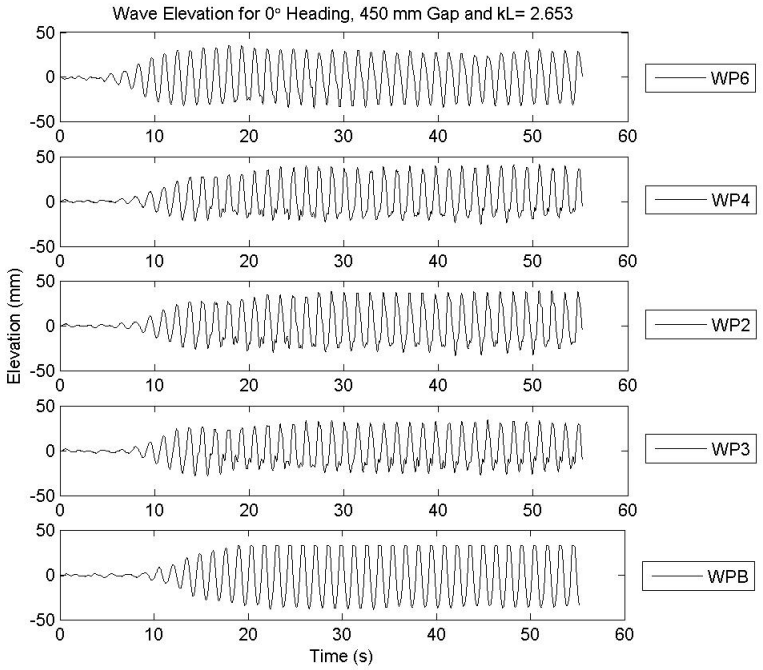
Wave Elevation for 0° Heading, 450 mm Gap and kL= 2.653
Elevation (mm)
Time (s)
WP6
WP4
WP2
WP3
WPB

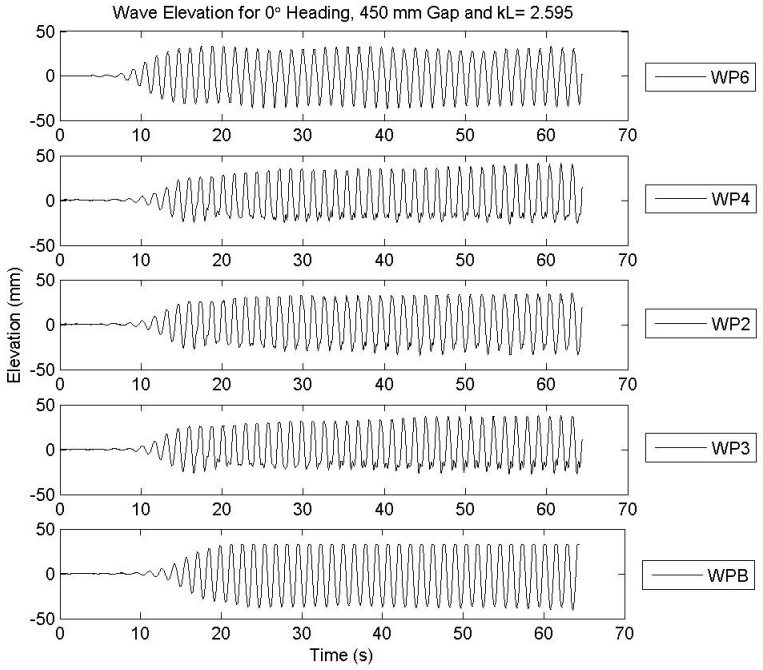
Wave Elevation for 0° Heading, 450 mm Gap and kL= 2.595
Elevation (mm)
Time (s)
WP6
WP4
WP2
WP3
WPB

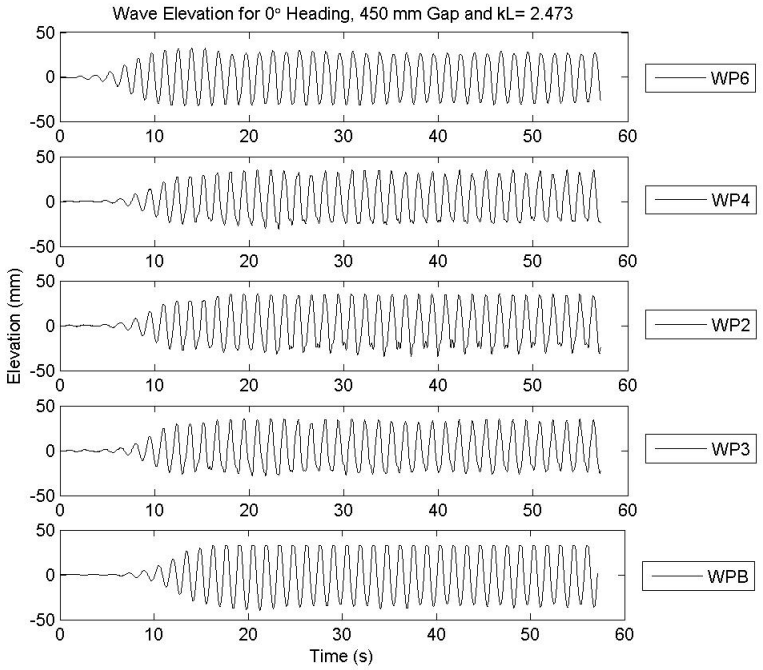
Wave Elevation for 0° Heading, 450 mm Gap and kL= 2.473
Elevation (mm)
Time (s)
WP6
WP4
WP2
WP3
WPB

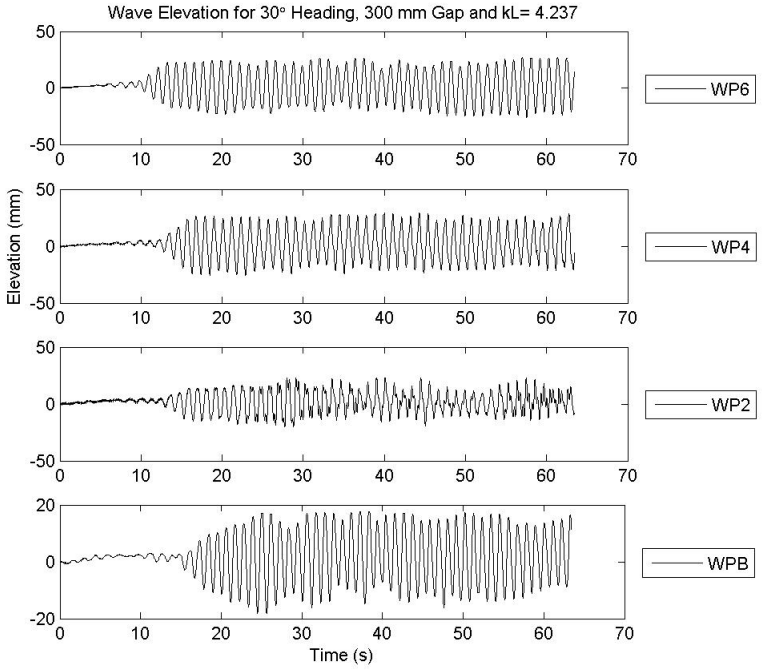
Wave Elevation for 30° Heading, 300 mm Gap and kL= 4.237
Elevation (mm)
Time (s)
WP6
WP4
WP2
WPB

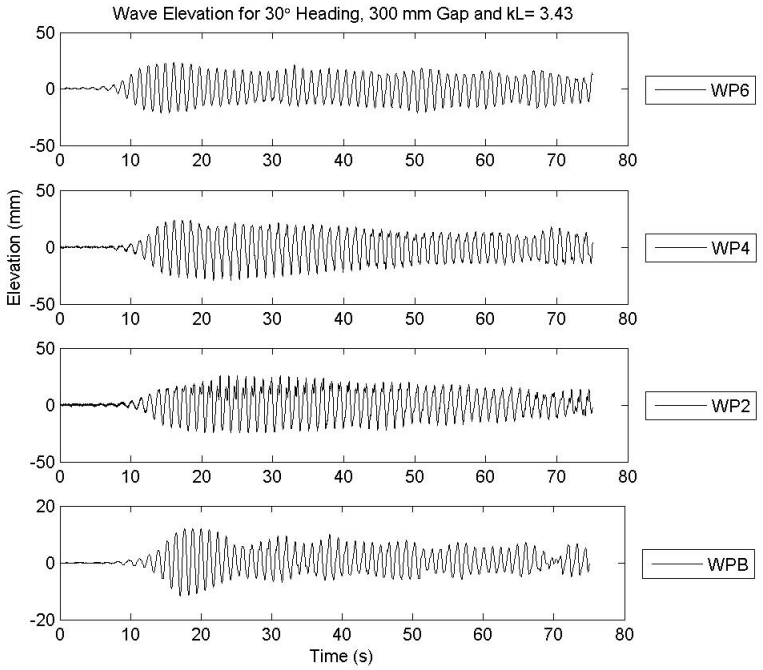
Wave Elevation for 30° Heading, 300 mm Gap and kL= 3.43
Elevation (mm)
Time (s)
WP6
WP4
WP2
WPB

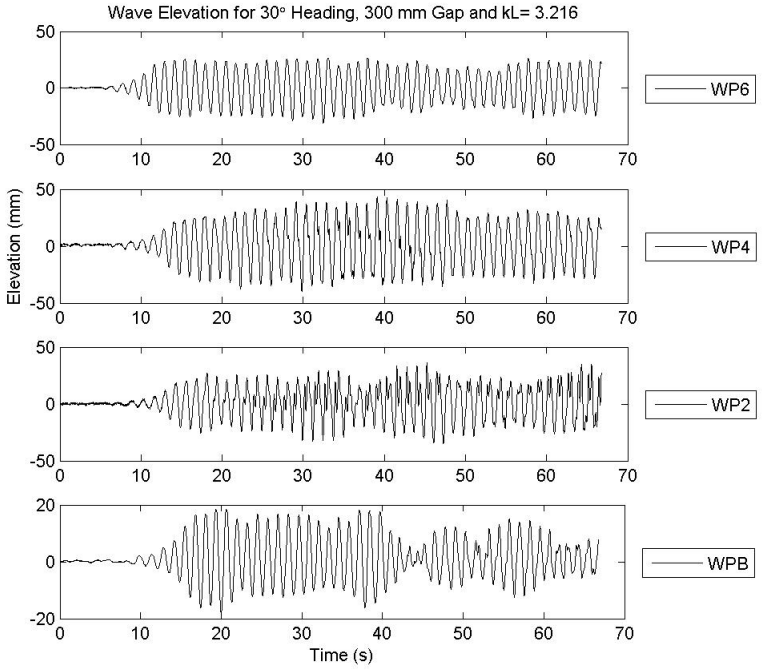
Wave Elevation for 30° Heading, 300 mm Gap and kL= 3.216
Elevation (mm)
Time (s)
WP6
WP4
WP2
WPB

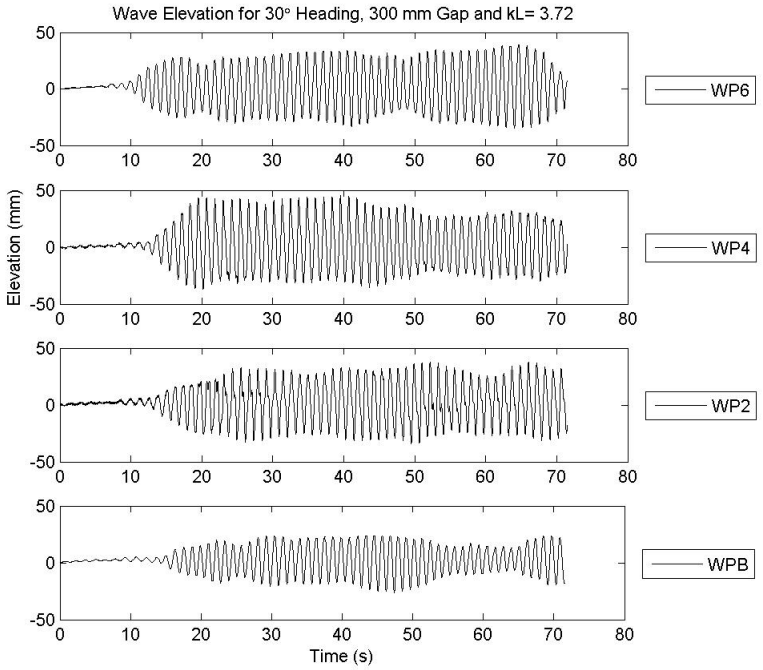
Wave Elevation for 30° Heading, 300 mm Gap and kL= 3.72
Elevation (mm)
Time (s)
WP6
WP4
WP2
WPB

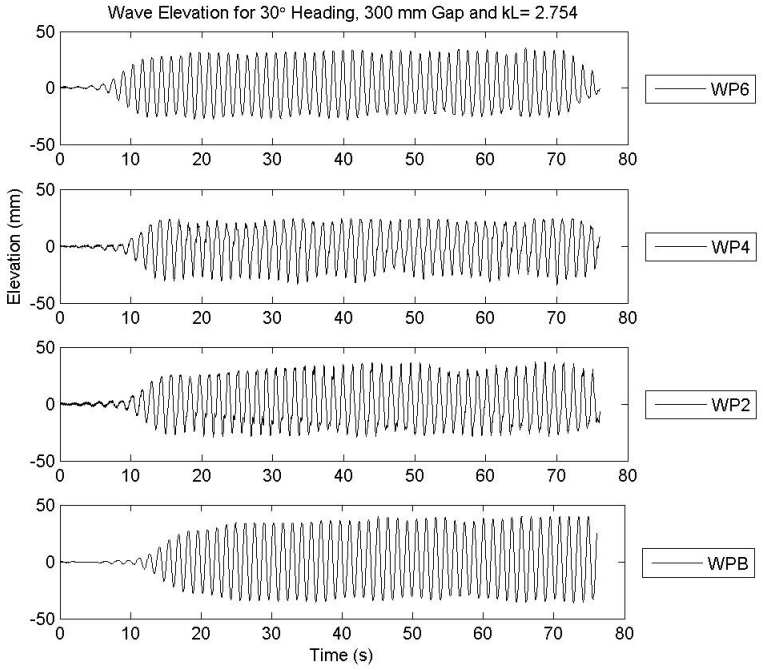
Wave Elevation for 30° Heading, 300 mm Gap and kL= 2.754
Elevation (mm)
Time (s)
WP6
WP4
WP2
WPB

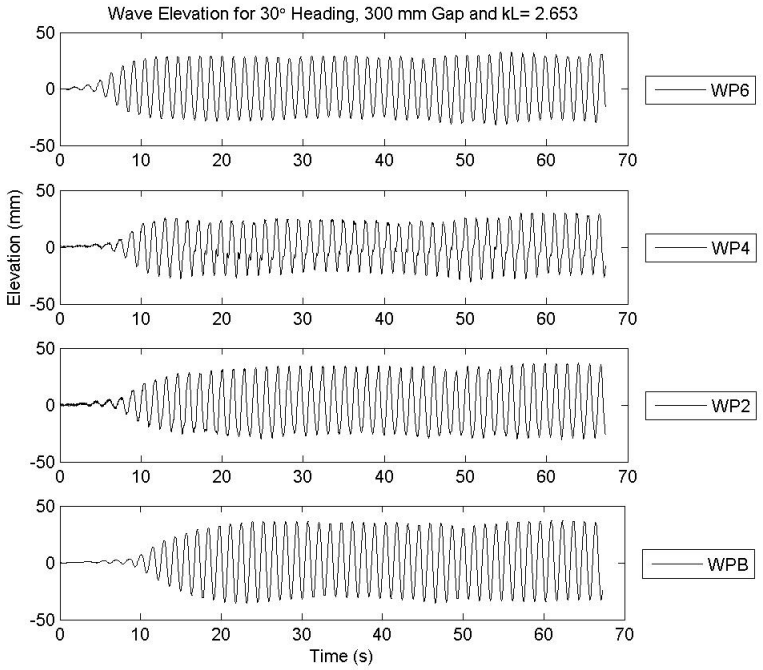
Wave Elevation for 30° Heading, 300 mm Gap and kL= 2.653
Elevation (mm)
Time (s)
WP6
WP4
WP2
WPB

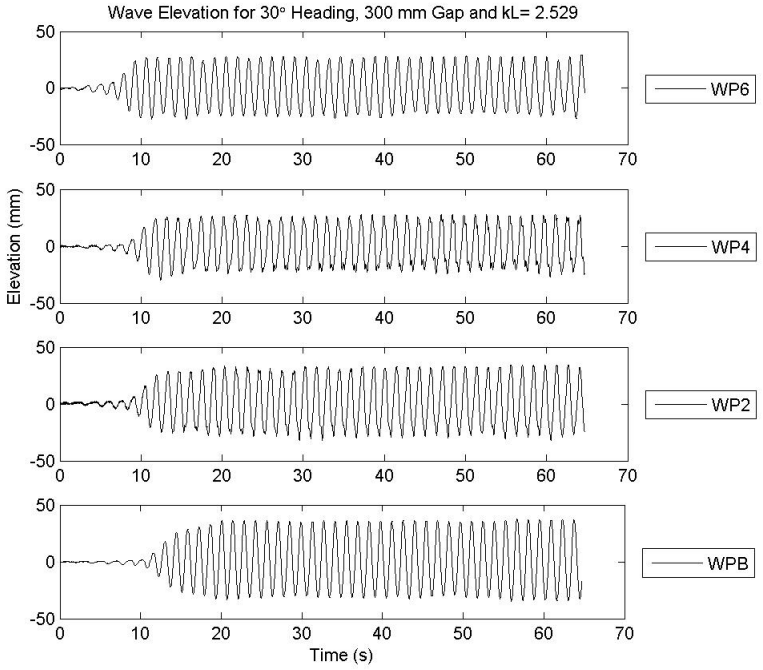
Wave Elevation for 30° Heading, 300 mm Gap and kL= 2.529
Elevation (mm)
Time (s)
WP6
WP4
WP2
WPB

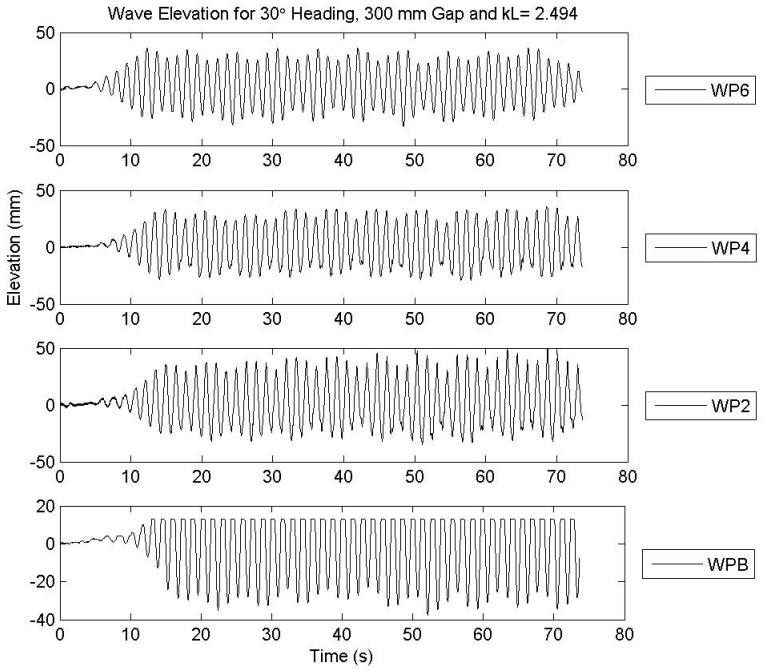
Wave Elevation for 30° Heading, 300 mm Gap and kL= 2.494
Elevation (mm)
Time (s)
WP6
WP4
WP2
WPB

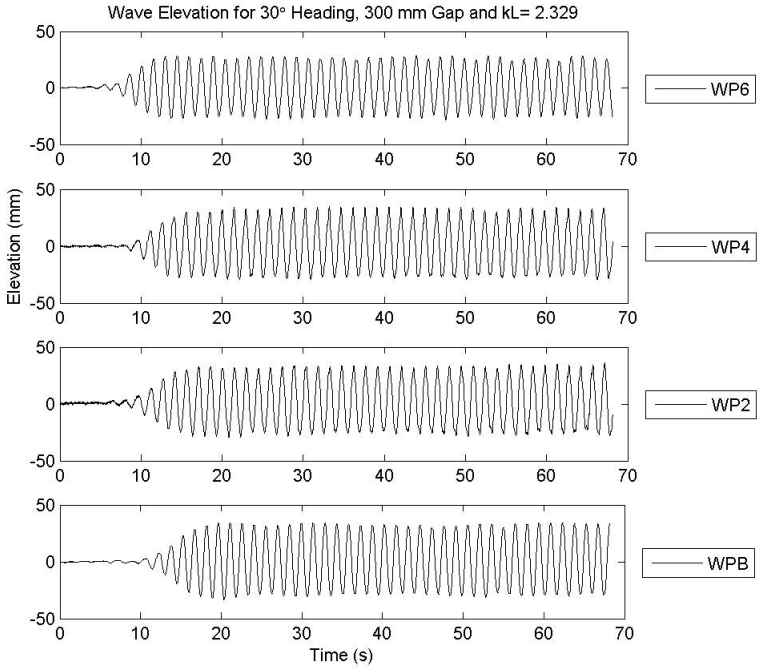
Wave Elevation for 30° Heading, 300 mm Gap and kL= 2.329
Elevation (mm)
Time (s)
WP6
WP4
WP2
WPB

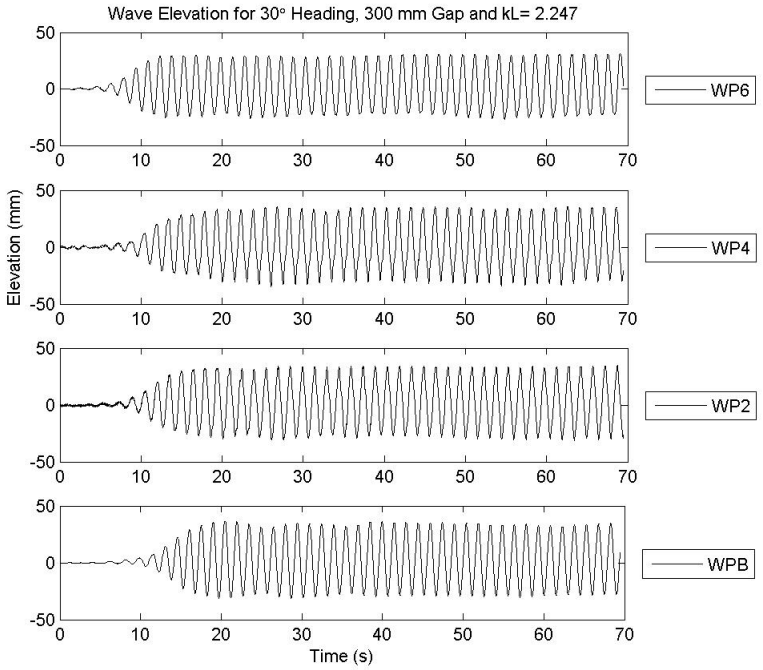
Wave Elevation for 30° Heading, 300 mm Gap and kL= 2.247
Elevation (mm)
Time (s)
WP6
WP4
WP2
WPB

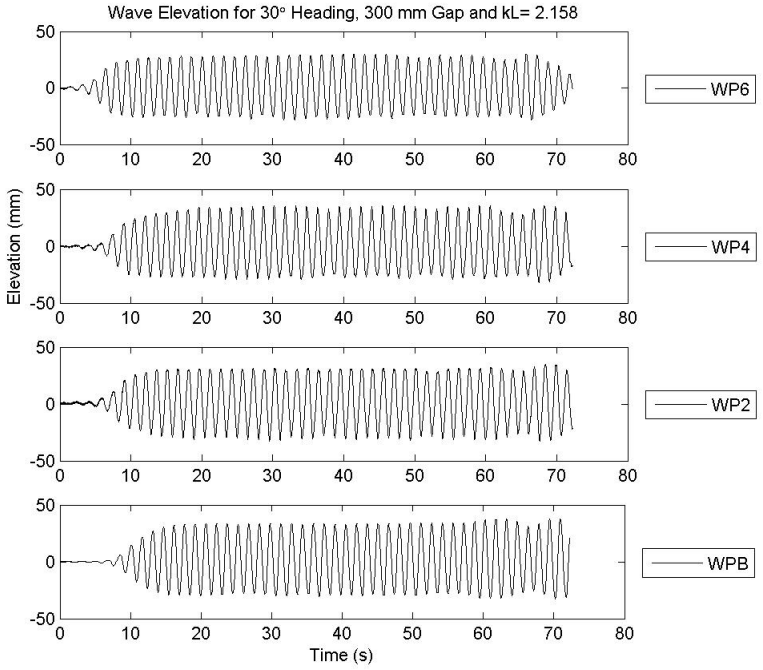
Wave Elevation for 30° Heading, 300 mm Gap and kL= 2.158
Elevation (mm)
Time (s)
WP6
WP4
WP2
WPB

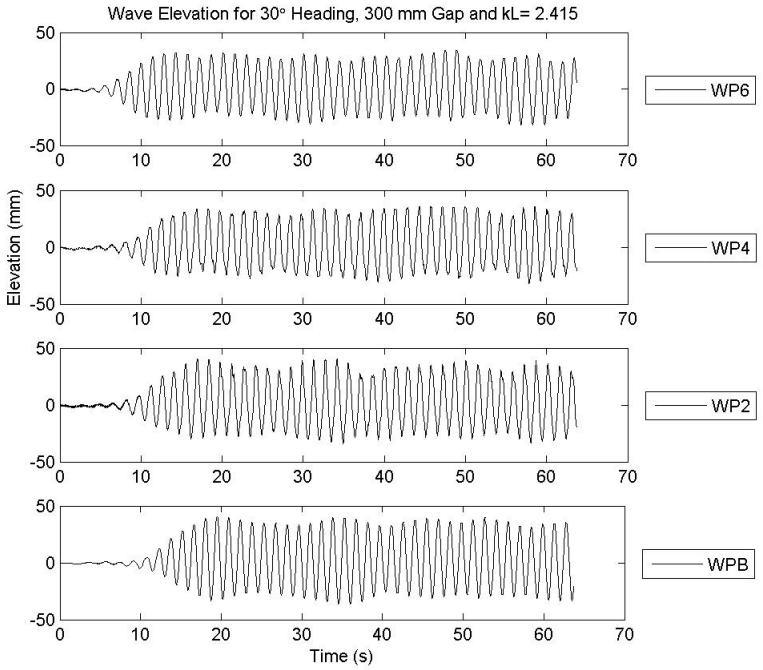
Wave Elevation for 30° Heading, 300 mm Gap and kL= 2.415
Elevation (mm)
Time (s)
WP6
WP4
WP2
WPB

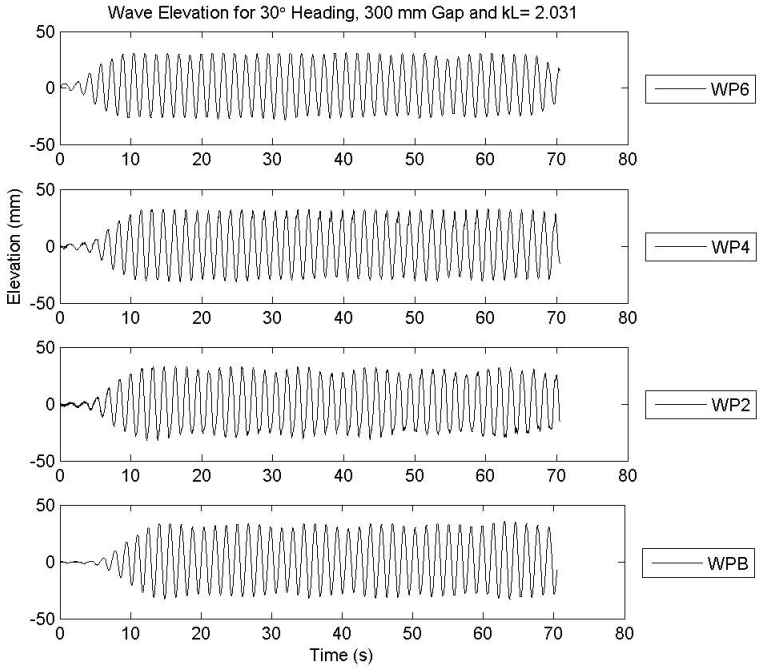
Wave Elevation for 30° Heading, 300 mm Gap and kL= 2.031
Elevation (mm)
Time (s)
WP6
WP4
WP2
WPB

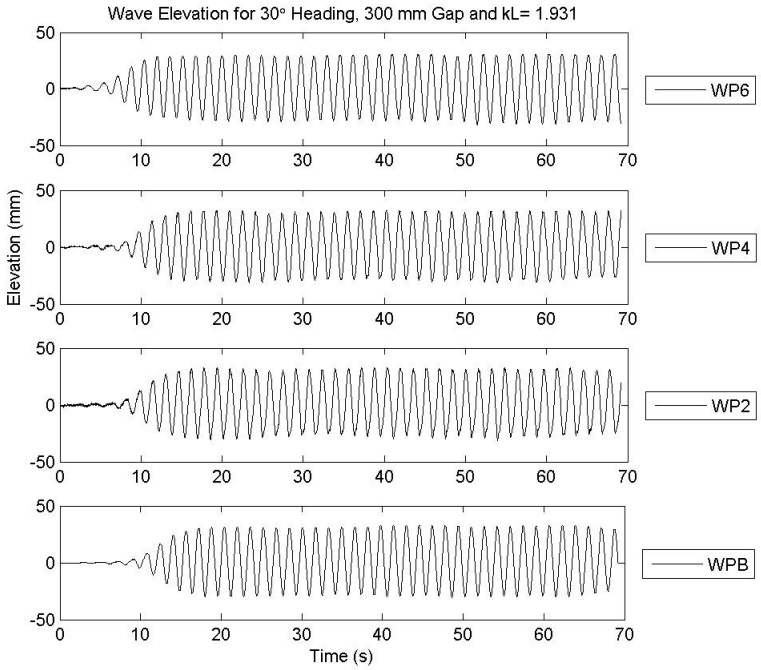
Wave Elevation for 30° Heading, 300 mm Gap and kL= 1.931
Elevation (mm)
Time (s)
WP6
WP4
WP2
WPB

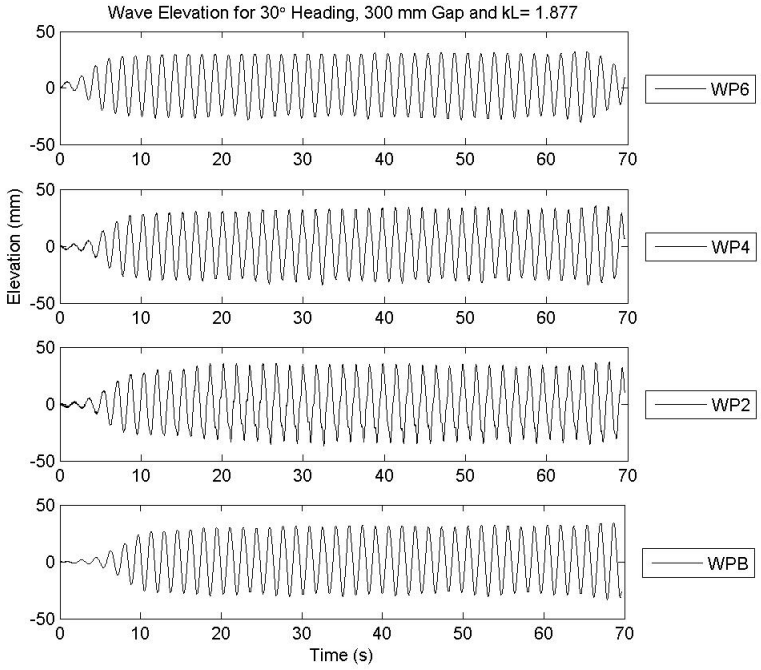
Wave Elevation for 30° Heading, 300 mm Gap and kL= 1.877
Elevation (mm)
Time (s)
WP6
WP4
WP2
WPB

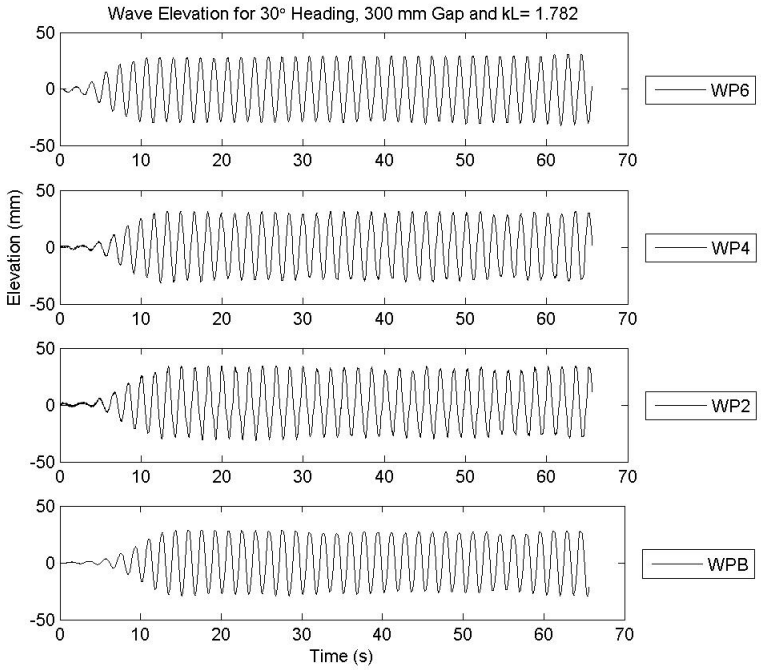
Wave Elevation for 30° Heading, 300 mm Gap and kL= 1.782
Elevation (mm)
Time (s)
WP6
WP4
WP2
WPB

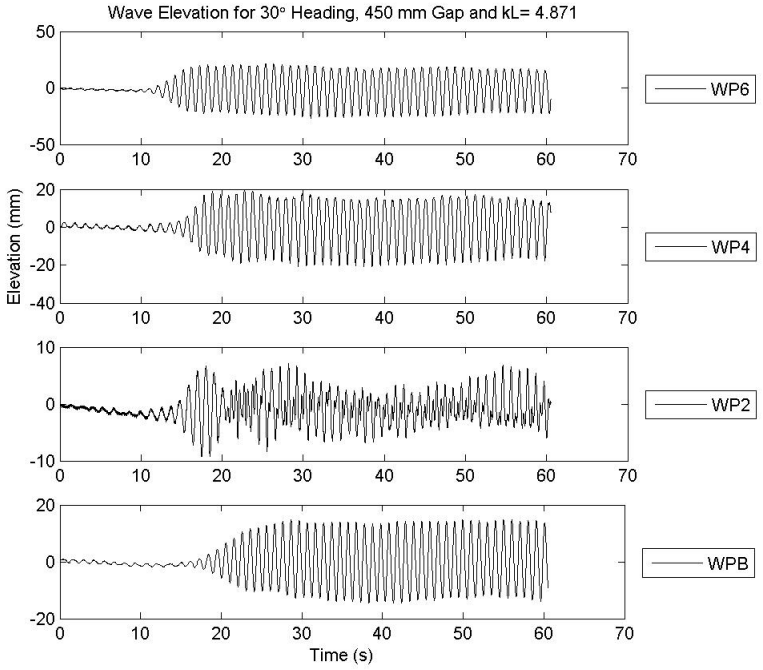
Wave Elevation for 30° Heading, 450 mm Gap and kL= 4.871
Elevation (mm)
Time (s)
WP6
WP4
WP2
WPB

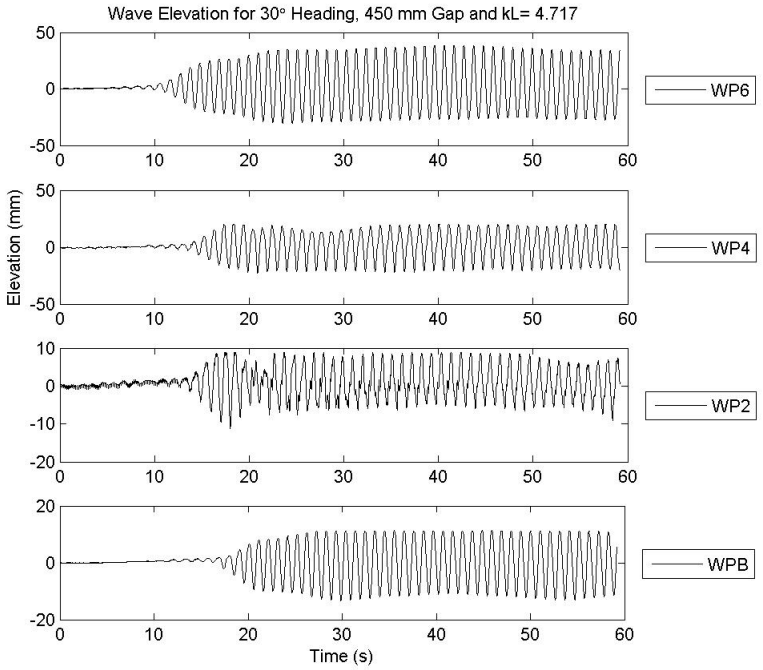
Wave Elevation for 30° Heading, 450 mm Gap and kL= 4.717
Elevation (mm)
Time (s)
WP6
WP4
WP2
WPB

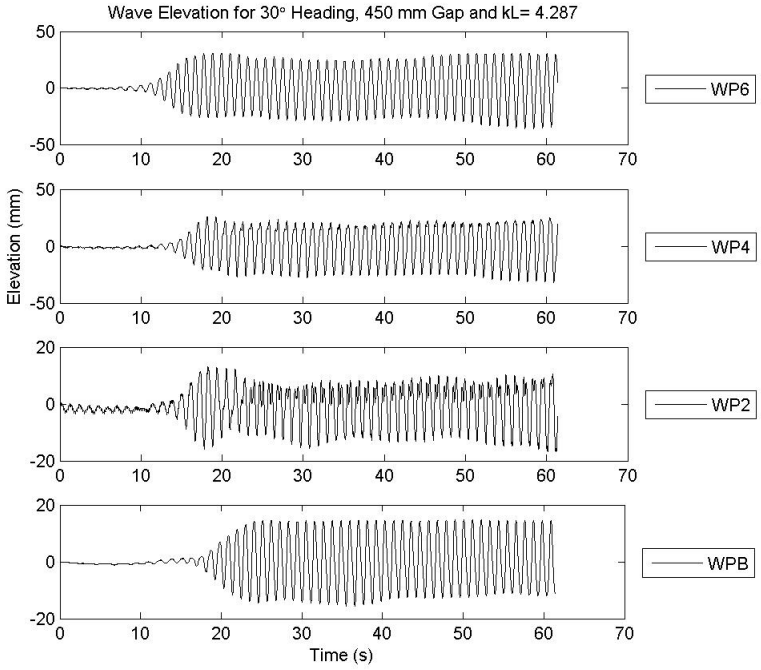
Wave Elevation for 30° Heading, 450 mm Gap and kL= 4.287
Elevation (mm)
Time (s)
WP6
WP4
WP2
WPB

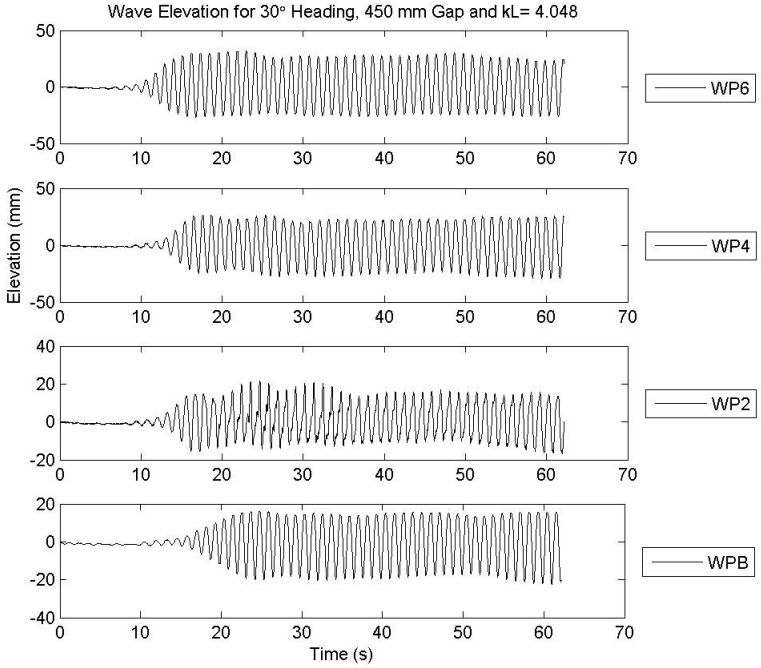
Wave Elevation for 30° Heading, 450 mm Gap and kL= 4.048
Elevation (mm)
Time (s)
WP6
WP4
WP2
WPB

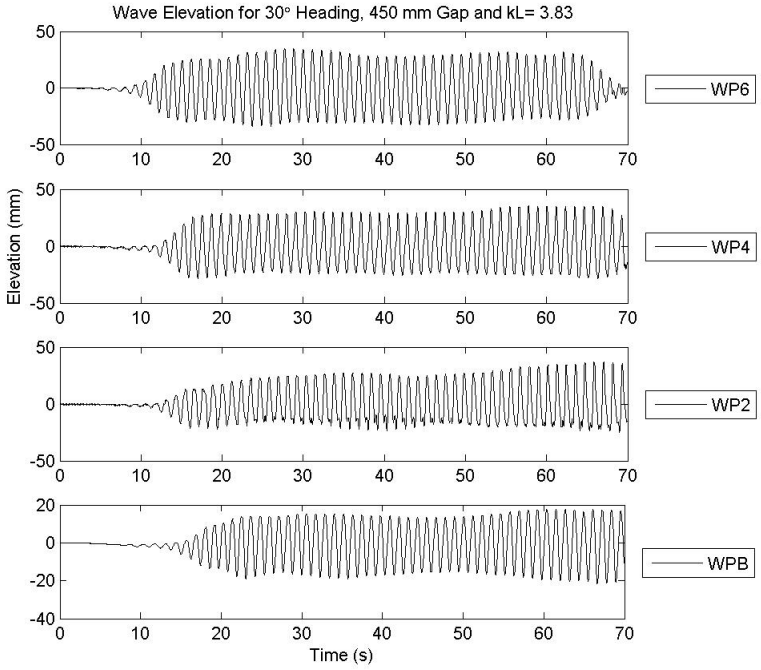
Wave Elevation for 30° Heading, 450 mm Gap and kL= 3.83
Elevation (mm)
Time (s)
WP6
WP4
WP2
WPB

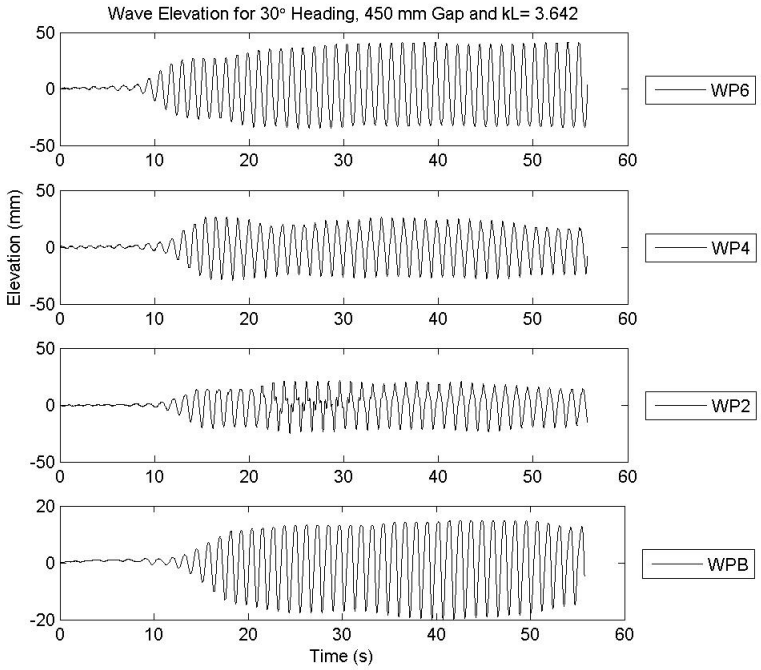
Wave Elevation for 30° Heading, 450 mm Gap and kL= 3.642
Elevation (mm)
Time (s)
WP6
WP4
WP2
WPB

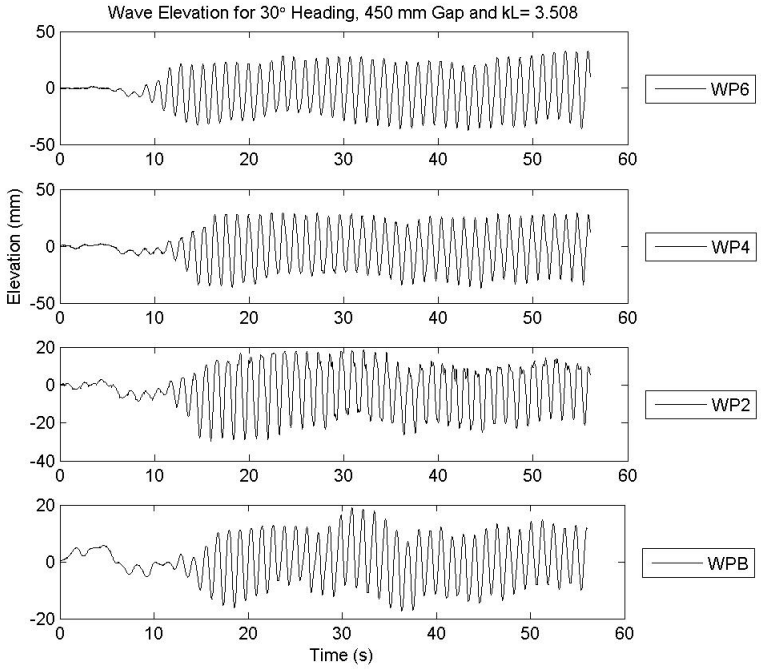
Wave Elevation for 30° Heading, 450 mm Gap and kL= 3.508
Elevation (mm)
Time (s)
WP6
WP4
WP2
WPB

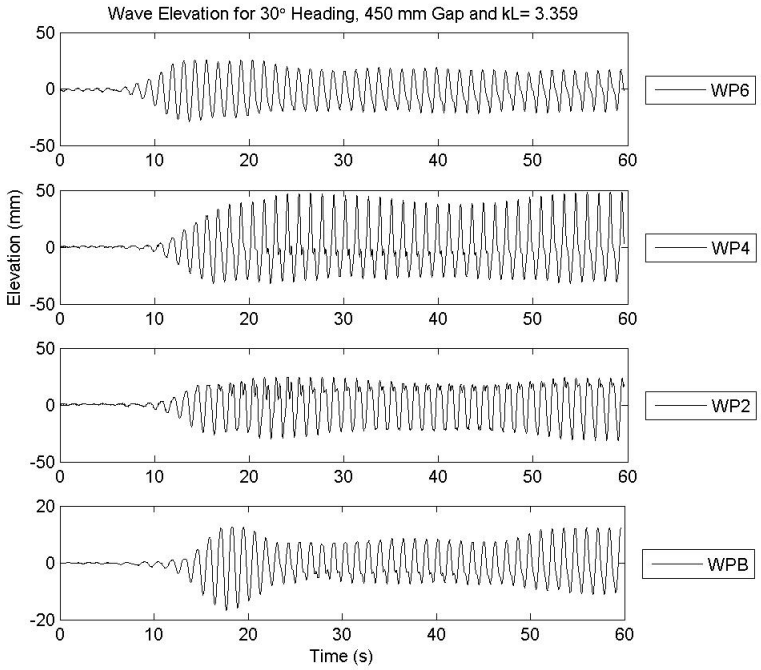
Wave Elevation for 30° Heading, 450 mm Gap and kL= 3.359
Elevation (mm)
Time (s)
WP6
WP4
WP2
WPB

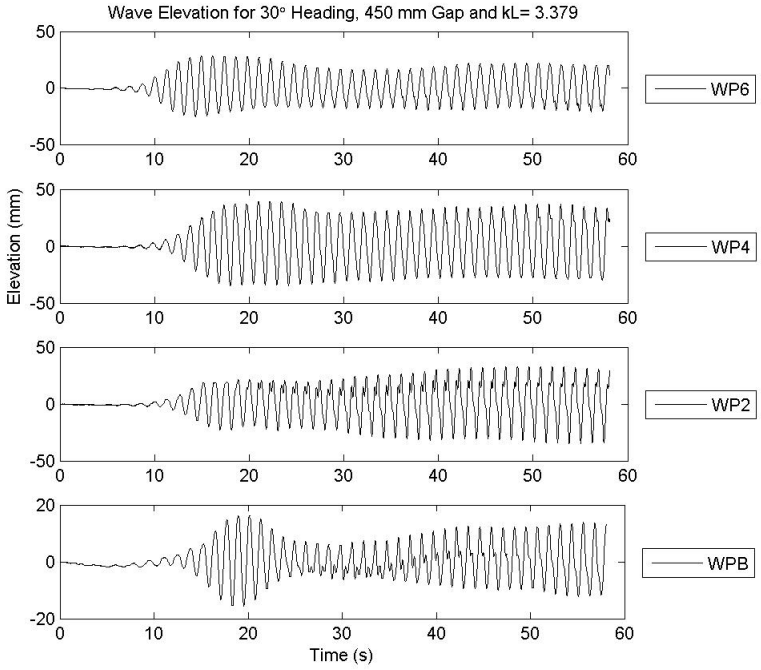
Wave Elevation for 30° Heading, 450 mm Gap and kL= 3.379
Elevation (mm)
Time (s)
WP6
WP4
WP2
WPB

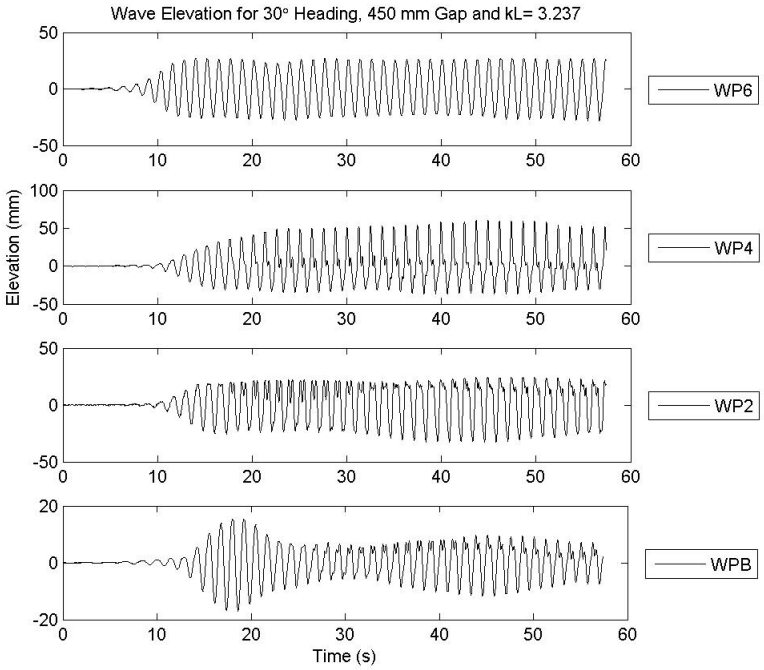
Wave Elevation for 30° Heading, 450 mm Gap and kL= 3.237
Elevation (mm)
Time (s)
WP6
WP4
WP2
WPB

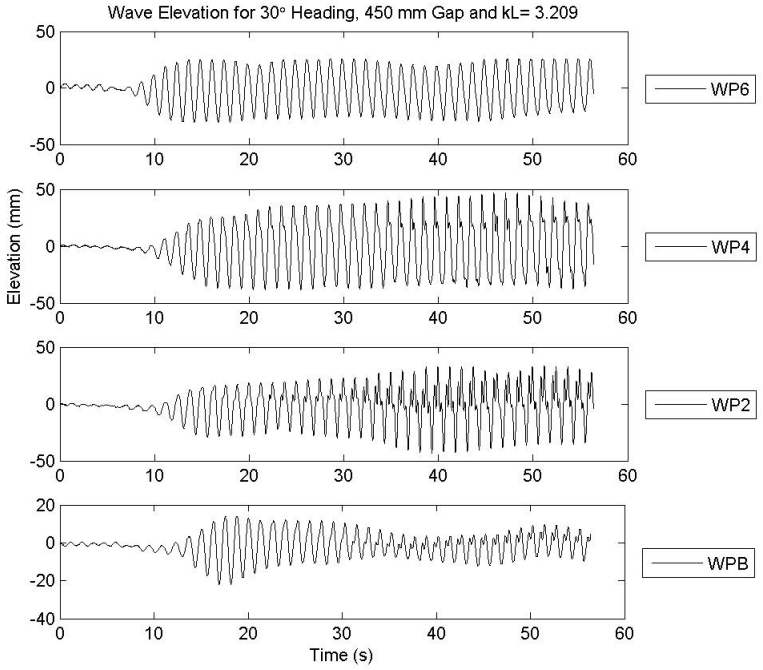
Wave Elevation for 30° Heading, 450 mm Gap and kL= 3.209
Elevation (mm)
Time (s)
WP6
WP4
WP2
WPB

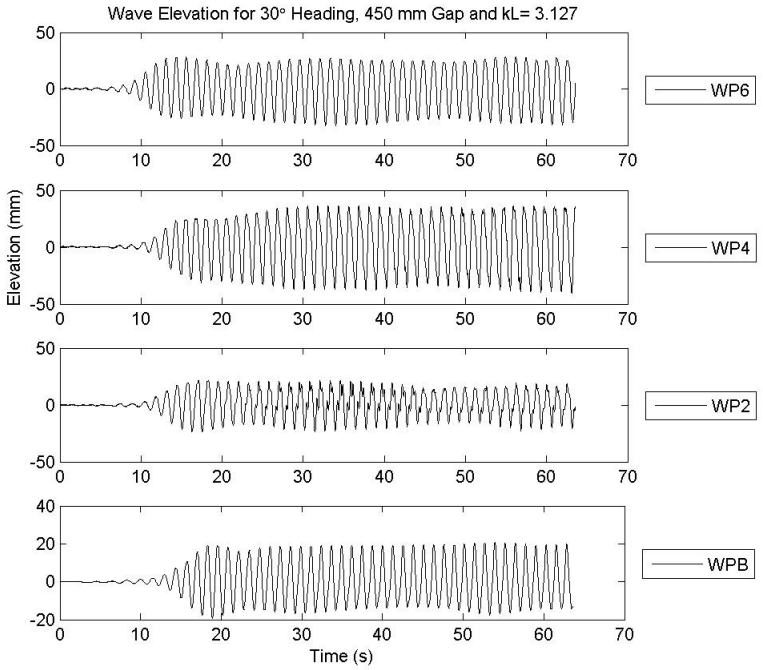
Wave Elevation for 30° Heading, 450 mm Gap and kL= 3.127
Elevation (mm)
Time (s)
WP6
WP4
WP2
WPB

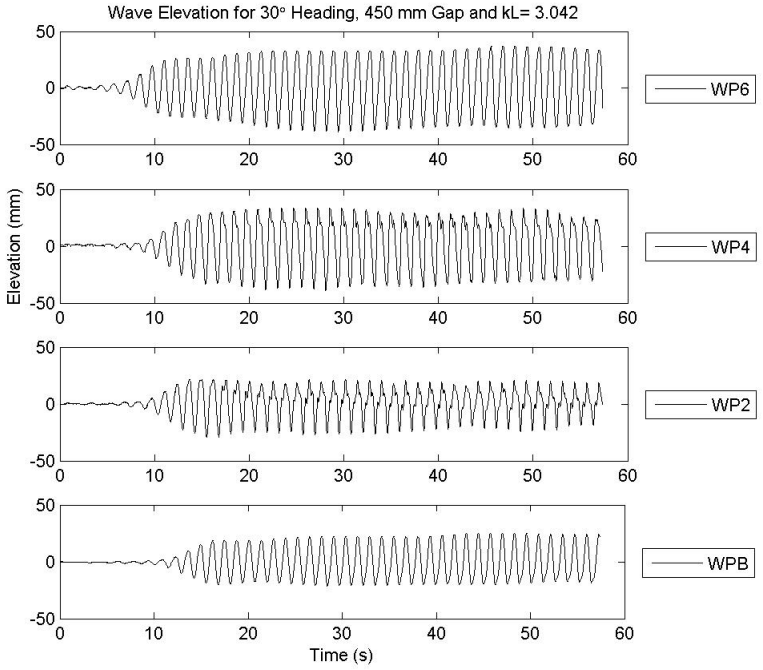
Wave Elevation for 30° Heading, 450 mm Gap and kL= 3.042
Elevation (mm)
Time (s)
WP6
WP4
WP2
WPB

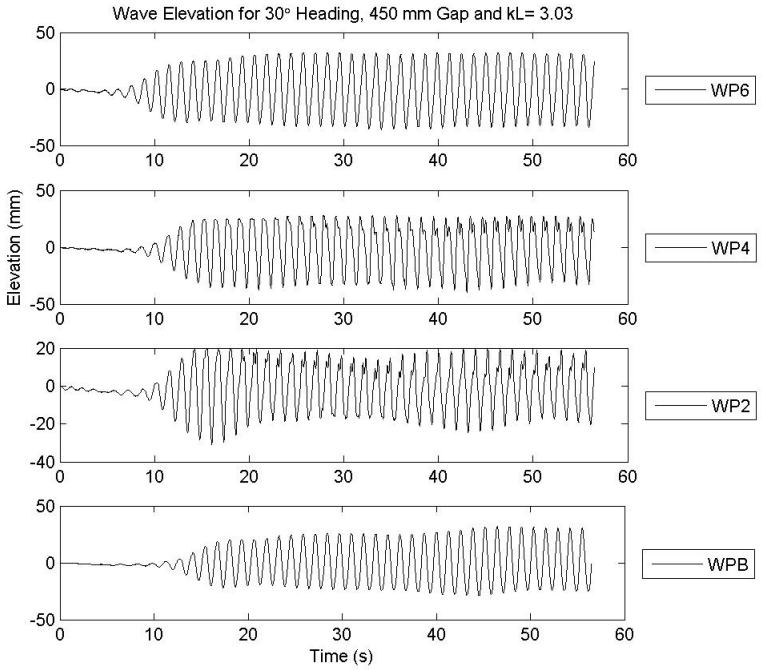
Wave Elevation for 30° Heading, 450 mm Gap and kL= 3.03
Elevation (mm)
Time (s)
WP6
WP4
WP2
WPB

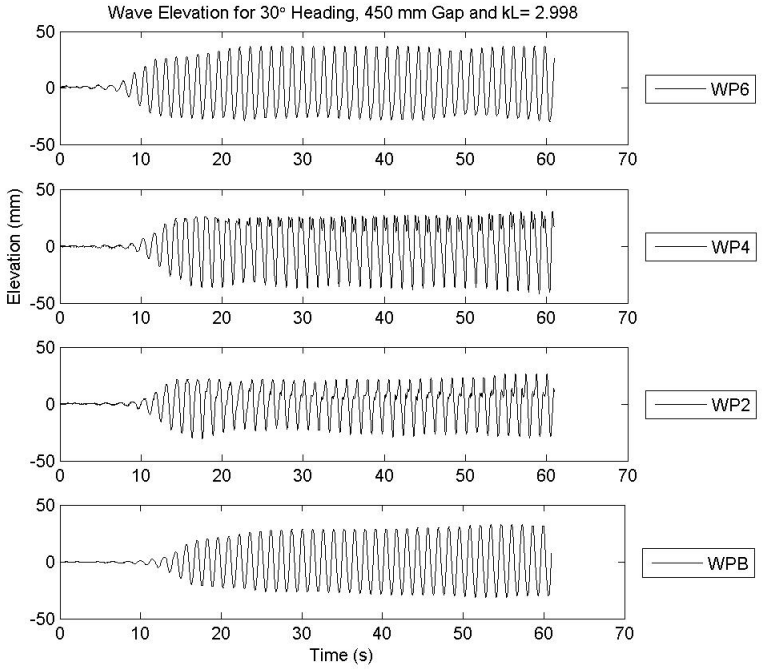
Wave Elevation for 30° Heading, 450 mm Gap and kL= 2.998
Elevation (mm)
Time (s)
WP6
WP4
WP2
WPB

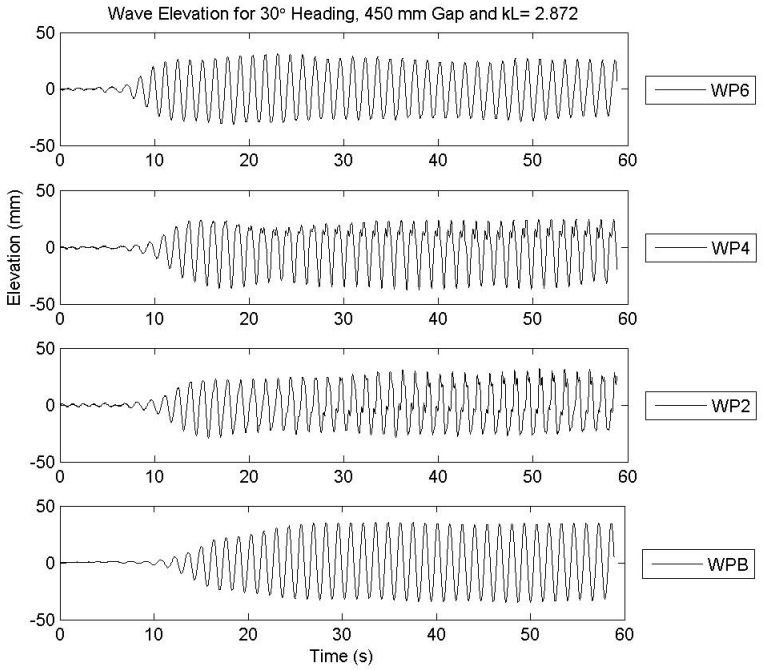
Wave Elevation for 30° Heading, 450 mm Gap and kL= 2.872
Elevation (mm)
Time (s)
WP6
WP4
WP2
WPB

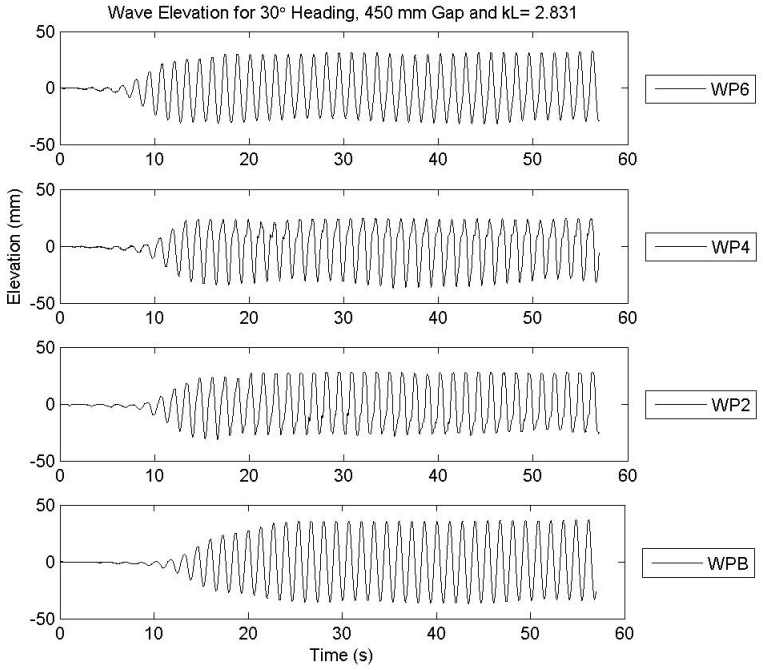
Wave Elevation for 30° Heading, 450 mm Gap and kL= 2.831
Elevation (mm)
Time (s)
WP6
WP4
WP2
WPB

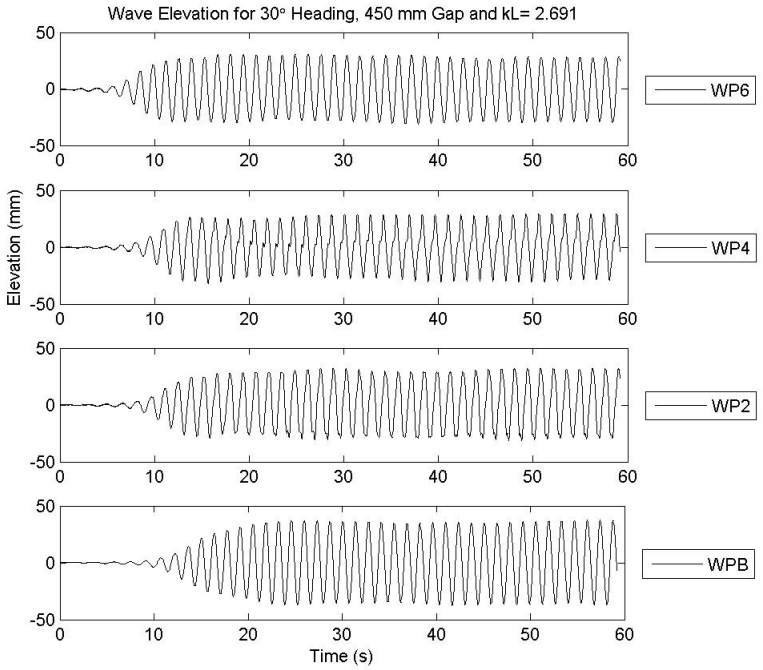
Wave Elevation for 30° Heading, 450 mm Gap and kL= 2.691
Elevation (mm)
Time (s)
WP6
WP4
WP2
WPB

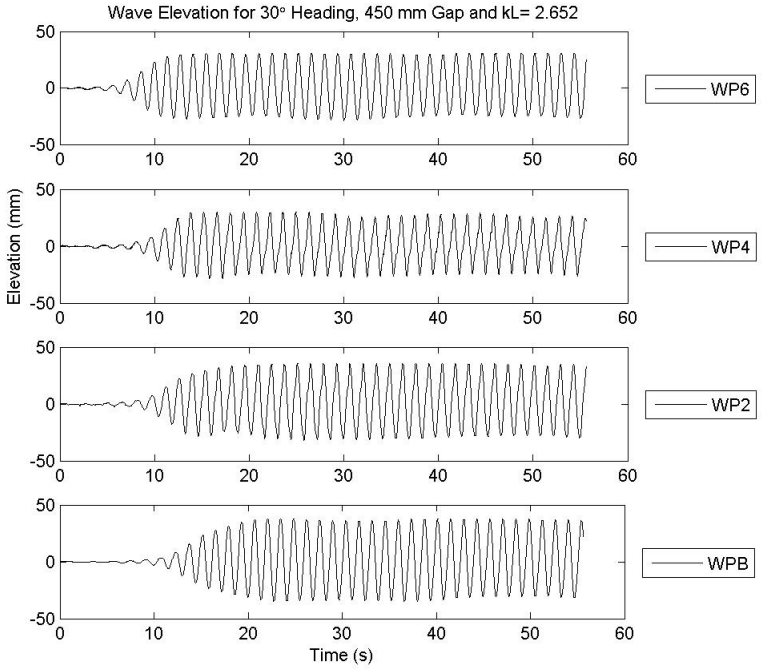
Wave Elevation for 30° Heading, 450 mm Gap and kL= 2.652
Elevation (mm)
Time (s)
WP6
WP4
WP2
WPB

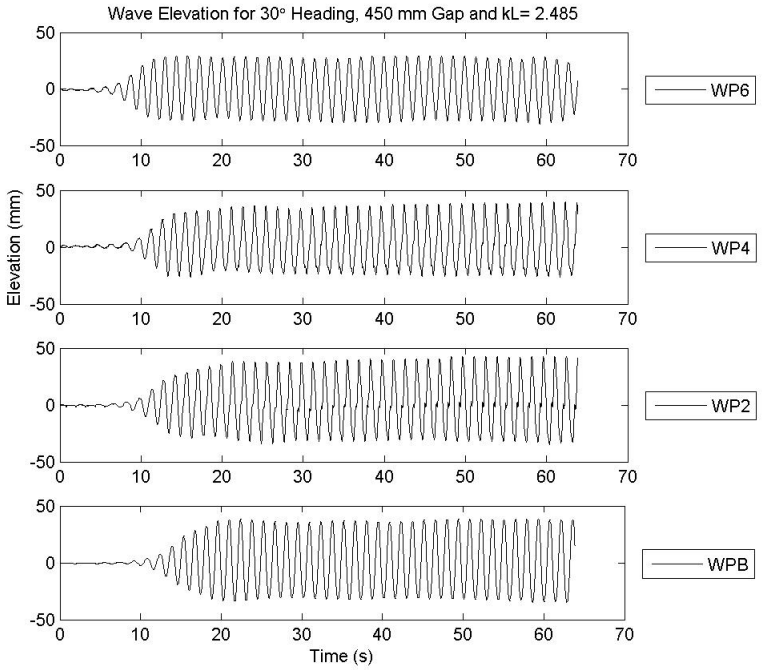
Wave Elevation for 30° Heading, 450 mm Gap and kL= 2.485
Elevation (mm)
Time (s)
WP6
WP4
WP2
WPB

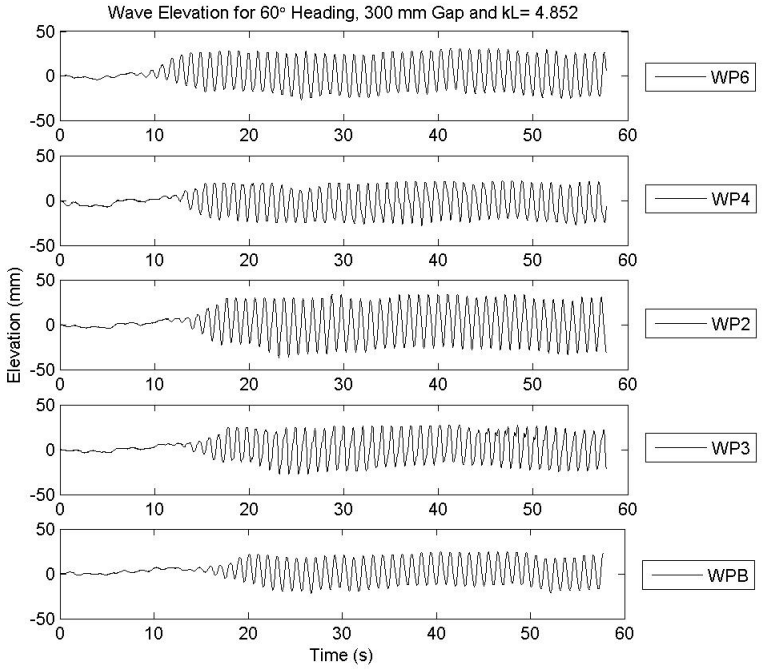
Wave Elevation for 60° Heading, 300 mm Gap and kL= 4.852
WP6
WP4
WP2
WP3
WPB
Elevation (mm)
Time (s)

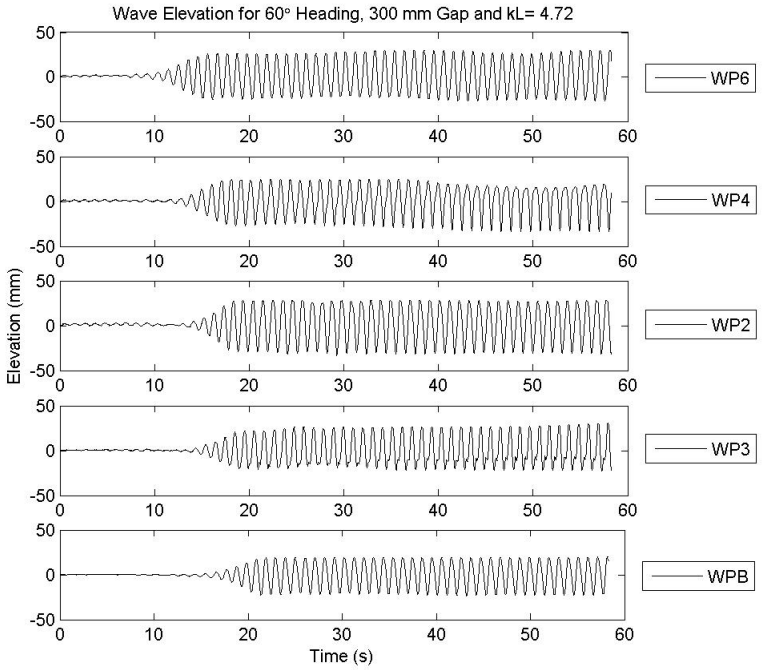
Wave Elevation for 60° Heading, 300 mm Gap and kL= 4.72
WP6
WP4
WP2
WP3
WPB
Elevation (mm)
Time (s)

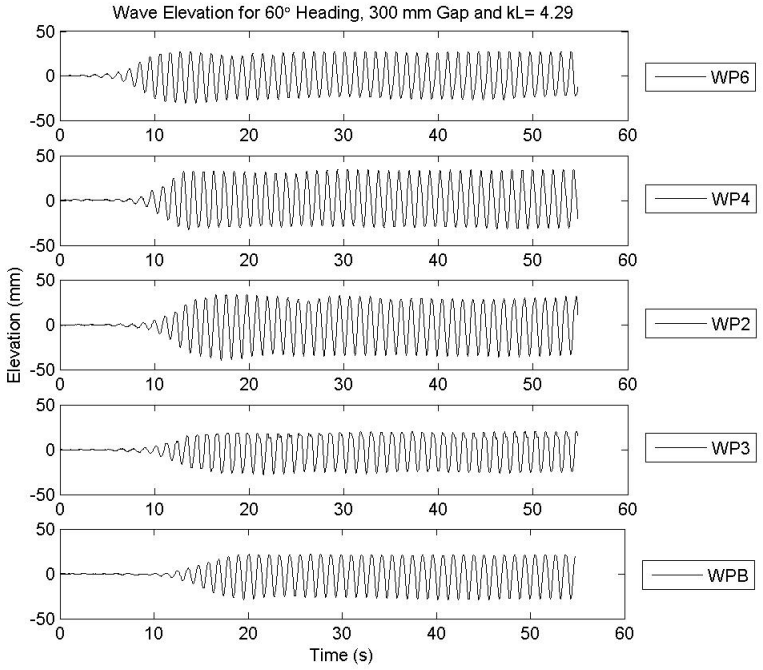
Wave Elevation for 60° Heading, 300 mm Gap and kL= 4.29
Elevation (mm)
Time (s)
WP6
WP4
WP2
WP3
WPB

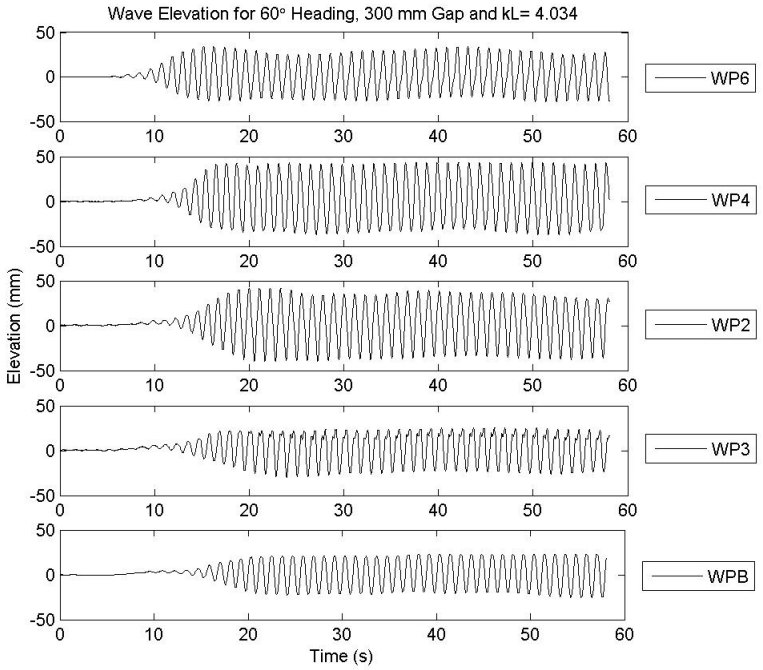
Wave Elevation for 60° Heading, 300 mm Gap and kL= 4.034
Elevation (mm)
Time (s)
WP6
WP4
WP2
WP3
WPB

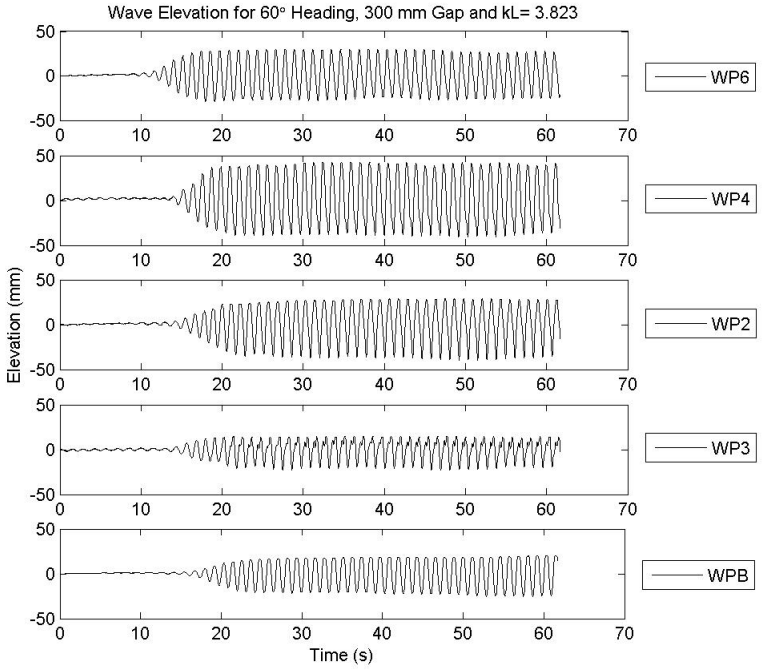
Wave Elevation for 60° Heading, 300 mm Gap and kL= 3.823
WP6
WP4
WP2
WP3
WPB
Elevation (mm)
Time (s)

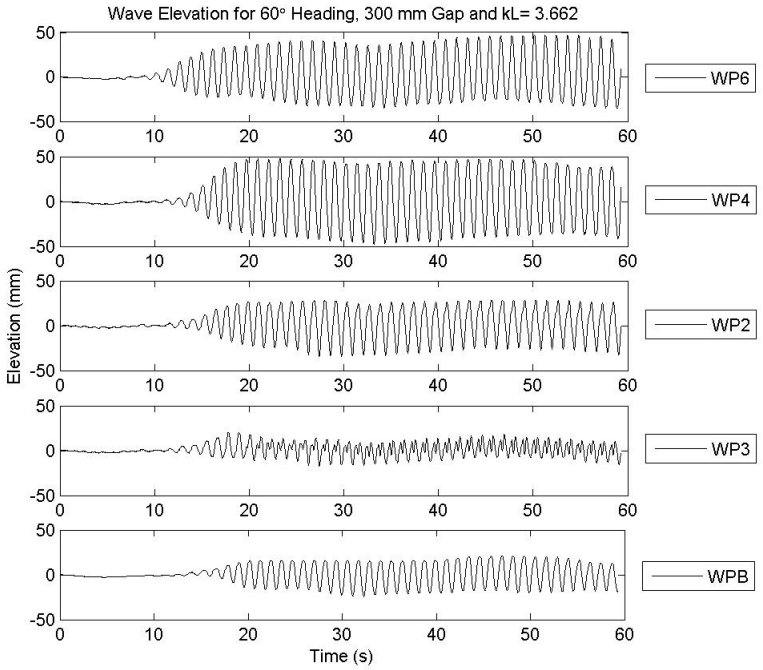
Wave Elevation for 60° Heading, 300 mm Gap and kL= 3.662
WP6
WP4
WP2
WP3
WPB
Elevation (mm)
Time (s)

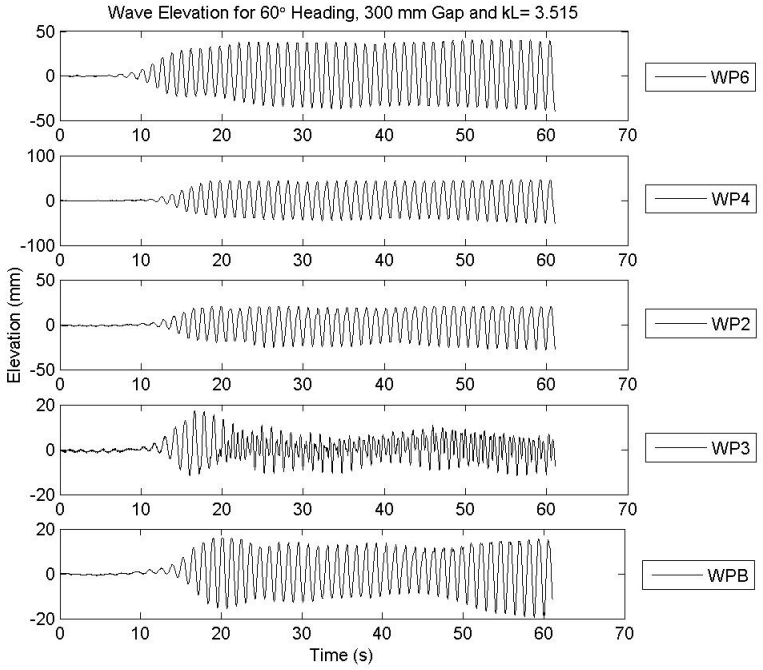
Wave Elevation for 60° Heading, 300 mm Gap and kL= 3.515
WP6
WP4
WP2
WP3
WPB
Elevation (mm)
Time (s)

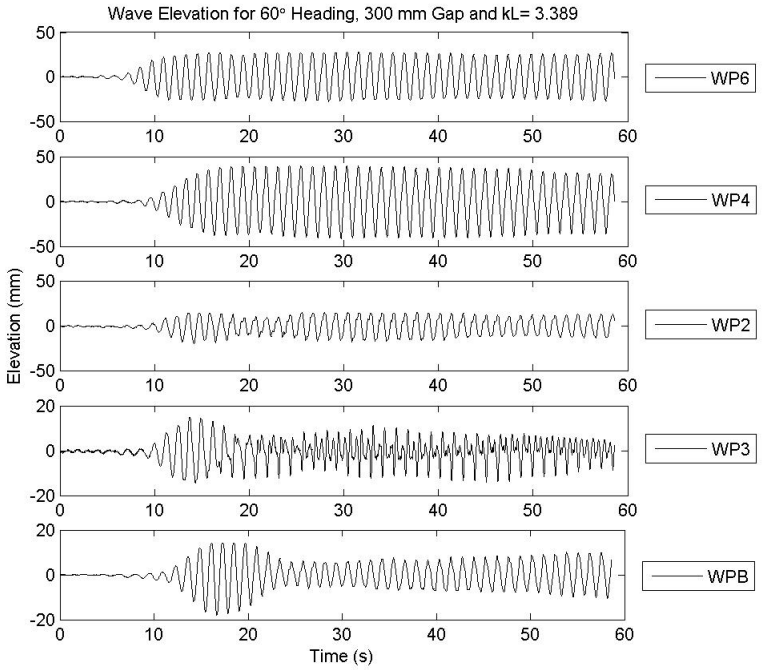
Wave Elevation for 60° Heading, 300 mm Gap and kL= 3.389
WP6
WP4
WP2
WP3
WPB
Elevation (mm)
Time (s)

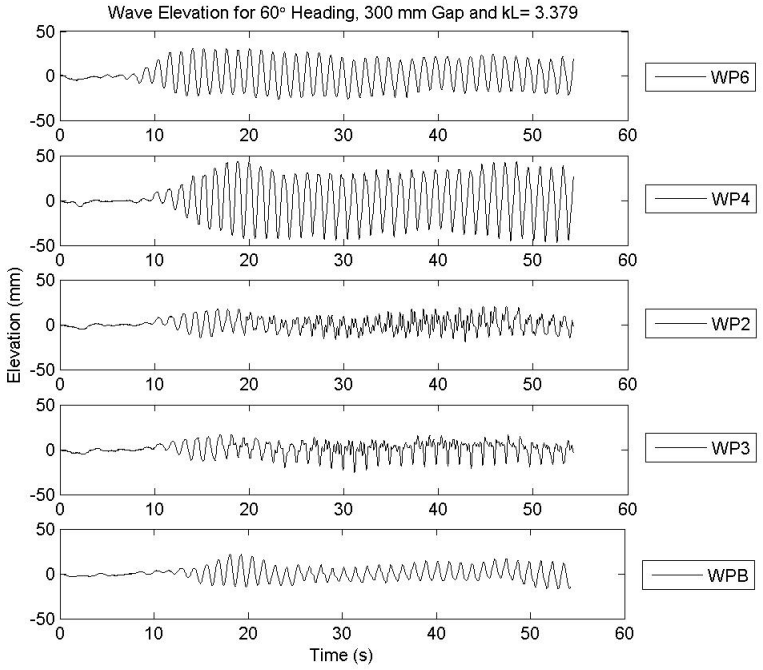
Wave Elevation for 60° Heading, 300 mm Gap and kL= 3.379
WP6
WP4
WP2
WP3
WPB
Elevation (mm)
Time (s)

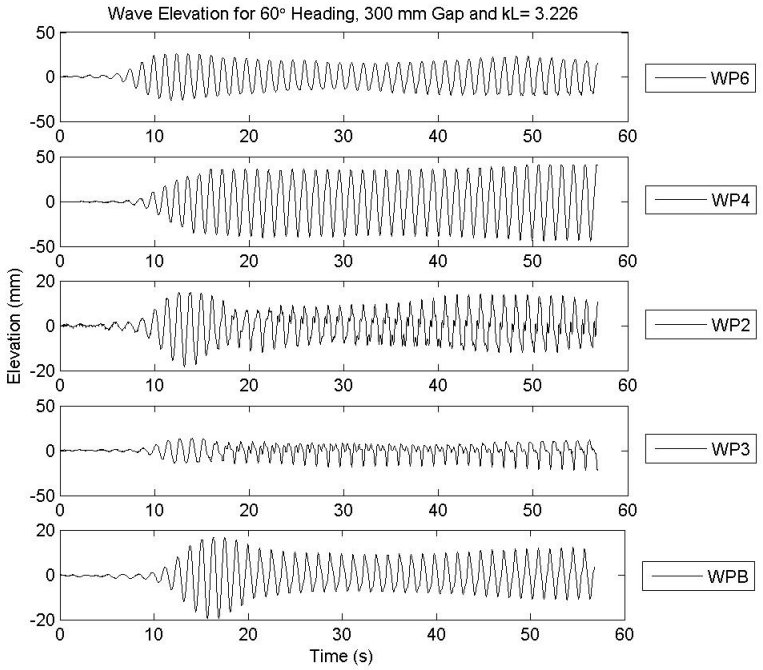
Wave Elevation for 60° Heading, 300 mm Gap and kL= 3.226
WP6
WP4
WP2
WP3
WPB
Elevation (mm)
Time (s)

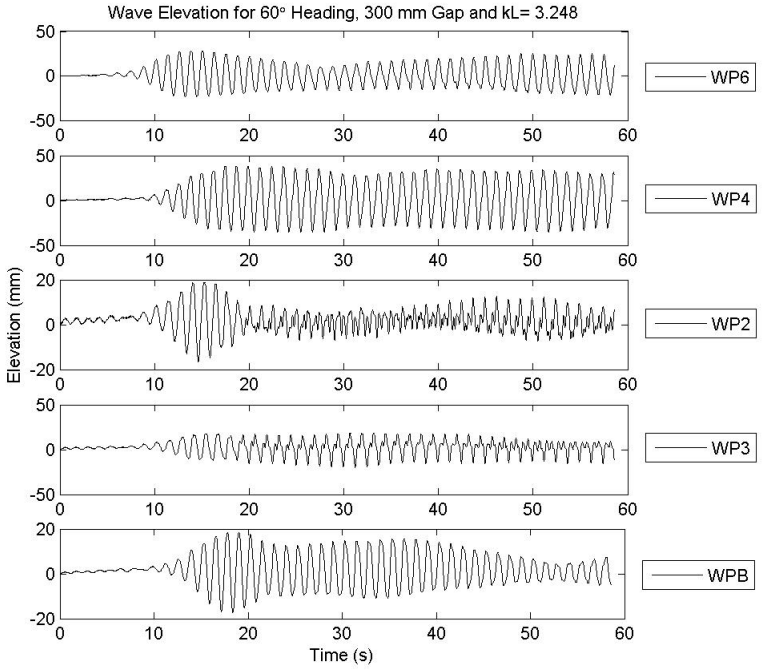
Wave Elevation for 60° Heading, 300 mm Gap and kL= 3.248
WP6
WP4
WP2
WP3
WPB
Elevation (mm)
Time (s)

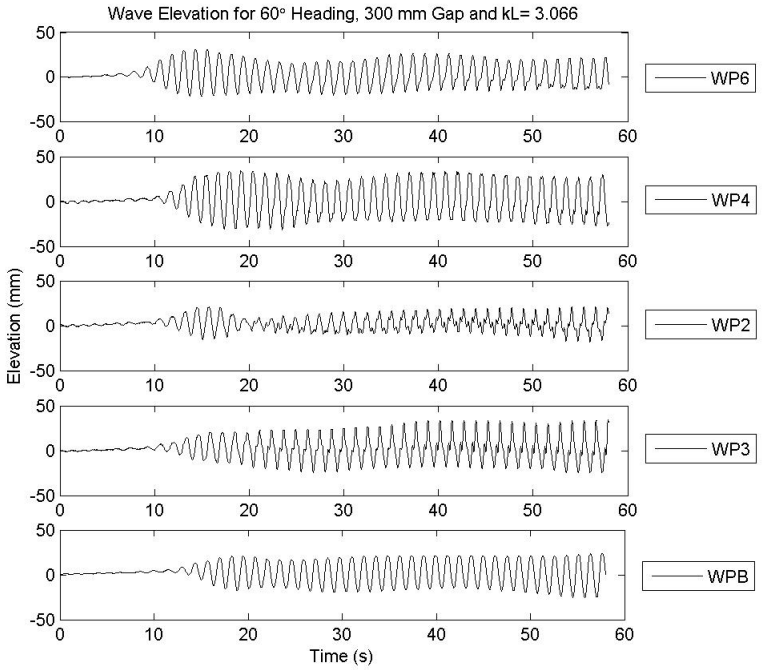
Wave Elevation for 60° Heading, 300 mm Gap and kL= 3.066
WP6
WP4
WP2
WP3
WPB
Elevation (mm)
Time (s)

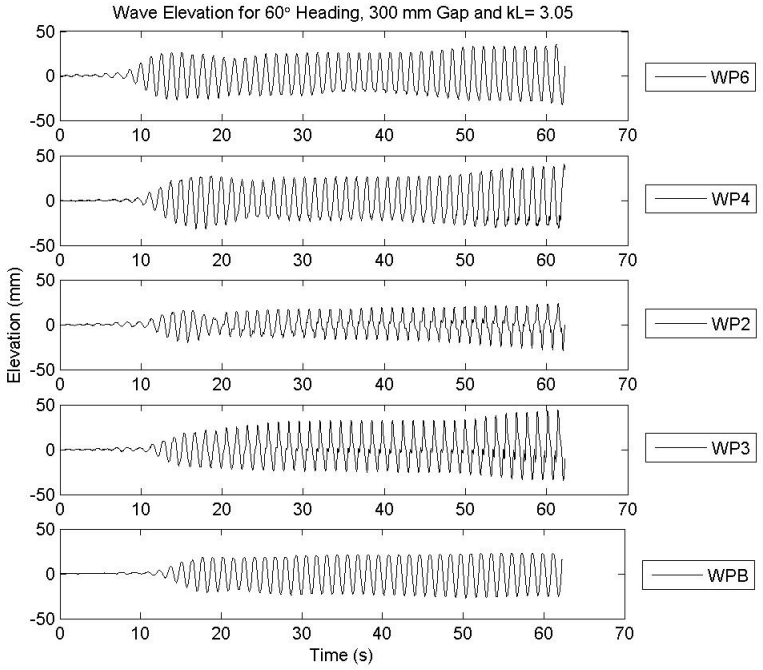
Wave Elevation for 60° Heading, 300 mm Gap and kL= 3.05
Elevation (mm)
Time (s)
WP6
WP4
WP2
WP3
WPB

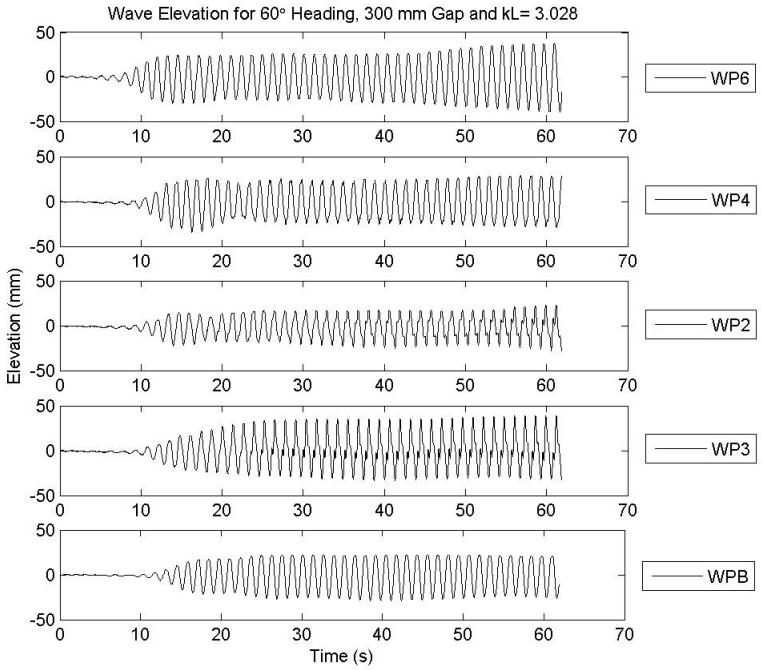
Wave Elevation for 60° Heading, 300 mm Gap and kL= 3.028
Elevation (mm)
Time (s)
WP6
WP4
WP2
WP3
WPB

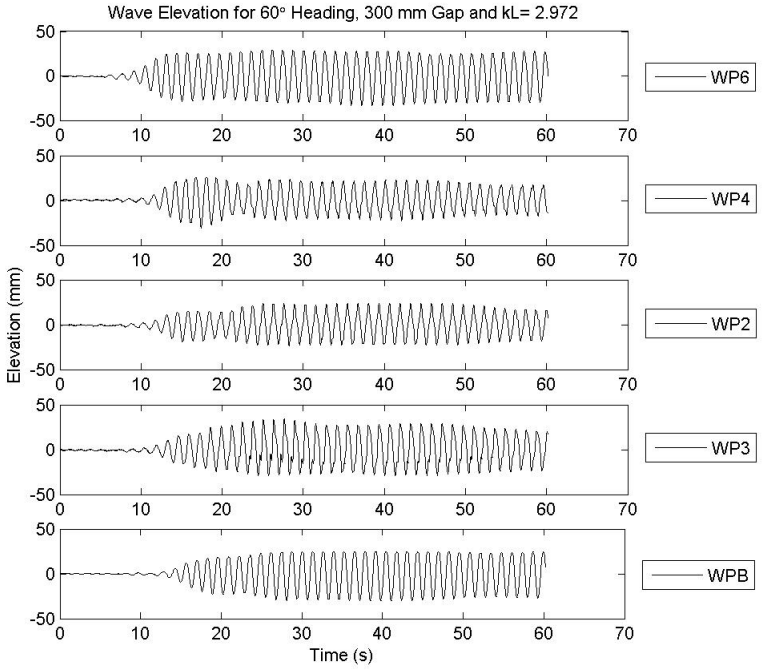
Wave Elevation for 60° Heading, 300 mm Gap and kL= 2.972
WP6
WP4
WP2
WP3
WPB
Elevation (mm)
Time (s)

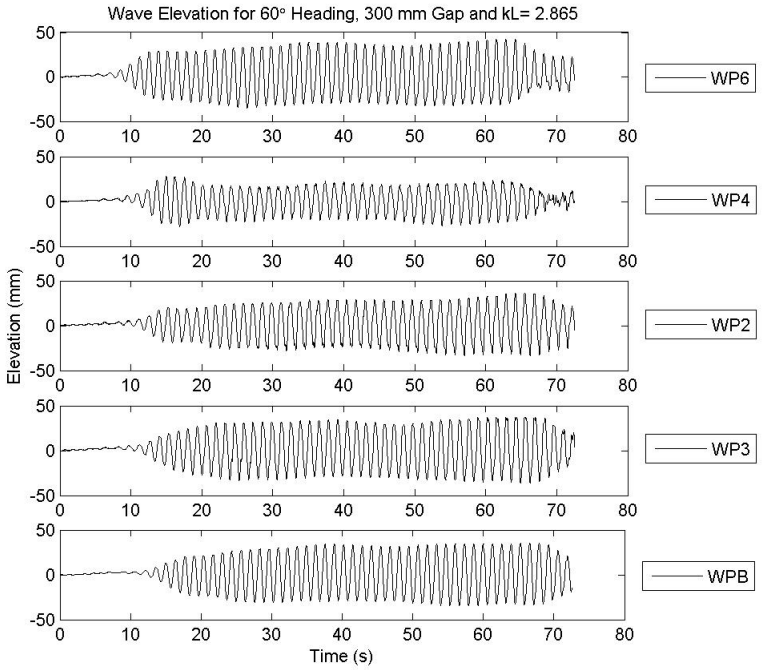
Wave Elevation for 60° Heading, 300 mm Gap and kL= 2.865
WP6
WP4
WP2
WP3
WPB
Elevation (mm)
Time (s)

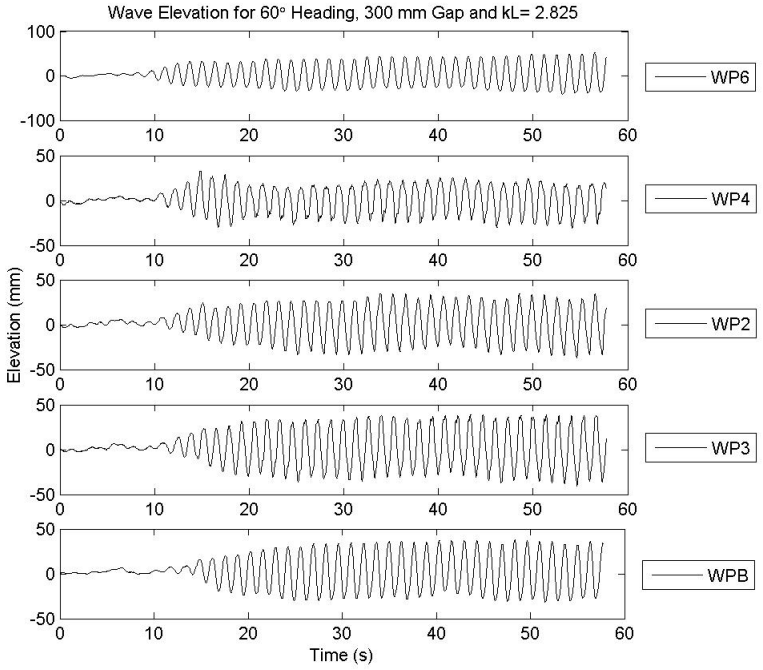
Wave Elevation for 60° Heading, 300 mm Gap and kL= 2.825
Elevation (mm)
Time (s)
WP6
WP4
WP2
WP3
WPB

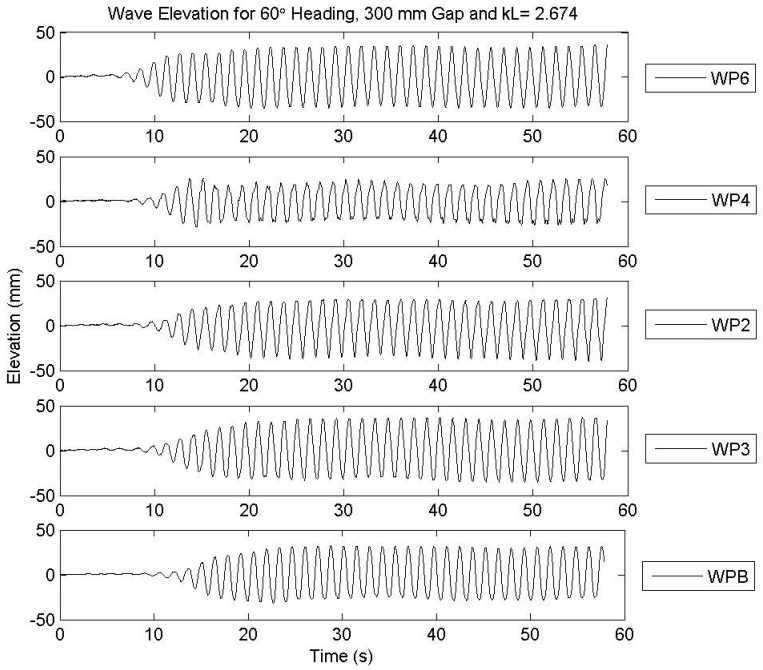
Wave Elevation for 60° Heading, 300 mm Gap and kL= 2.674
Elevation (mm)
Time (s)
WP6
WP4
WP2
WP3
WPB

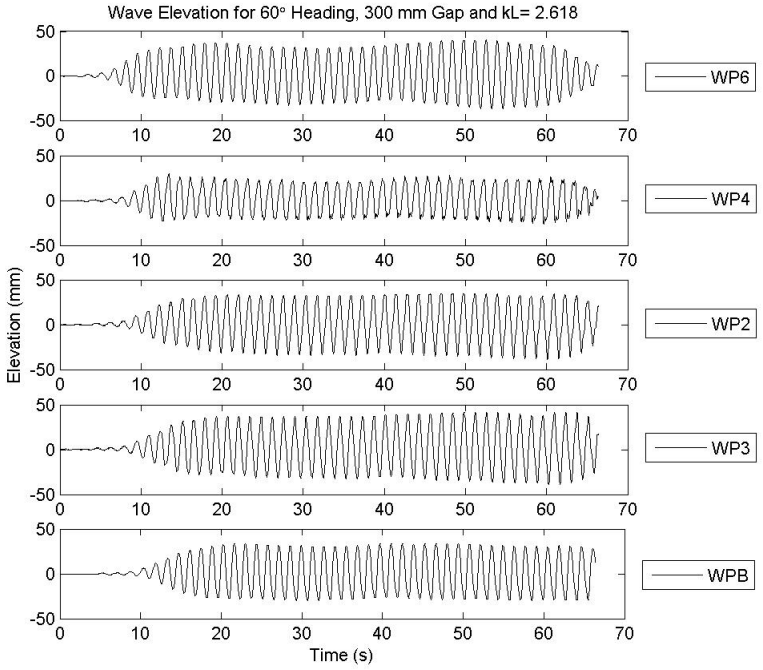
Wave Elevation for 60° Heading, 300 mm Gap and kL= 2.618
WP6
WP4
WP2
WP3
WPB
Elevation (mm)
Time (s)

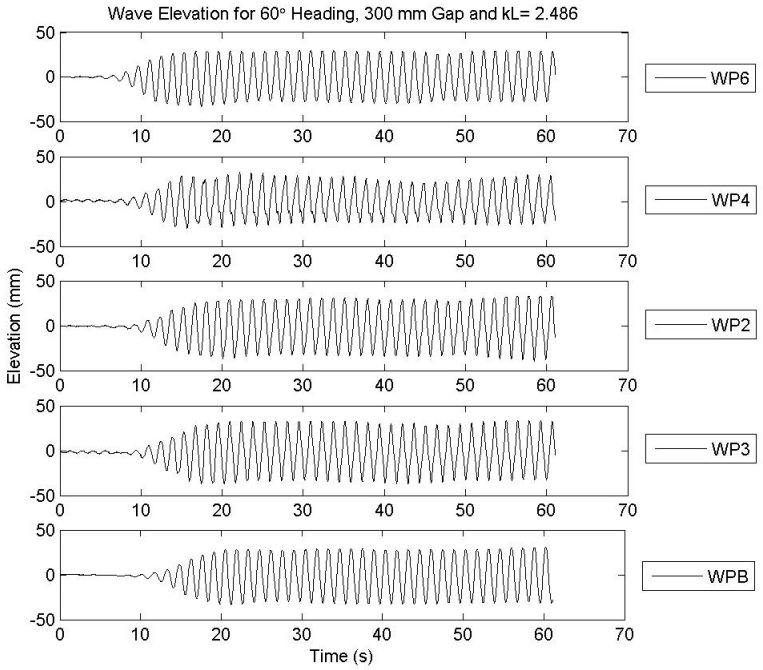
Wave Elevation for 60° Heading, 300 mm Gap and kL= 2.486
WP6
WP4
WP2
WP3
WPB
Elevation (mm)
Time (s)

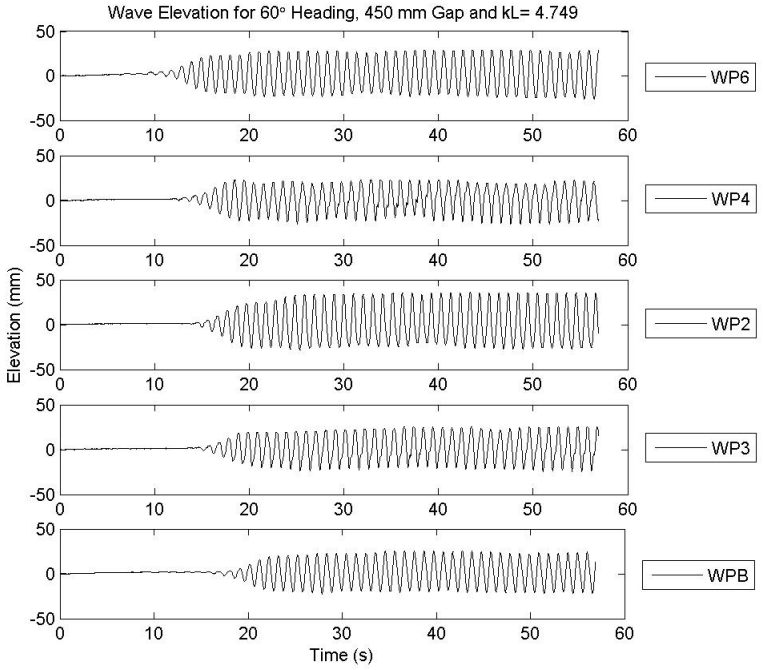
Wave Elevation for 60° Heading, 450 mm Gap and kL= 4.749
WP6
WP4
WP2
WP3
WPB
Elevation (mm)
Time (s)

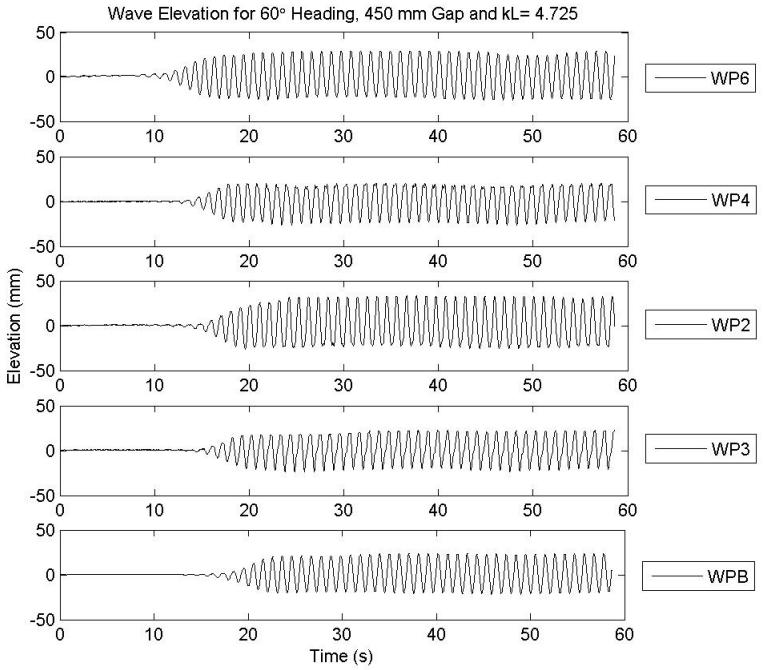
Wave Elevation for 60° Heading, 450 mm Gap and kL= 4.725
WP6
WP4
WP2
WP3
WPB
Elevation (mm)
Time (s)

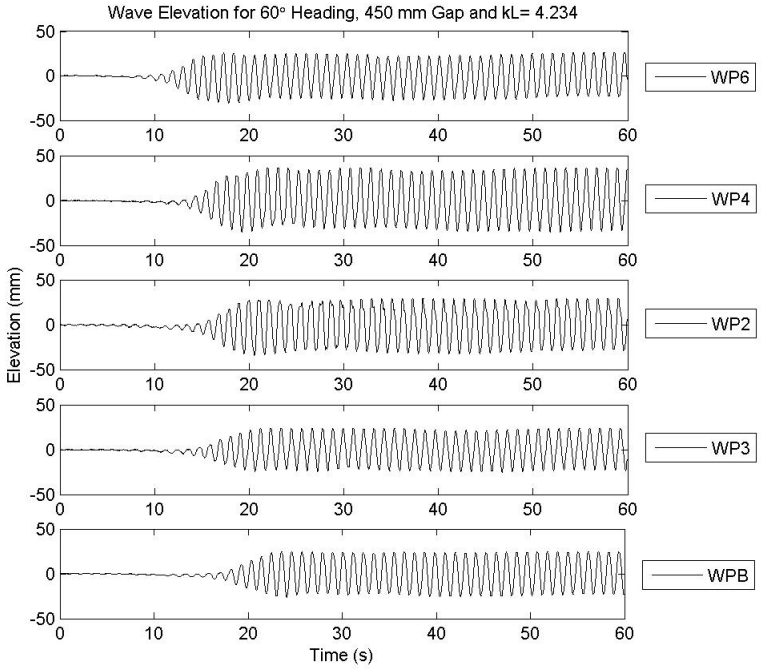
Wave Elevation for 60° Heading, 450 mm Gap and kL= 4.234
WP6
WP4
WP2
WP3
WPB
Elevation (mm)
Time (s)

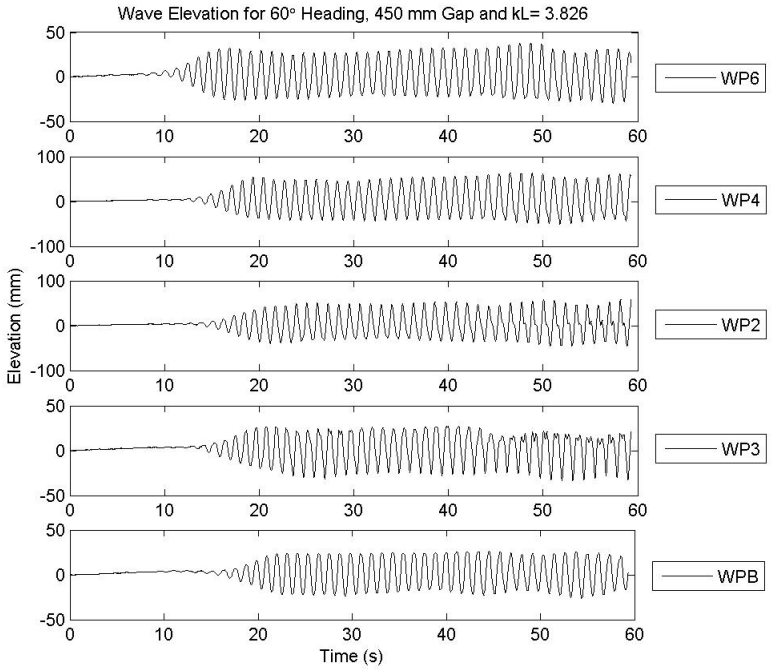
Wave Elevation for 60° Heading, 450 mm Gap and kL= 3.826
WP6
WP4
WP2
WP3
WPB
Elevation (mm)
Time (s)

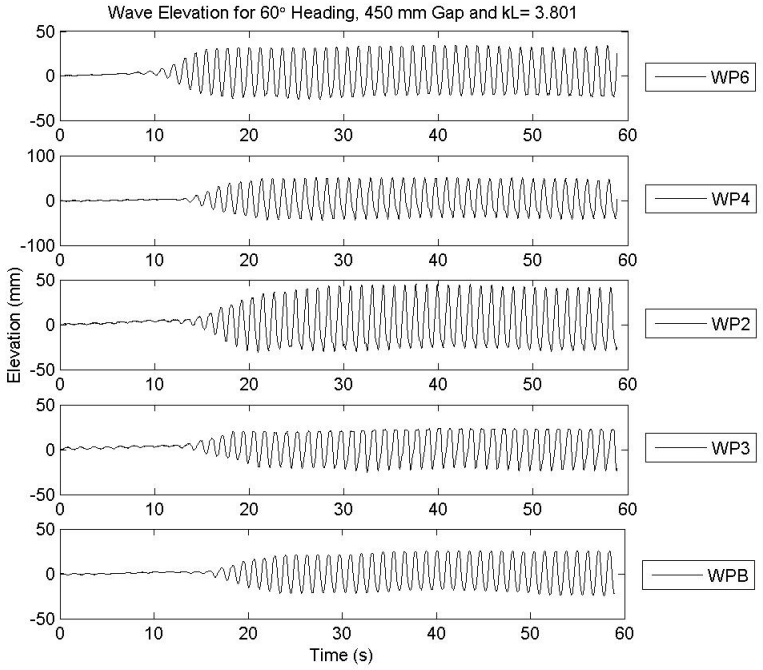
Wave Elevation for 60° Heading, 450 mm Gap and kL= 3.801
WP6
WP4
WP2
WP3
WPB
Elevation (mm)
Time (s)

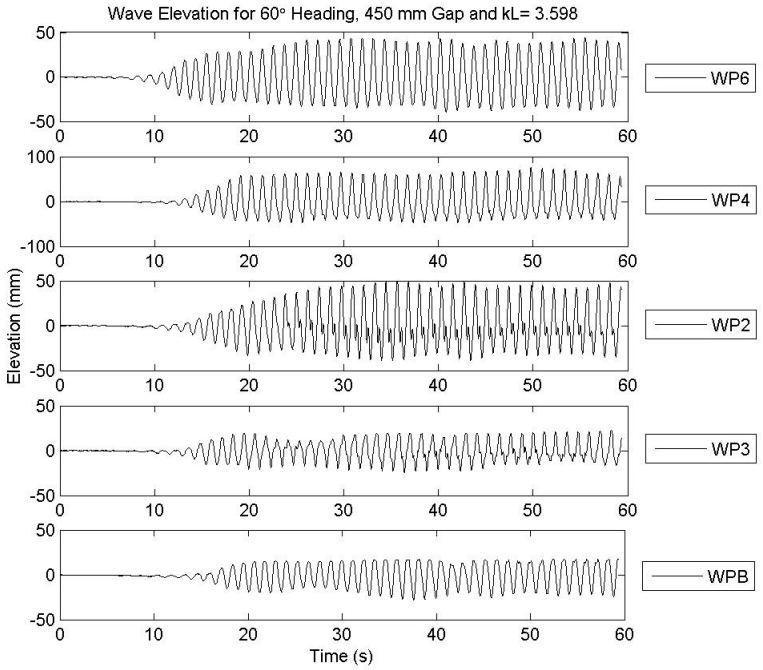
Wave Elevation for 60° Heading, 450 mm Gap and kL= 3.598
WP6
WP4
WP2
WP3
WPB
Elevation (mm)
Time (s)

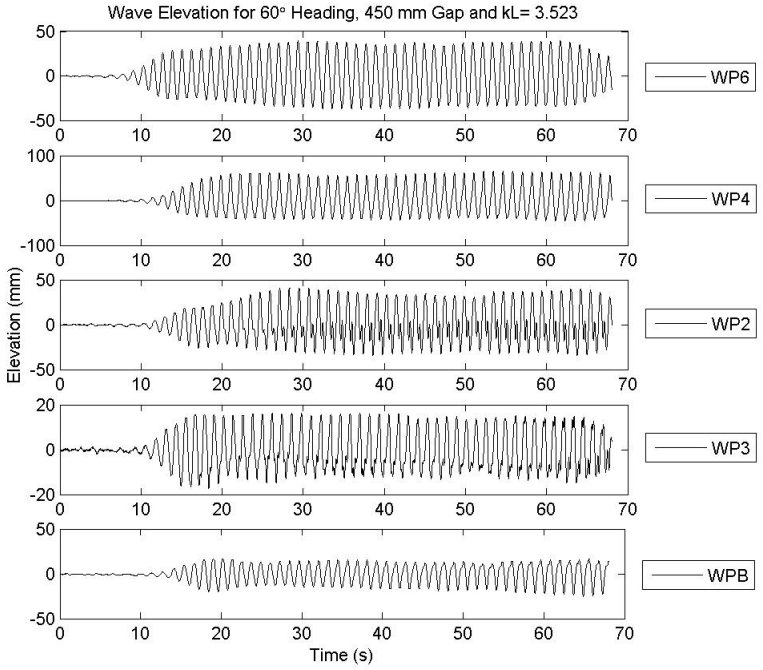
Wave Elevation for 60° Heading, 450 mm Gap and kL= 3.523
WP6
WP4
WP2
WP3
WPB
Elevation (mm)
Time (s)

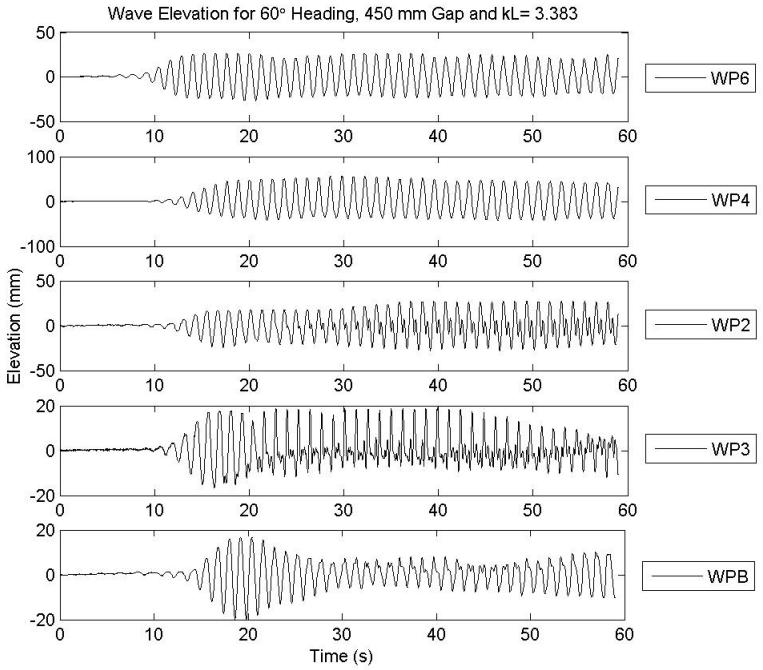
Wave Elevation for 60° Heading, 450 mm Gap and kL= 3.383
WP6
WP4
WP2
WP3
WPB
Elevation (mm)
Time (s)

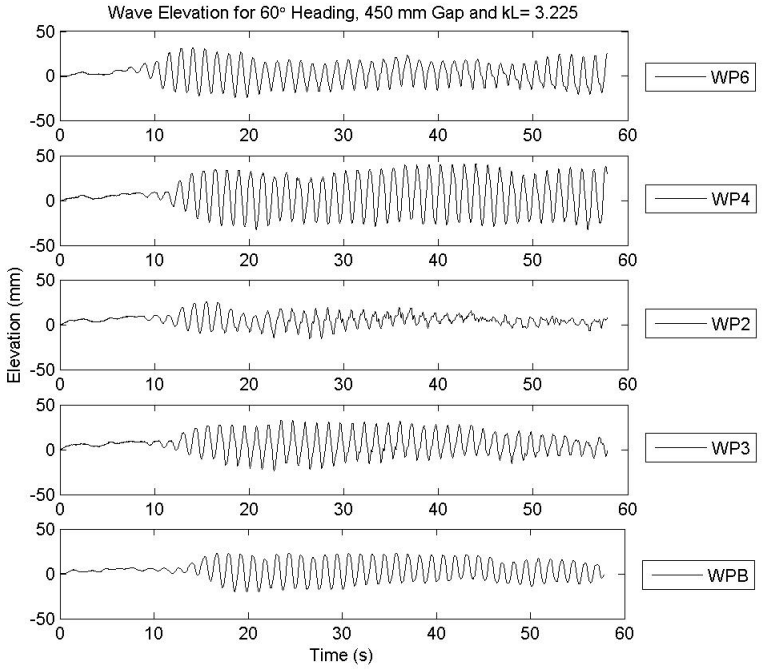
Wave Elevation for 60° Heading, 450 mm Gap and kL= 3.225
WP6
WP4
WP2
WP3
WPB
Elevation (mm)
Time (s)

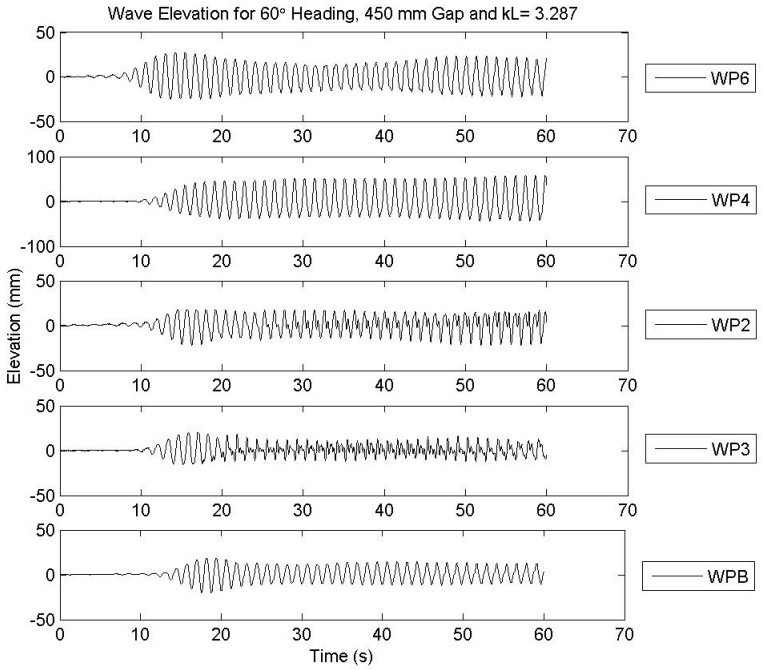
Wave Elevation for 60° Heading, 450 mm Gap and kL= 3.287
WP6
WP4
WP2
WP3
WPB
Elevation (mm)
Time (s)

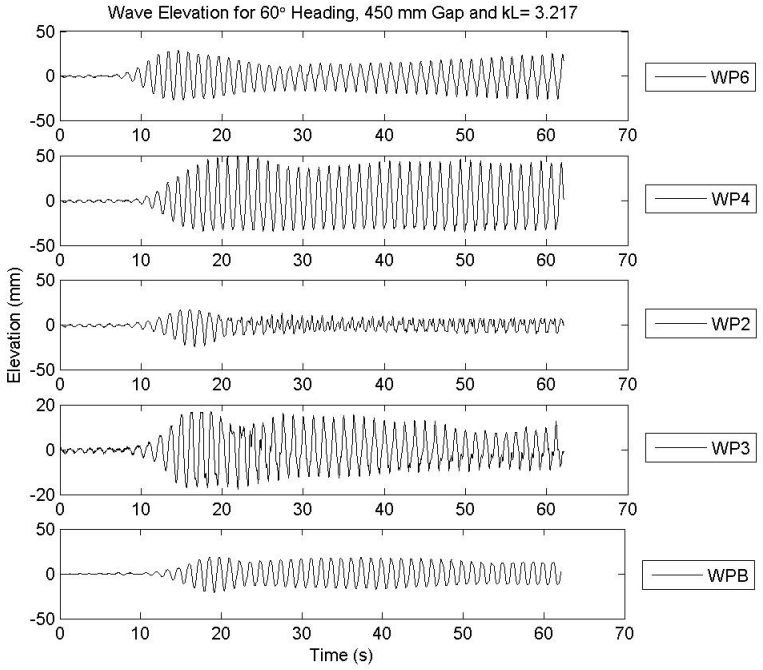
Wave Elevation for 60° Heading, 450 mm Gap and kL= 3.217
WP6
WP4
WP2
WP3
WPB
Elevation (mm)
Time (s)

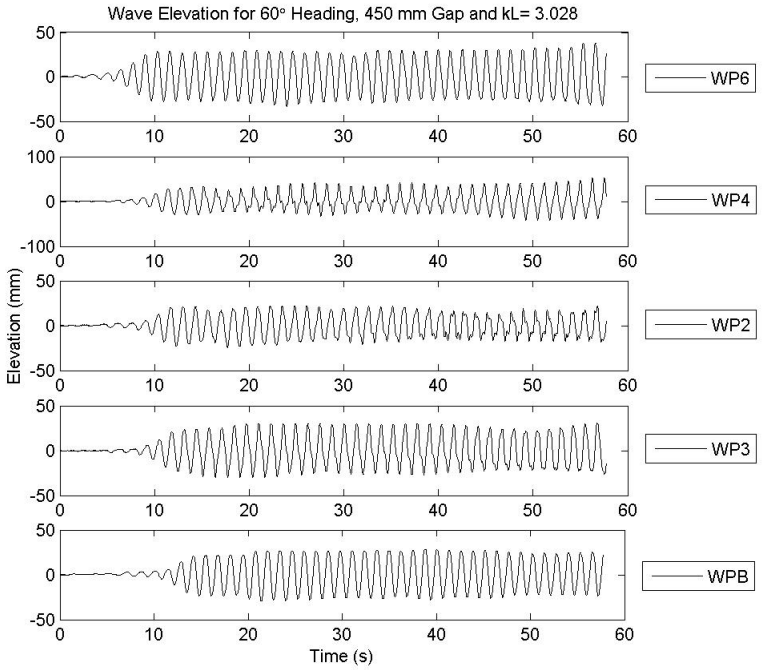
Wave Elevation for 60° Heading, 450 mm Gap and kL= 3.028
WP6
WP4
WP2
WP3
WPB
Elevation (mm)
Time (s)

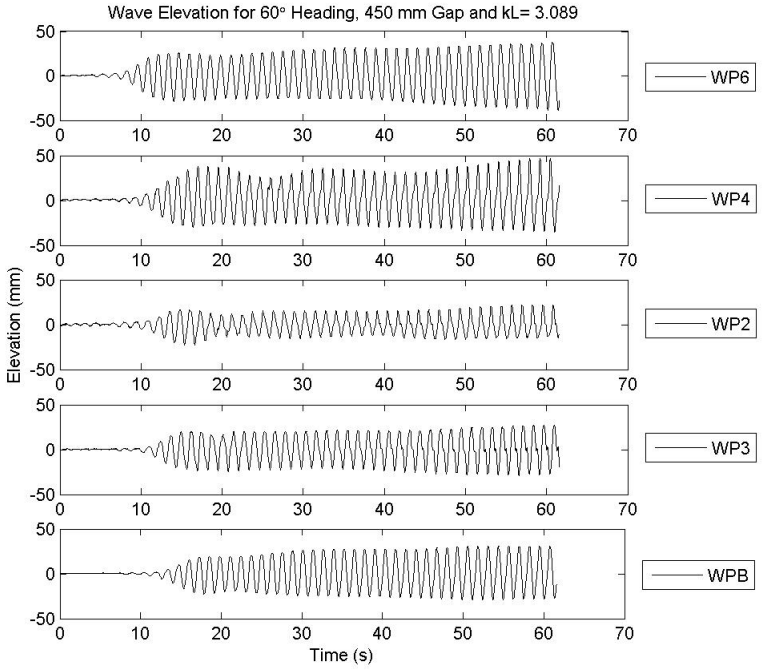
Wave Elevation for 60° Heading, 450 mm Gap and kL= 3.089
Elevation (mm)
Time (s)
WP6
WP4
WP2
WP3
WPB

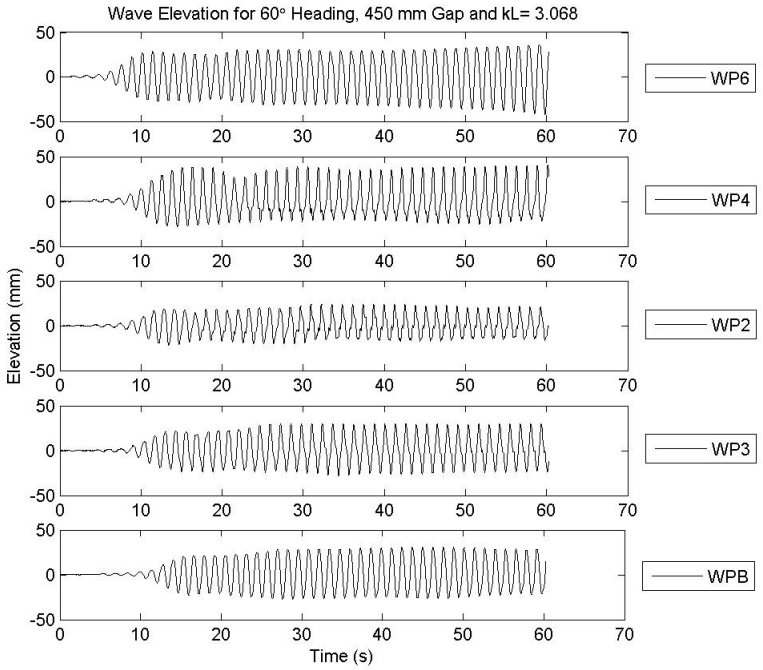
Wave Elevation for 60° Heading, 450 mm Gap and kL= 3.068
Elevation (mm)
Time (s)
WP6
WP4
WP2
WP3
WPB

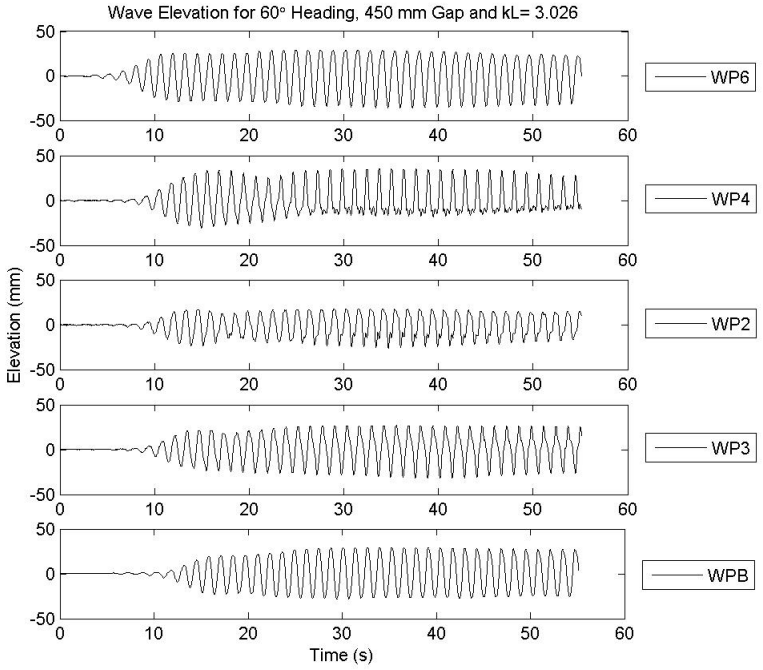
Wave Elevation for 60° Heading, 450 mm Gap and kL= 3.026
Elevation (mm)
Time (s)
WP6
WP4
WP2
WP3
WPB

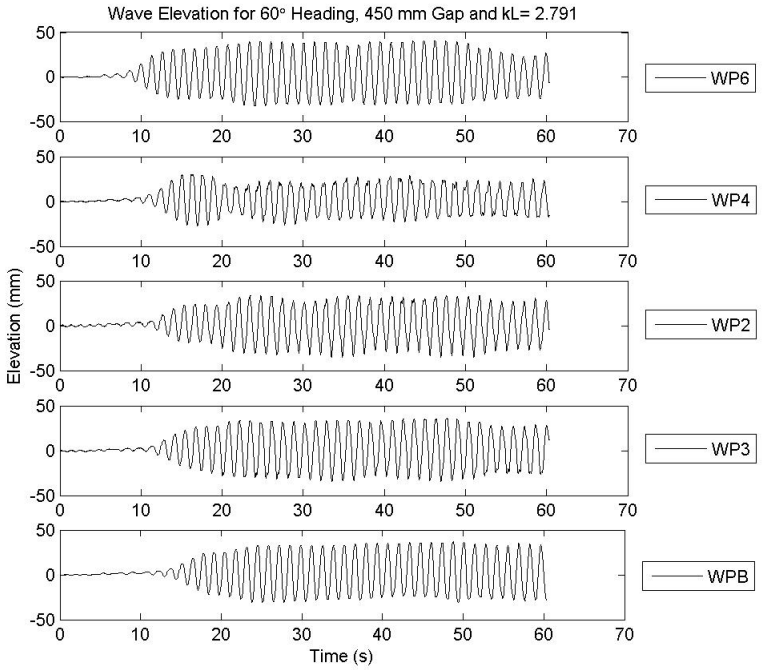
Wave Elevation for 60° Heading, 450 mm Gap and kL= 2.791
Elevation (mm)
Time (s)
WP6
WP4
WP2
WP3
WPB

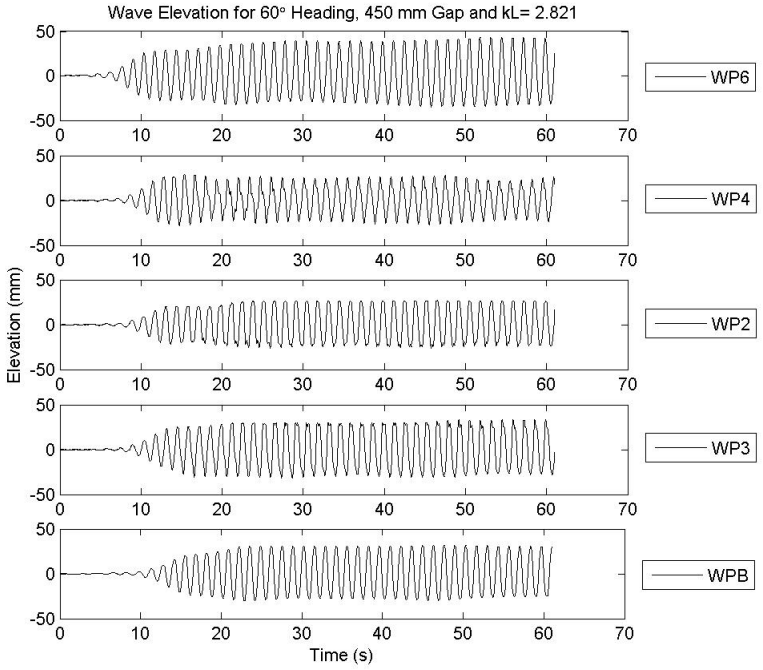
Wave Elevation for 60° Heading, 450 mm Gap and kL= 2.821
WP6
WP4
WP2
WP3
WPB
Elevation (mm)
Time (s)

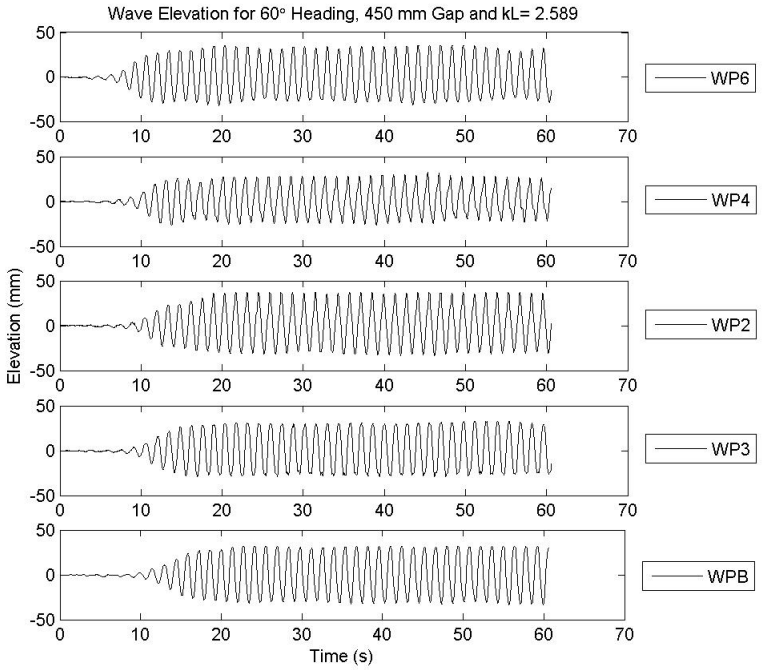
Wave Elevation for 60° Heading, 450 mm Gap and kL= 2.589
WP6
WP4
WP2
WP3
WPB
Elevation (mm)
Time (s)

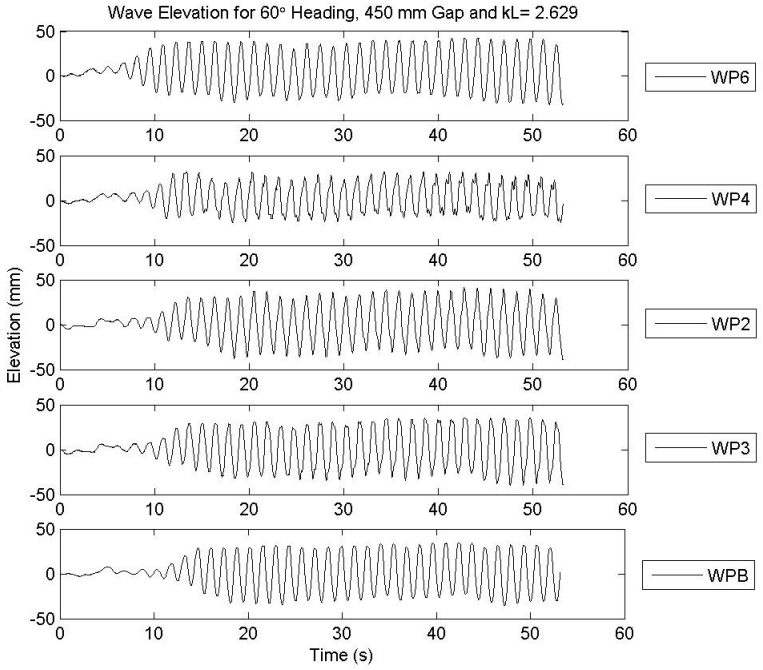
Wave Elevation for 60° Heading, 450 mm Gap and kL= 2.629
Elevation (mm)
Time (s)
WP6
WP4
WP2
WP3
WPB

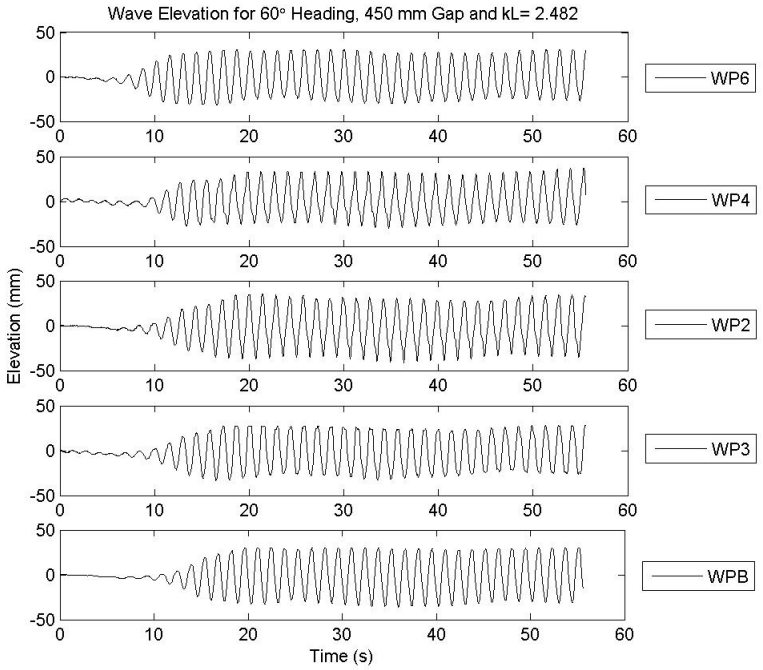
Wave Elevation for 60° Heading, 450 mm Gap and kL= 2.482
Elevation (mm)
Time (s)
WP6
WP4
WP2
WP3
WPB

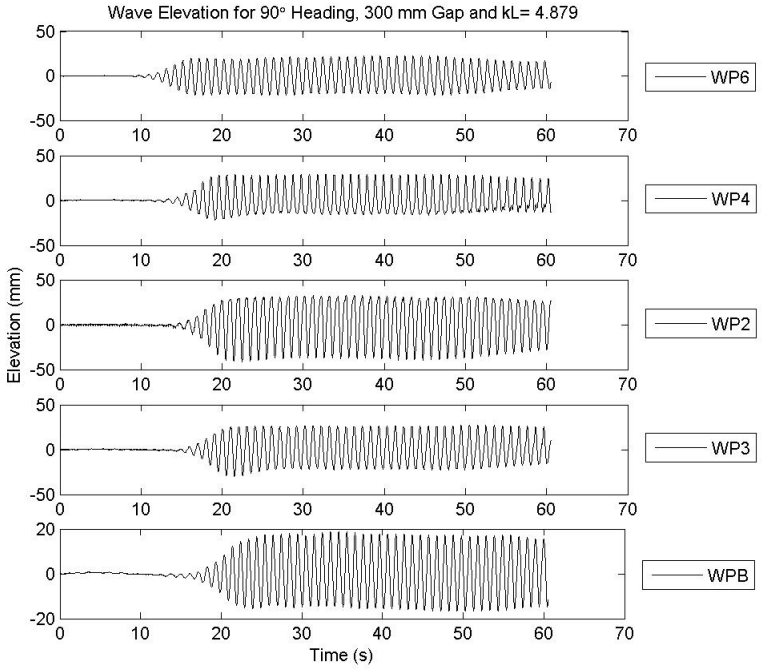
Wave Elevation for 90° Heading, 300 mm Gap and kL= 4.879
WP6
WP4
WP2
WP3
WPB
Elevation (mm)
Time (s)

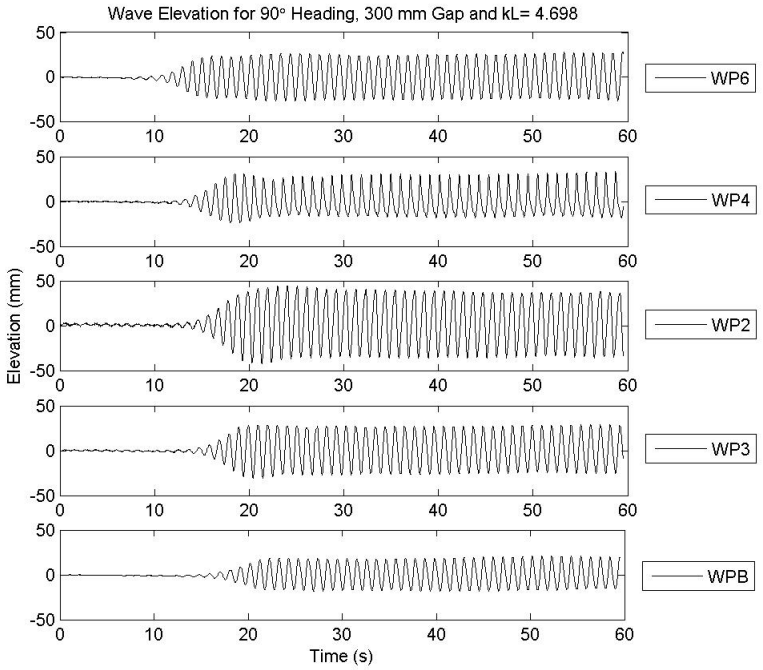
Wave Elevation for 90° Heading, 300 mm Gap and kL= 4.698
WP6
WP4
WP2
WP3
WPB
Elevation (mm)
Time (s)

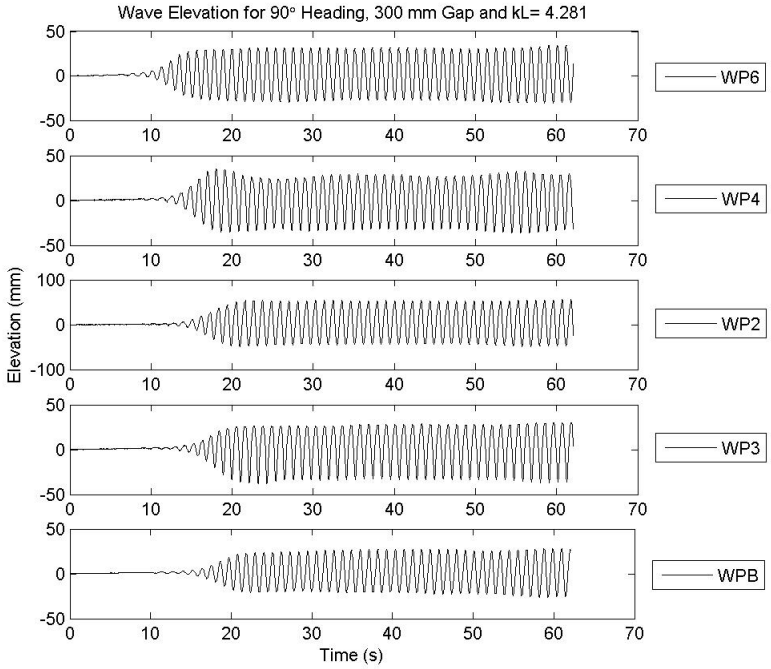
Wave Elevation for 90° Heading, 300 mm Gap and kL= 4.281
WP6
WP4
WP2
WP3
WPB
Elevation (mm)
Time (s)

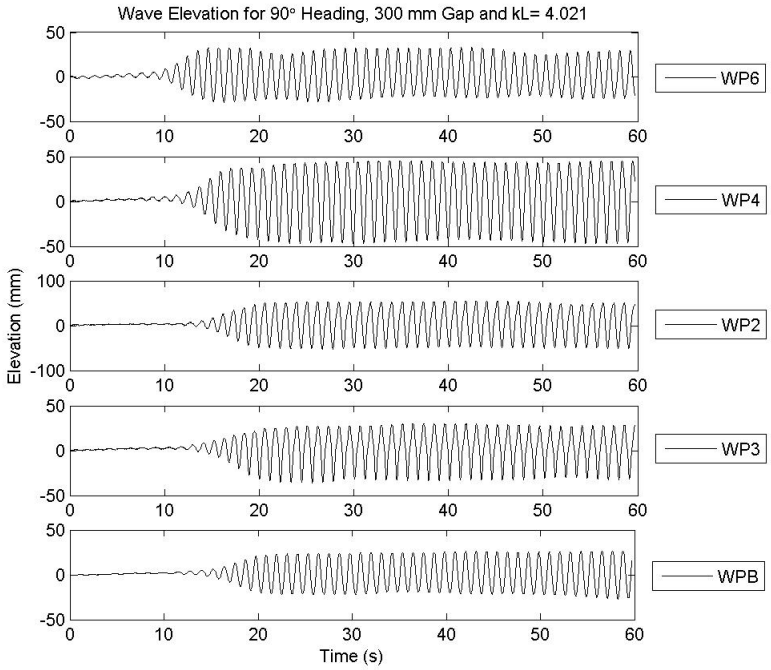
Wave Elevation for 90° Heading, 300 mm Gap and kL= 4.021
WP6
WP4
WP2
WP3
WPB
Elevation (mm)
Time (s)

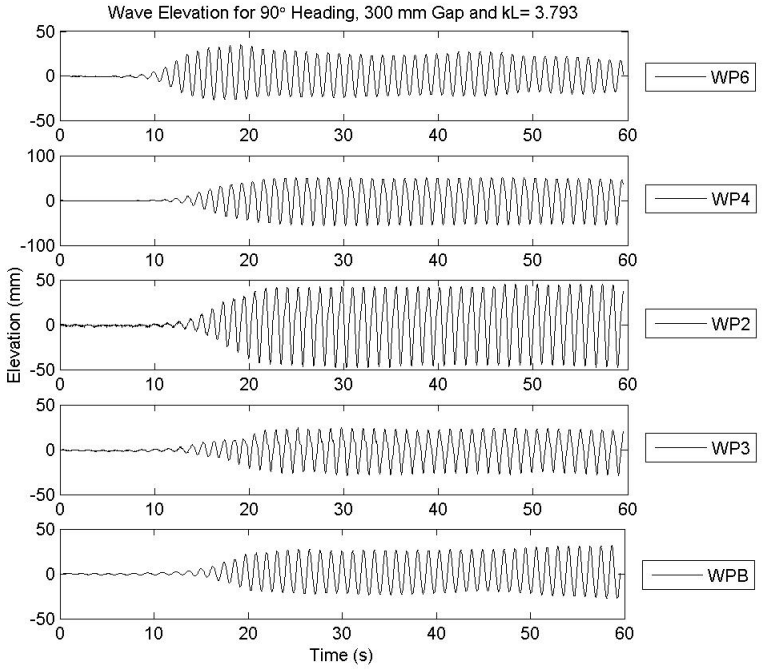
Wave Elevation for 90° Heading, 300 mm Gap and kL= 3.793
WP6
WP4
WP2
WP3
WPB
Elevation (mm)
Time (s)

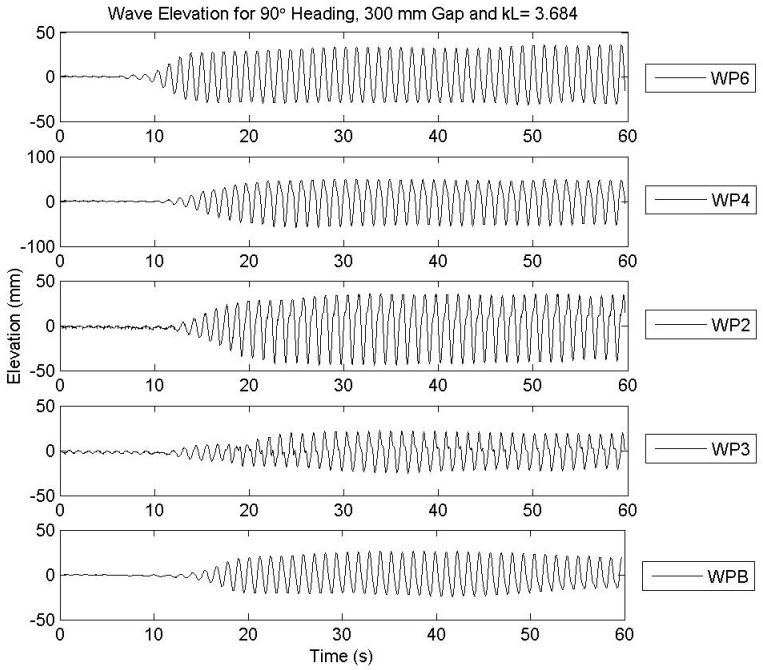
Wave Elevation for 90° Heading, 300 mm Gap and kL= 3.684
WP6
WP4
WP2
WP3
WPB
Elevation (mm)
Time (s)

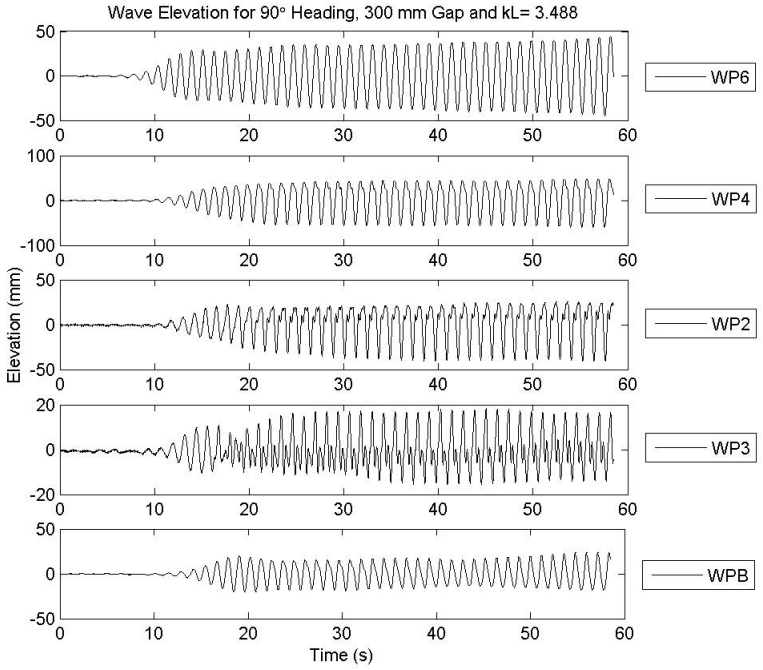
Wave Elevation for 90° Heading, 300 mm Gap and kL= 3.488
WP6
WP4
WP2
WP3
WPB
Elevation (mm)
Time (s)

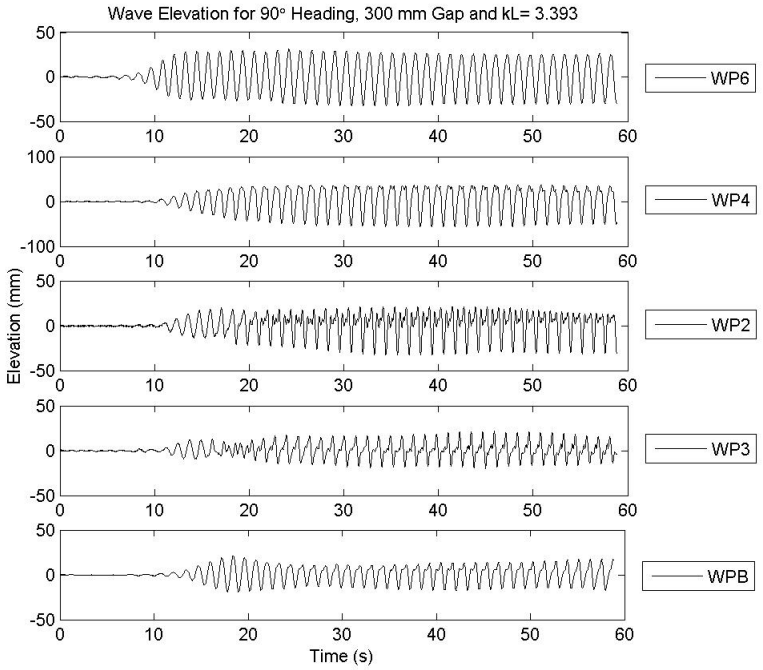
Wave Elevation for 90° Heading, 300 mm Gap and kL= 3.393
WP6
WP4
WP2
WP3
WPB
Elevation (mm)
Time (s)

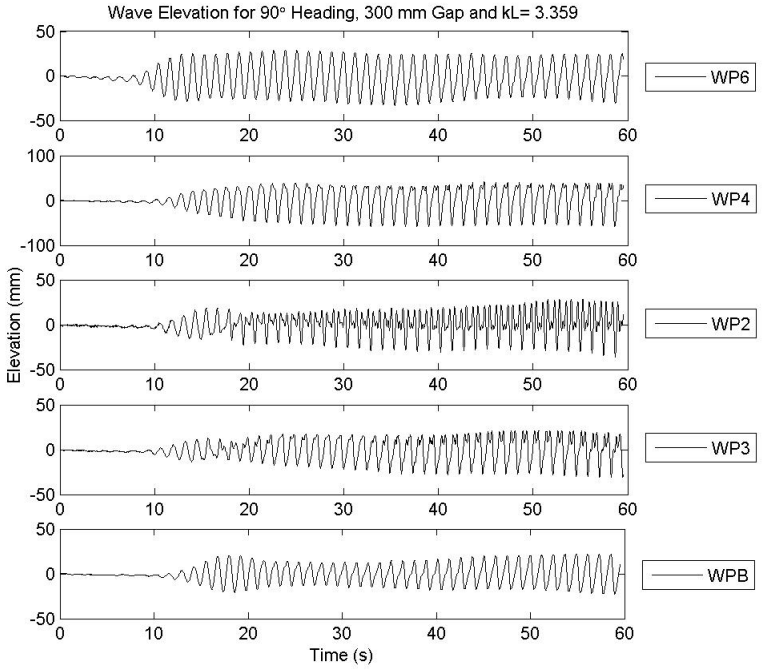
Wave Elevation for 90° Heading, 300 mm Gap and kL= 3.359
WP6
WP4
WP2
WP3
WPB
Elevation (mm)
Time (s)

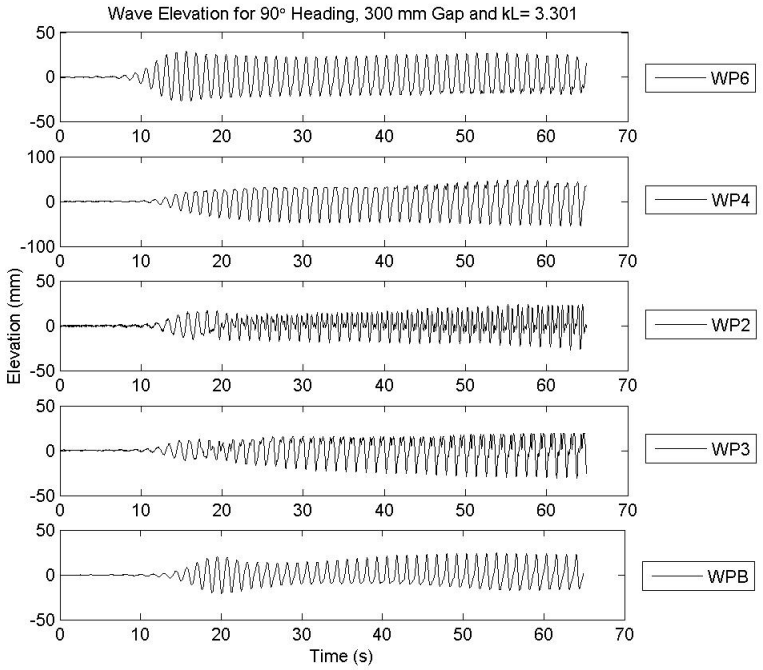
Wave Elevation for 90° Heading, 300 mm Gap and kL= 3.301
WP6
WP4
WP2
WP3
WPB
Elevation (mm)
Time (s)

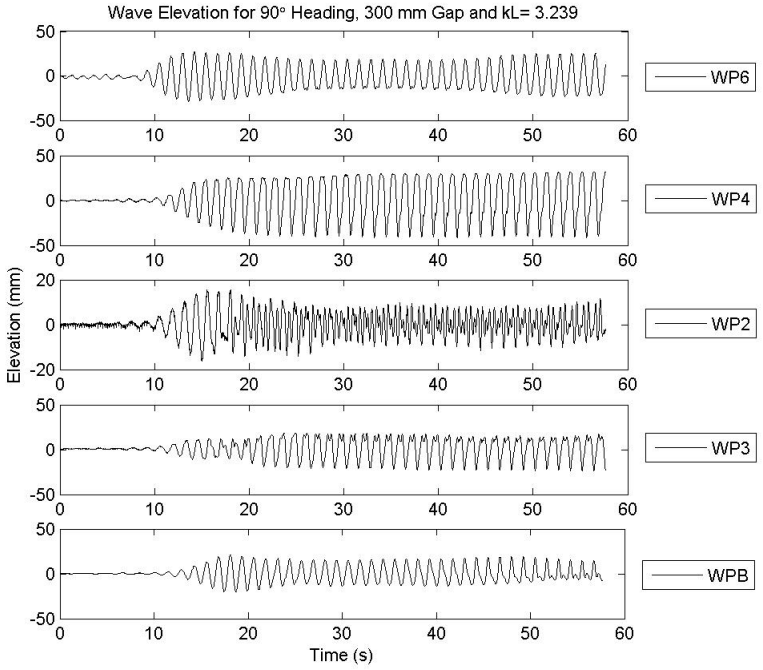
Wave Elevation for 90° Heading, 300 mm Gap and kL= 3.239
WP6
WP4
WP2
WP3
WPB
Elevation (mm)
Time (s)

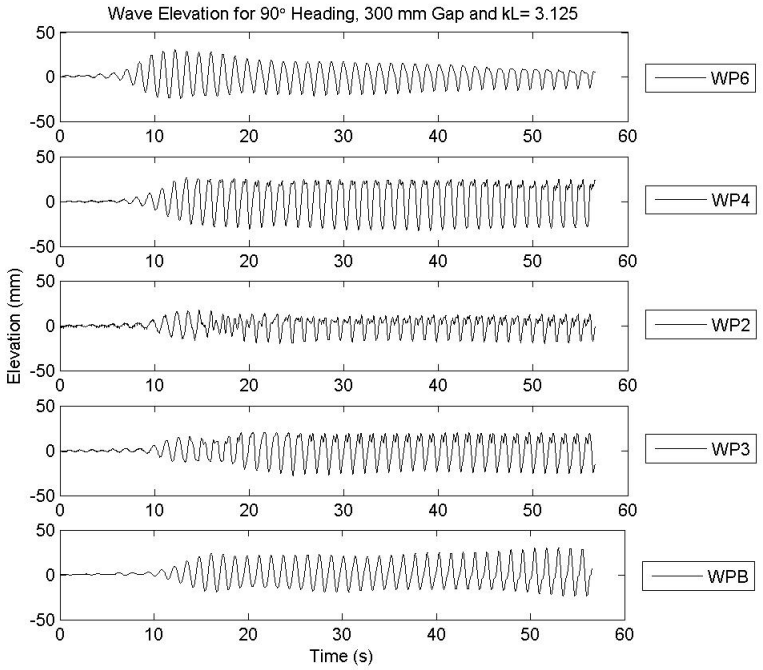
Wave Elevation for 90° Heading, 300 mm Gap and kL= 3.125
WP6
WP4
WP2
WP3
WPB
Elevation (mm)
Time (s)

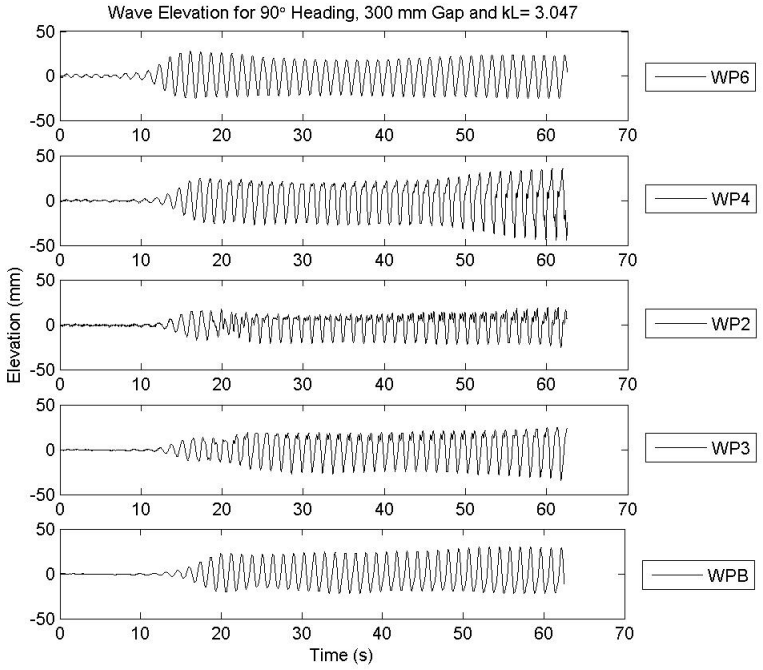
Wave Elevation for 90° Heading, 300 mm Gap and kL= 3.047
Elevation (mm)
Time (s)
WP6
WP4
WP2
WP3
WPB

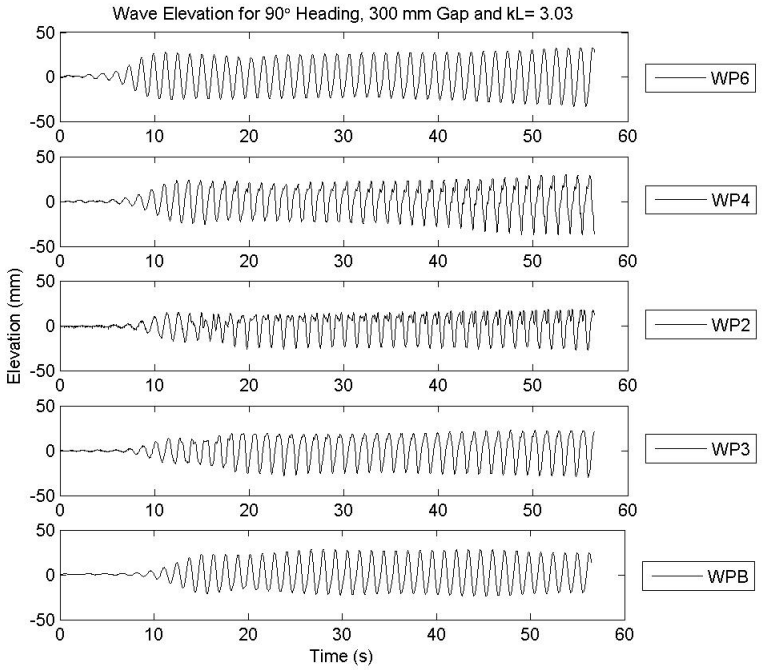
Wave Elevation for 90° Heading, 300 mm Gap and kL= 3.03
Elevation (mm)
Time (s)
WP6
WP4
WP2
WP3
WPB

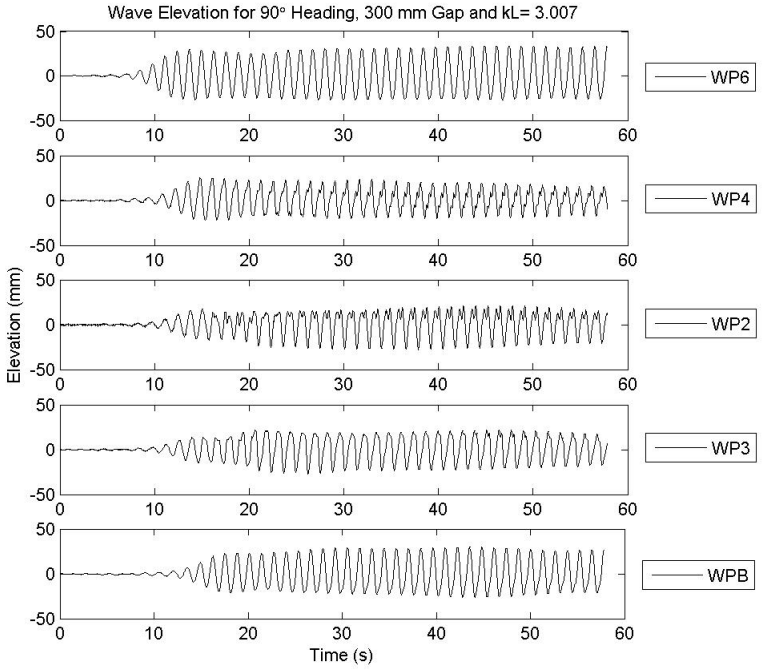
Wave Elevation for 90° Heading, 300 mm Gap and kL= 3.007
WP6
WP4
WP2
WP3
WPB
Elevation (mm)
Time (s)

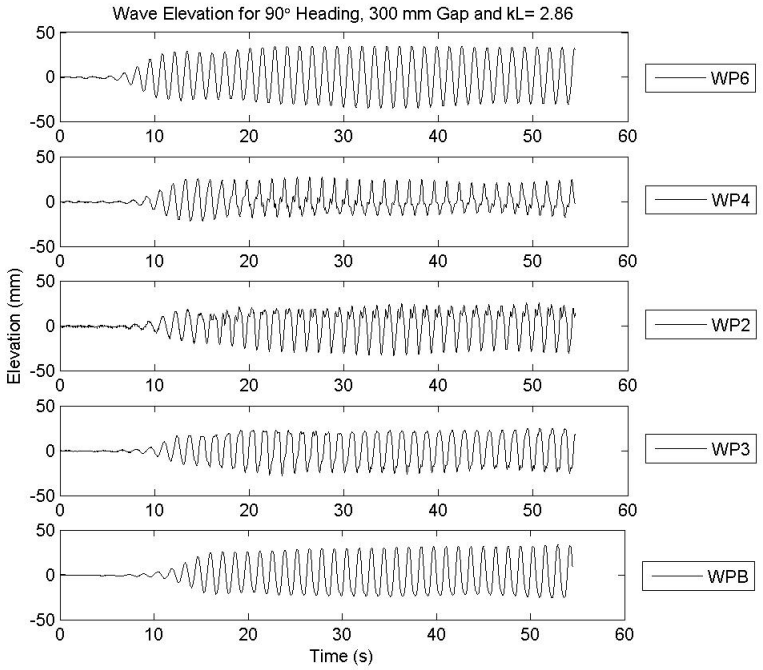
Wave Elevation for 90° Heading, 300 mm Gap and kL= 2.86
WP6
WP4
WP2
WP3
WPB
Elevation (mm)
Time (s)

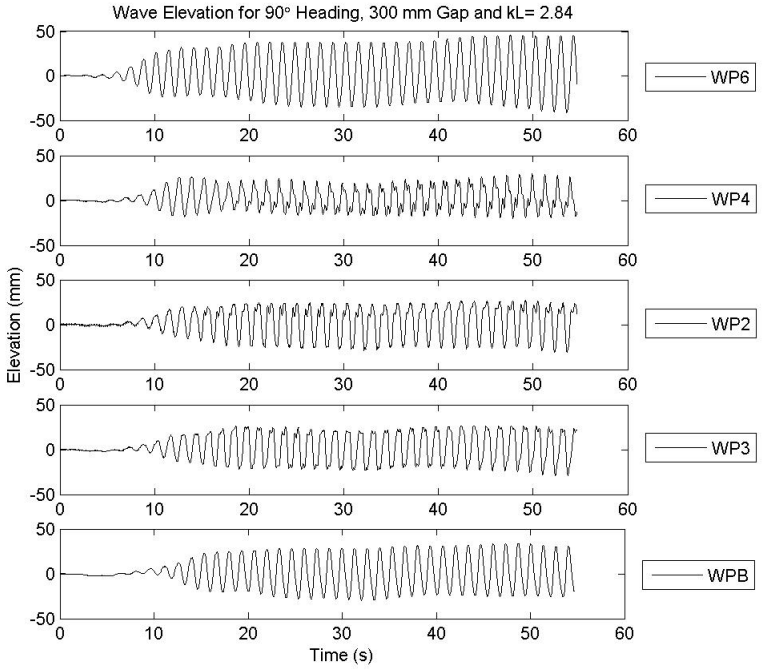
Wave Elevation for 90° Heading, 300 mm Gap and kL= 2.84
WP6
WP4
WP2
WP3
WPB
Elevation (mm)
Time (s)

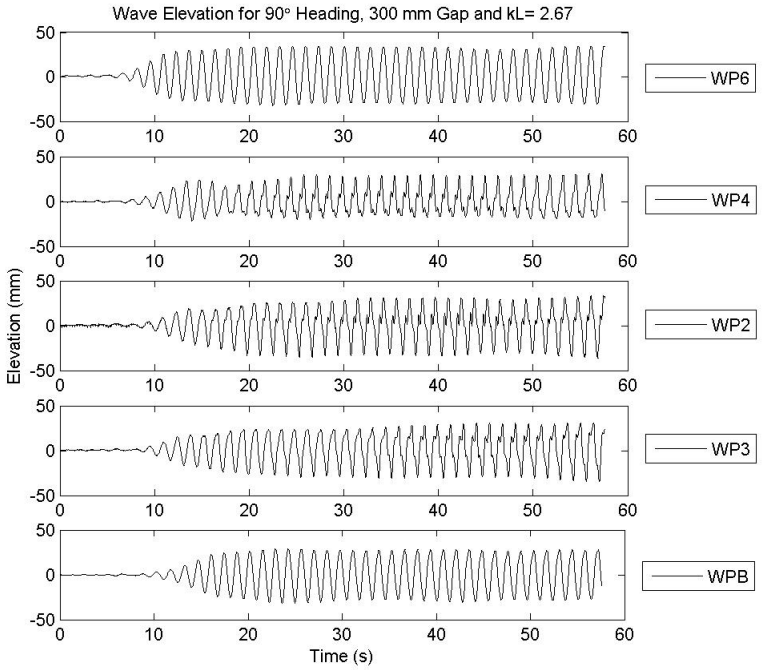
Wave Elevation for 90° Heading, 300 mm Gap and kL= 2.67
WP6
WP4
WP2
WP3
WPB
Elevation (mm)
Time (s)

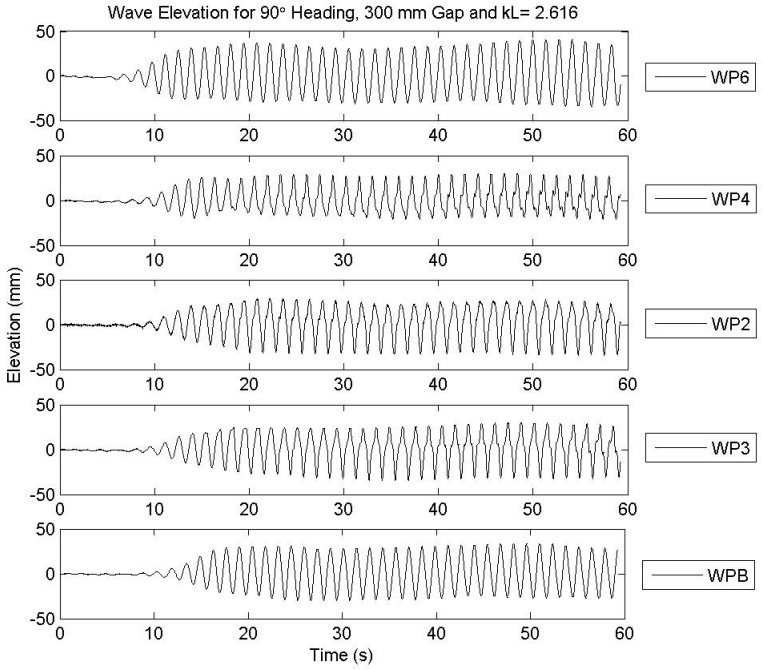
Wave Elevation for 90° Heading, 300 mm Gap and kL= 2.616
Elevation (mm)
Time (s)
WP6
WP4
WP2
WP3
WPB

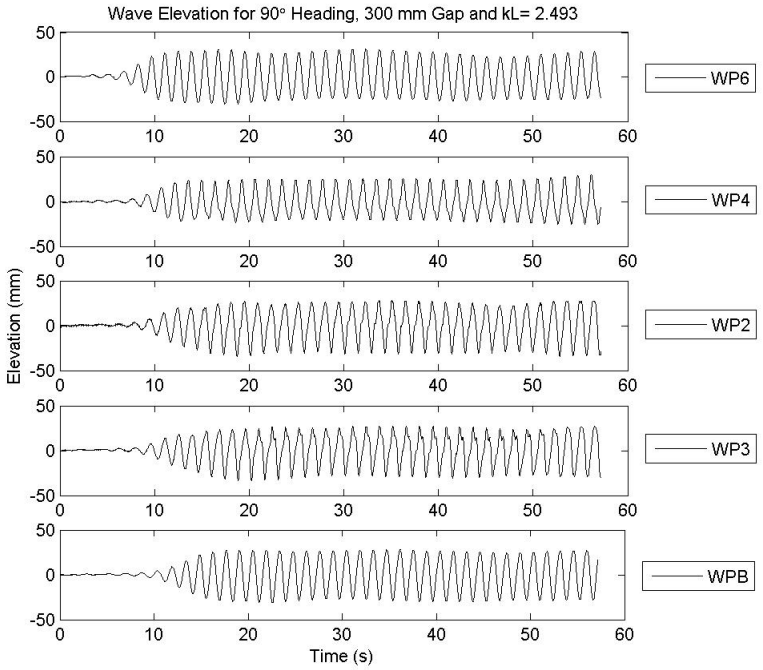
Wave Elevation for 90° Heading, 300 mm Gap and kL= 2.493
Elevation (mm)
Time (s)
WP6
WP4
WP2
WP3
WPB

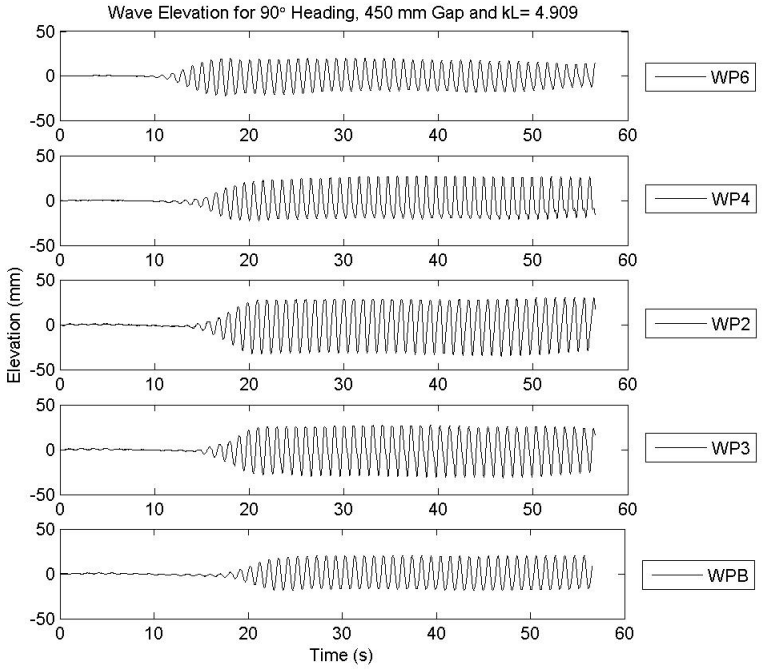
Wave Elevation for 90° Heading, 450 mm Gap and kL= 4.909
Elevation (mm)
Time (s)
WP6
WP4
WP2
WP3
WPB

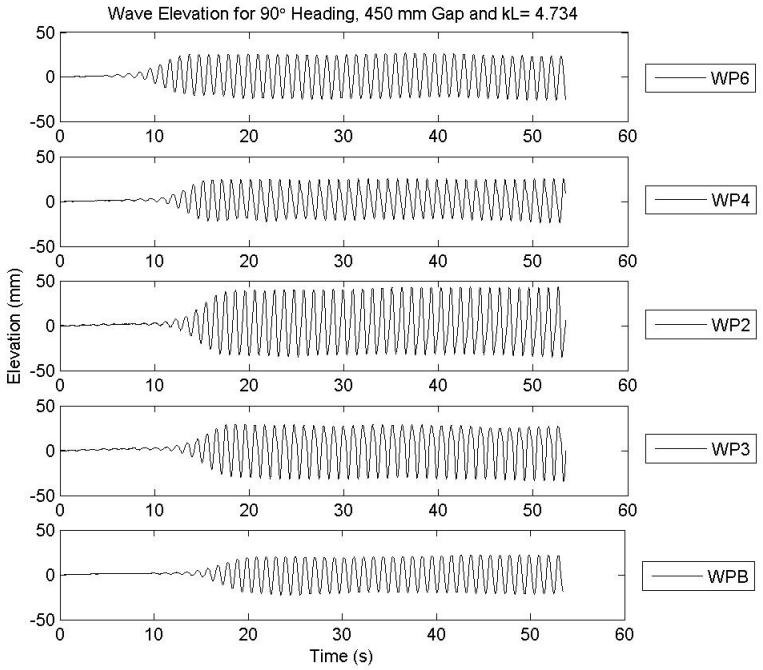
Wave Elevation for 90° Heading, 450 mm Gap and kL= 4.734
Elevation (mm)
Time (s)
WP6
WP4
WP2
WP3
WPB

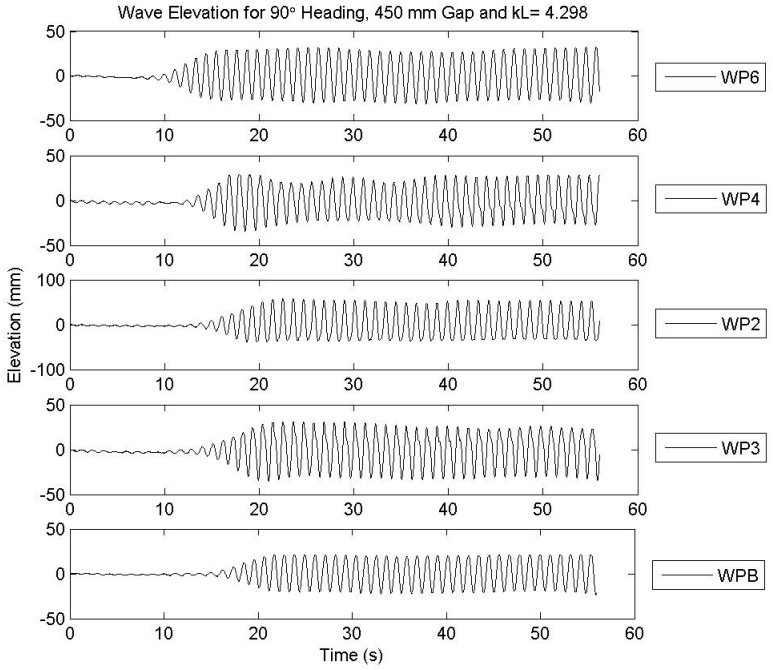
Wave Elevation for 90° Heading, 450 mm Gap and kL= 4.298
WP6
WP4
WP2
WP3
WPB
Elevation (mm)
Time (s)

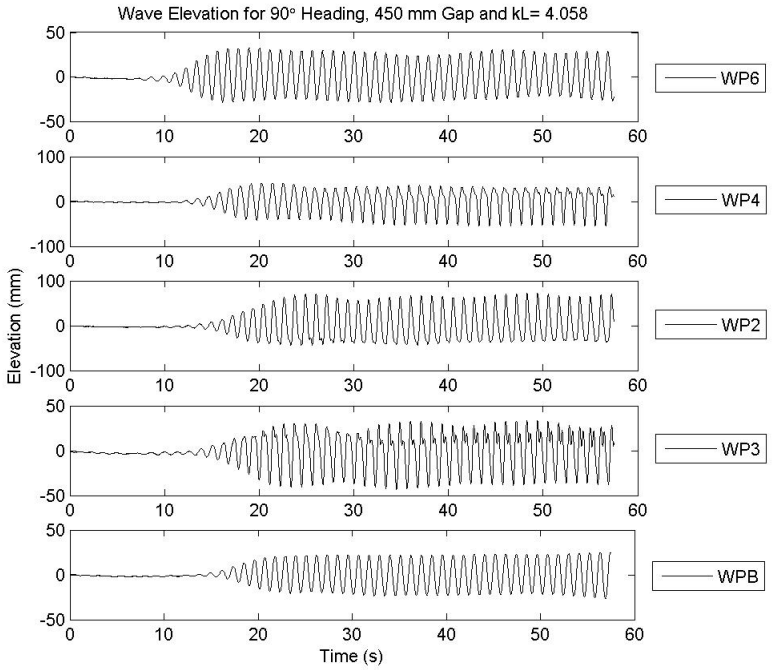
Wave Elevation for 90° Heading, 450 mm Gap and kL= 4.058
WP6
WP4
WP2
WP3
WPB
Elevation (mm)
Time (s)

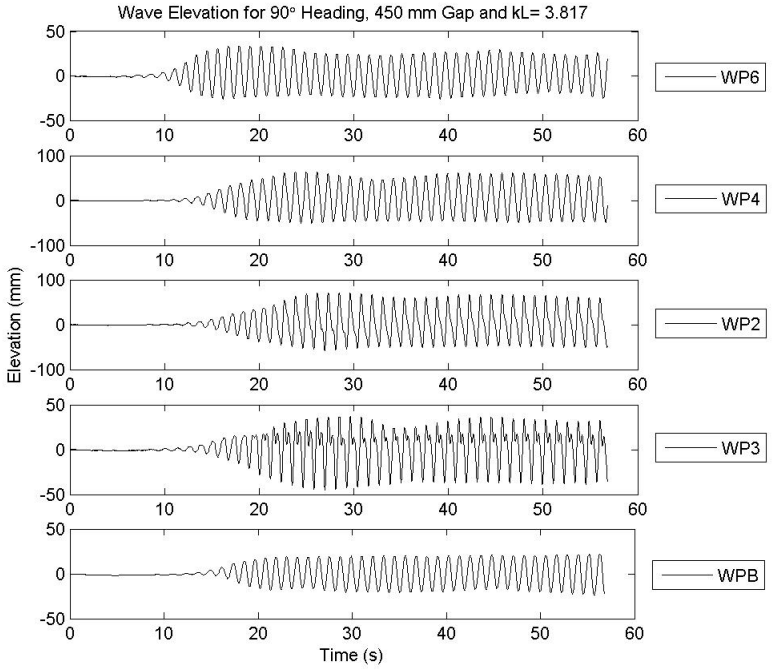
Wave Elevation for 90° Heading, 450 mm Gap and kL= 3.817
WP6
WP4
WP2
WP3
WPB
Elevation (mm)
Time (s)

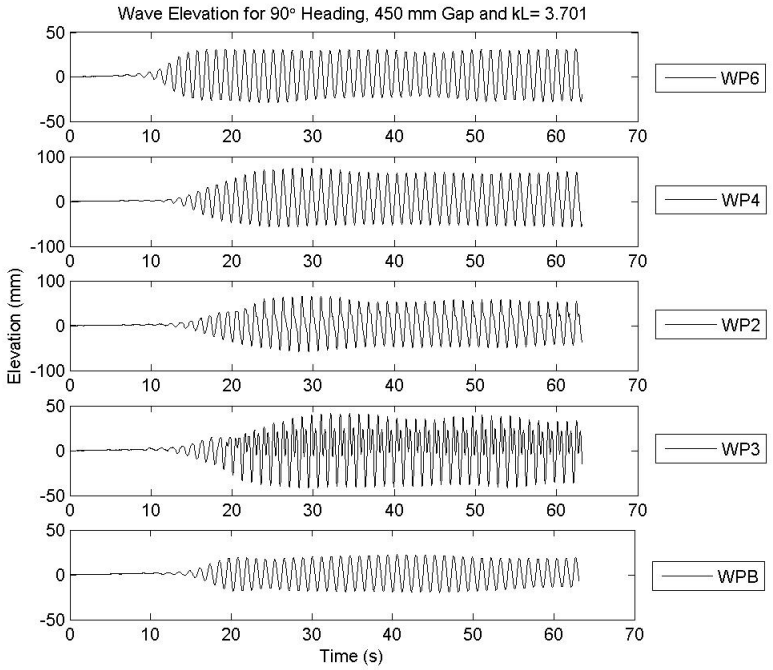
Wave Elevation for 90° Heading, 450 mm Gap and kL= 3.701
WP6
WP4
WP2
WP3
WPB
Elevation (mm)
Time (s)

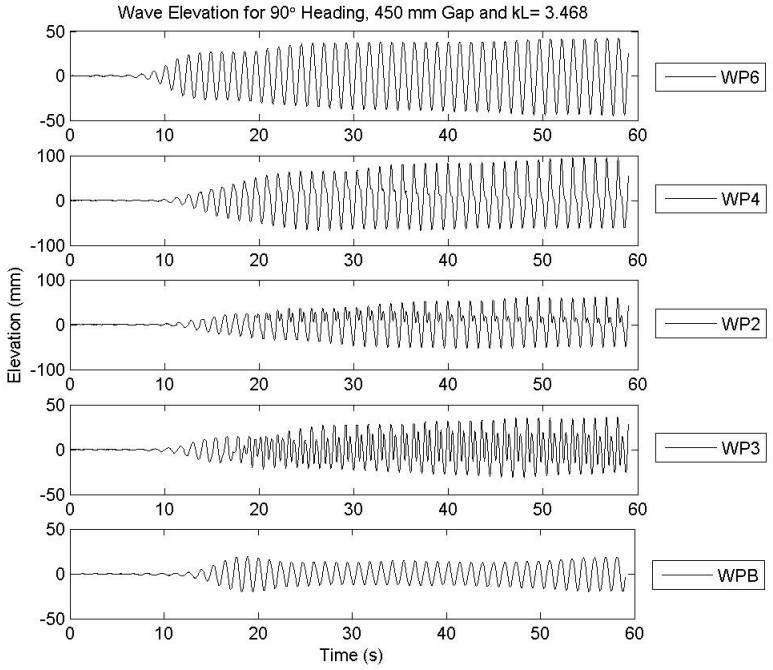
Wave Elevation for 90° Heading, 450 mm Gap and kL= 3.468
WP6
WP4
WP2
WP3
WPB
Elevation (mm)
Time (s)

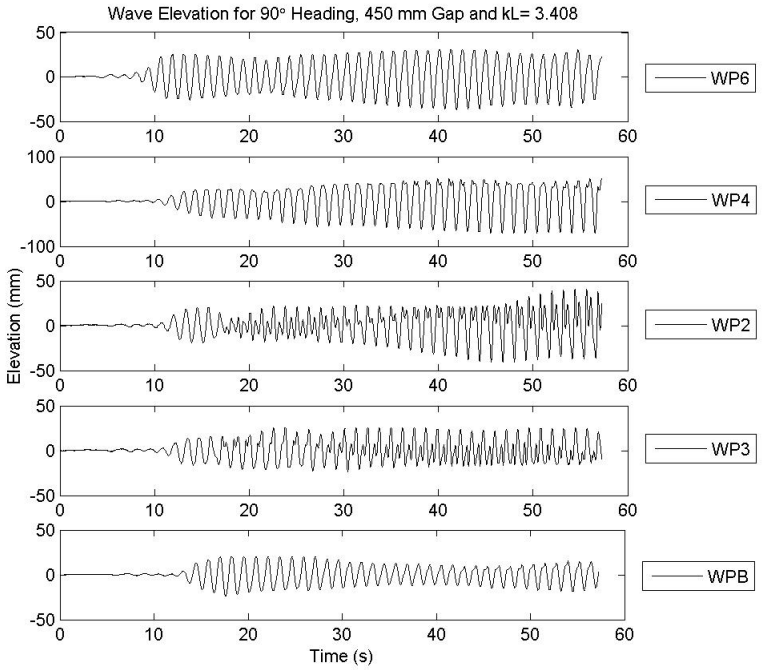
Wave Elevation for 90° Heading, 450 mm Gap and kL= 3.408
WP6
WP4
WP2
WP3
WPB
Elevation (mm)
Time (s)

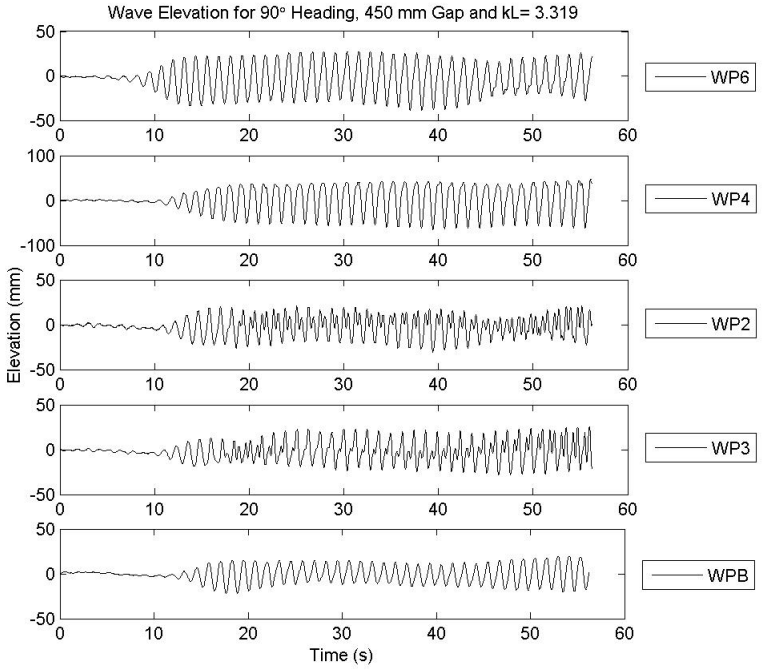
Wave Elevation for 90° Heading, 450 mm Gap and kL= 3.319
WP6
WP4
WP2
WP3
WPB
Elevation (mm)
Time (s)

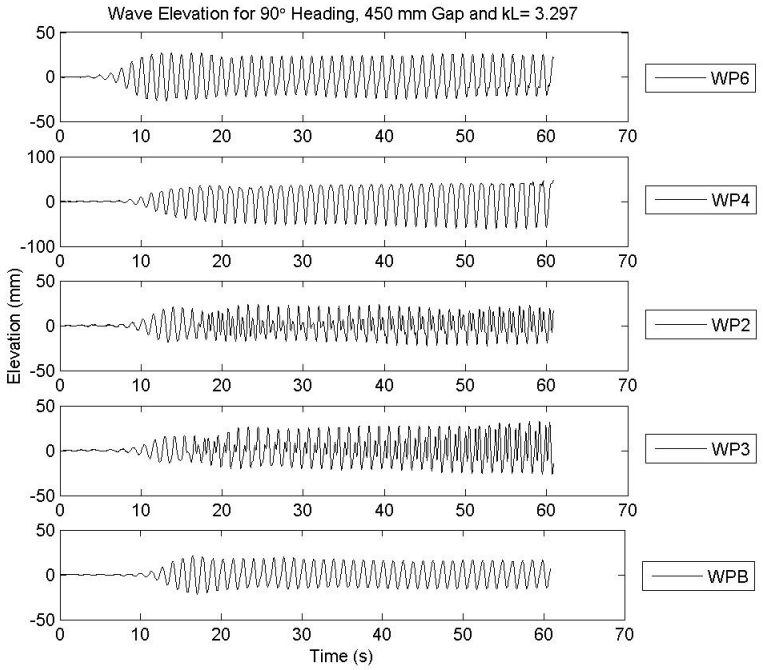
Wave Elevation for 90° Heading, 450 mm Gap and kL= 3.297
WP6
WP4
WP2
WP3
WPB
Elevation (mm)
Time (s)

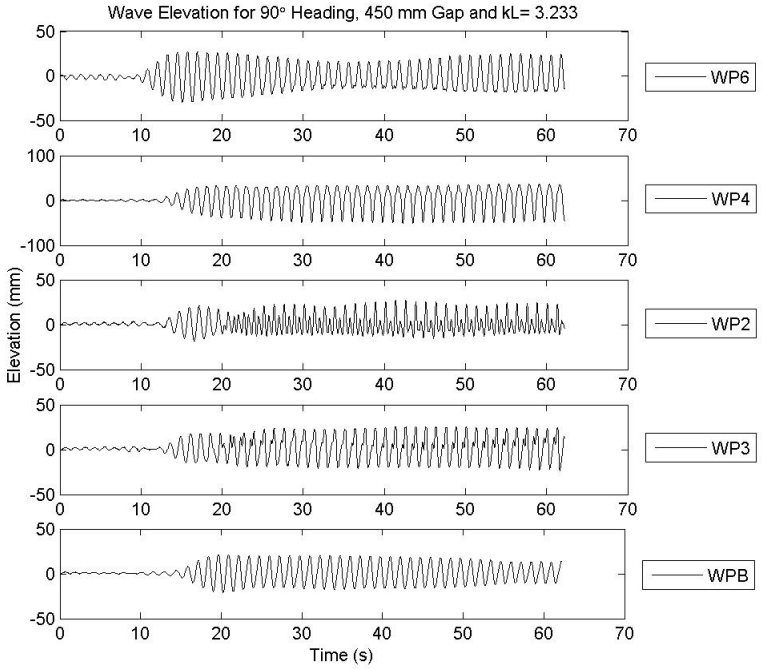
Wave Elevation for 90° Heading, 450 mm Gap and kL= 3.233
WP6
WP4
WP2
WP3
WPB
Elevation (mm)
Time (s)

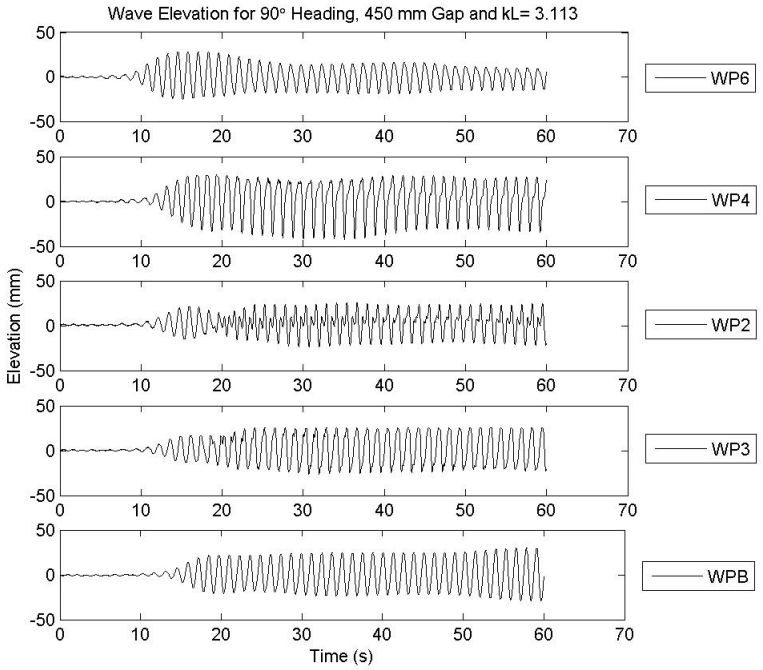
Wave Elevation for 90° Heading, 450 mm Gap and kL= 3.113
WP6
WP4
WP2
WP3
WPB
Elevation (mm)
Time (s)

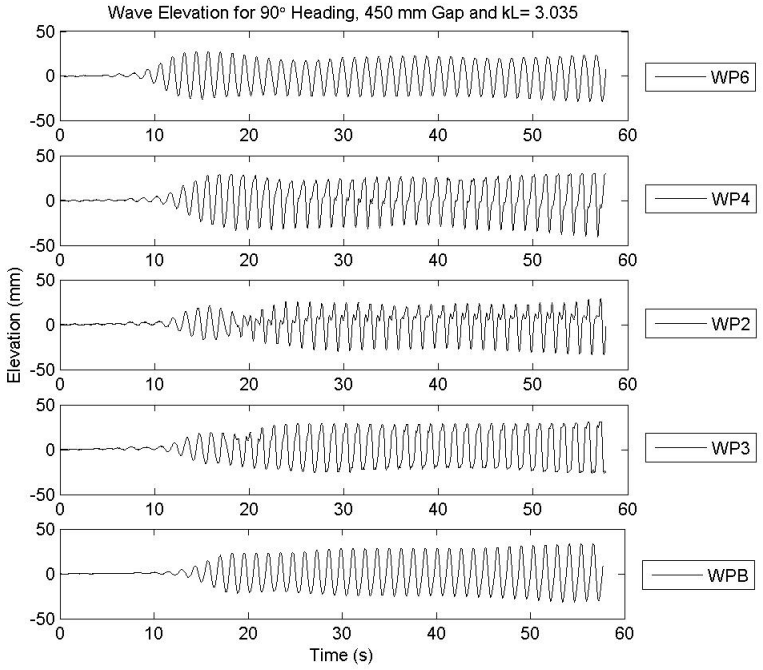
Wave Elevation for 90° Heading, 450 mm Gap and kL= 3.035
Elevation (mm)
Time (s)
WP6
WP4
WP2
WP3
WPB

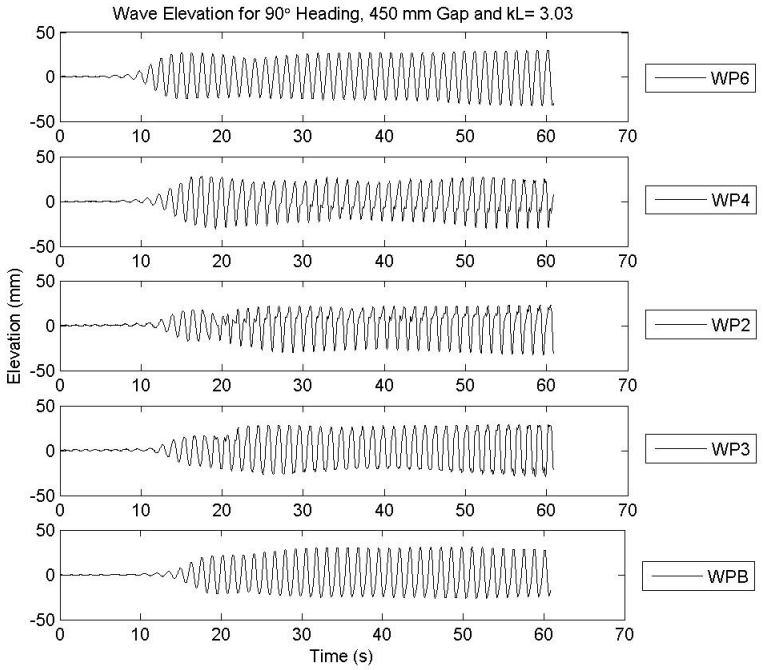
Wave Elevation for 90° Heading, 450 mm Gap and kL= 3.03
Elevation (mm)
Time (s)
WP6
WP4
WP2
WP3
WPB

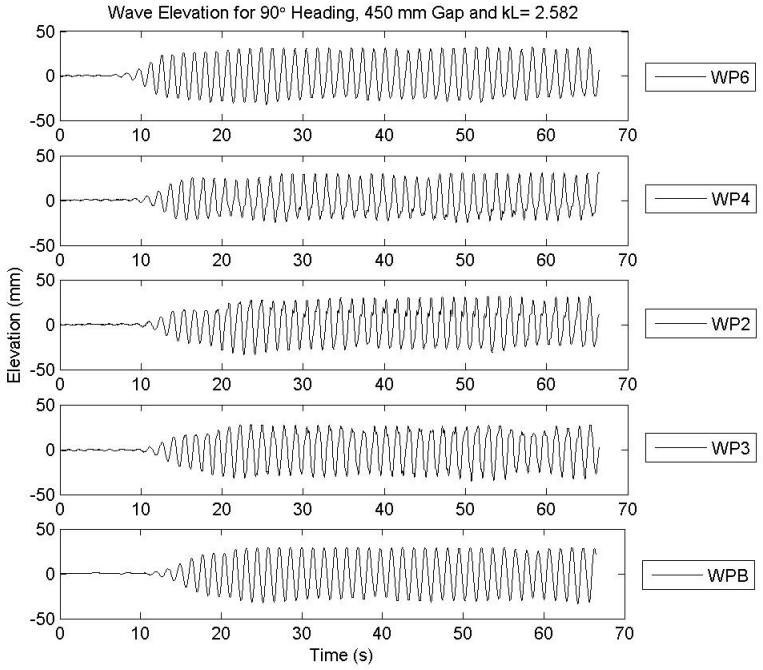
Wave Elevation for 90° Heading, 450 mm Gap and kL= 2.582
WP6
WP4
WP2
WP3
WPB
Elevation (mm)
Time (s)

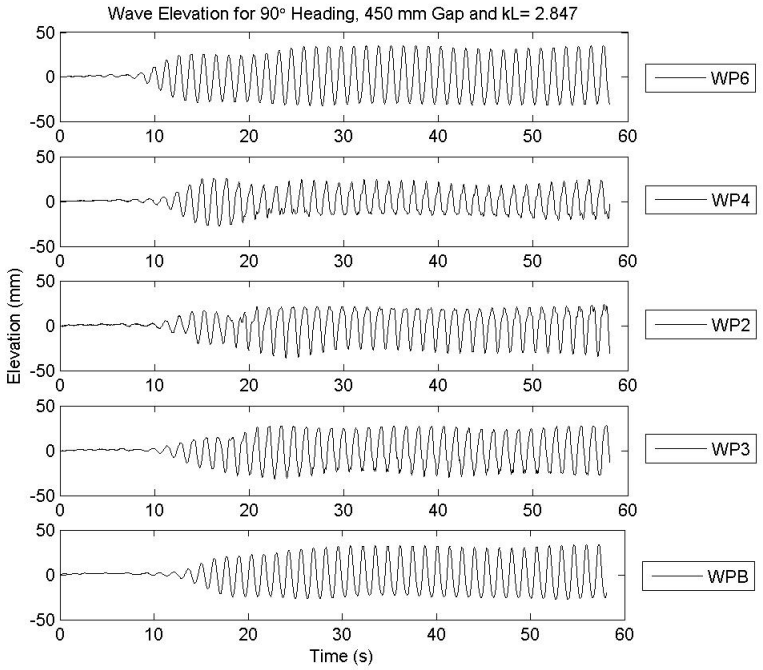
Wave Elevation for 90° Heading, 450 mm Gap and kL= 2.847
WP6
WP4
WP2
WP3
WPB
Elevation (mm)
Time (s)

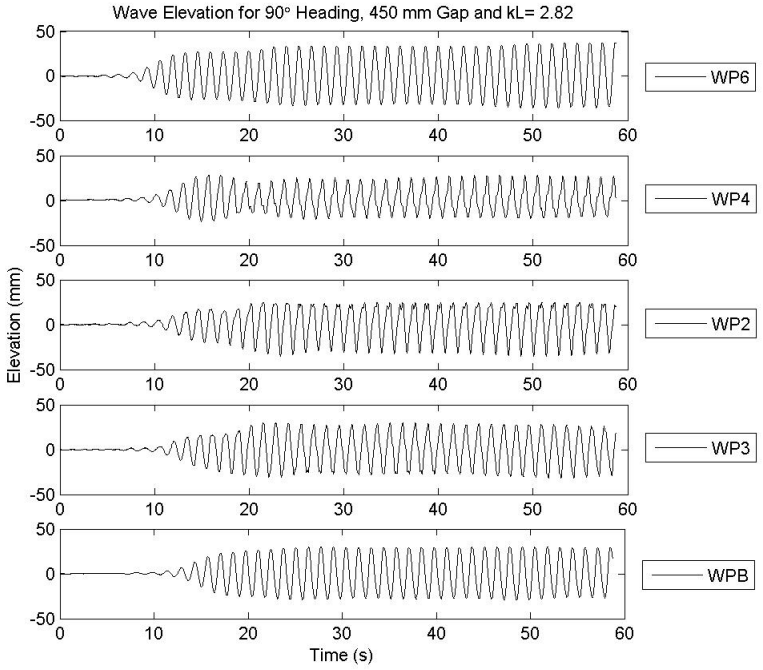
Wave Elevation for 90° Heading, 450 mm Gap and kL= 2.82
Elevation (mm)
Time (s)
WP6
WP4
WP2
WP3
WPB

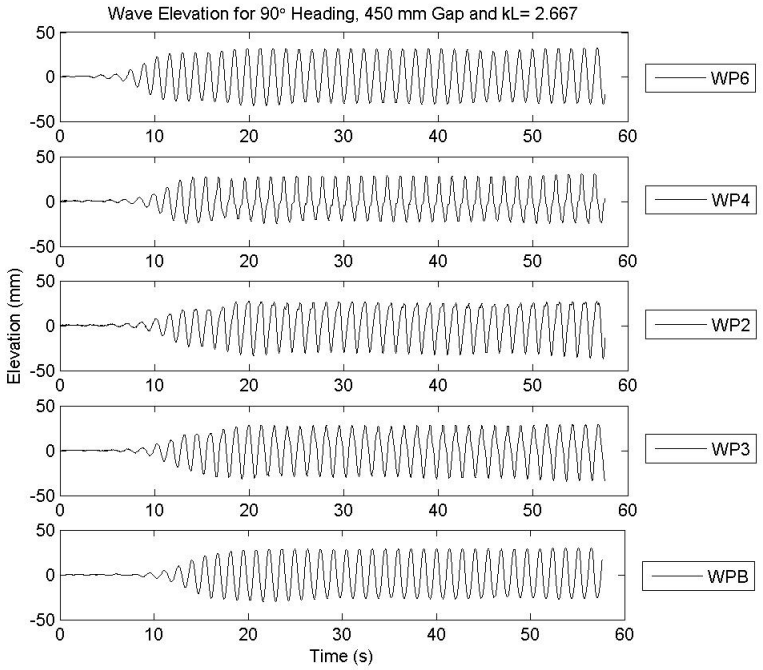
Wave Elevation for 90° Heading, 450 mm Gap and kL= 2.667
Elevation (mm)
Time (s)
WP6
WP4
WP2
WP3
WPB

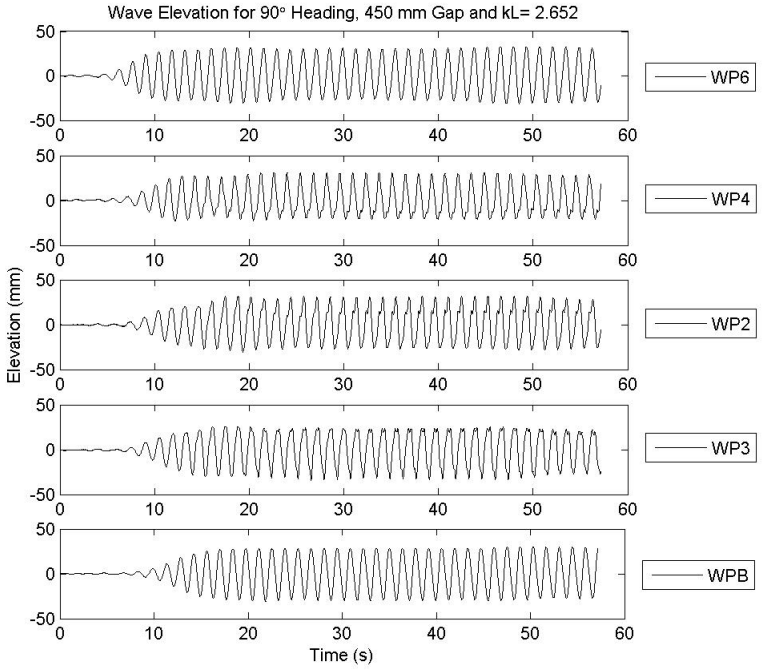
Wave Elevation for 90° Heading, 450 mm Gap and kL= 2.652
WP6
WP4
WP2
WP3
WPB
Elevation (mm)
Time (s)

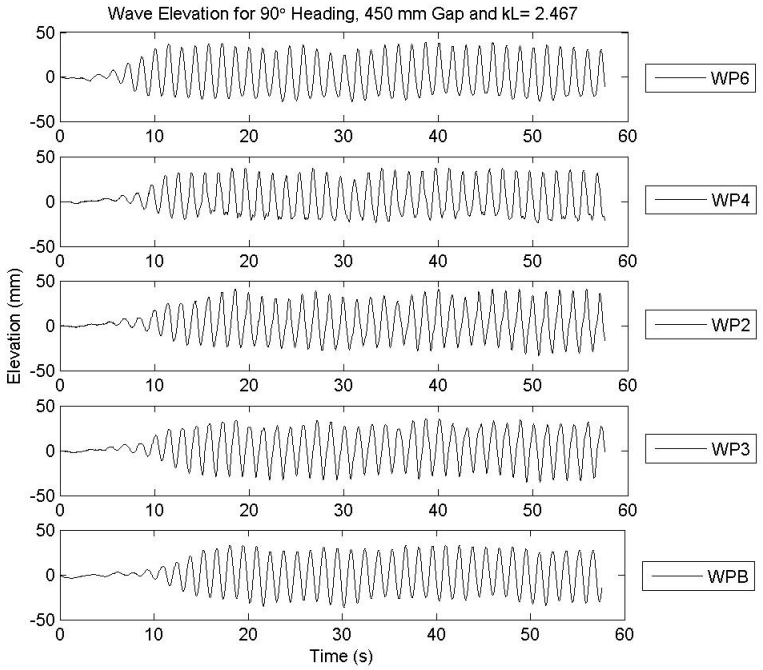
Wave Elevation for 90° Heading, 450 mm Gap and kL= 2.467
WP6
WP4
WP2
WP3
WPB
Elevation (mm)
Time (s)

Appendix B

Body Motions

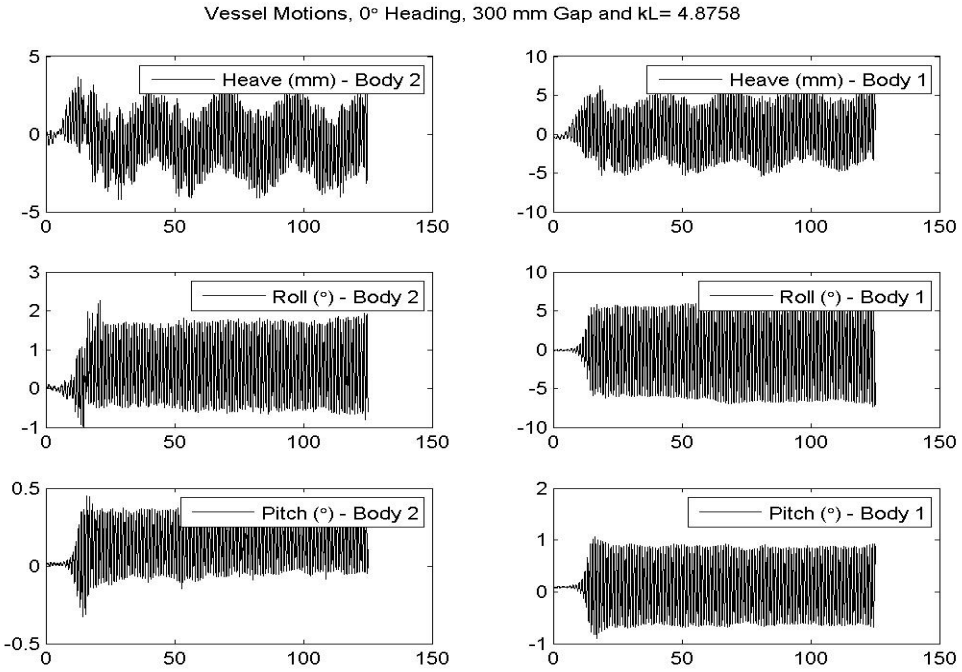

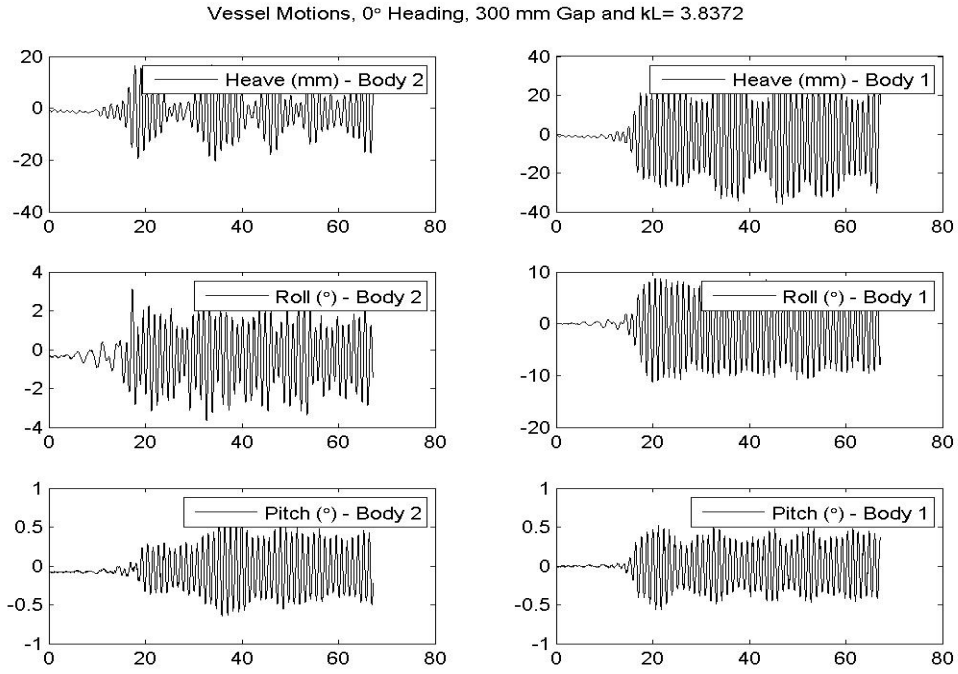
Vessel Motions, 0° Heading, 300 mm Gap and kL= 3.8372
Heave (mm) - Body 2
Heave (mm) - Body 1
Roll (°) - Body 2
Roll (°) - Body 1
Pitch (°) - Body 2
Pitch (°) - Body 1

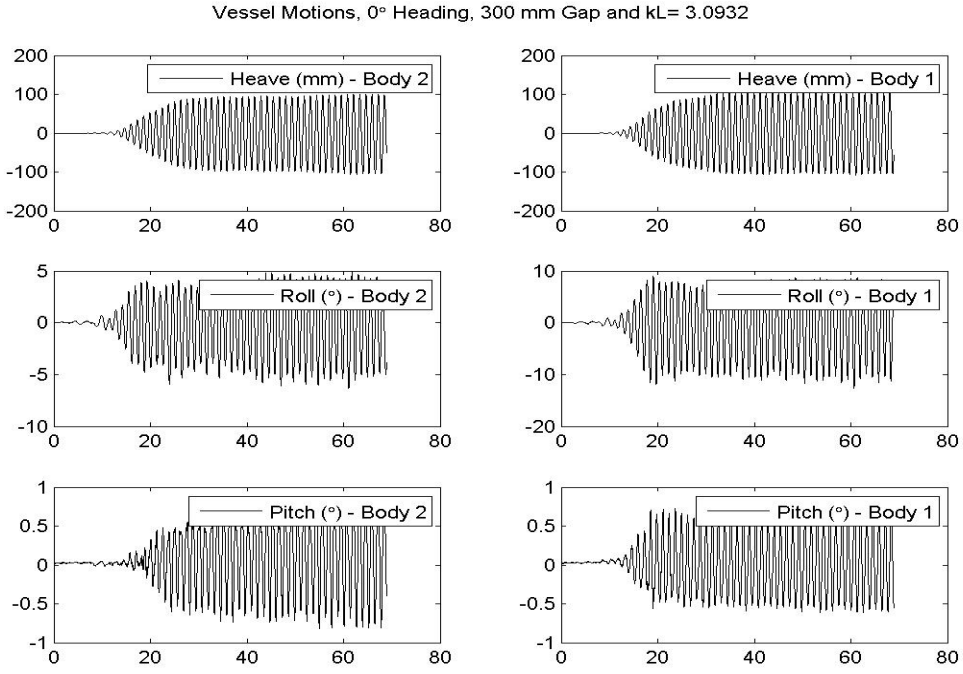
Vessel Motions, 0° Heading, 300 mm Gap and kL= 3.0932
Heave (mm) - Body 2
Heave (mm) - Body 1
Roll (°) - Body 2
Roll (°) - Body 1
Pitch (°) - Body 2
Pitch (°) - Body 1

Vessel Motions, 0° Heading, 300 mm Gap and kL= 2.7996

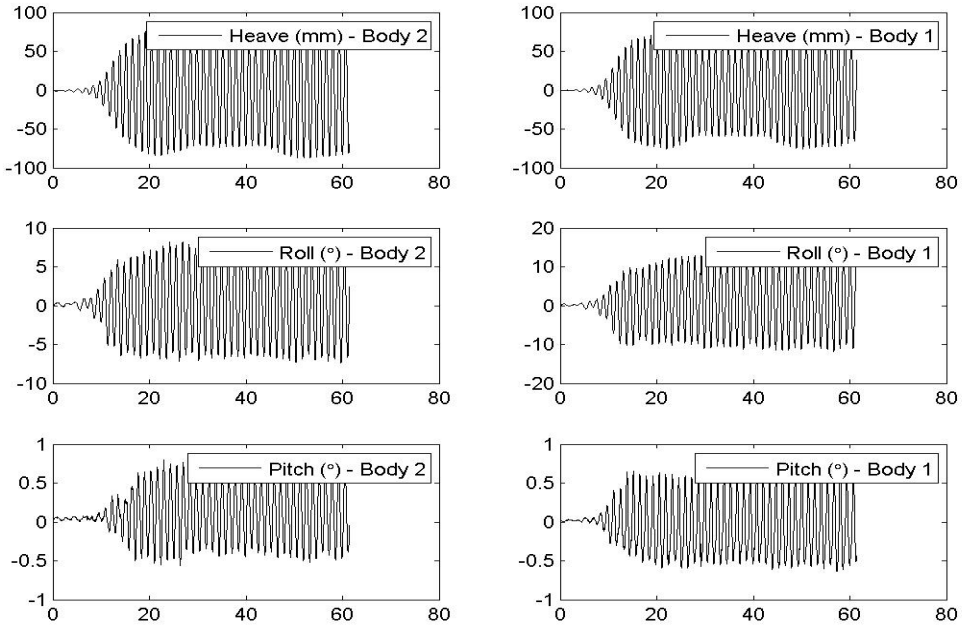

Vessel Motions, 0° Heading, 300 mm Gap and kL= 3.6941

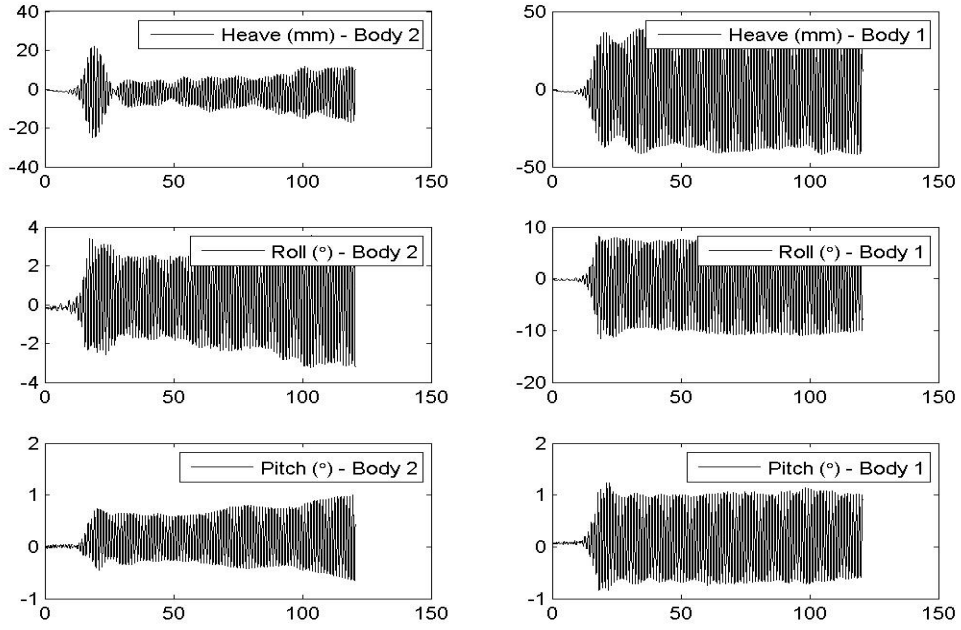

Vessel Motions, 0° Heading, 300 mm Gap and kL= 3.5045

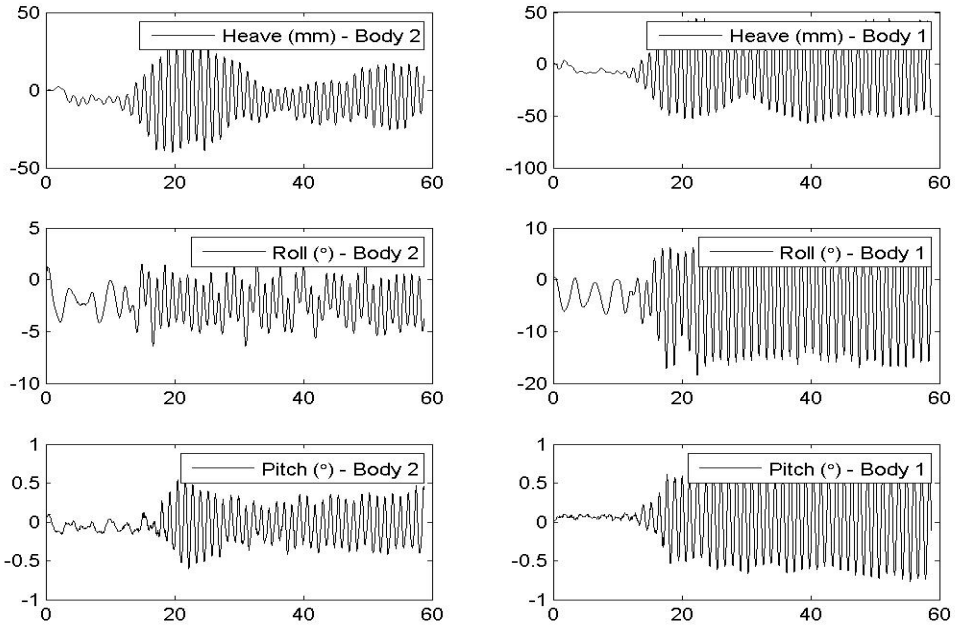

Vessel Motions, 0° Heading, 300 mm Gap and kL= 2.4895

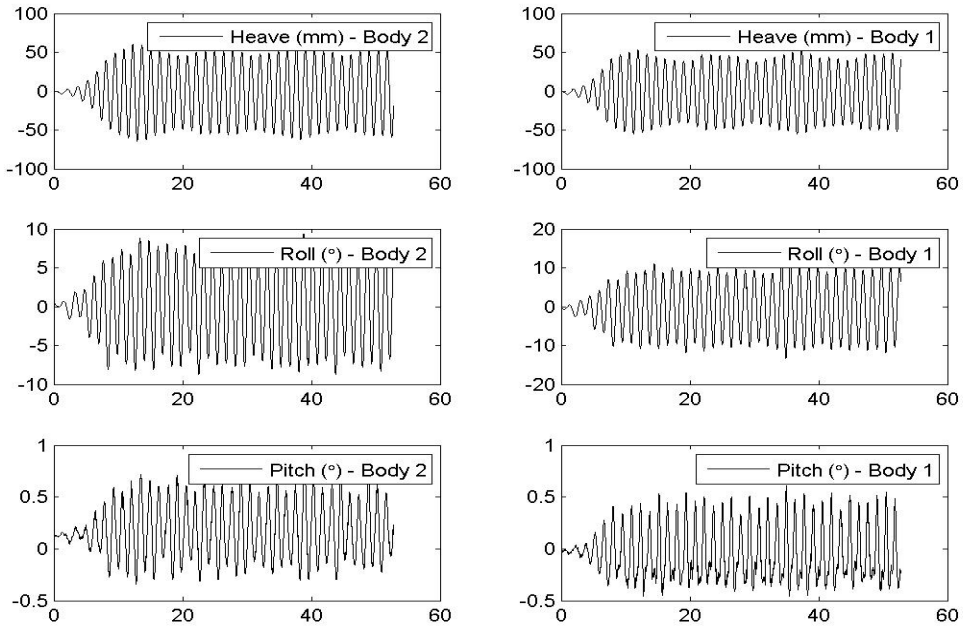

Vessel Motions, 0° Heading, 300 mm Gap and kL= 3.3304

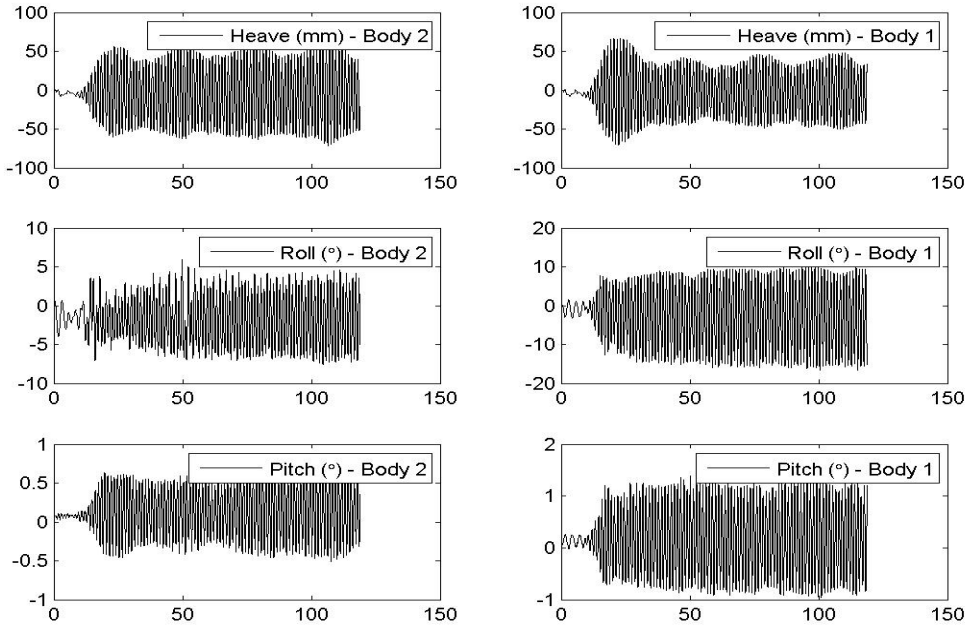

Vessel Motions, 0° Heading, 300 mm Gap and kL= 3.2524

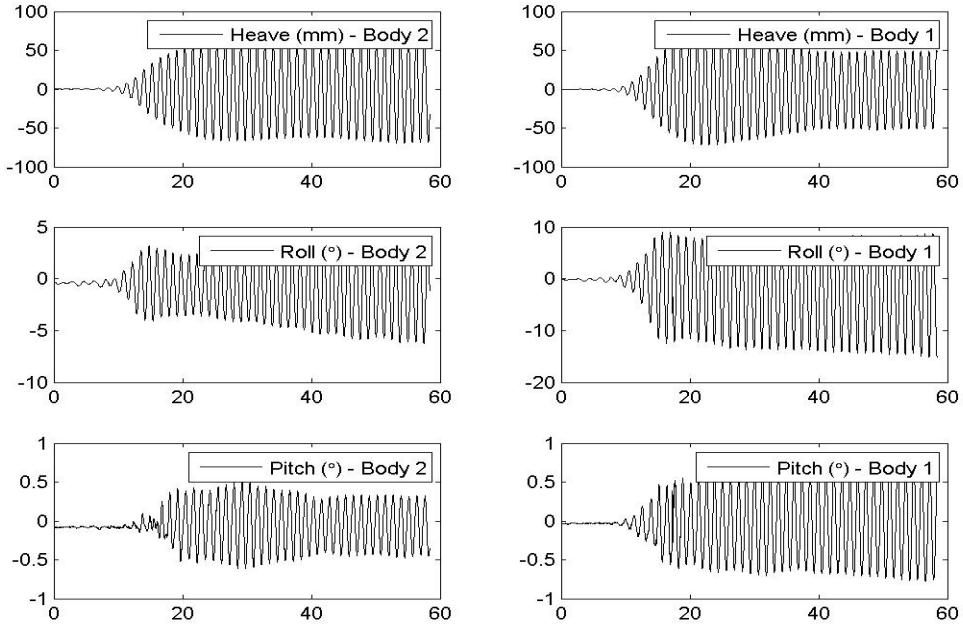

Vessel Motions, 0° Heading, 300 mm Gap and kL= 3.2741

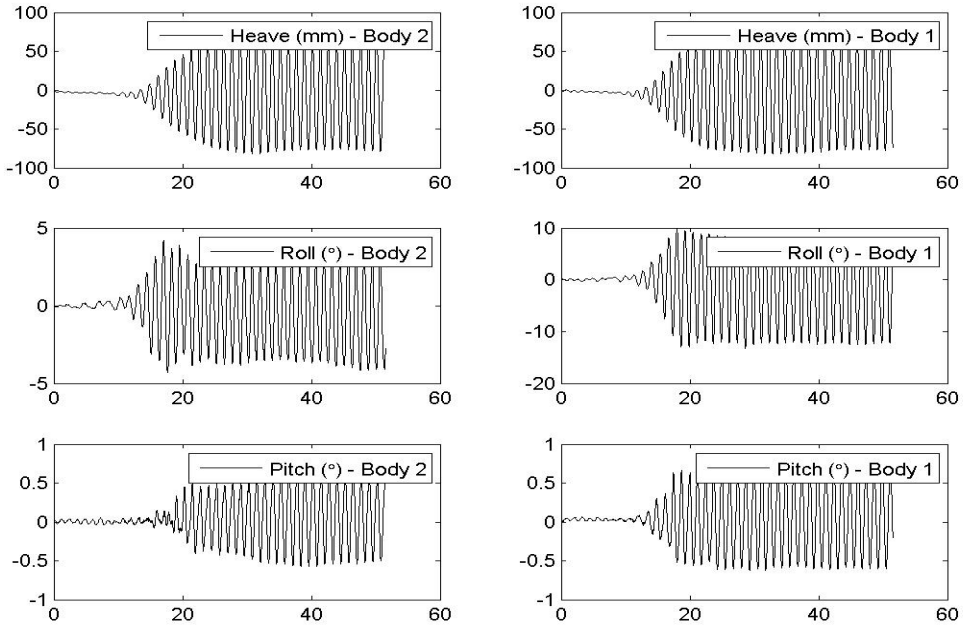

Vessel Motions, 0° Heading, 300 mm Gap and kL= 3.1265

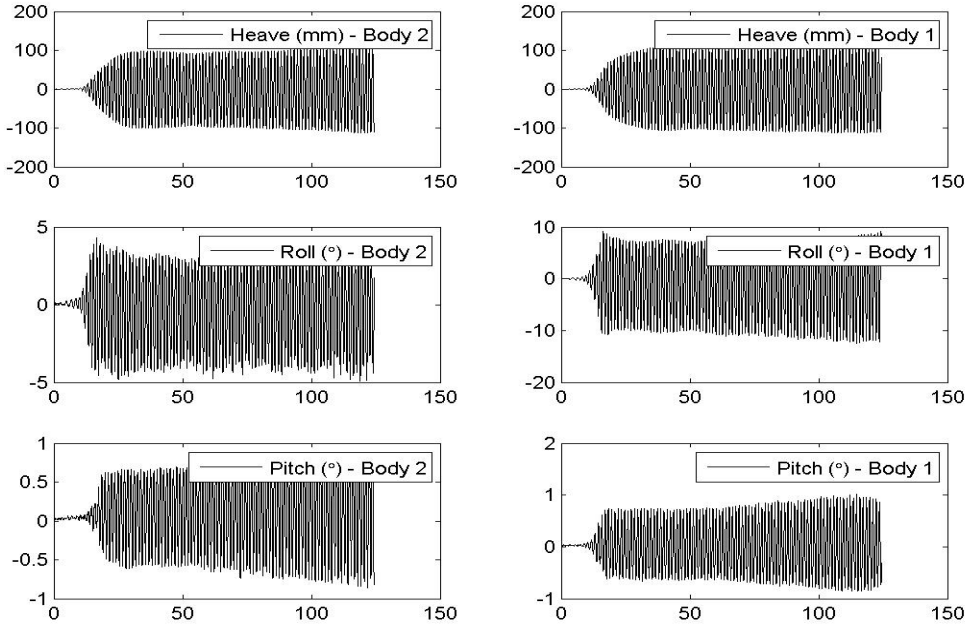

Vessel Motions, 0° Heading, 300 mm Gap and kL= 2.302

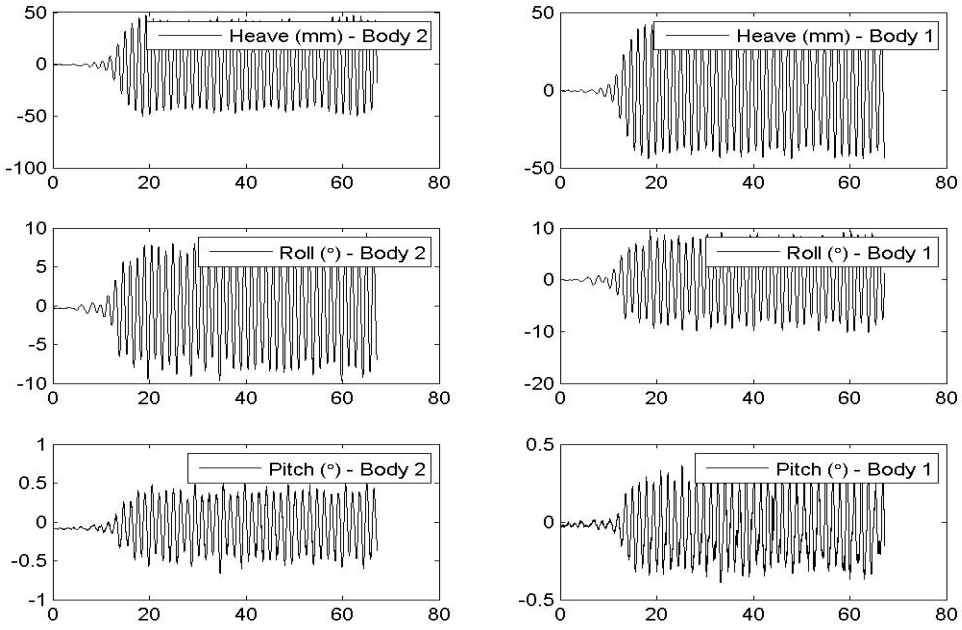

Vessel Motions, 0° Heading, 300 mm Gap and kL= 3.0204

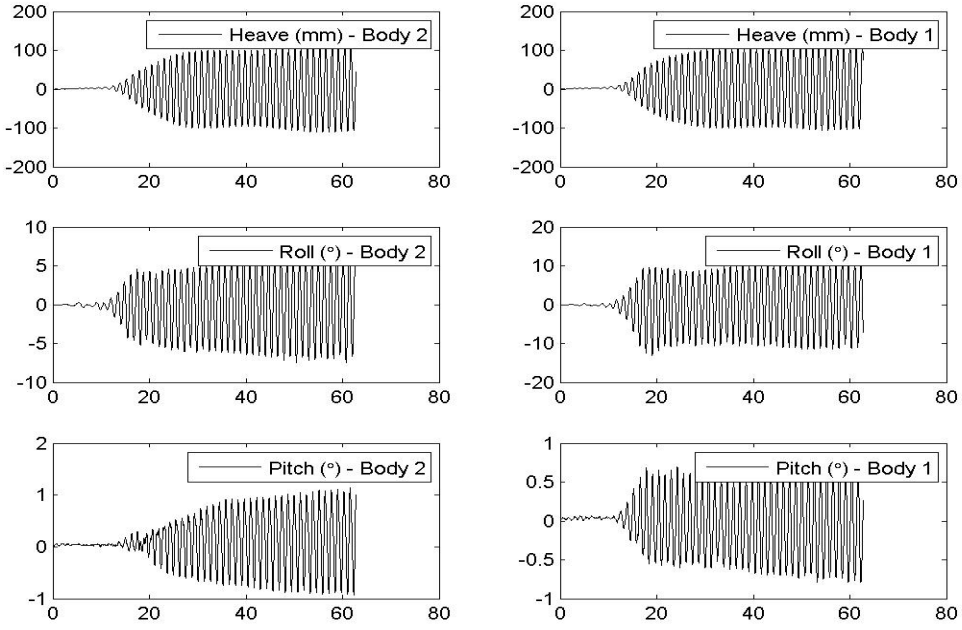

Vessel Motions, 0° Heading, 300 mm Gap and kL= 2.2327

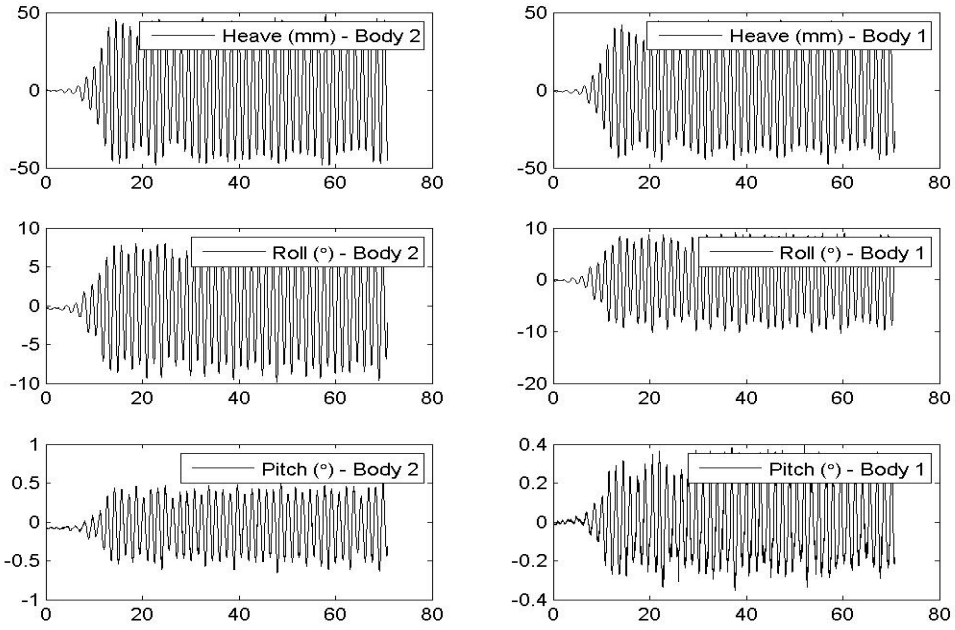

Vessel Motions, 0° Heading, 300 mm Gap and kL= 2.8897

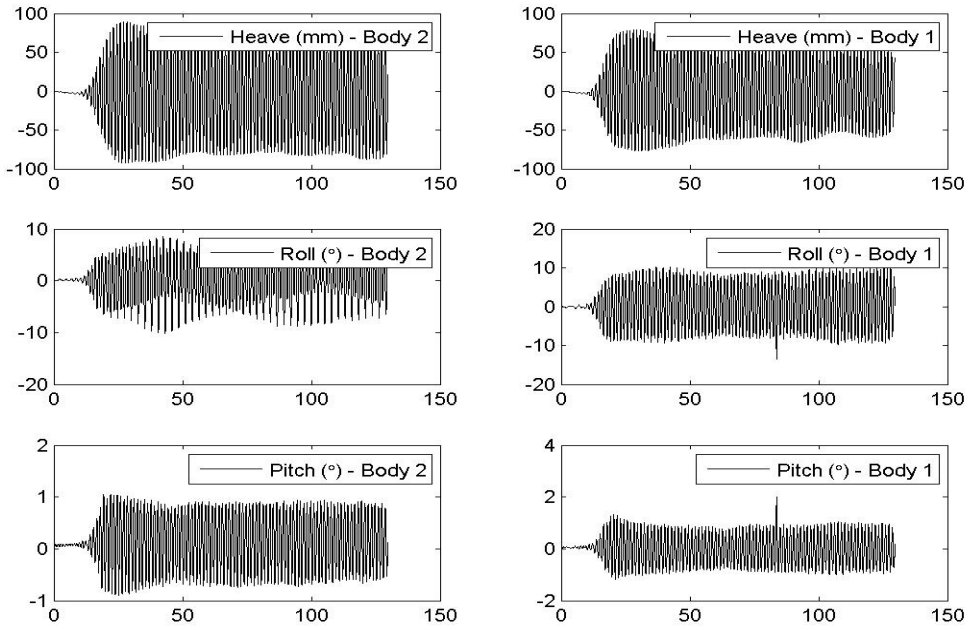

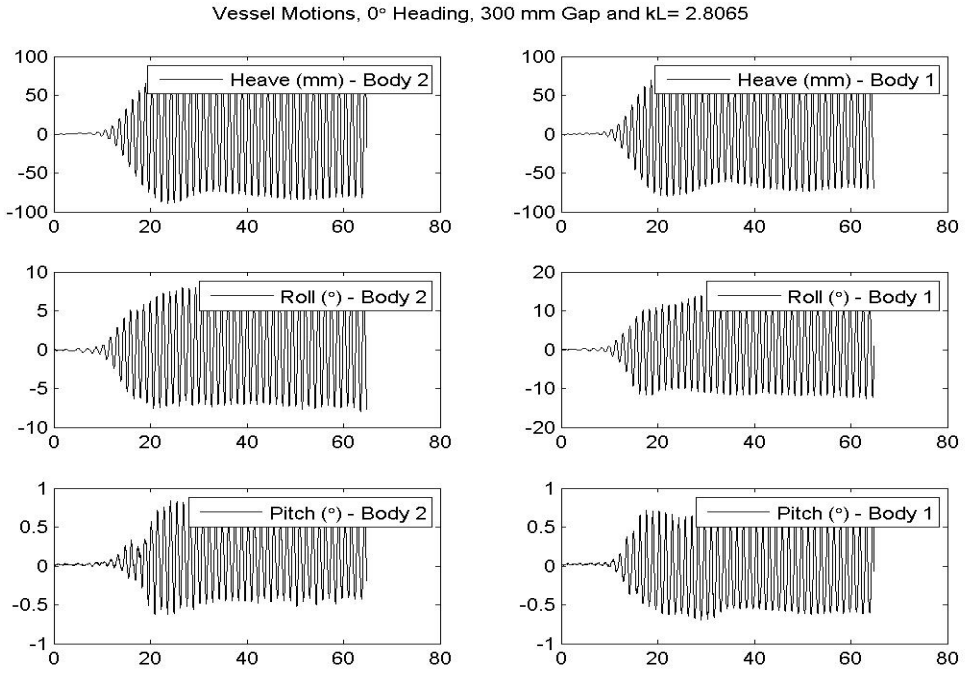
Vessel Motions, 0° Heading, 300 mm Gap and kL= 2.8065
Heave (mm) - Body 2
Heave (mm) - Body 1
Roll (°) - Body 2
Roll (°) - Body 1
Pitch (°) - Body 2
Pitch (°) - Body 1

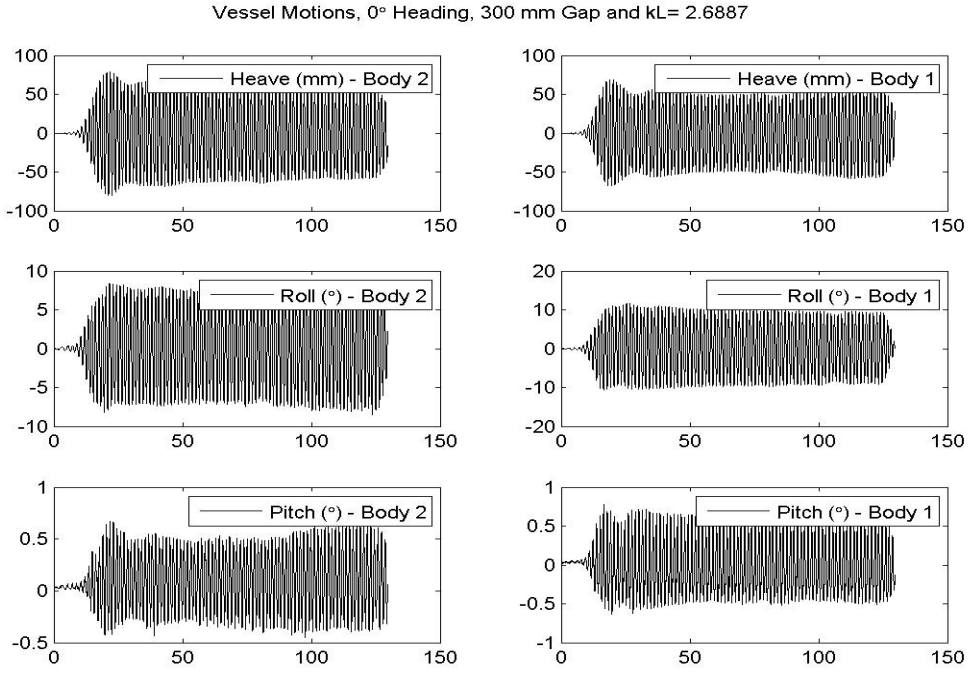
Vessel Motions, 0° Heading, 300 mm Gap and kL= 2.6887
Heave (mm) - Body 2
Heave (mm) - Body 1
Roll (°) - Body 2
Roll (°) - Body 1
Pitch (°) - Body 2
Pitch (°) - Body 1

Vessel Motions, 0° Heading, 300 mm Gap and kL= 1.8815

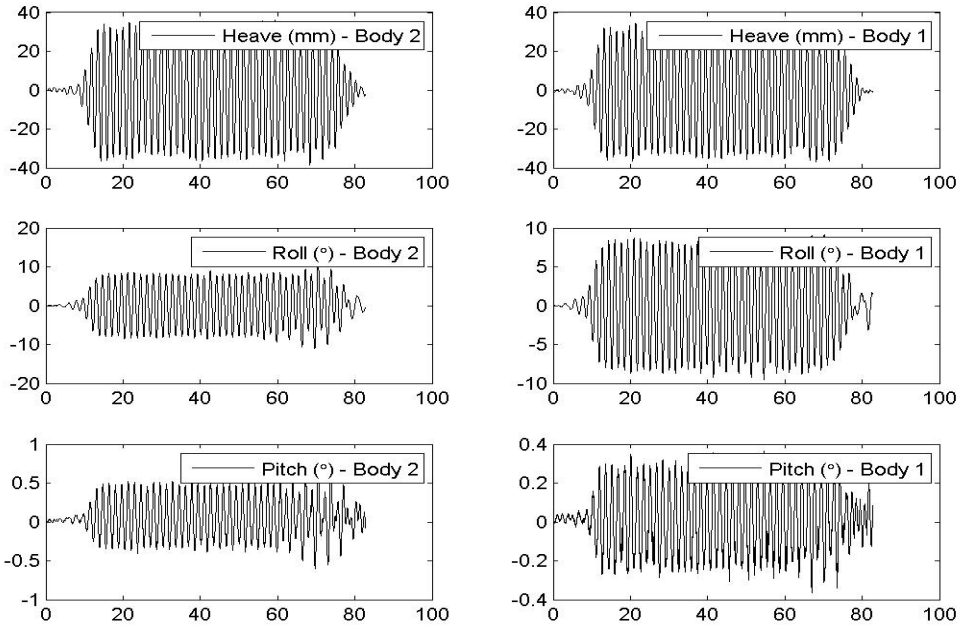

Vessel Motions, 0° Heading, 300 mm Gap and kL= 1.7789

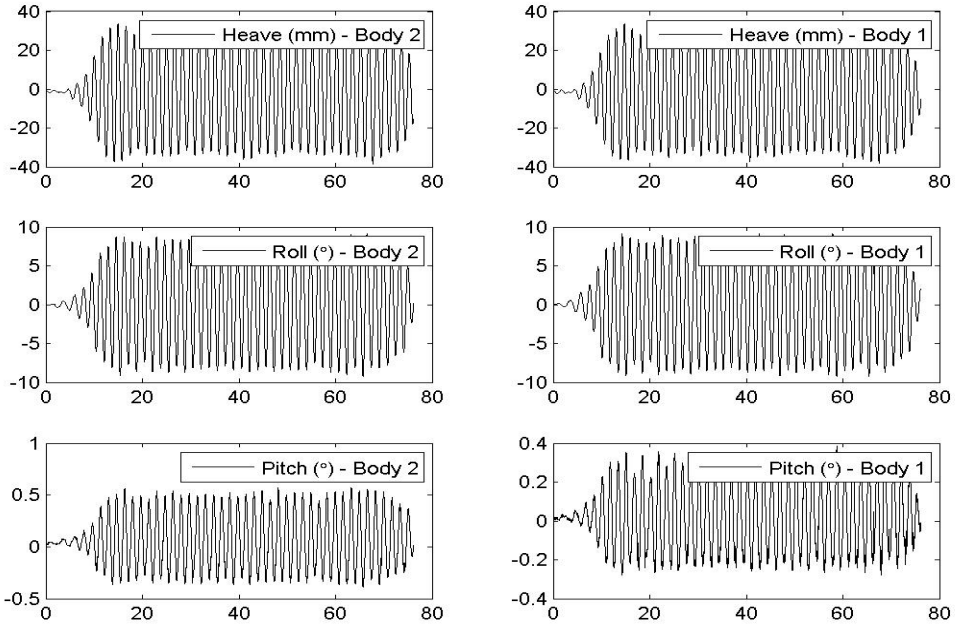

Vessel Motions, 0° Heading, 450 mm Gap and kL= 4.962

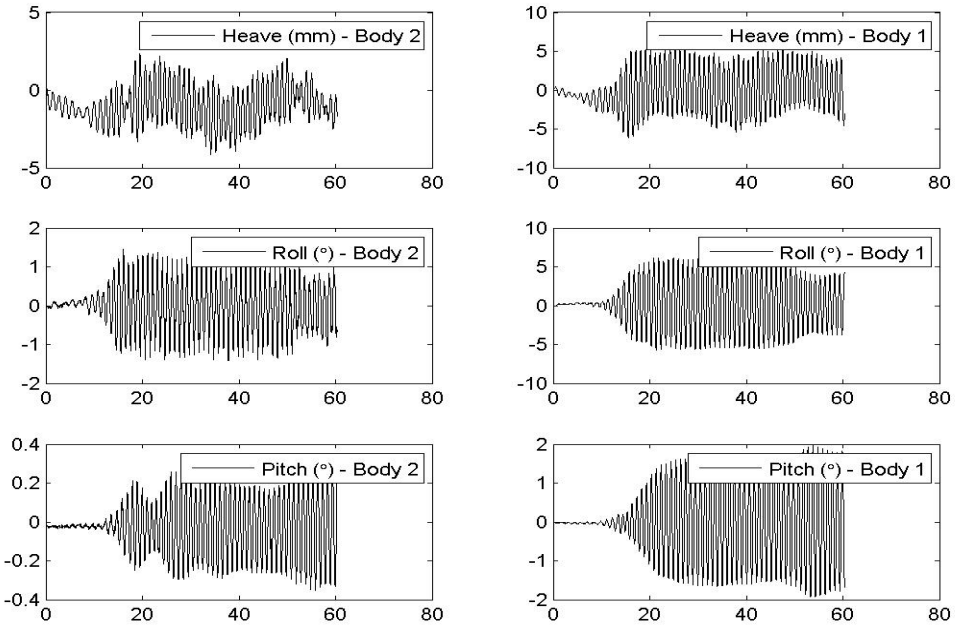

Vessel Motions, 0° Heading, 450 mm Gap and kL= 4.692

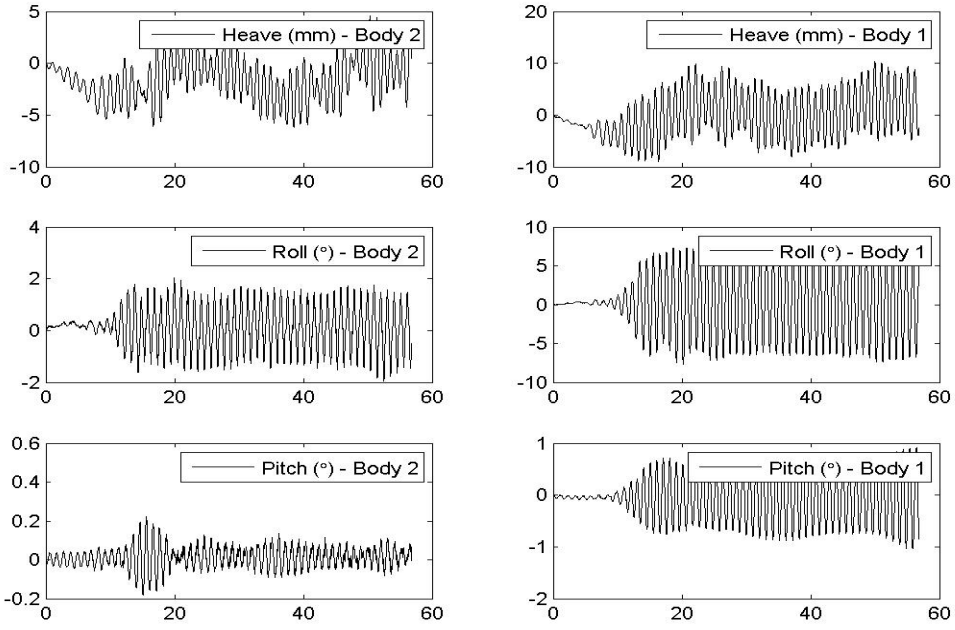

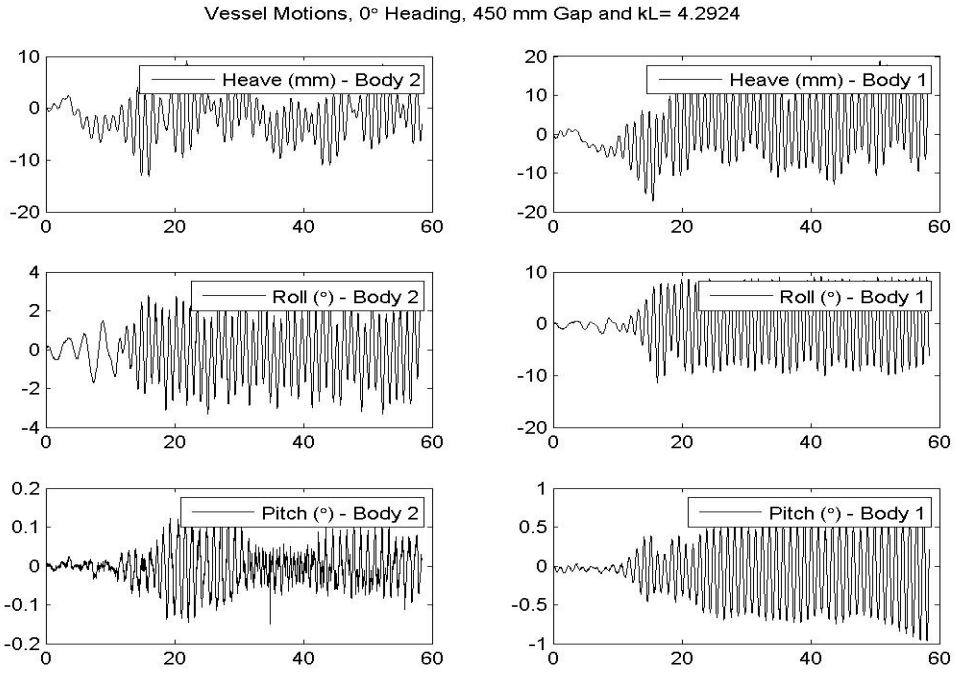
Vessel Motions, 0° Heading, 450 mm Gap and kL= 4.2924
Heave (mm) - Body 2
Heave (mm) - Body 1
Roll (°) - Body 2
Roll (°) - Body 1
Pitch (°) - Body 2
Pitch (°) - Body 1

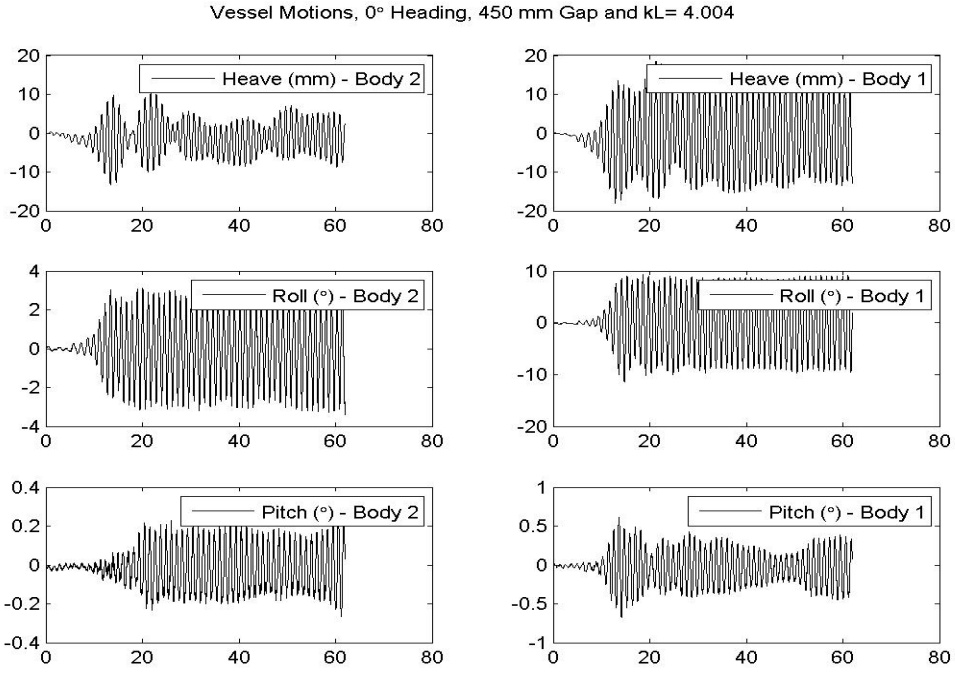
Vessel Motions, 0° Heading, 450 mm Gap and kL= 4.004
Heave (mm) - Body 2
Heave (mm) - Body 1
Roll (°) - Body 2
Roll (°) - Body 1
Pitch (°) - Body 2
Pitch (°) - Body 1

Vessel Motions, 0° Heading, 450 mm Gap and kL= 3.8304

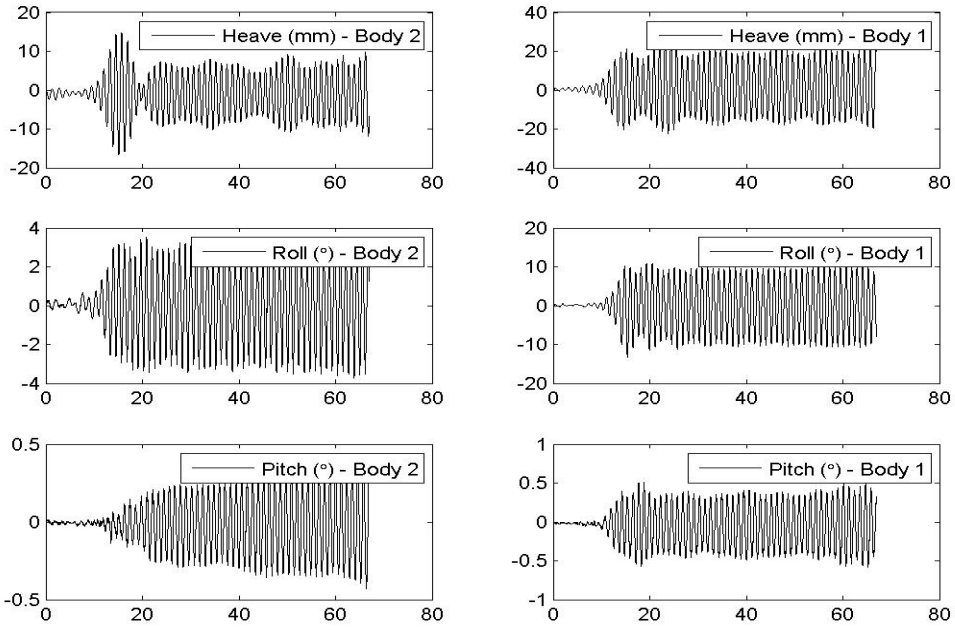

Vessel Motions, 0° Heading, 450 mm Gap and kL= 3.665

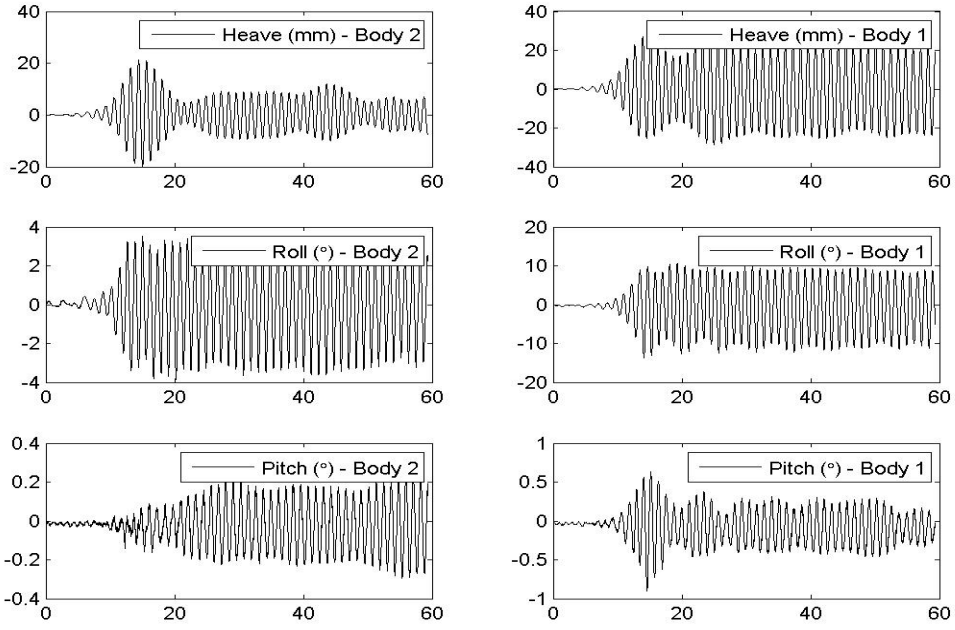

Vessel Motions, 0° Heading, 450 mm Gap and kL= 3.4922

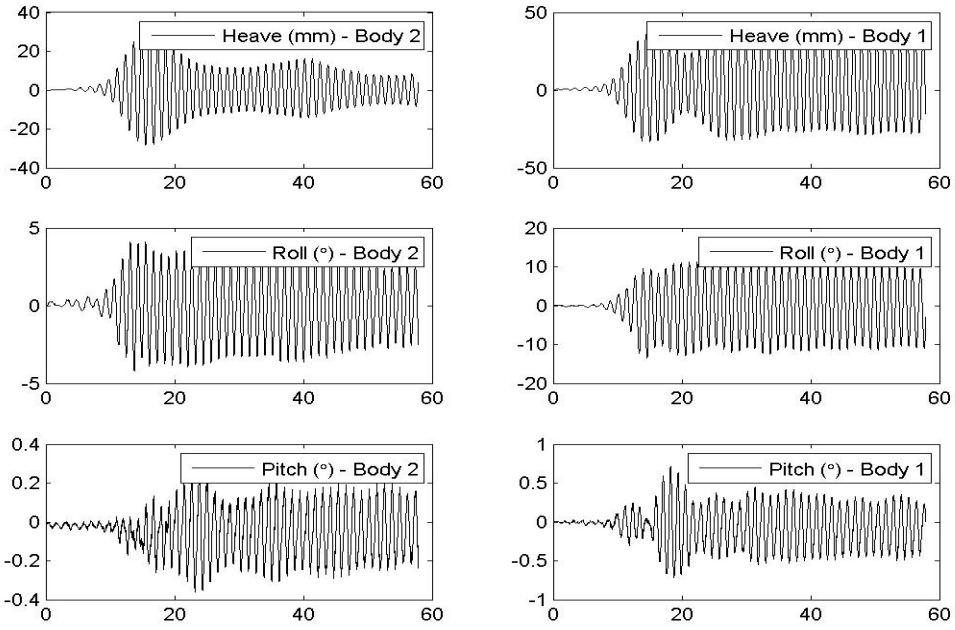

Vessel Motions, 0° Heading, 450 mm Gap and kL= 3.3832

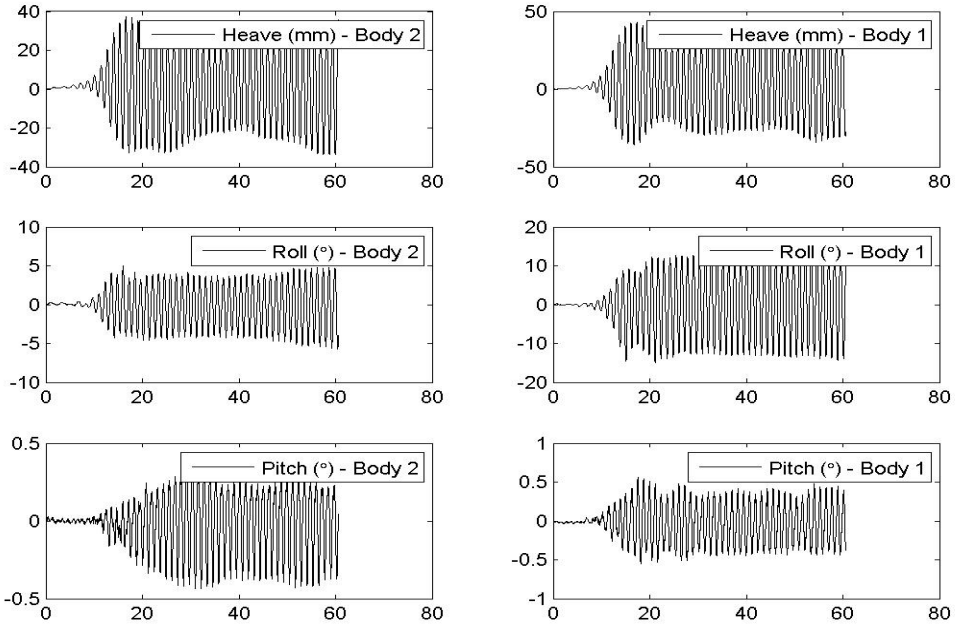

Vessel Motions, 0° Heading, 450 mm Gap and kL= 3.3463

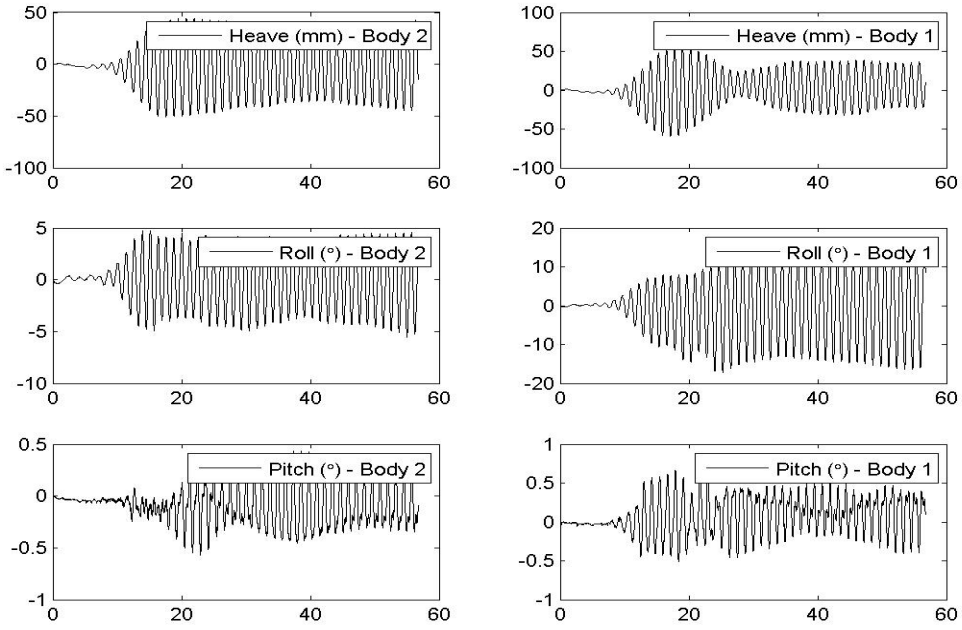

Vessel Motions, 0° Heading, 450 mm Gap and kL= 3.2642

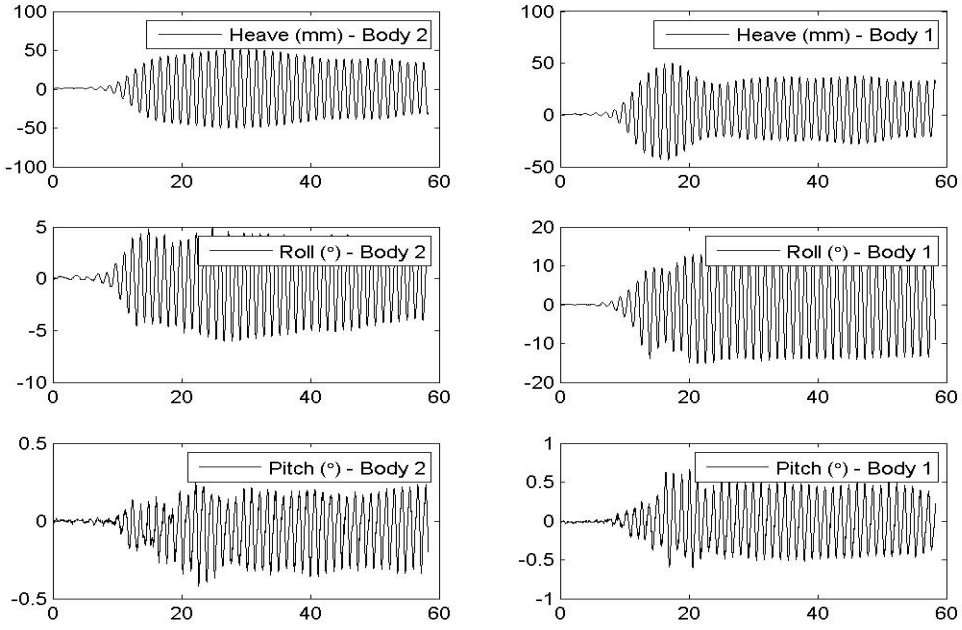

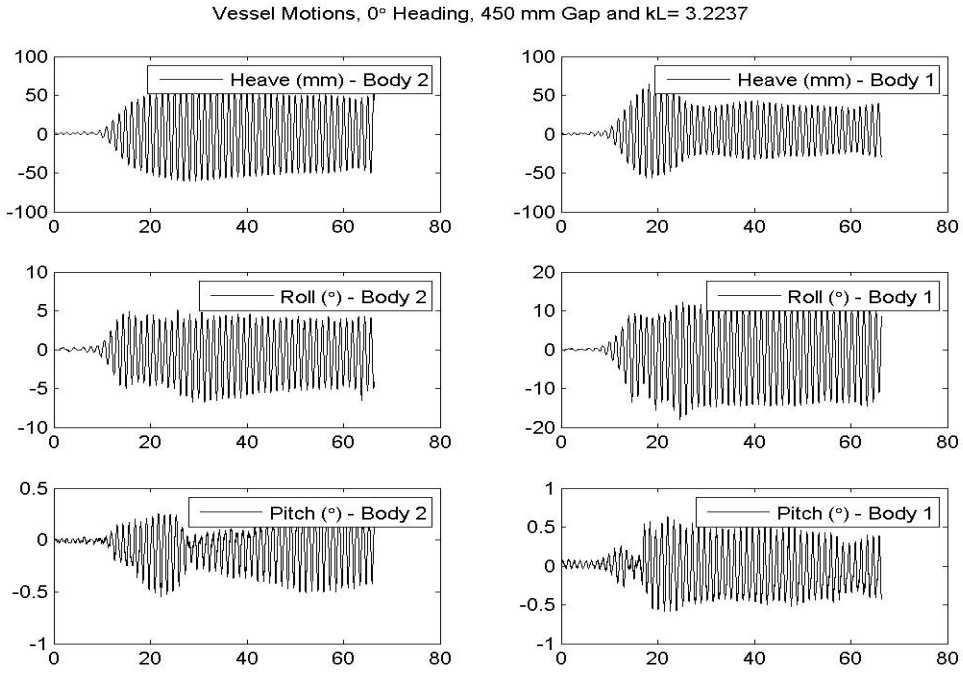
Vessel Motions, 0° Heading, 450 mm Gap and kL= 3.2237
Heave (mm) - Body 2
Heave (mm) - Body 1
Roll (°) - Body 2
Roll (°) - Body 1
Pitch (°) - Body 2
Pitch (°) - Body 1

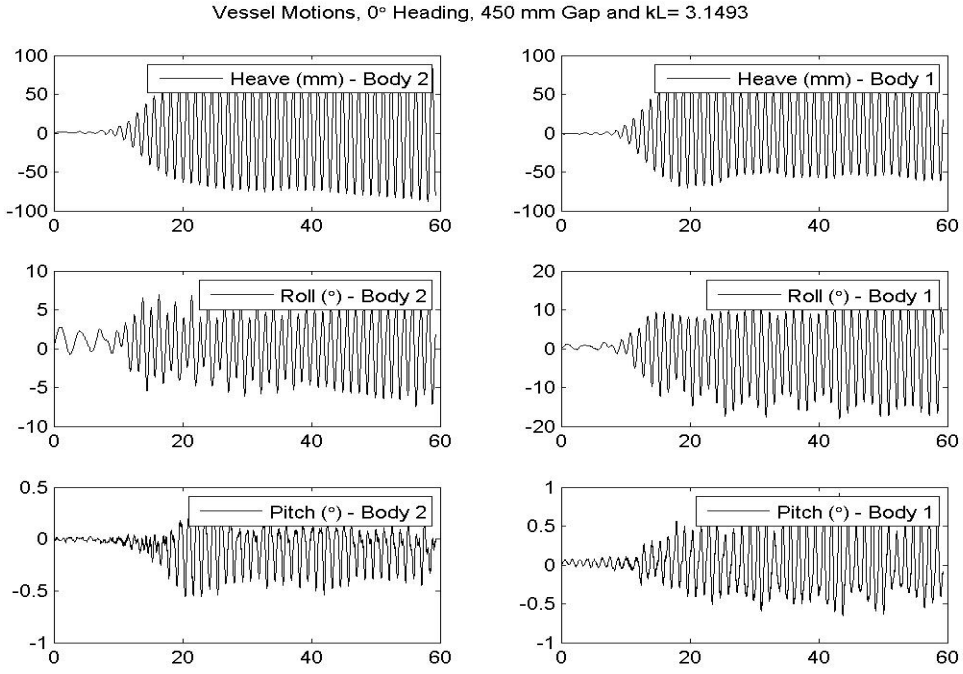
Vessel Motions, 0° Heading, 450 mm Gap and kL= 3.1493
Heave (mm) - Body 2
Heave (mm) - Body 1
Roll (°) - Body 2
Roll (°) - Body 1
Pitch (°) - Body 2
Pitch (°) - Body 1

Vessel Motions, 0° Heading, 450 mm Gap and kL= 3.0993

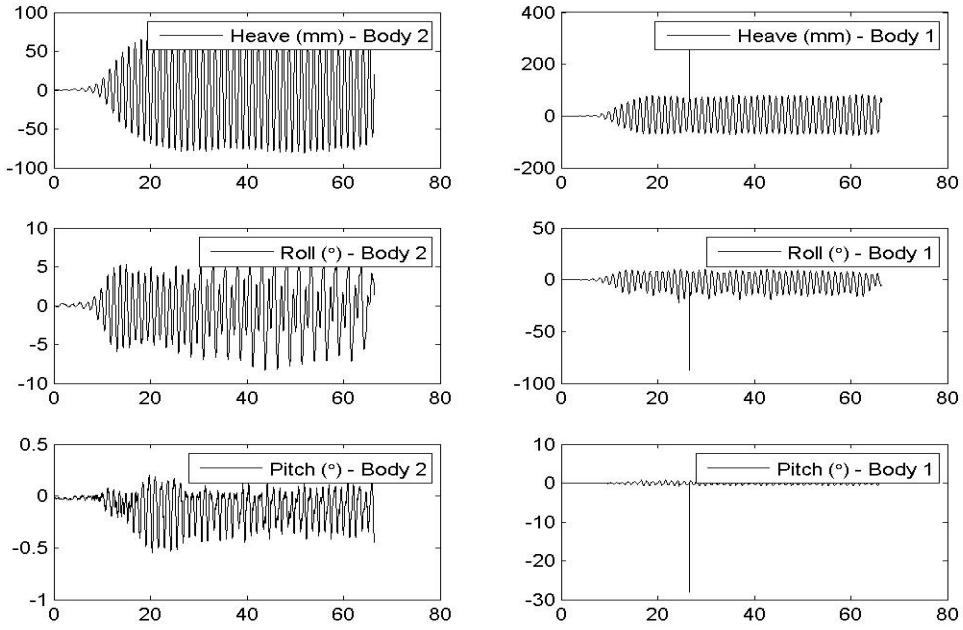

Vessel Motions, 0° Heading, 450 mm Gap and kL= 3.029

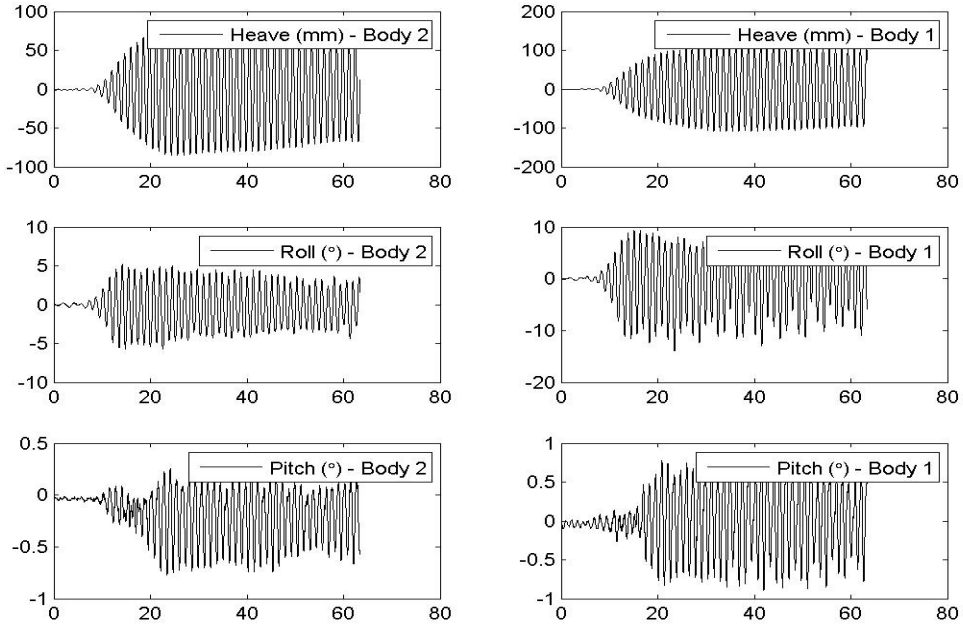

Vessel Motions, 0° Heading, 450 mm Gap and kL= 3.0005

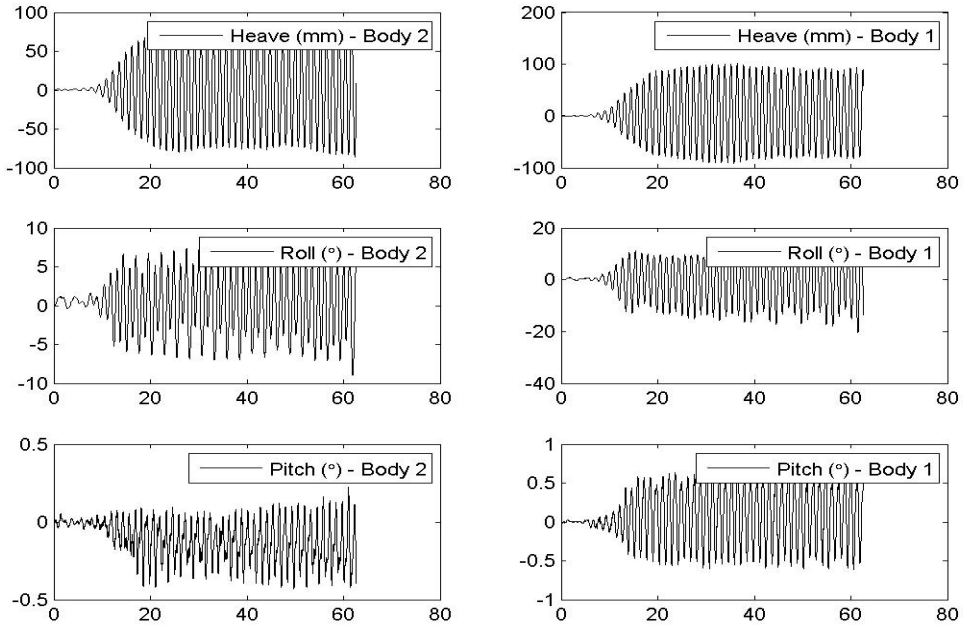

Vessel Motions, 0° Heading, 450 mm Gap and kL= 2.9078

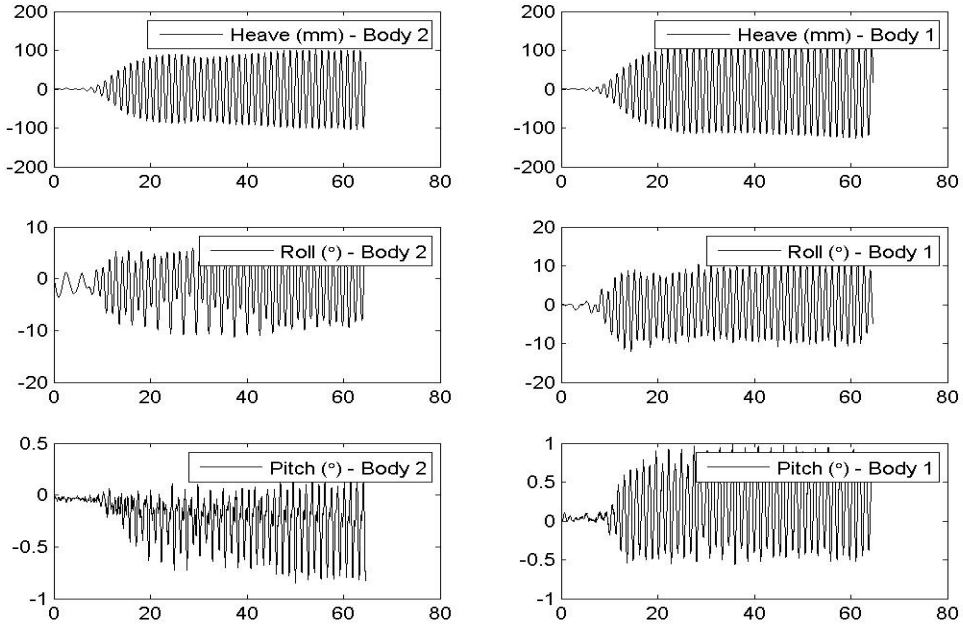

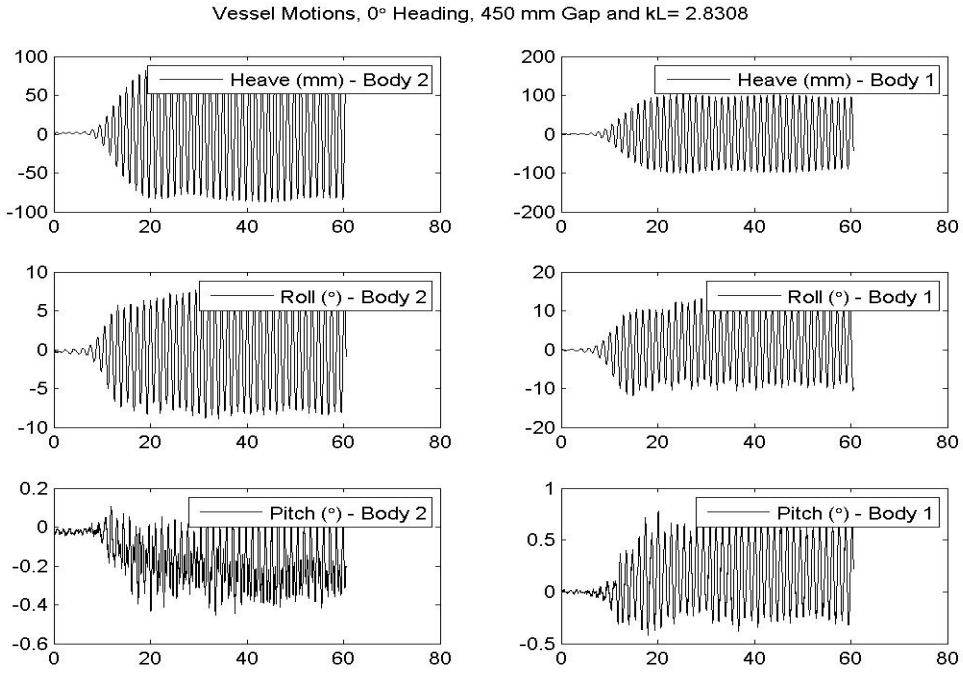
Vessel Motions, 0° Heading, 450 mm Gap and kL= 2.8308
Heave (mm) - Body 2
Heave (mm) - Body 1
Roll (°) - Body 2
Roll (°) - Body 1
Pitch (°) - Body 2
Pitch (°) - Body 1

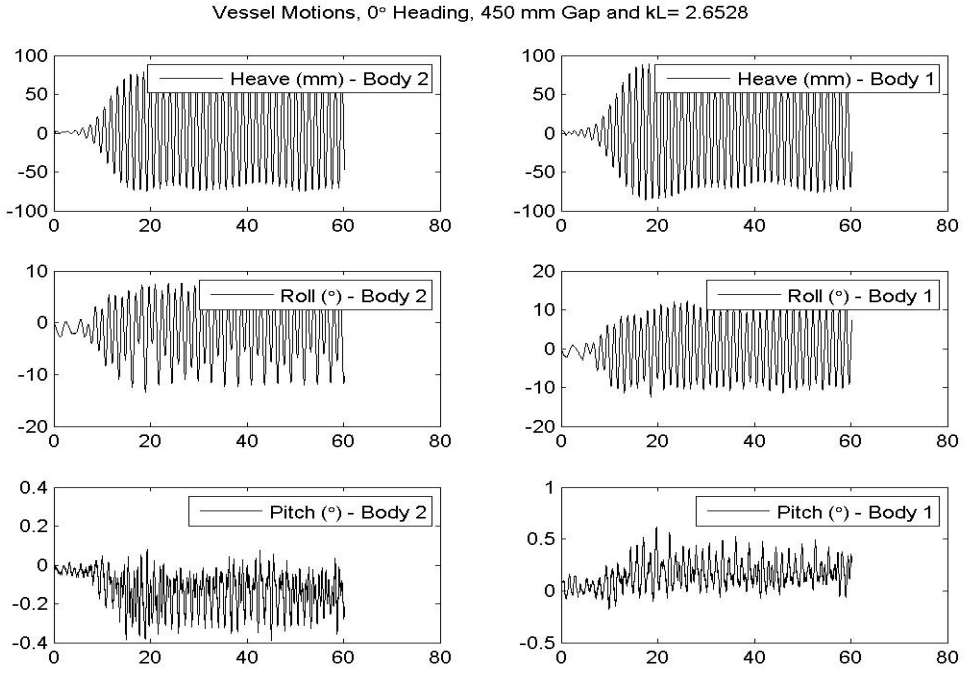
Vessel Motions, 0° Heading, 450 mm Gap and kL= 2.6528
Heave (mm) - Body 2
Heave (mm) - Body 1
Roll (°) - Body 2
Roll (°) - Body 1
Pitch (°) - Body 2
Pitch (°) - Body 1

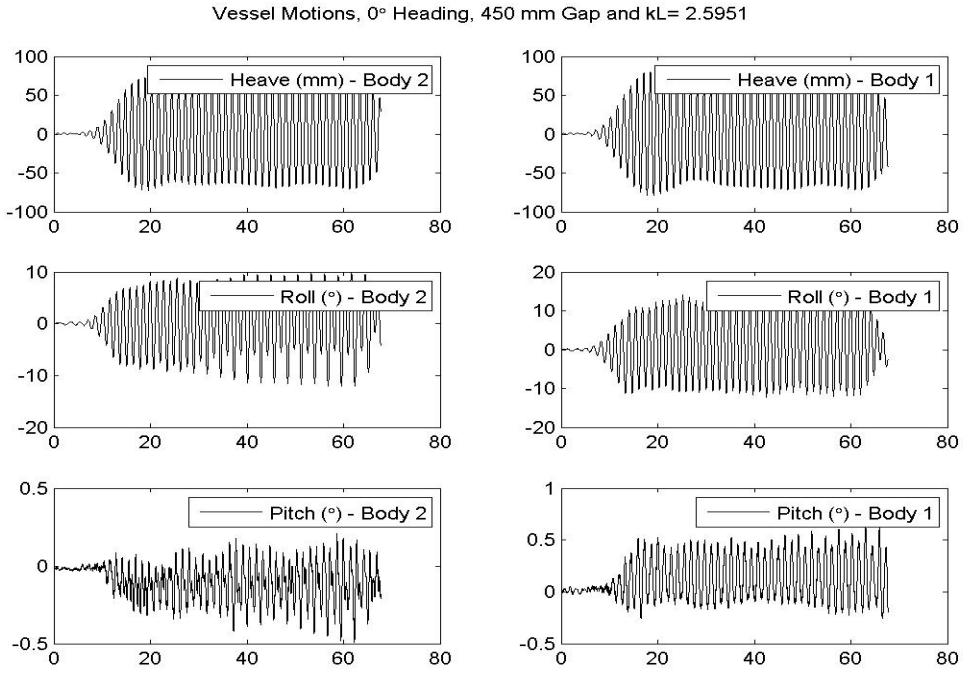
Vessel Motions, 0° Heading, 450 mm Gap and kL= 2.5951
Heave (mm) - Body 2
Heave (mm) - Body 1
Roll (°) - Body 2
Roll (°) - Body 1
Pitch (°) - Body 2
Pitch (°) - Body 1

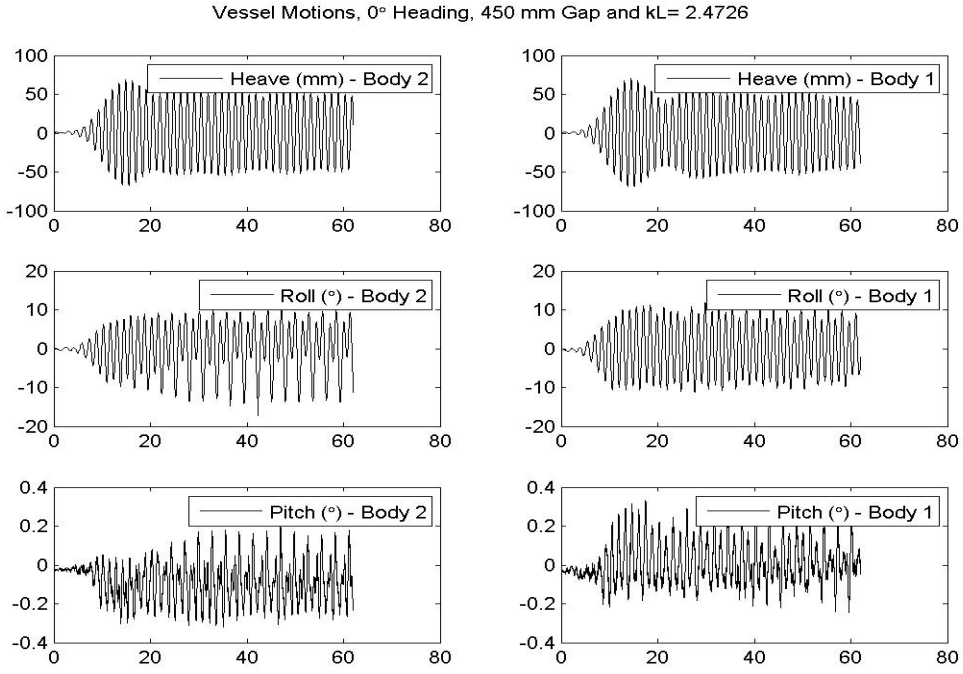
Vessel Motions, 0° Heading, 450 mm Gap and kL= 2.4726
Heave (mm) - Body 2
Heave (mm) - Body 1
Roll (°) - Body 2
Roll (°) - Body 1
Pitch (°) - Body 2
Pitch (°) - Body 1

Vessel Motions, 30° Heading, 300 mm Gap and kL= 4.2366

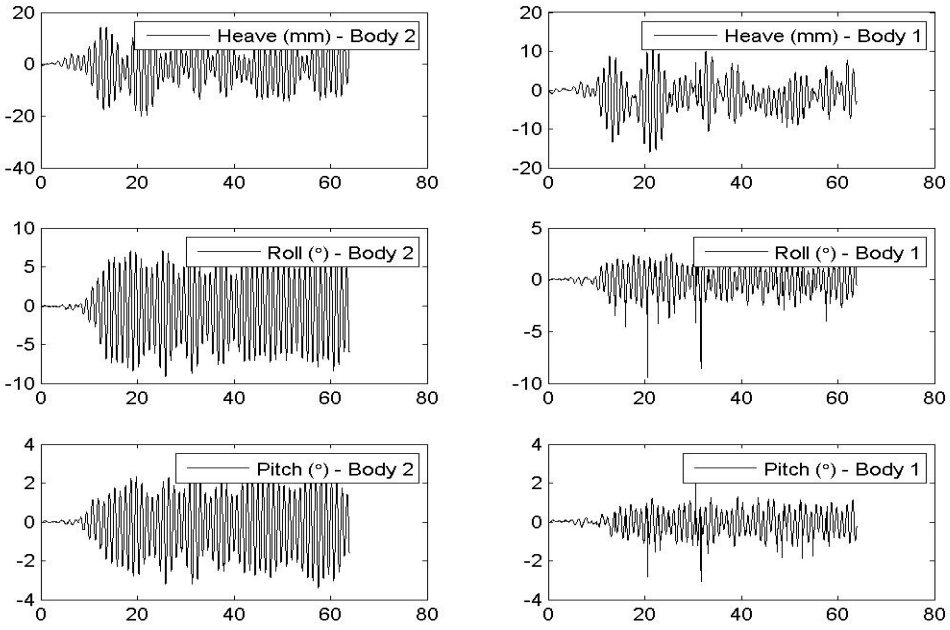

Vessel Motions, 30° Heading, 300 mm Gap and kL= 3.4298

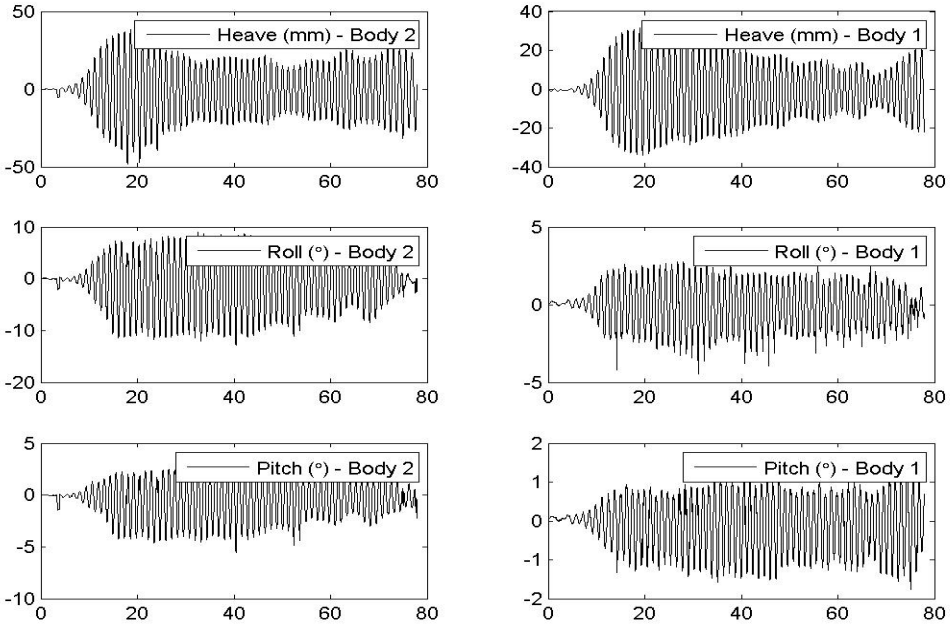

Vessel Motions, 30° Heading, 300 mm Gap and kL= 3.2165

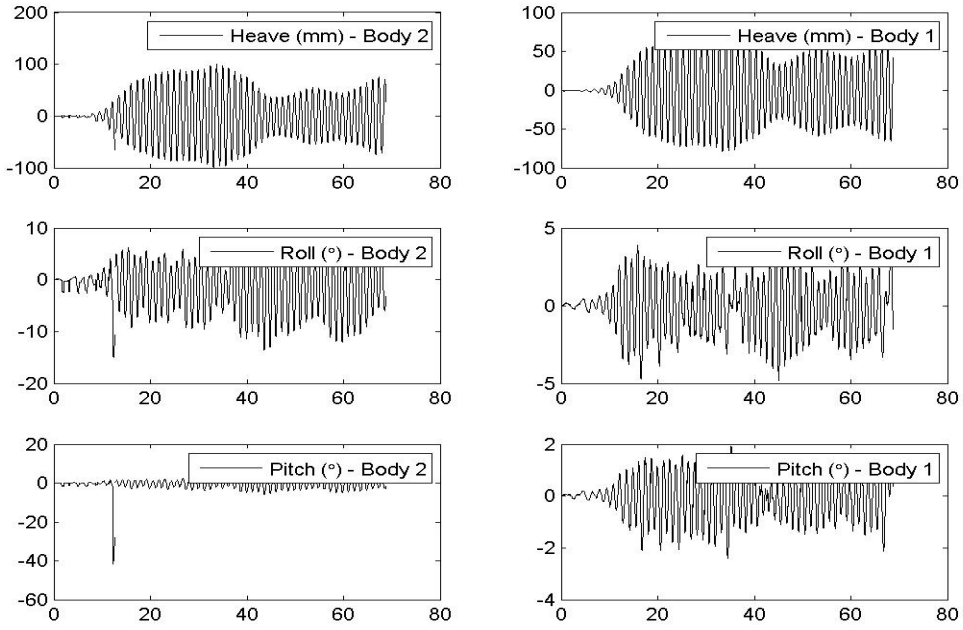

Vessel Motions, 30° Heading, 300 mm Gap and kL= 3.7199

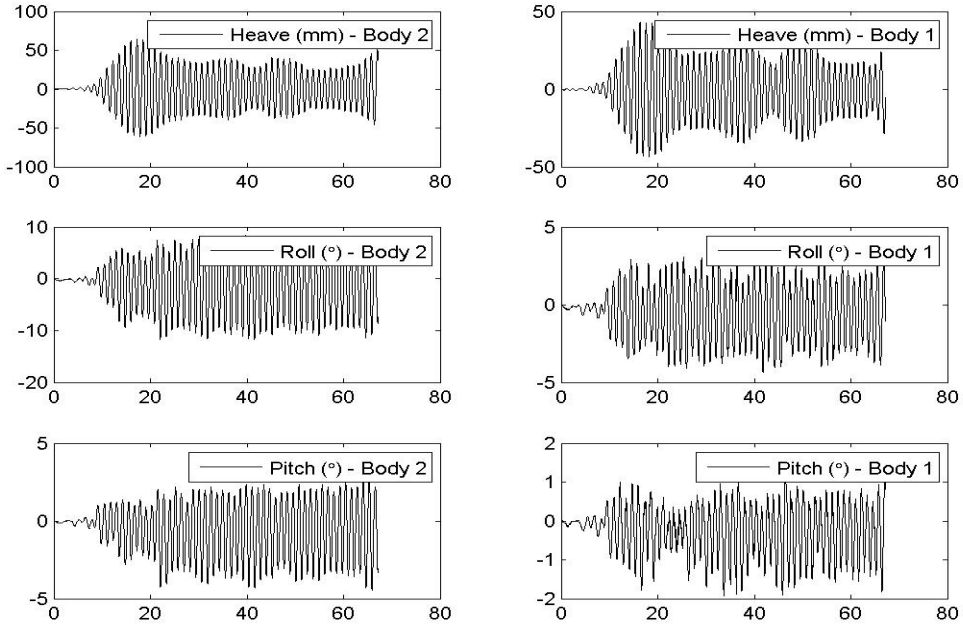

Vessel Motions, 30° Heading, 300 mm Gap and kL= 2.7535

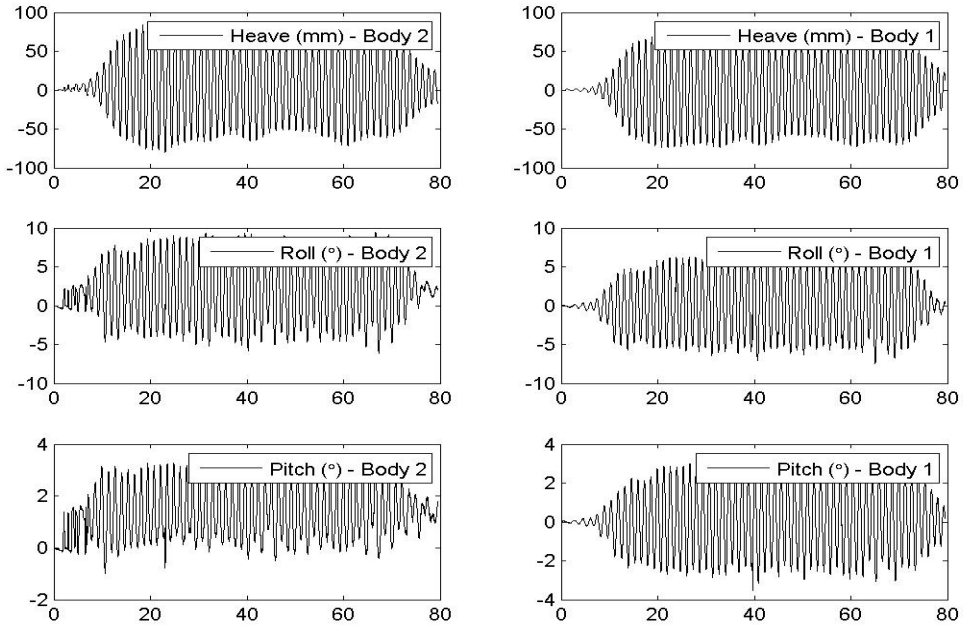

Vessel Motions, 30° Heading, 300 mm Gap and kL= 2.6525

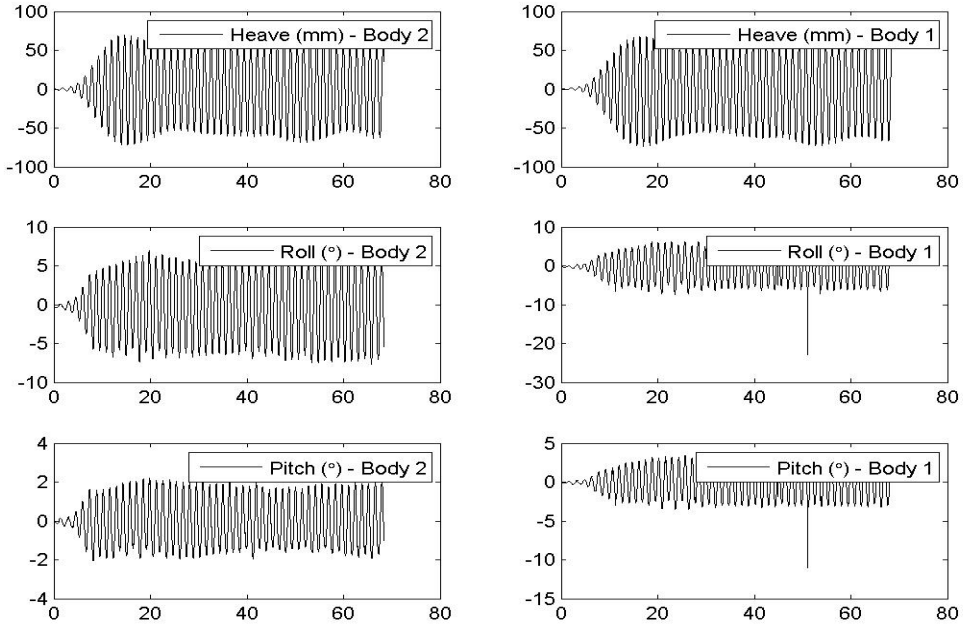

Vessel Motions, 30° Heading, 300 mm Gap and kL= 2.529

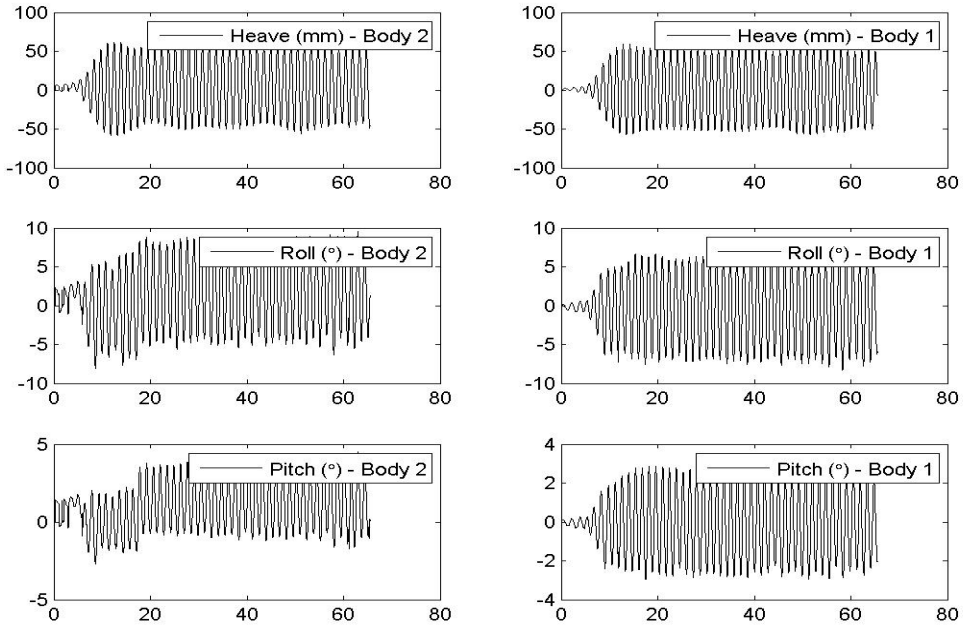

Vessel Motions, 30° Heading, 300 mm Gap and kL= 2.4944

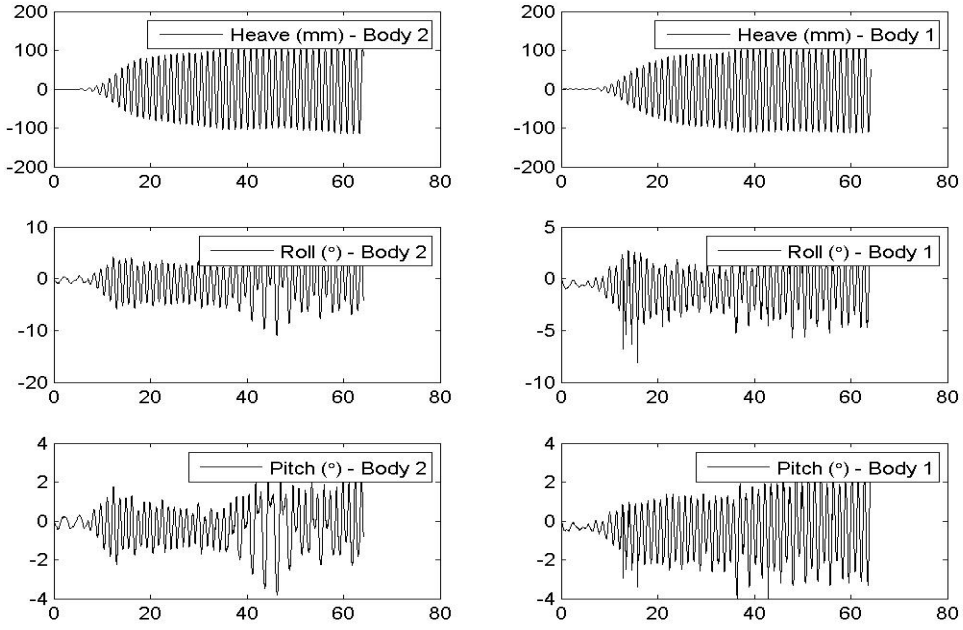

Vessel Motions, 30° Heading, 300 mm Gap and kL= 2.3294

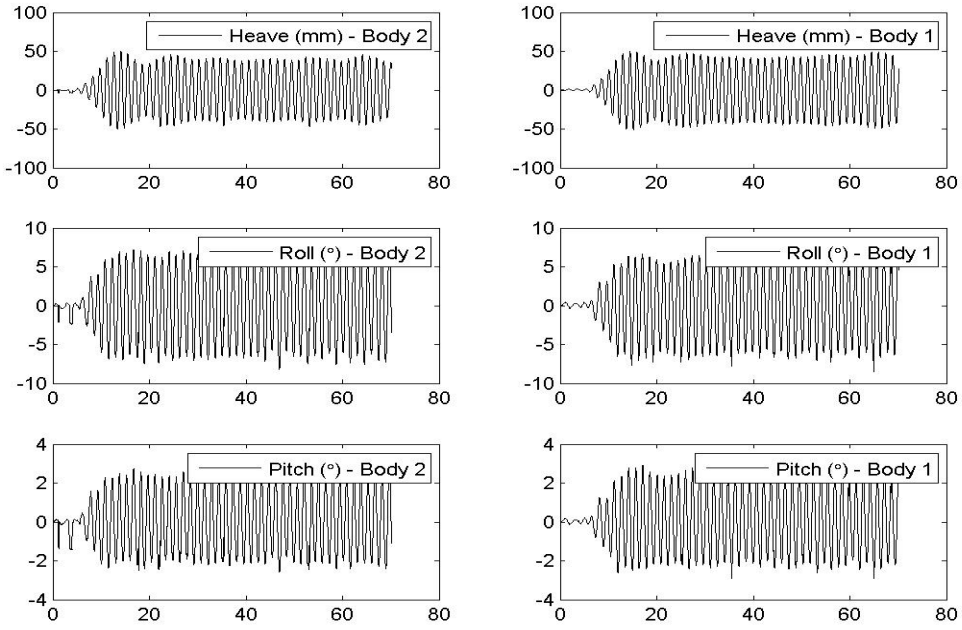

Vessel Motions, 30° Heading, 300 mm Gap and kL= 2.2474

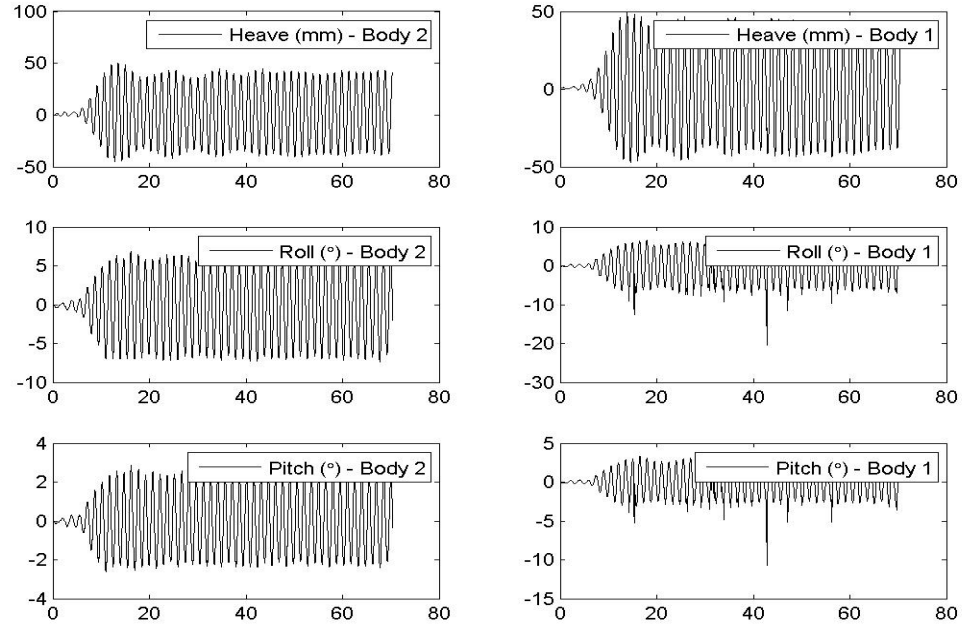

Vessel Motions, 30° Heading, 300 mm Gap and kL= 2.1579

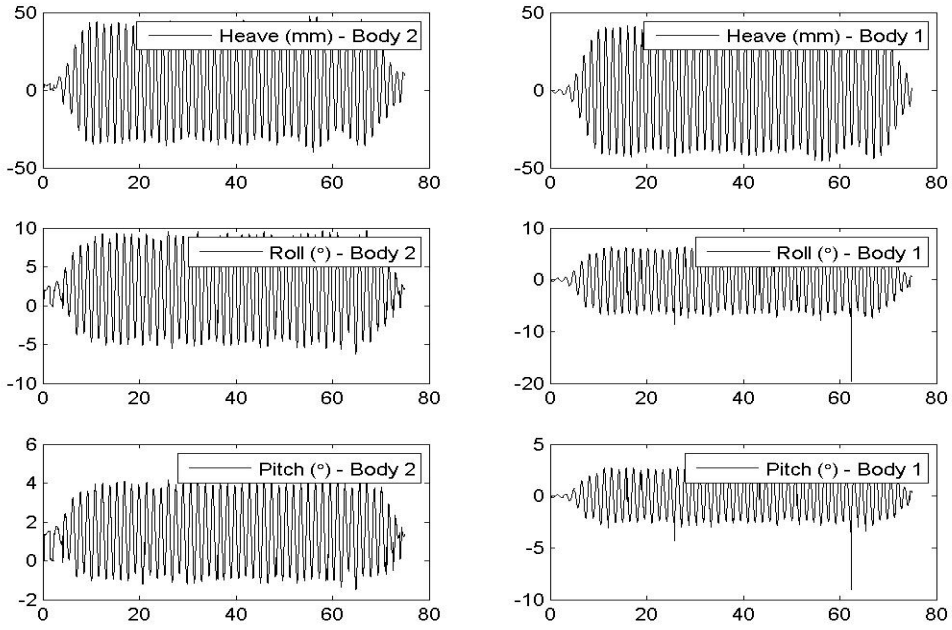

Vessel Motions, 30° Heading, 300 mm Gap and kL= 2.4148

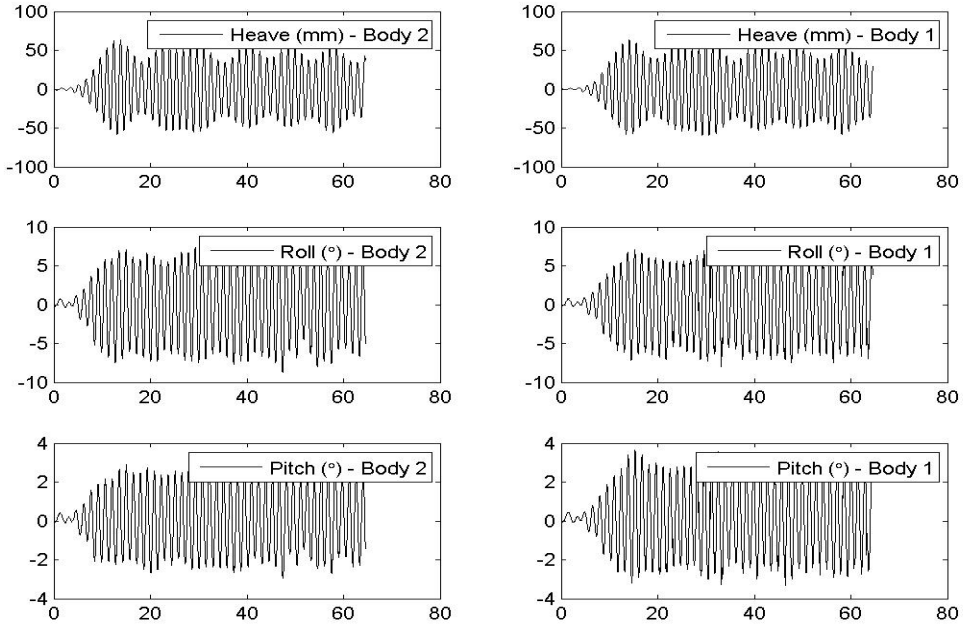

Vessel Motions, 30° Heading, 300 mm Gap and kL= 2.031

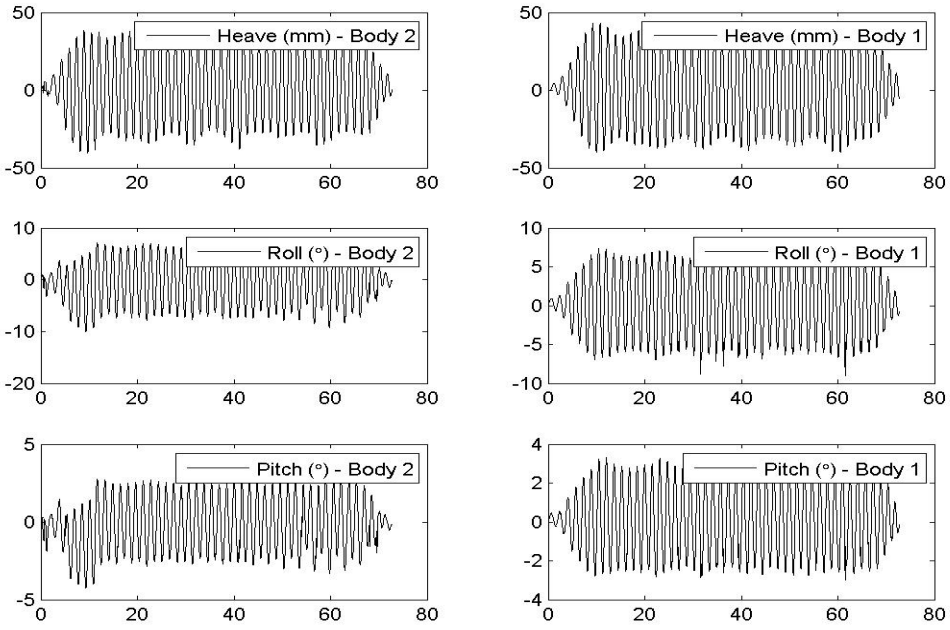

Vessel Motions, 30° Heading, 300 mm Gap and kL= 1.9306

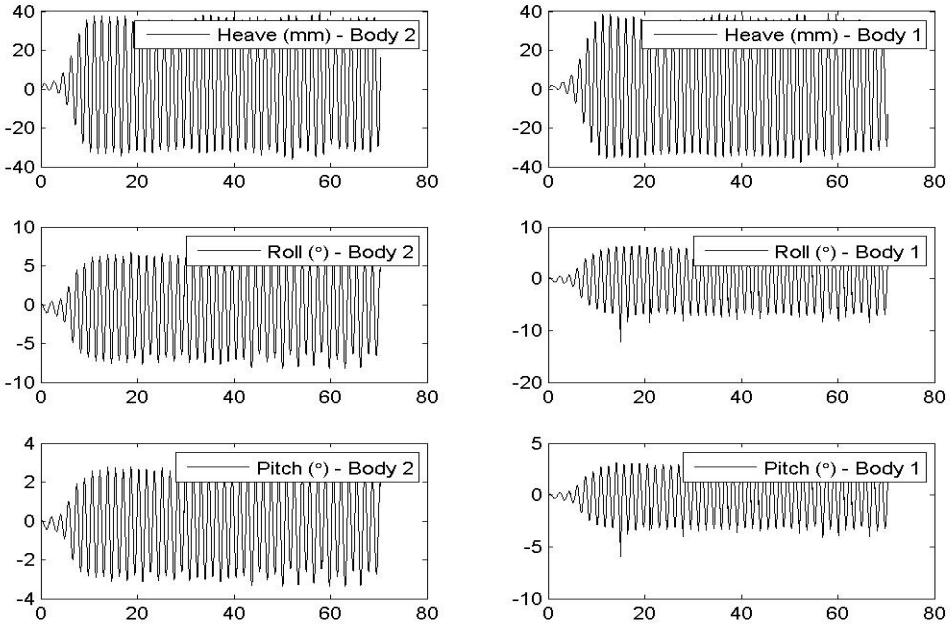

Vessel Motions, 30° Heading, 300 mm Gap and kL= 1.8772

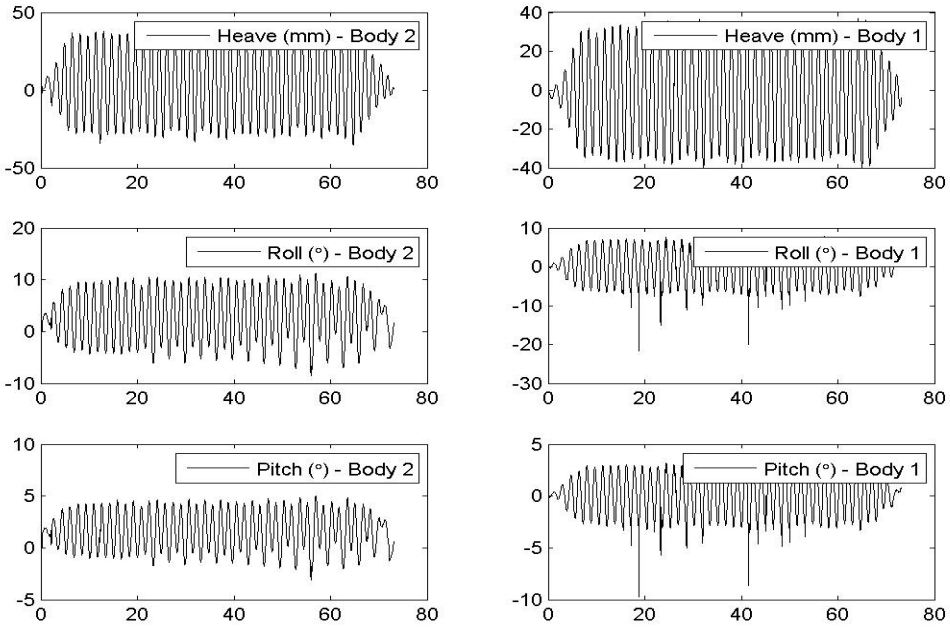

Vessel Motions, 30° Heading, 300 mm Gap and kL= 1.7822

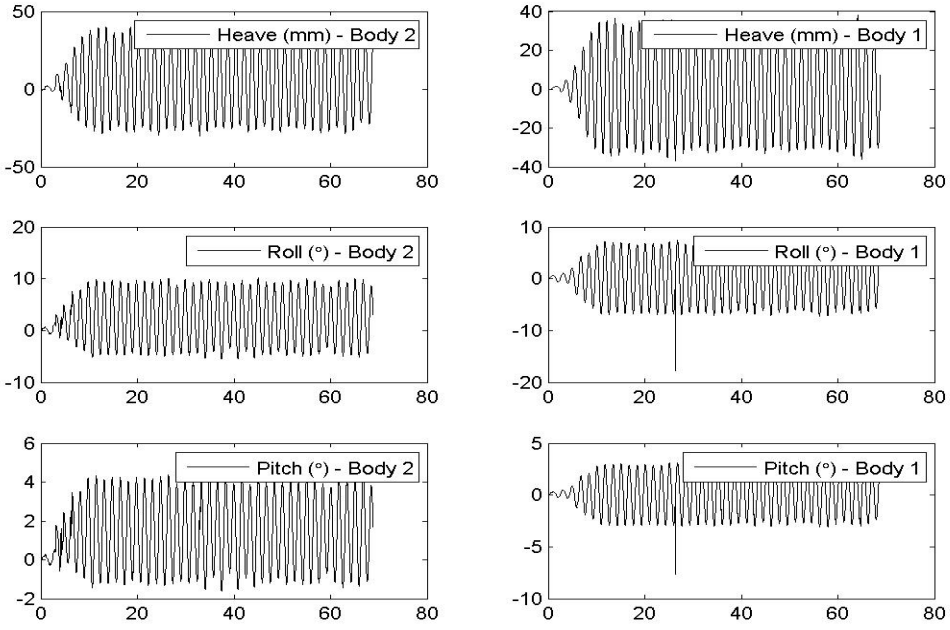

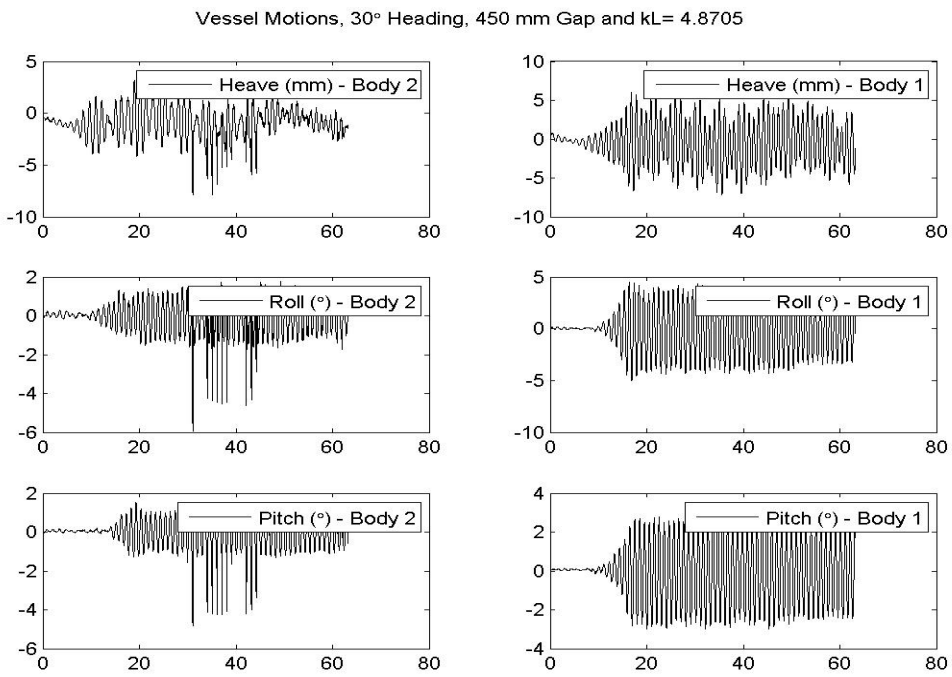
Vessel Motions, 30° Heading, 450 mm Gap and kL= 4.8705
Heave (mm) - Body 2
Heave (mm) - Body 1
Roll (°) - Body 2
Roll (°) - Body 1
Pitch (°) - Body 2
Pitch (°) - Body 1

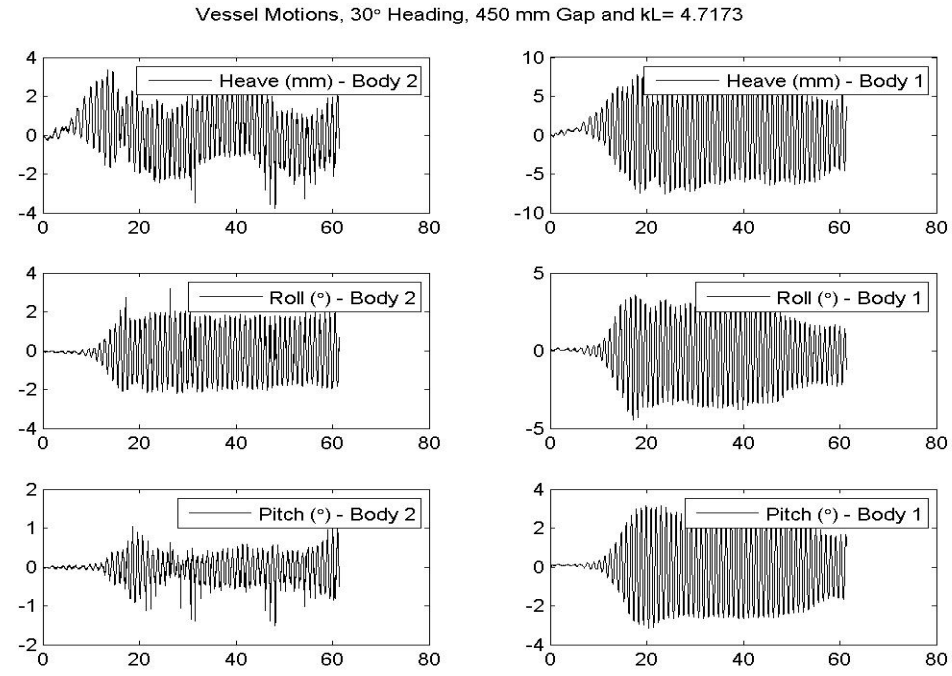
Vessel Motions, 30° Heading, 450 mm Gap and kL= 4.7173
Heave (mm) - Body 2
Heave (mm) - Body 1
Roll (°) - Body 2
Roll (°) - Body 1
Pitch (°) - Body 2
Pitch (°) - Body 1

Vessel Motions, 30° Heading, 450 mm Gap and kL= 4.2869

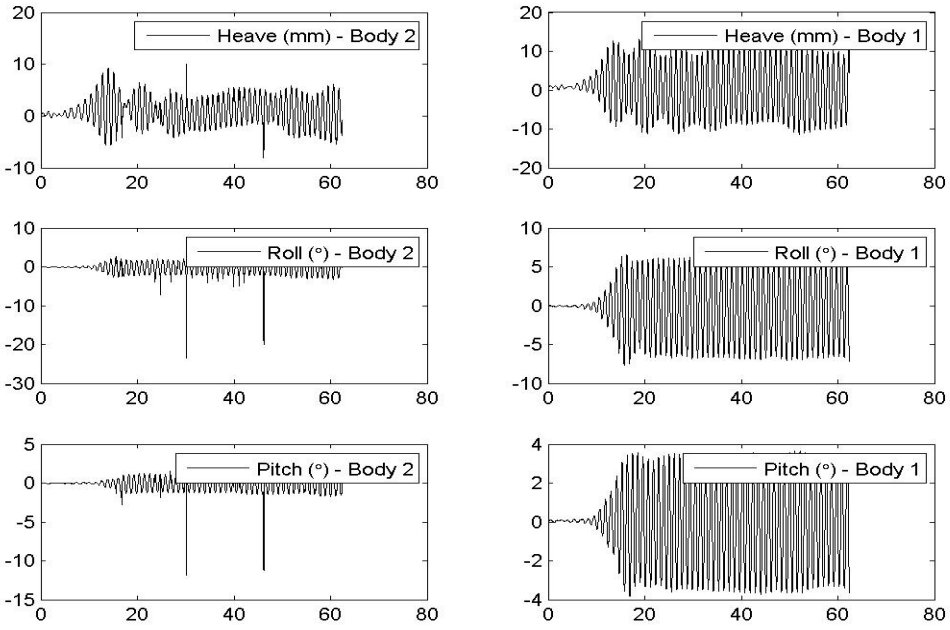

Vessel Motions, 30° Heading, 450 mm Gap and kL= 4.0479

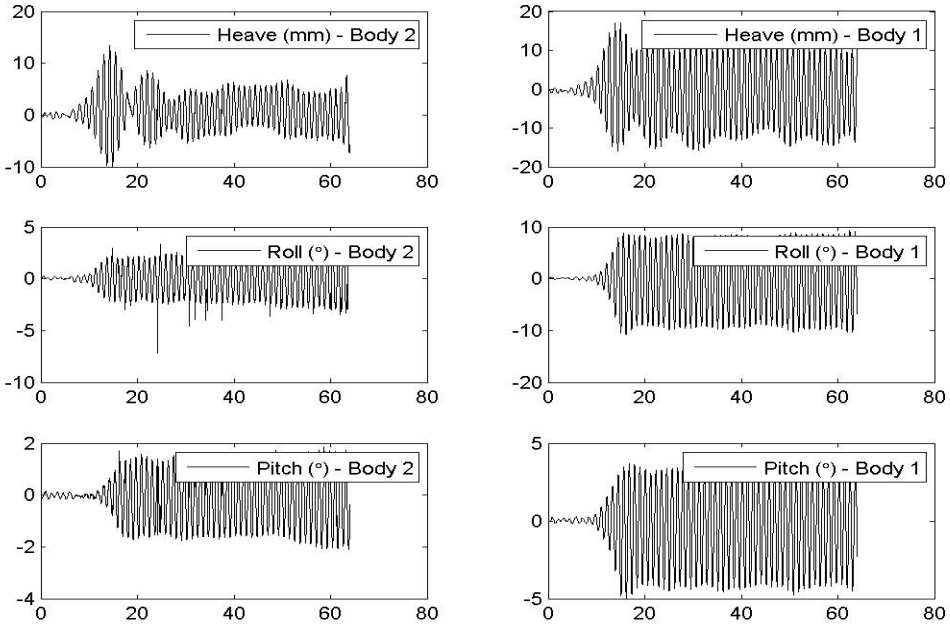

Vessel Motions, 30° Heading, 450 mm Gap and kL= 3.8302

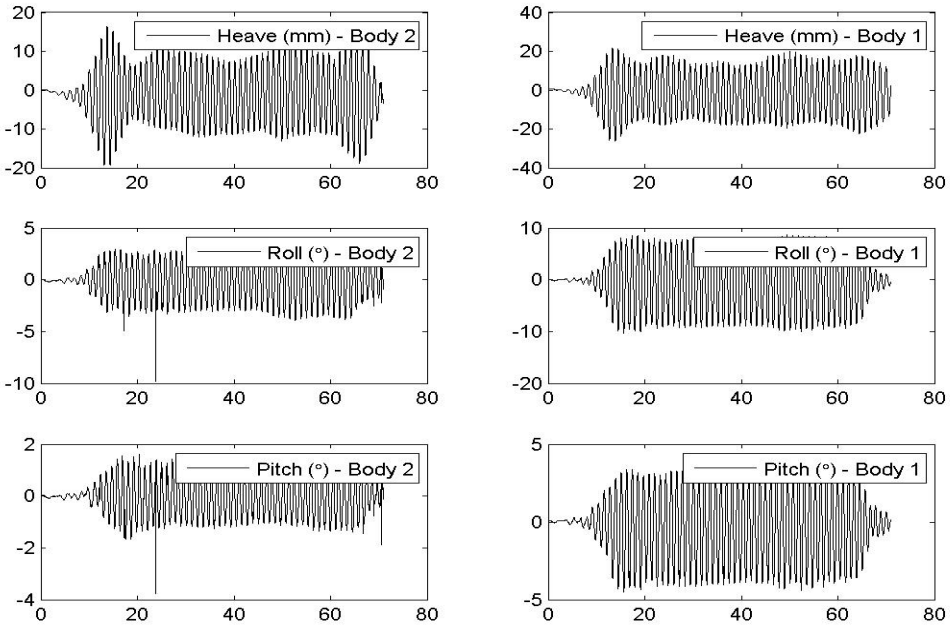

Vessel Motions, 30° Heading, 450 mm Gap and kL= 3.642

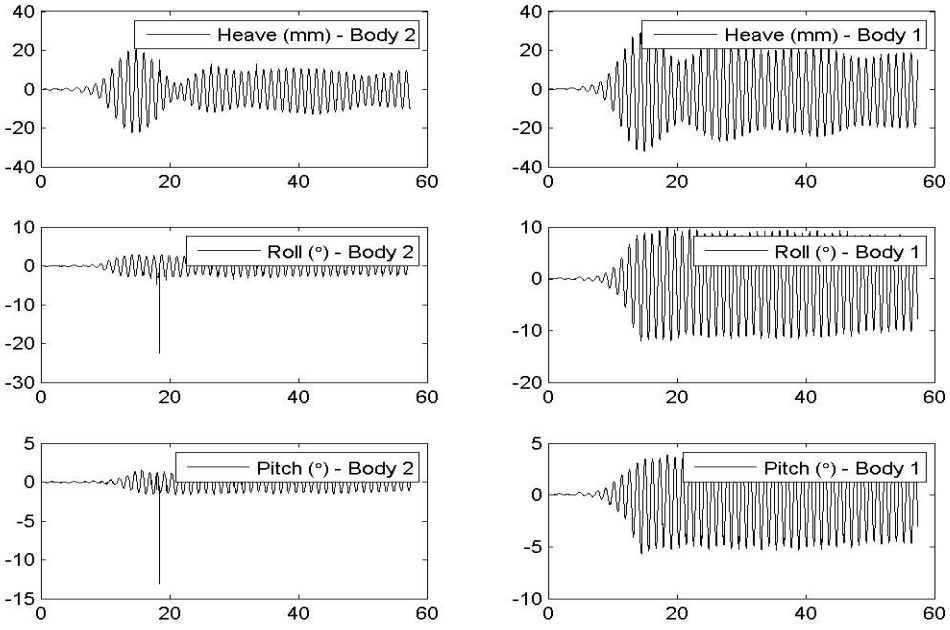

Vessel Motions, 30° Heading, 450 mm Gap and kL= 3.5078

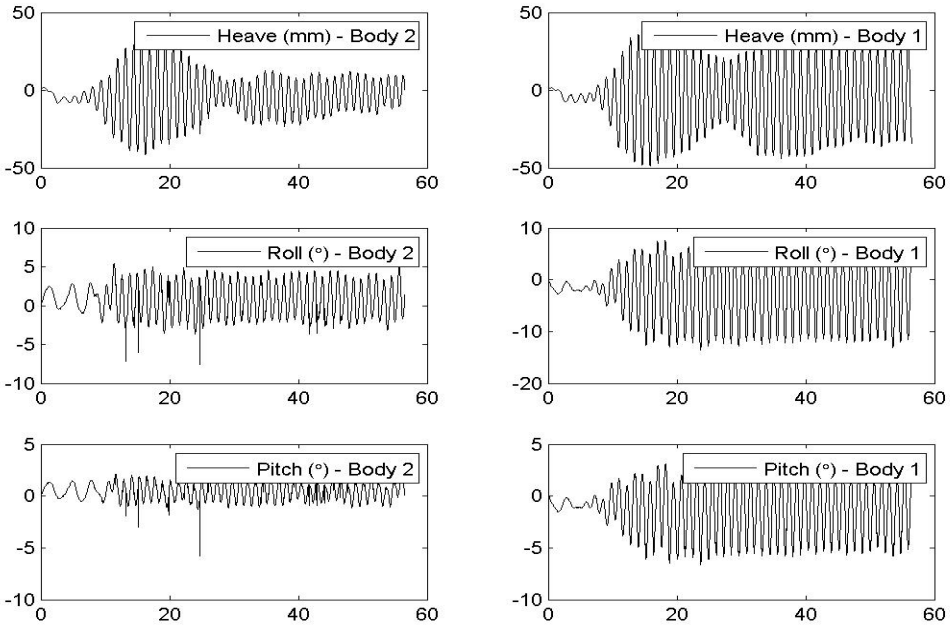

Vessel Motions, 30° Heading, 450 mm Gap and kL= 3.3595

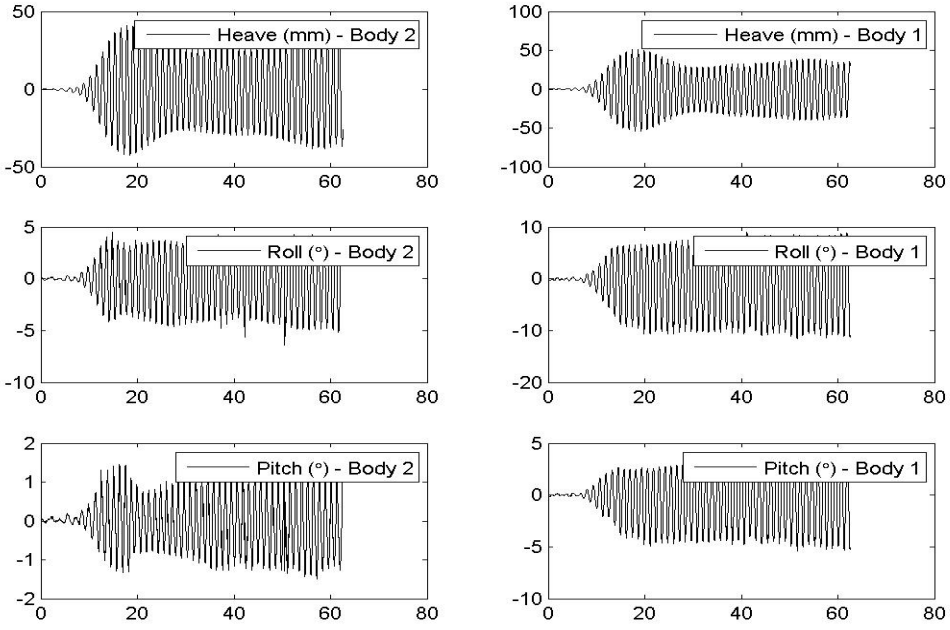

Vessel Motions, 30° Heading, 450 mm Gap and kL= 3.379

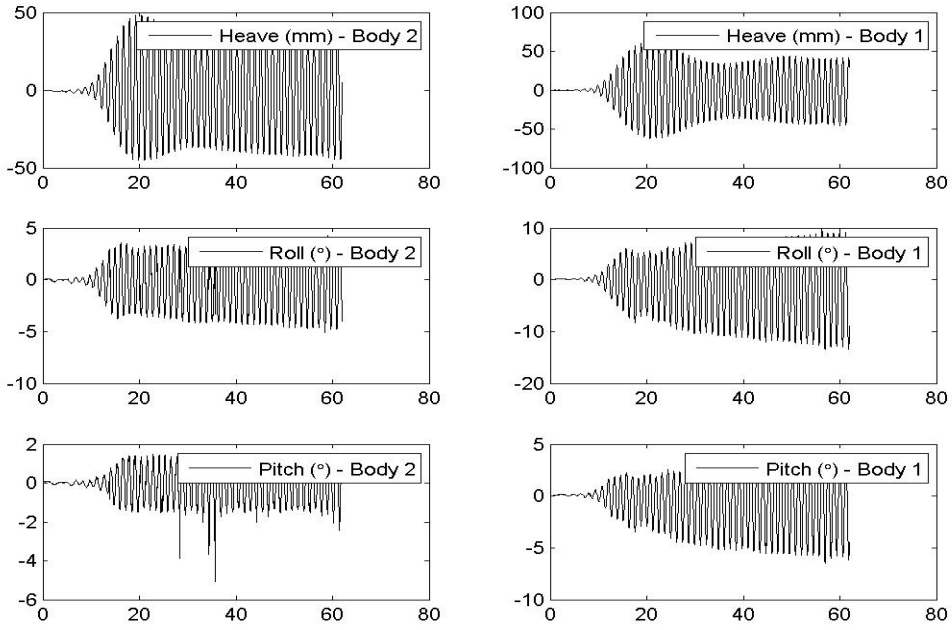

Vessel Motions, 30° Heading, 450 mm Gap and kL= 3.2373

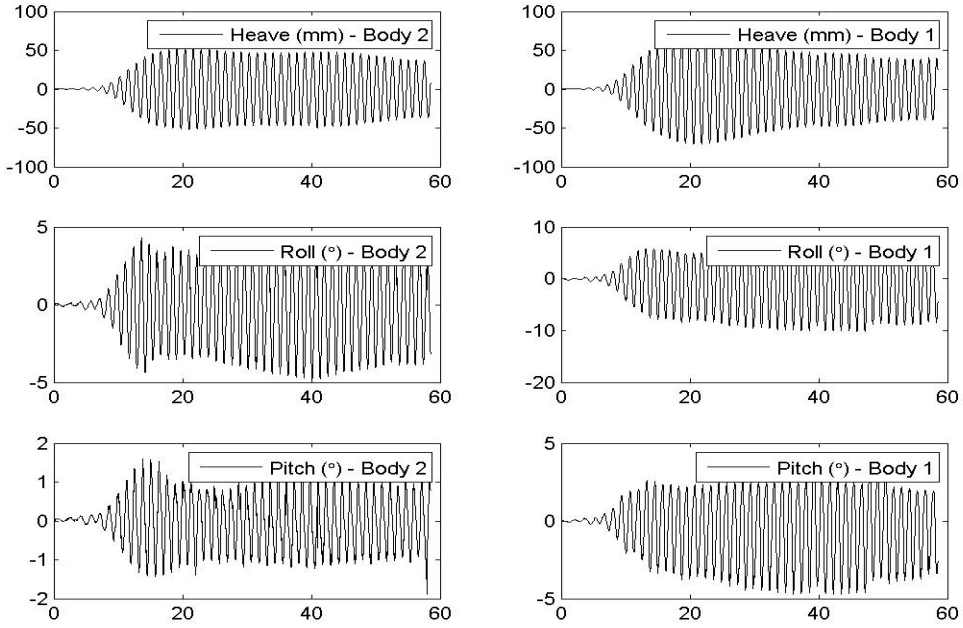

Vessel Motions, 30° Heading, 450 mm Gap and kL= 3.209

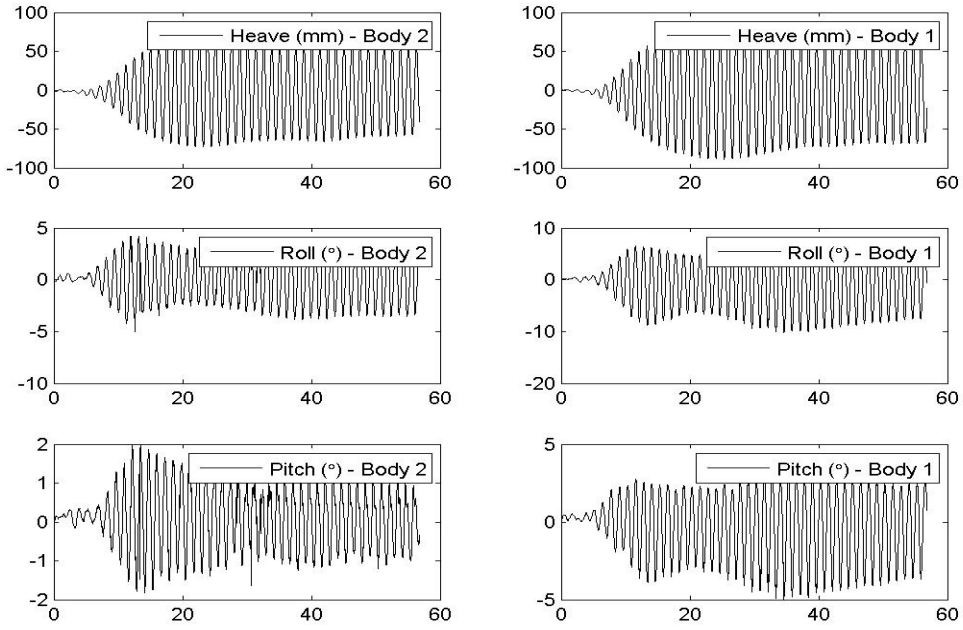

Vessel Motions, 30° Heading, 450 mm Gap and kL= 3.127

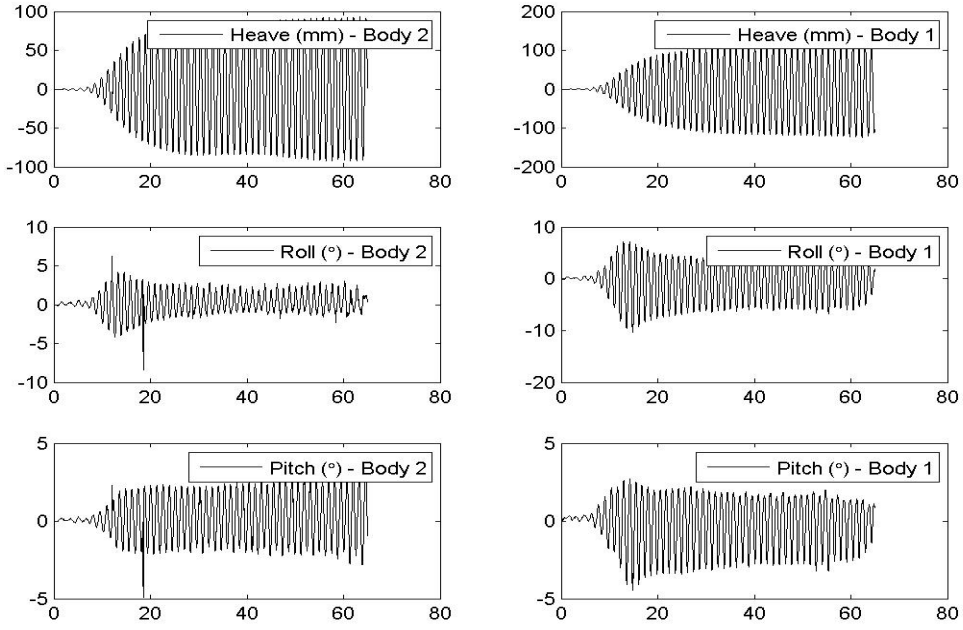

Vessel Motions, 30° Heading, 450 mm Gap and kL= 3.0419

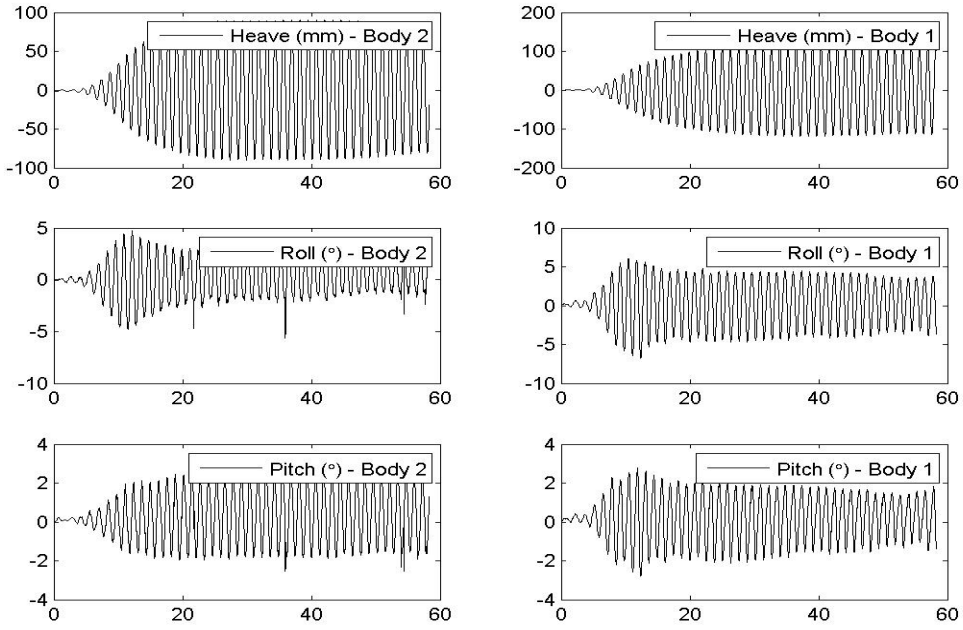

Vessel Motions, 30° Heading, 450 mm Gap and kL= 3.0304

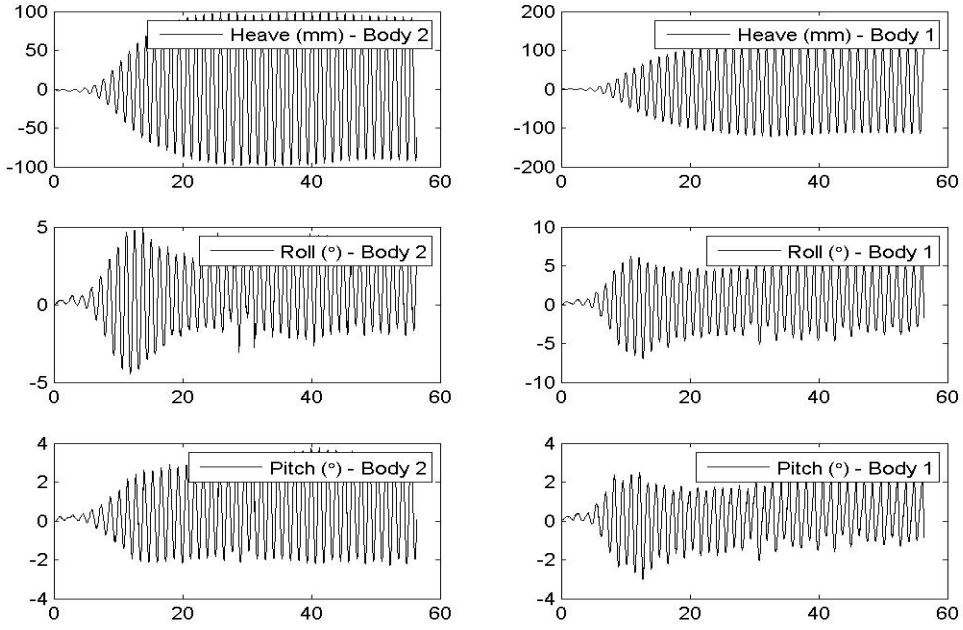

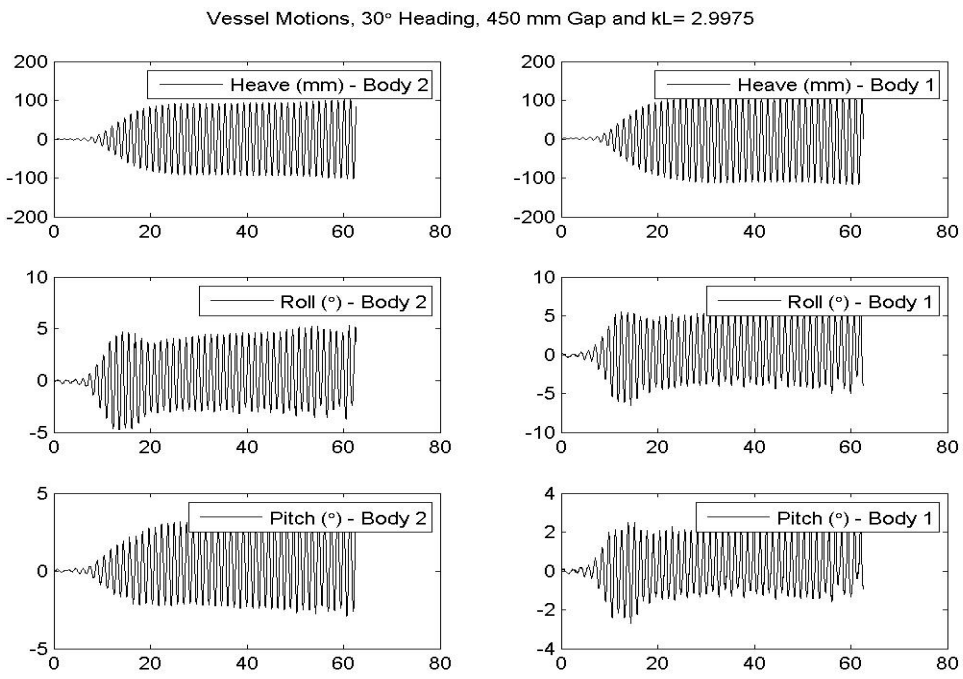
Vessel Motions, 30° Heading, 450 mm Gap and kL= 2.9975
Heave (mm) - Body 2
Heave (mm) - Body 1
Roll (°) - Body 2
Roll (°) - Body 1
Pitch (°) - Body 2
Pitch (°) - Body 1

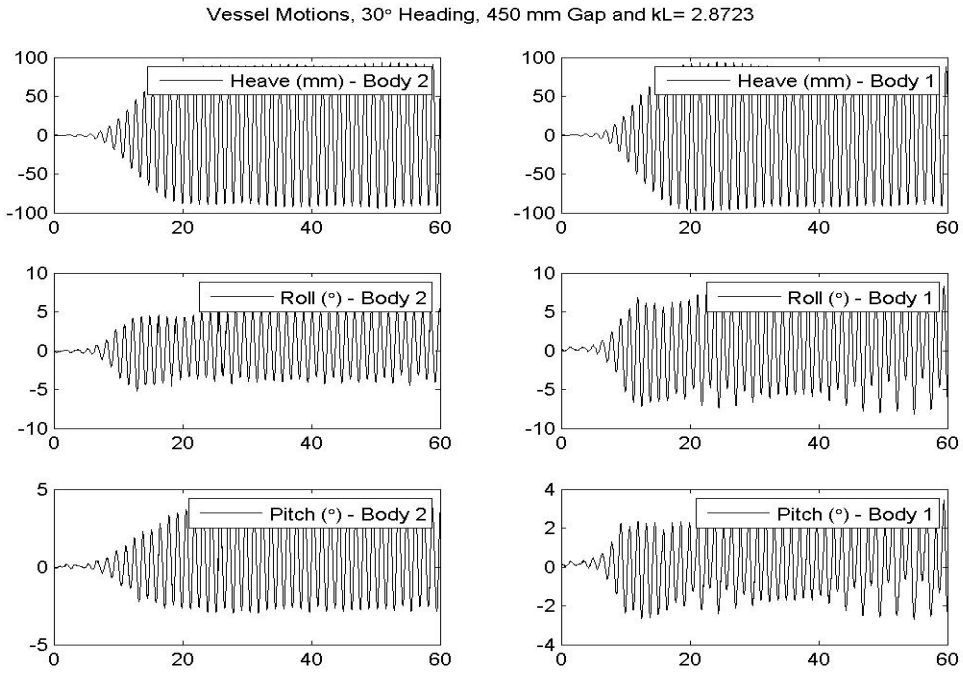
Vessel Motions, 30° Heading, 450 mm Gap and kL= 2.8723
Heave (mm) - Body 2
Heave (mm) - Body 1
Roll (°) - Body 2
Roll (°) - Body 1
Pitch (°) - Body 2
Pitch (°) - Body 1

Vessel Motions, 30° Heading, 450 mm Gap and kL= 2.8307

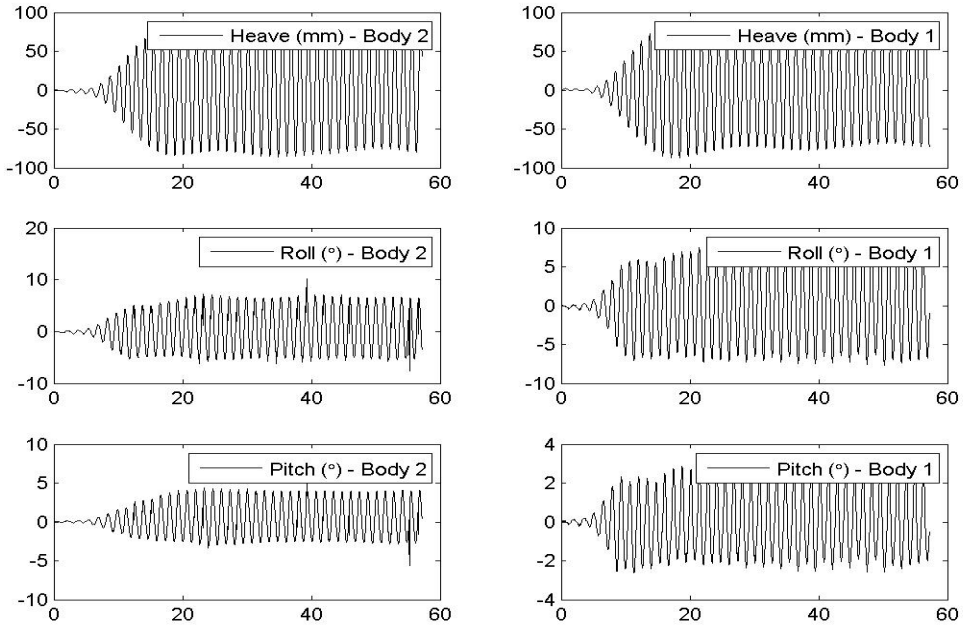

Vessel Motions, 30° Heading, 450 mm Gap and kL= 2.6906

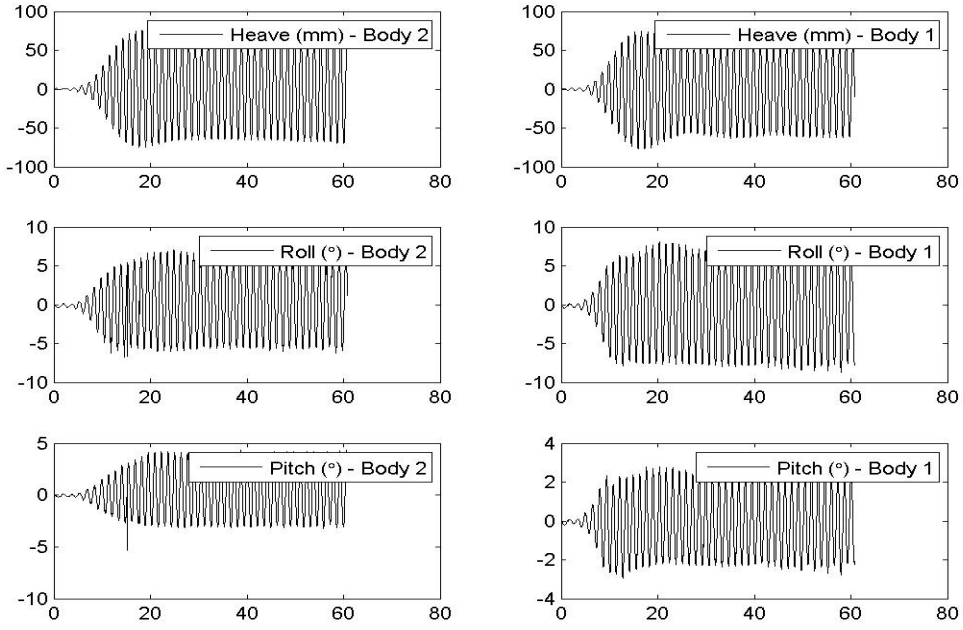

Vessel Motions, 30° Heading, 450 mm Gap and kL= 2.652

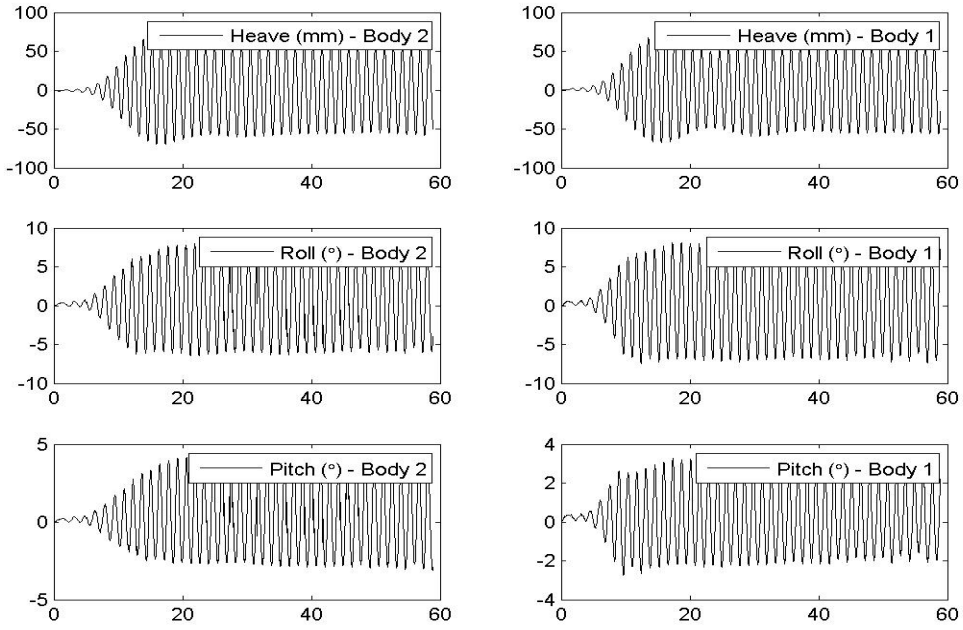

Vessel Motions, 30° Heading, 450 mm Gap and kL= 2.4848

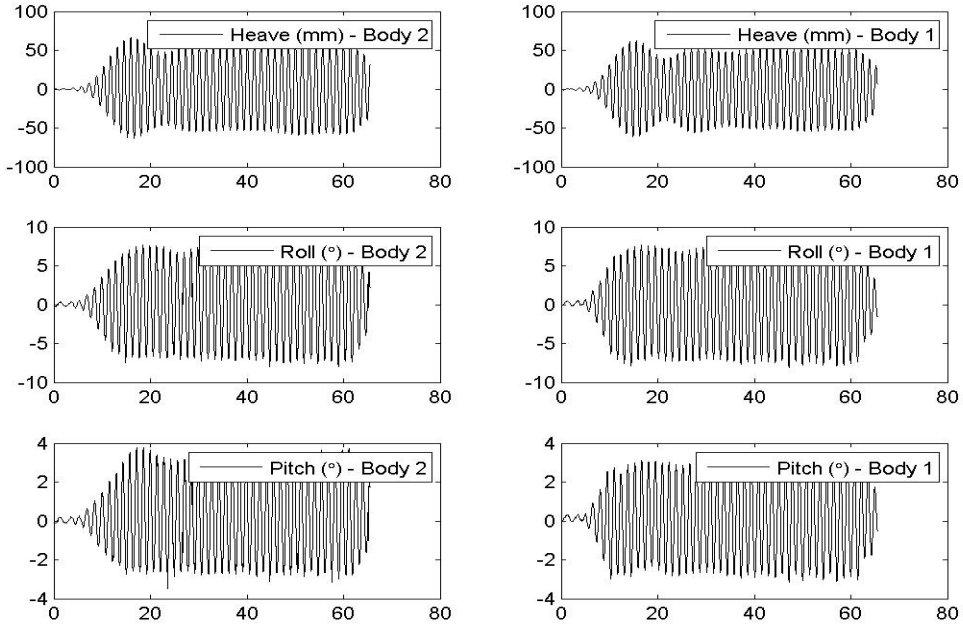

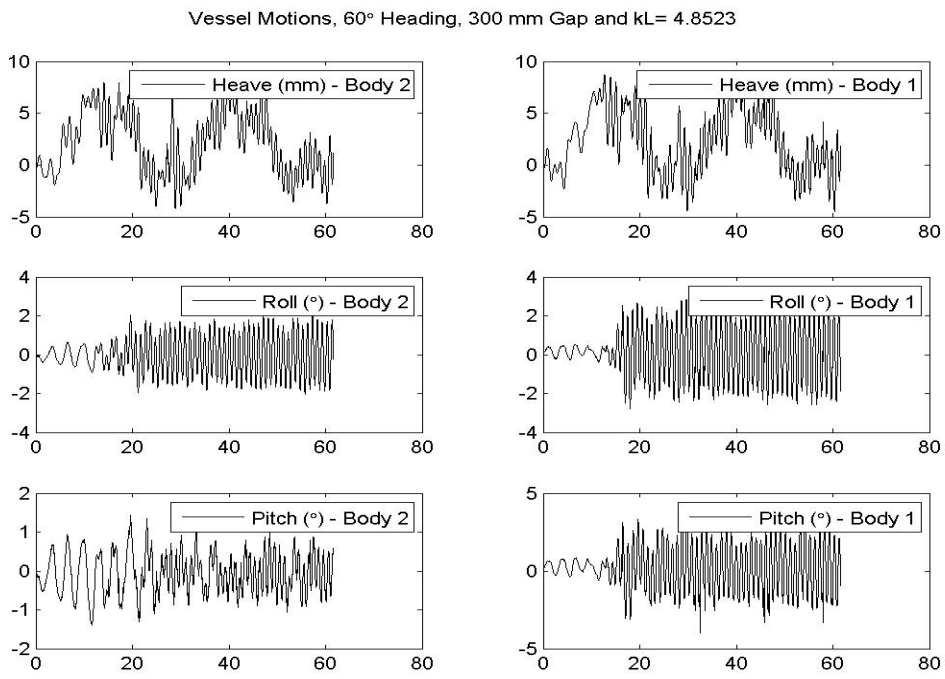
Vessel Motions, 60° Heading, 300 mm Gap and kL= 4.8523
Heave (mm) - Body 2
Heave (mm) - Body 1
Roll (°) - Body 2
Roll (°) - Body 1
Pitch (°) - Body 2
Pitch (°) - Body 1

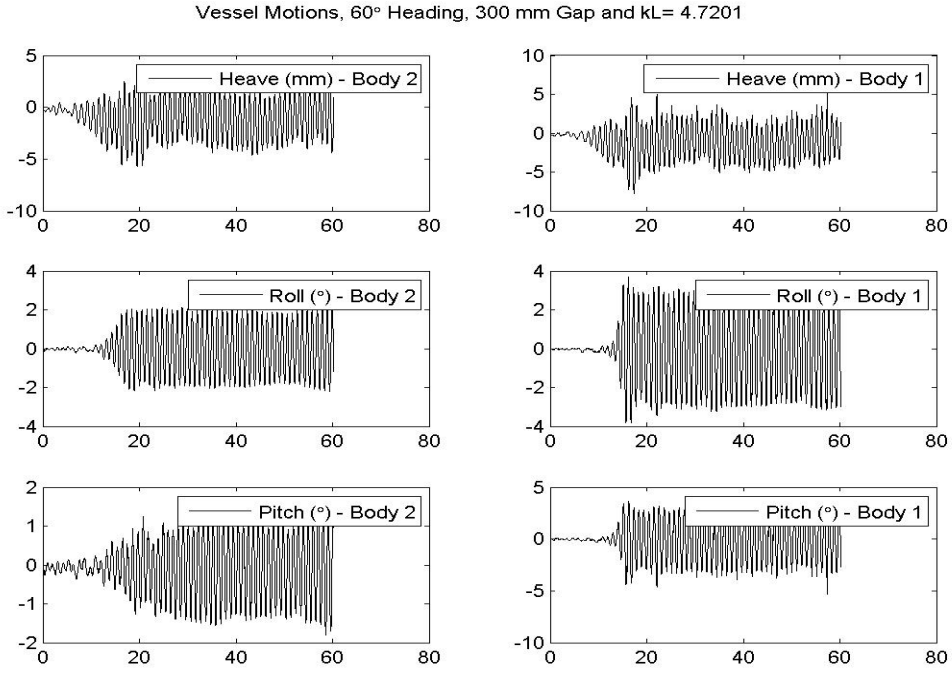
Vessel Motions, 60° Heading, 300 mm Gap and kL= 4.7201
Heave (mm) - Body 2
Heave (mm) - Body 1
Roll (°) - Body 2
Roll (°) - Body 1
Pitch (°) - Body 2
Pitch (°) - Body 1

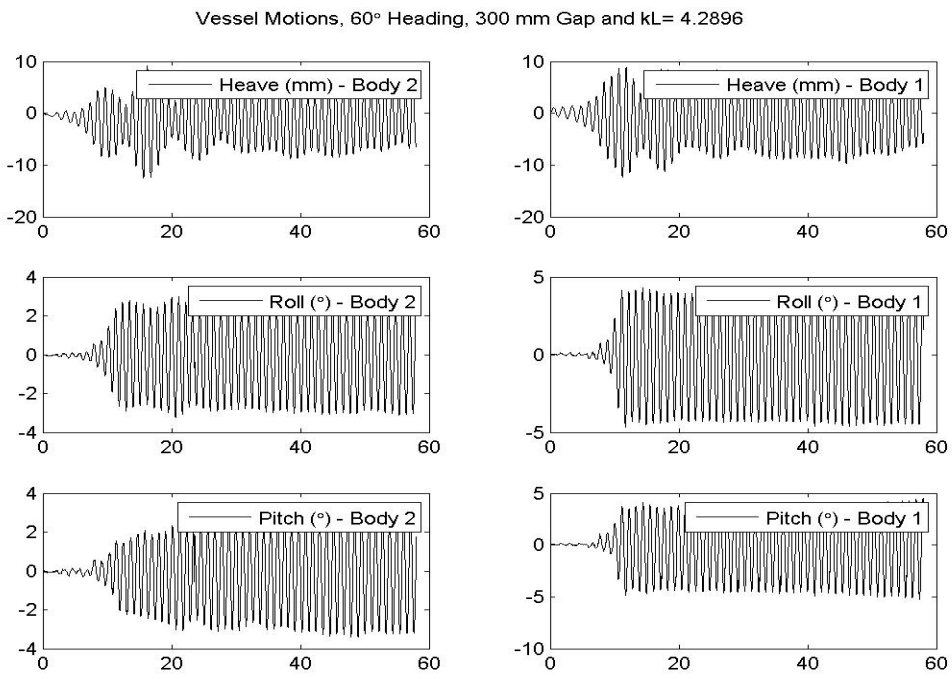
Vessel Motions, 60° Heading, 300 mm Gap and kL= 4.2896
Heave (mm) - Body 2
Heave (mm) - Body 1
Roll (°) - Body 2
Roll (°) - Body 1
Pitch (°) - Body 2
Pitch (°) - Body 1

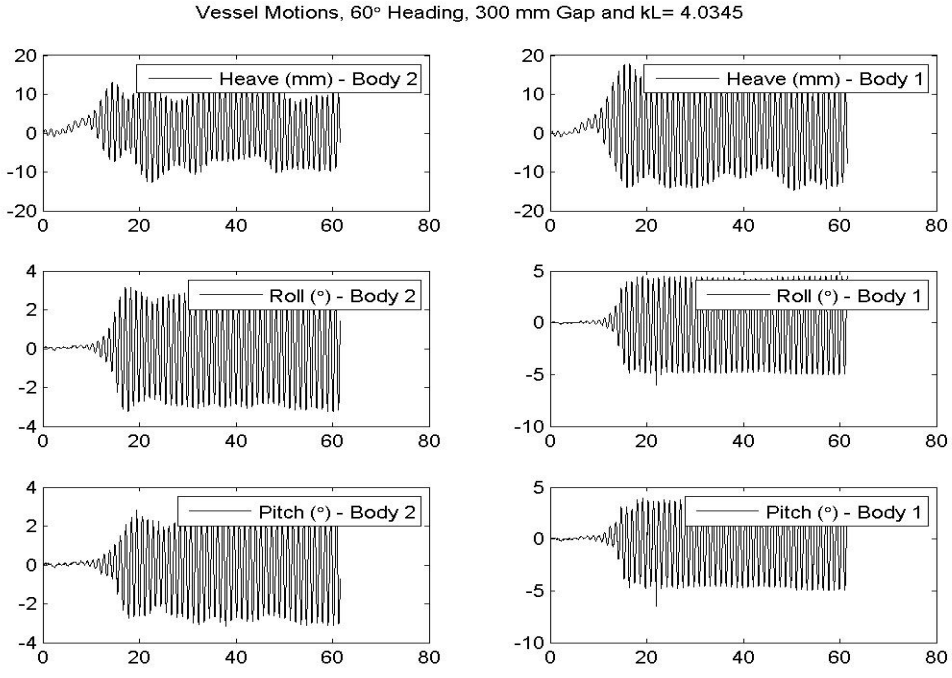
Vessel Motions, 60° Heading, 300 mm Gap and kL= 4.0345
Heave (mm) - Body 2
Heave (mm) - Body 1
Roll (°) - Body 2
Roll (°) - Body 1
Pitch (°) - Body 2
Pitch (°) - Body 1

Vessel Motions, 60° Heading, 300 mm Gap and kL= 3.8226

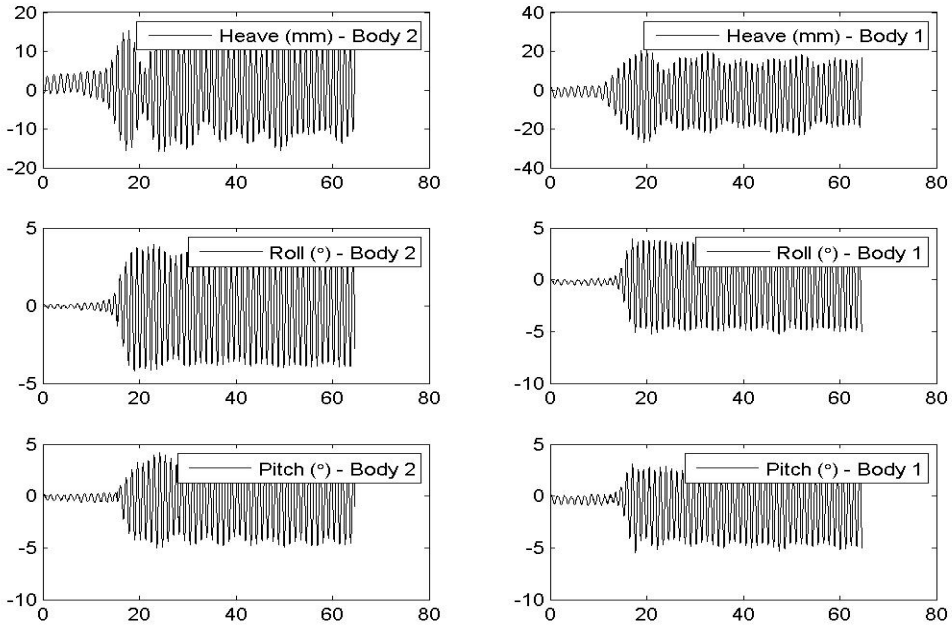

Vessel Motions, 60° Heading, 300 mm Gap and kL= 3.662

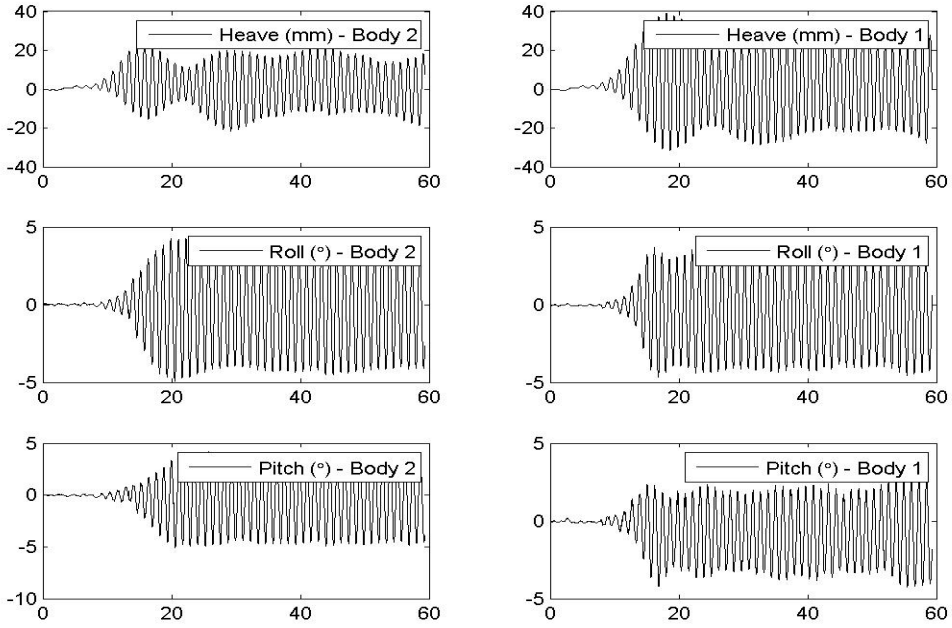

Vessel Motions, 60° Heading, 300 mm Gap and kL= 3.5152

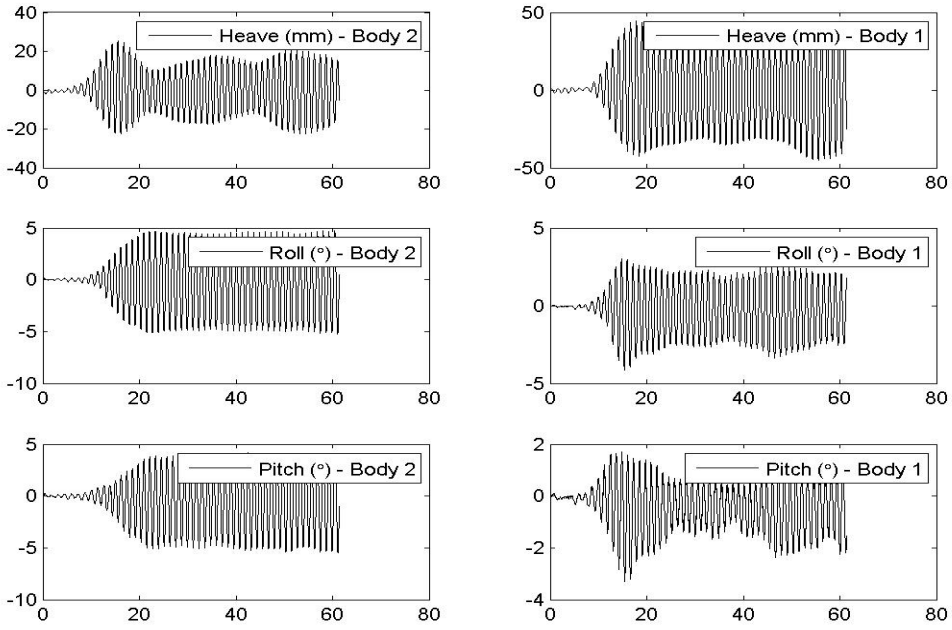

Vessel Motions, 60° Heading, 300 mm Gap and kL= 3.389

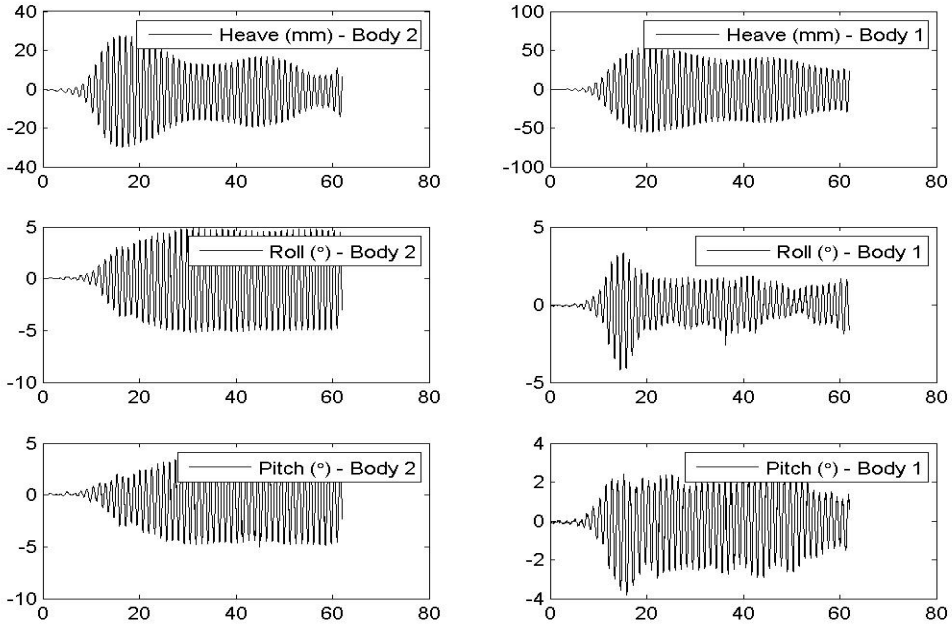

Vessel Motions, 60° Heading, 300 mm Gap and kL= 3.3792

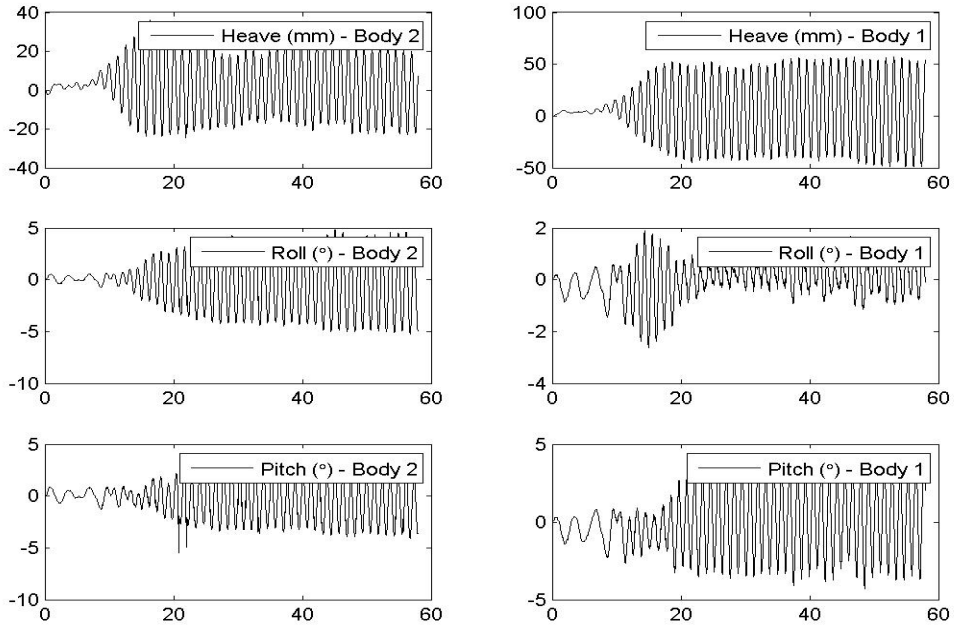

Vessel Motions, 60° Heading, 300 mm Gap and kL= 3.2261

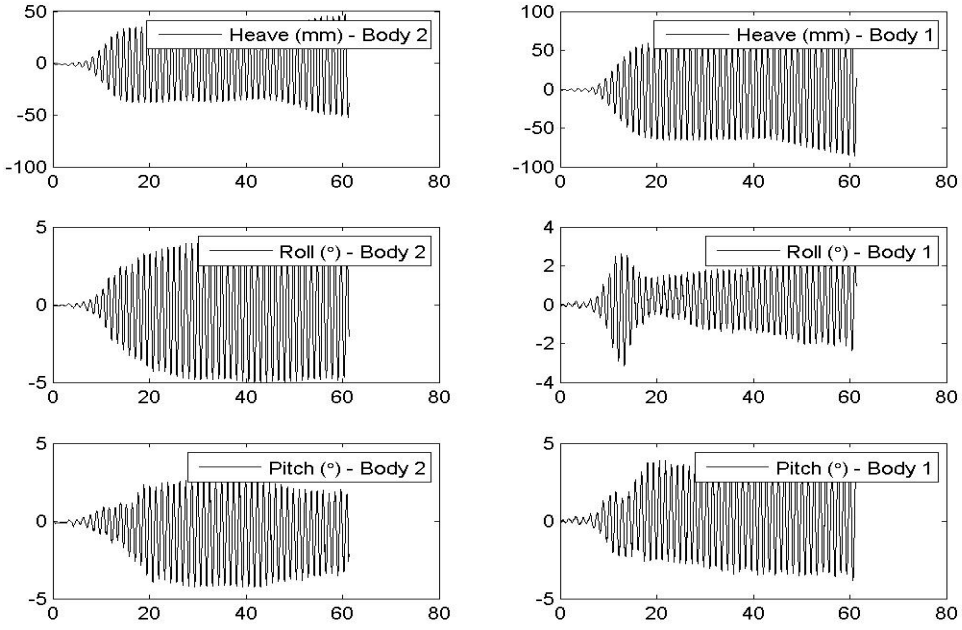

Vessel Motions, 60° Heading, 300 mm Gap and kL= 3.2481

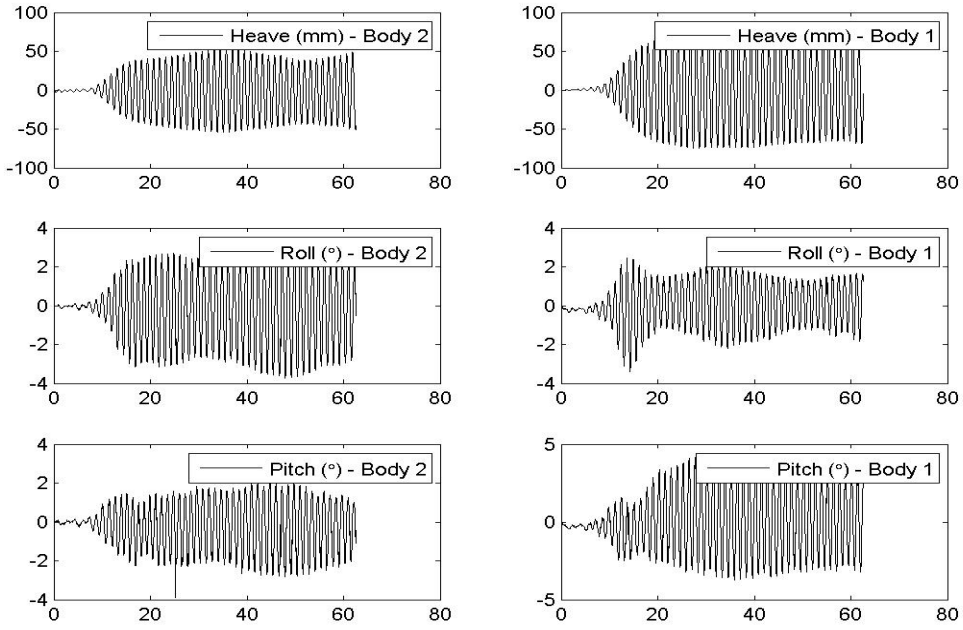

Vessel Motions, 60° Heading, 300 mm Gap and kL= 3.0658

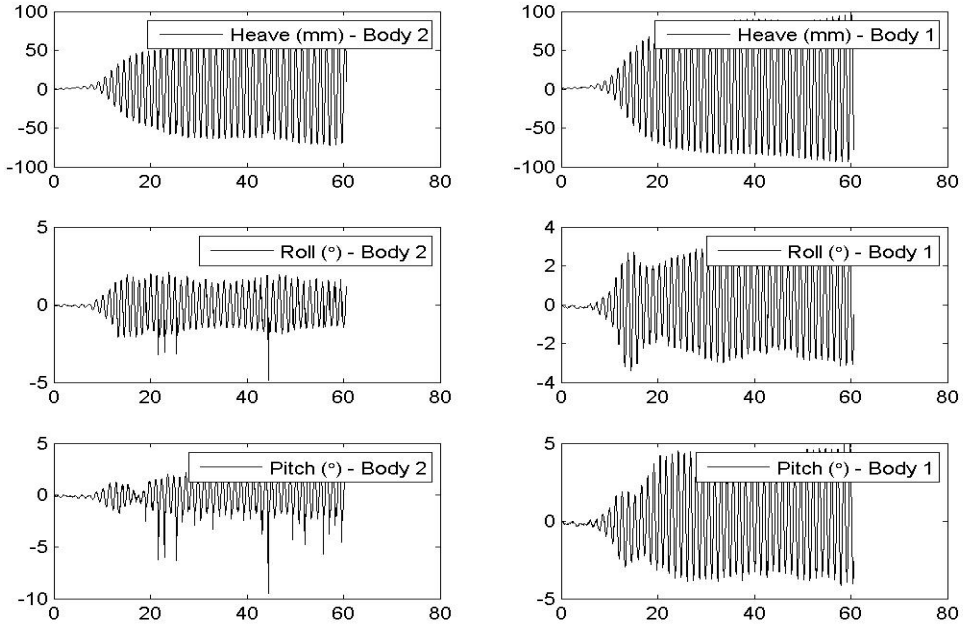

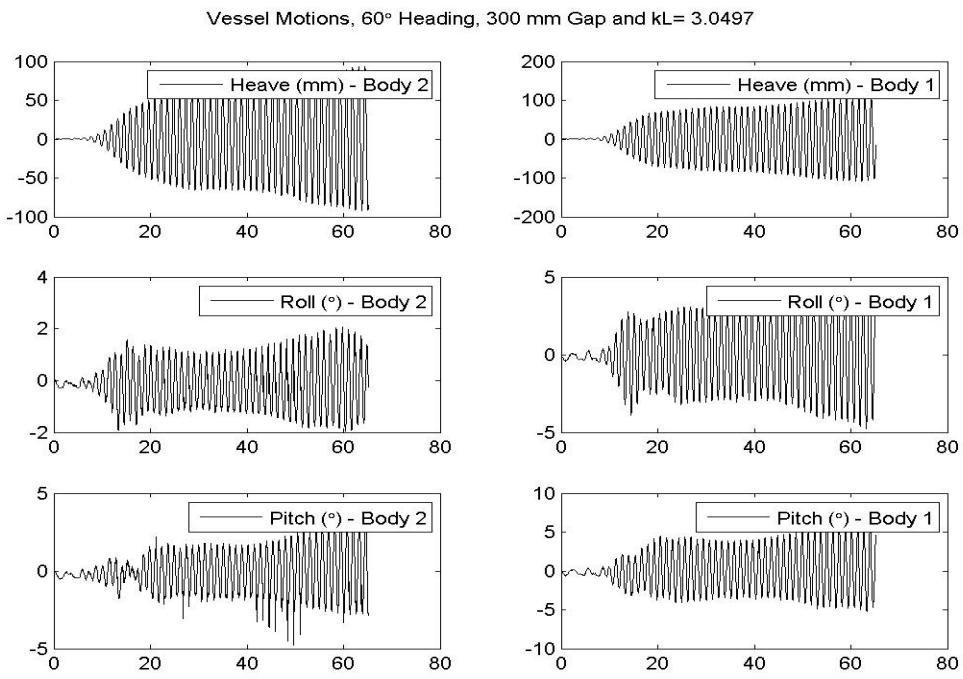
Vessel Motions, 60° Heading, 300 mm Gap and kL= 3.0497
Heave (mm) - Body 2
Heave (mm) - Body 1
Roll (°) - Body 2
Roll (°) - Body 1
Pitch (°) - Body 2
Pitch (°) - Body 1

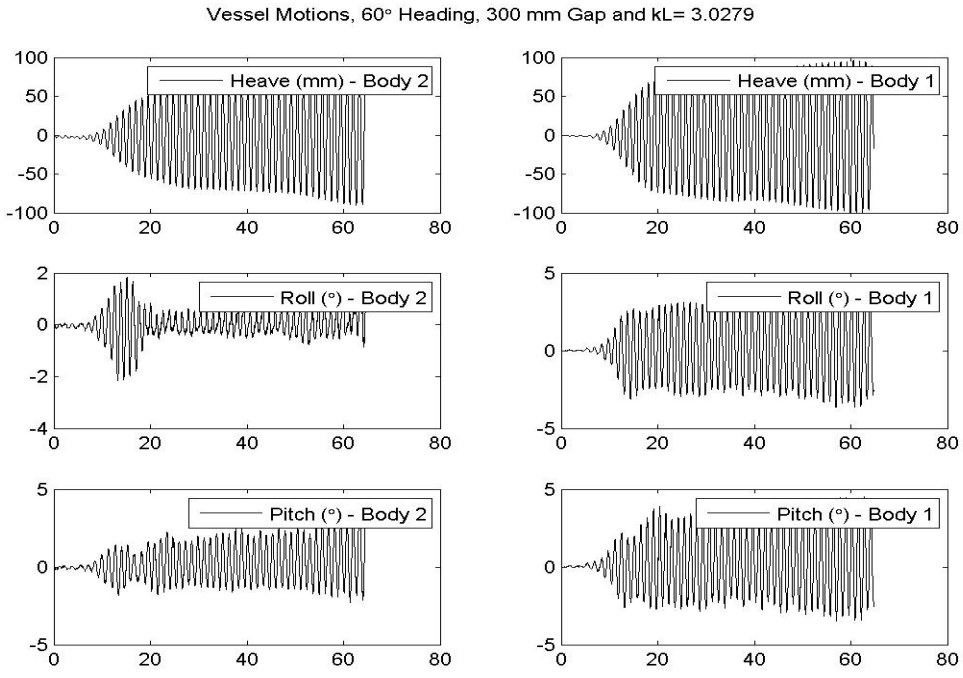
Vessel Motions, 60° Heading, 300 mm Gap and kL= 3.0279
Heave (mm) - Body 2
Heave (mm) - Body 1
Roll (°) - Body 2
Roll (°) - Body 1
Pitch (°) - Body 2
Pitch (°) - Body 1

Vessel Motions, 60° Heading, 300 mm Gap and kL= 2.9725

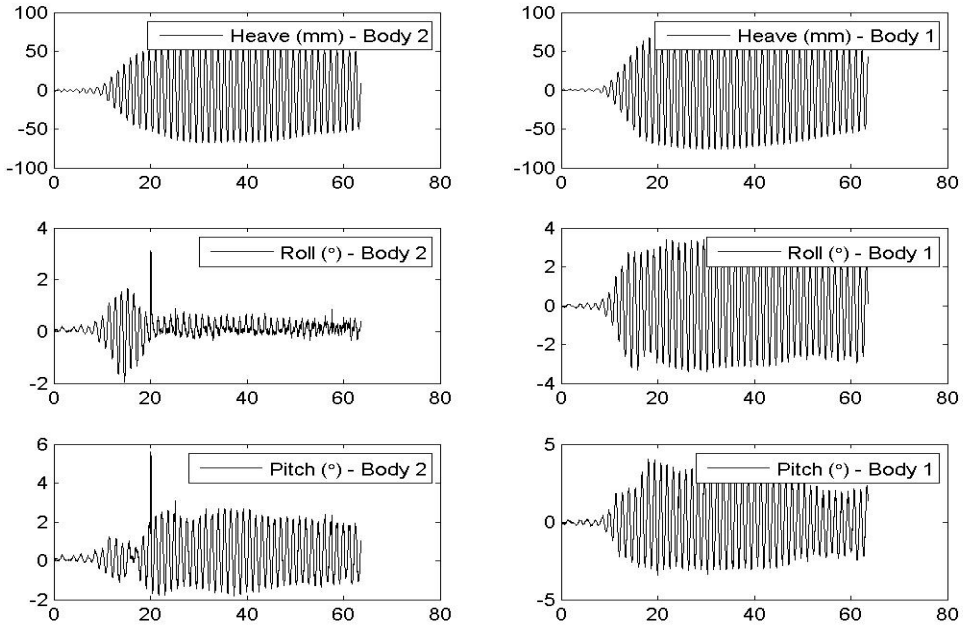

Vessel Motions, 60° Heading, 300 mm Gap and kL= 2.8647

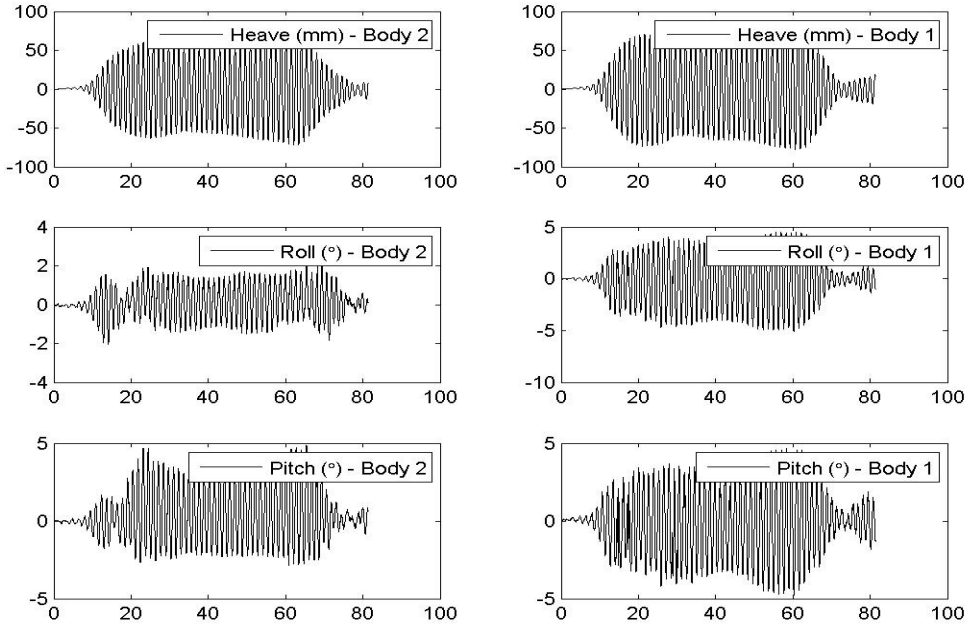

Vessel Motions, 60° Heading, 300 mm Gap and kL= 2.8255

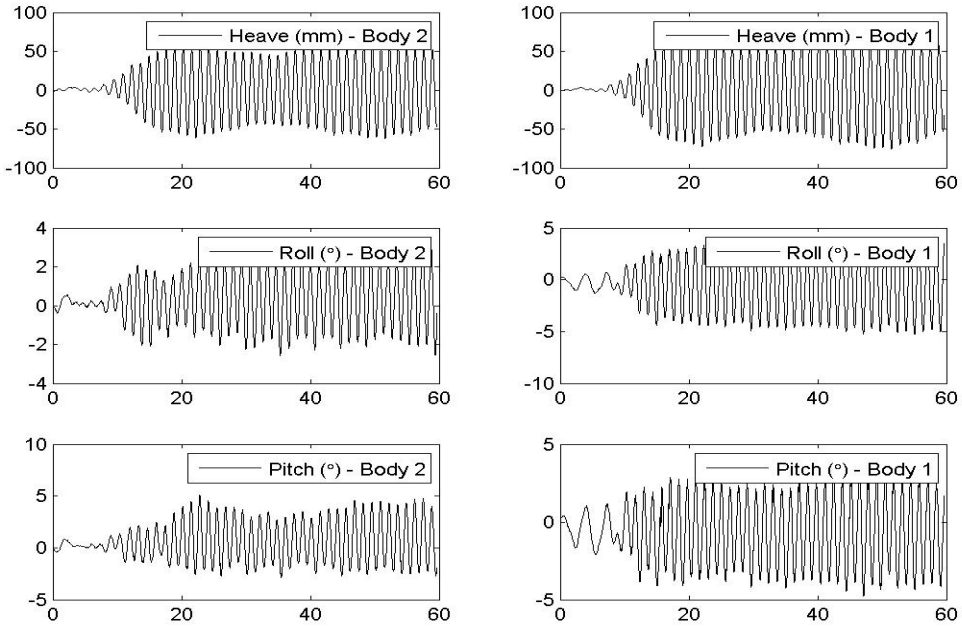

Vessel Motions, 60° Heading, 300 mm Gap and kL= 2.6737

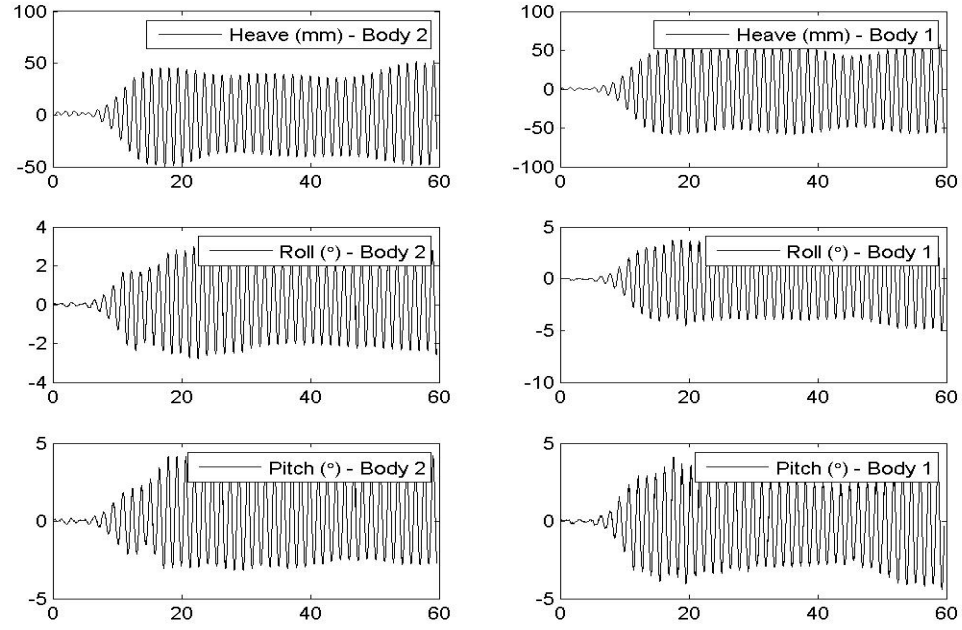

Vessel Motions, 60° Heading, 300 mm Gap and kL= 2.6181

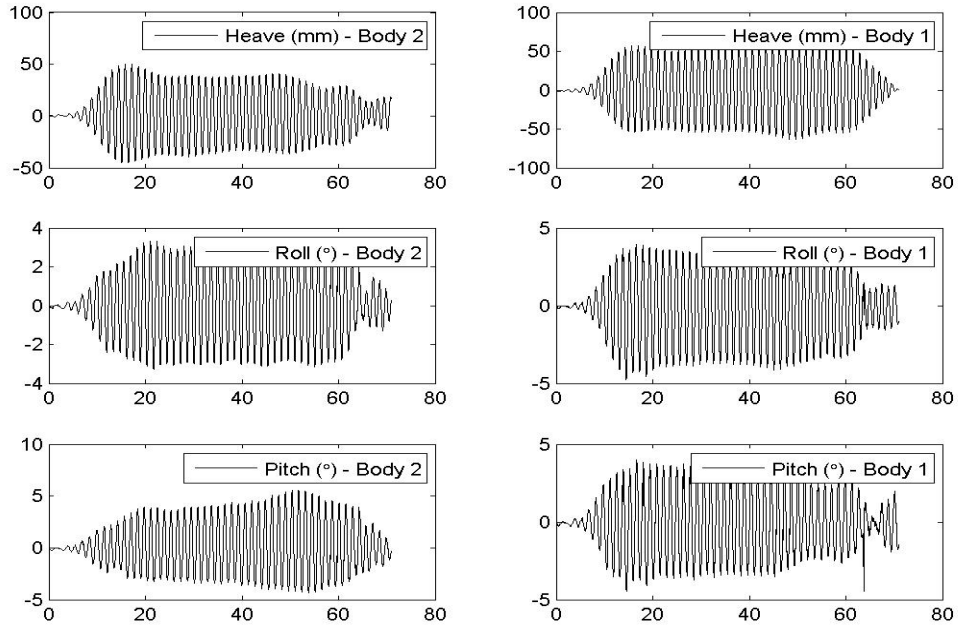

Vessel Motions, 60° Heading, 300 mm Gap and kL= 2.4855

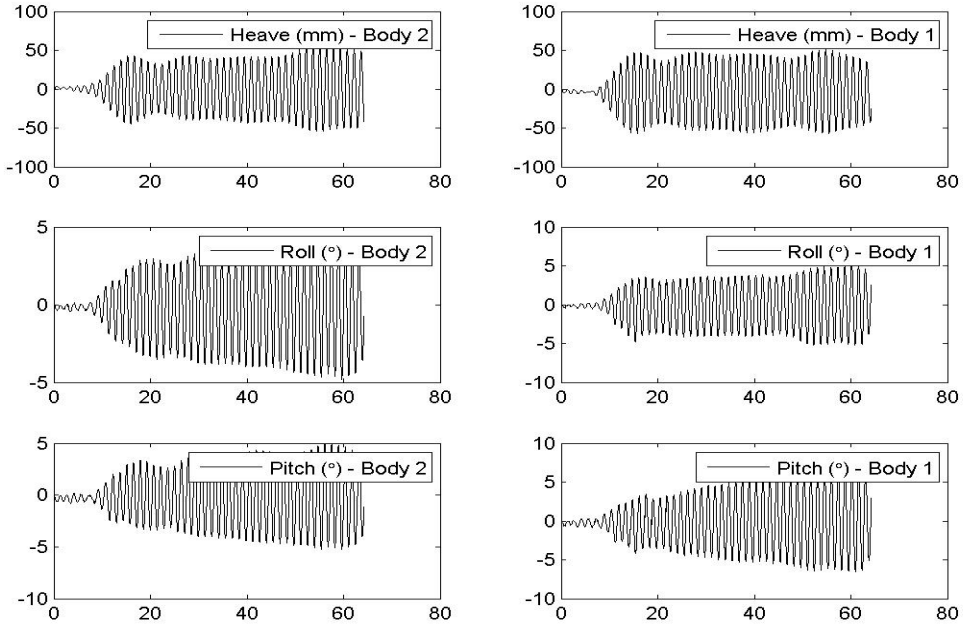

Vessel Motions, 60° Heading, 450 mm Gap and kL= 4.7491

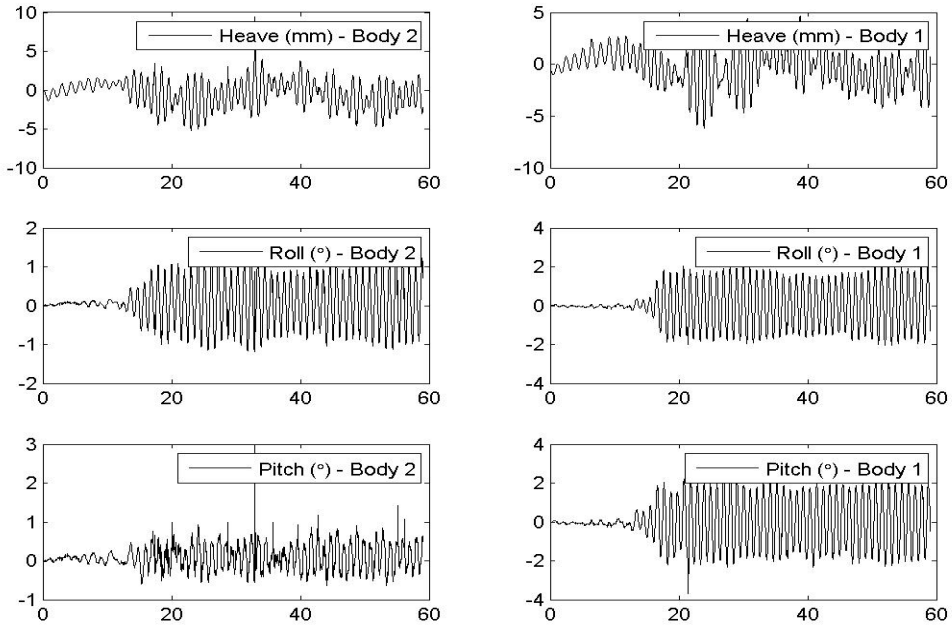

Vessel Motions, 60° Heading, 450 mm Gap and kL= 4.7248

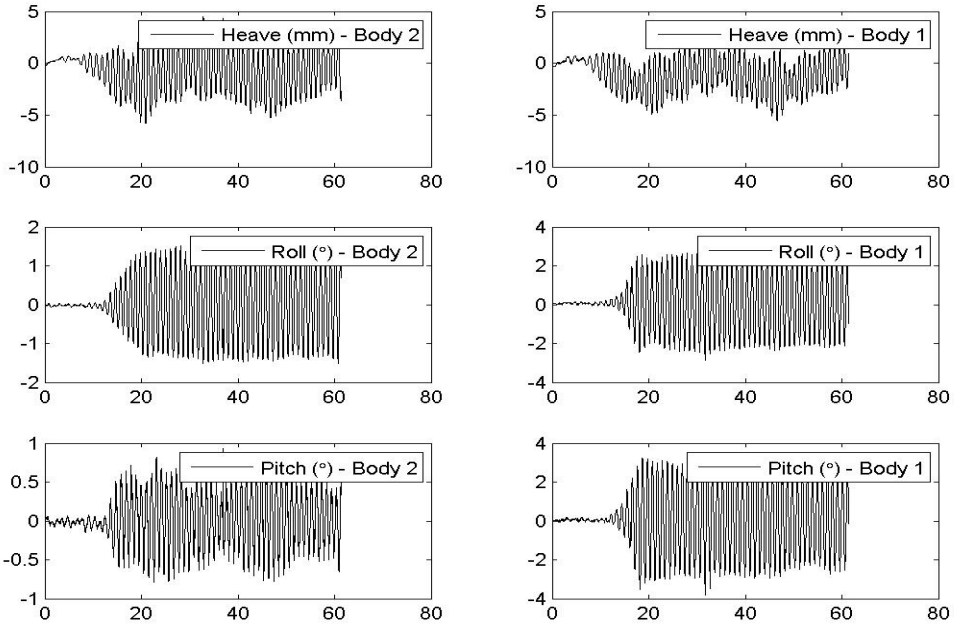

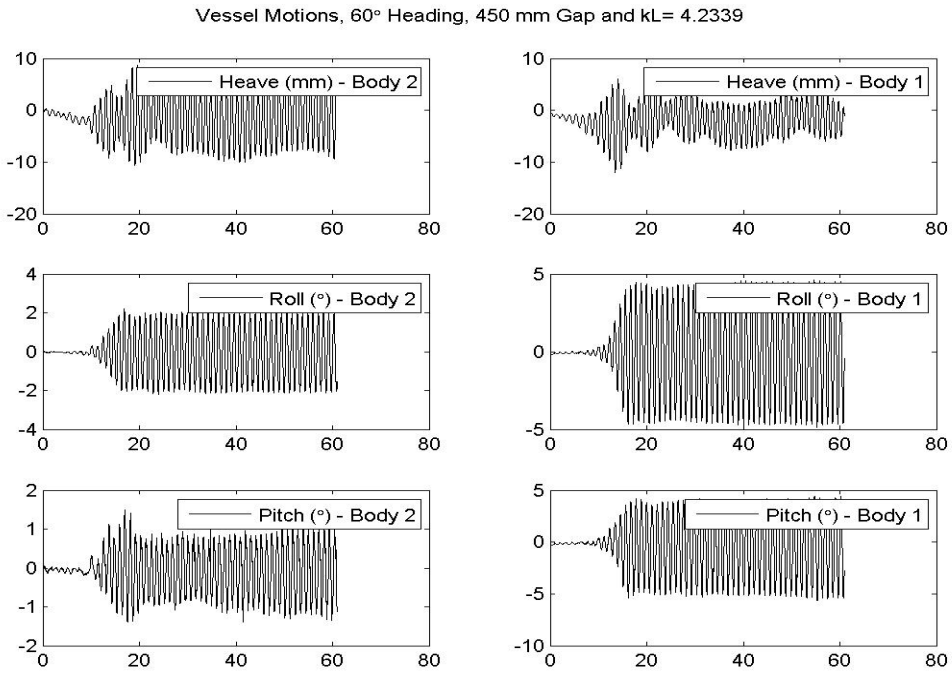
Vessel Motions, 60° Heading, 450 mm Gap and kL= 4.2339
Heave (mm) - Body 2
Heave (mm) - Body 1
Roll (°) - Body 2
Roll (°) - Body 1
Pitch (°) - Body 2
Pitch (°) - Body 1

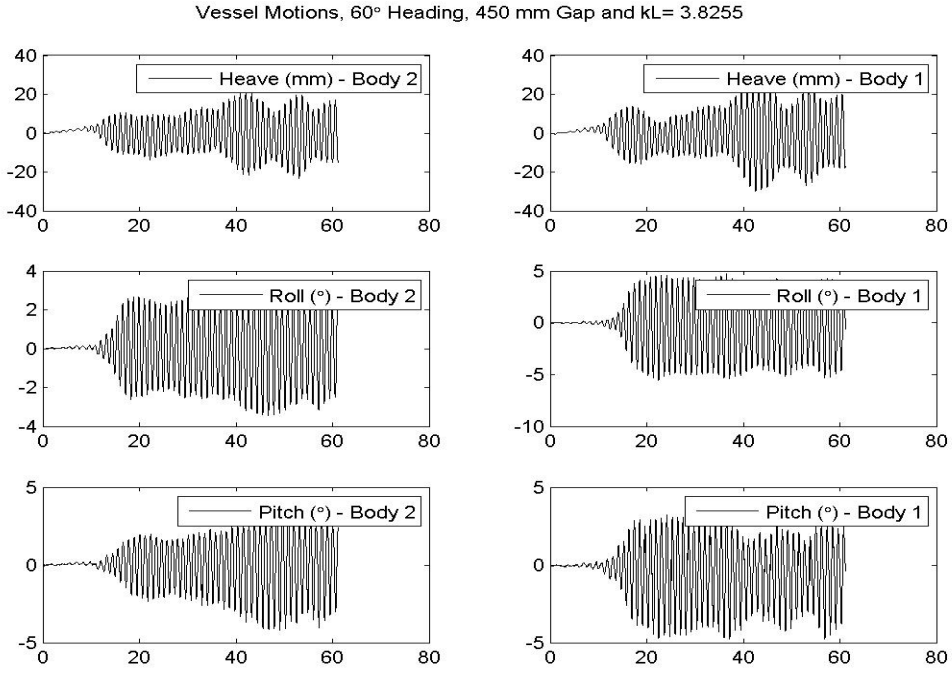
Vessel Motions, 60° Heading, 450 mm Gap and kL= 3.8255
Heave (mm) - Body 2
Heave (mm) - Body 1
Roll (°) - Body 2
Roll (°) - Body 1
Pitch (°) - Body 2
Pitch (°) - Body 1

Vessel Motions, 60° Heading, 450 mm Gap and kL= 3.8007

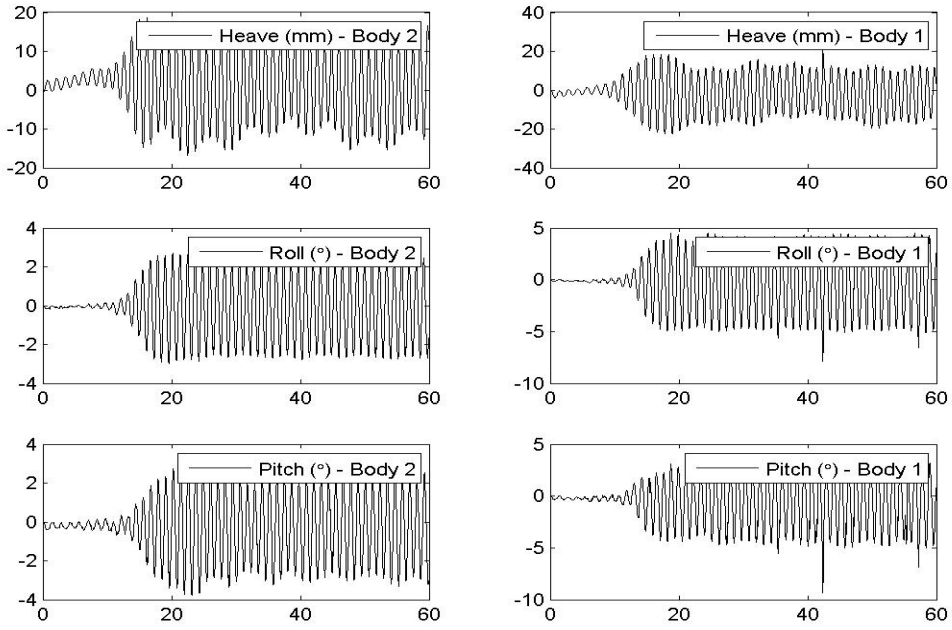

Vessel Motions, 60° Heading, 450 mm Gap and kL= 3.5979

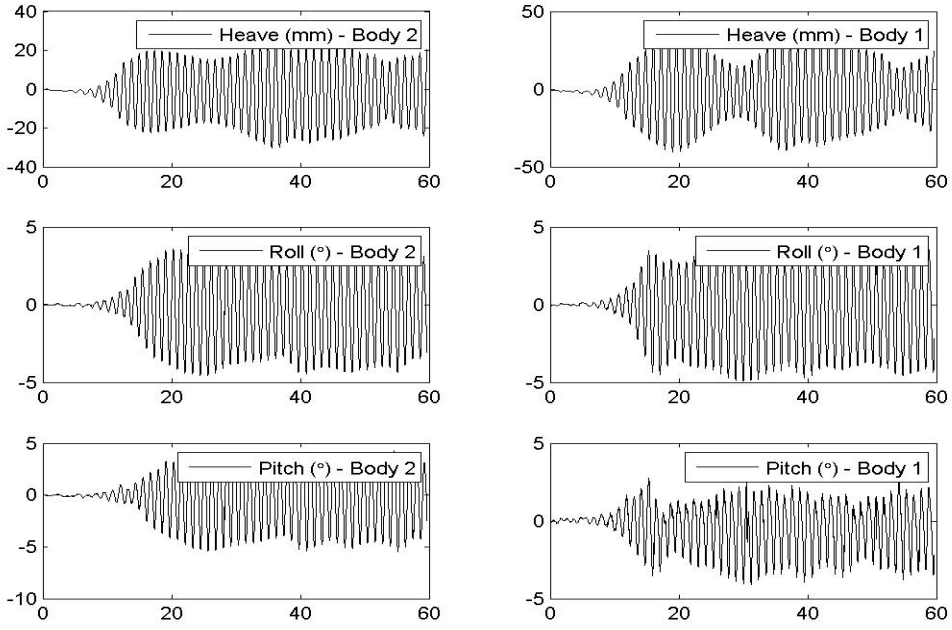

Vessel Motions, 60° Heading, 450 mm Gap and kL= 3.5226

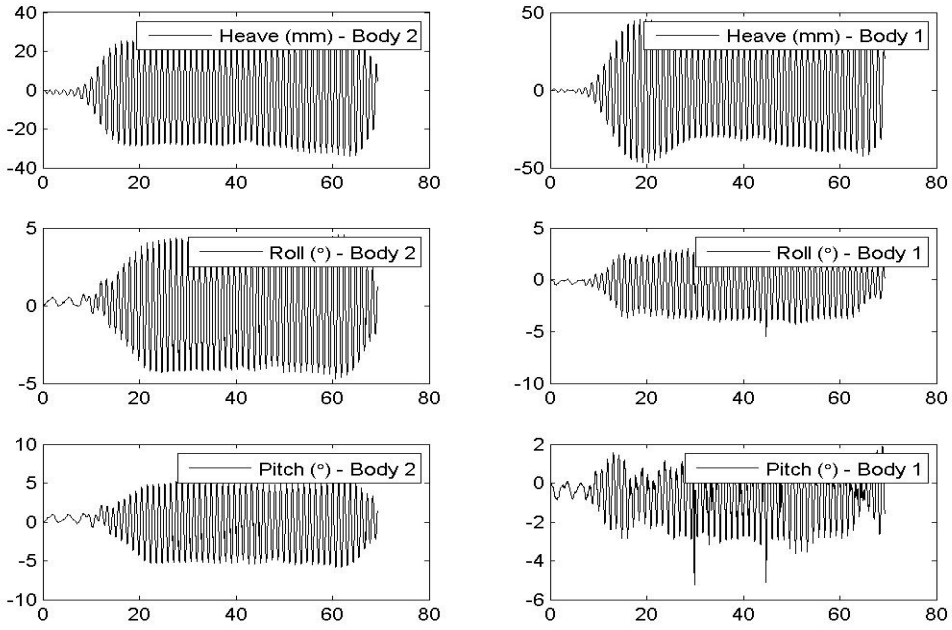

Vessel Motions, 60° Heading, 450 mm Gap and kL= 3.3831

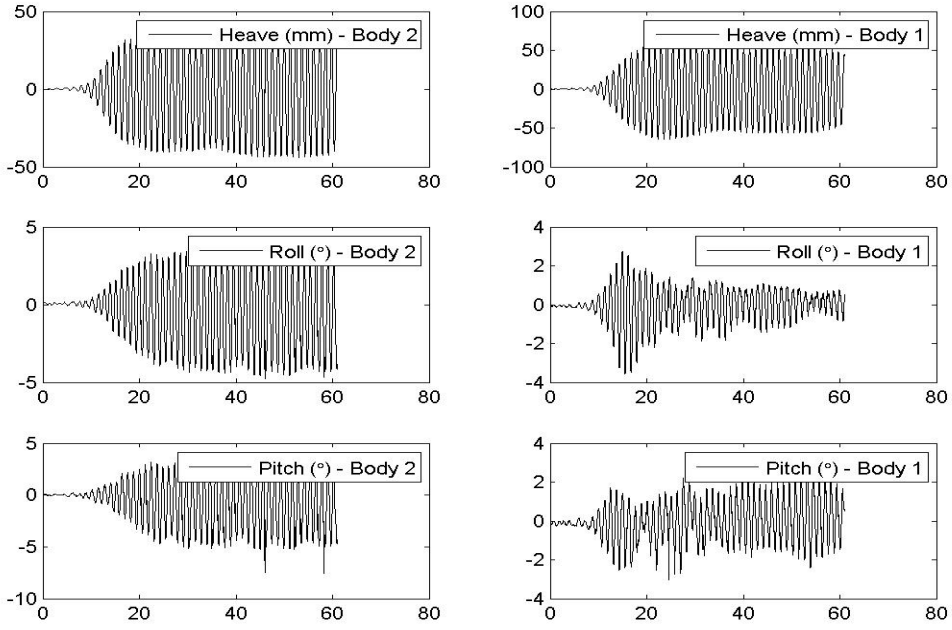

Vessel Motions, 60° Heading, 450 mm Gap and kL= 3.2252

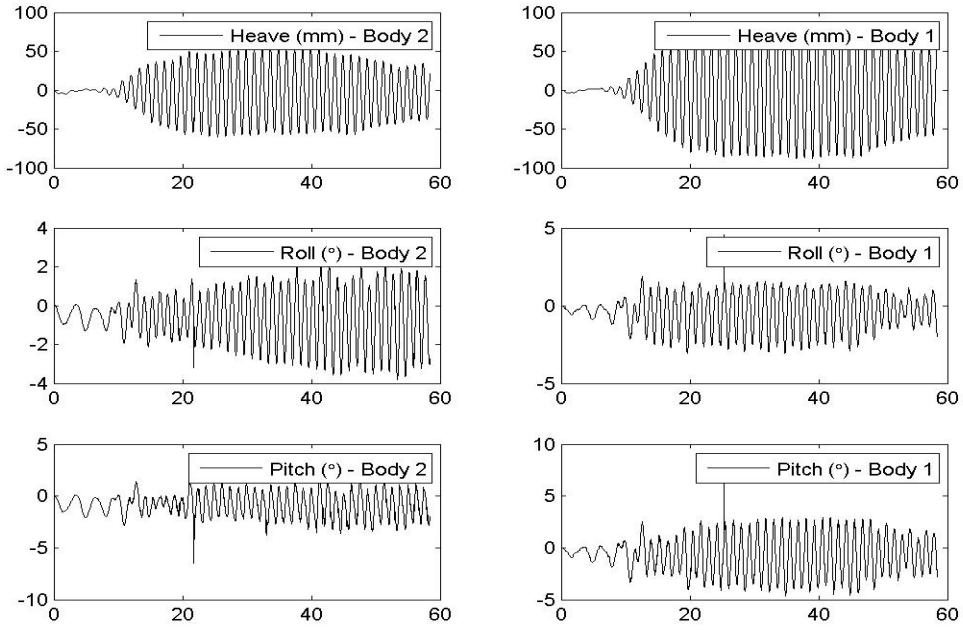

Vessel Motions, 60° Heading, 450 mm Gap and kL= 3.2873

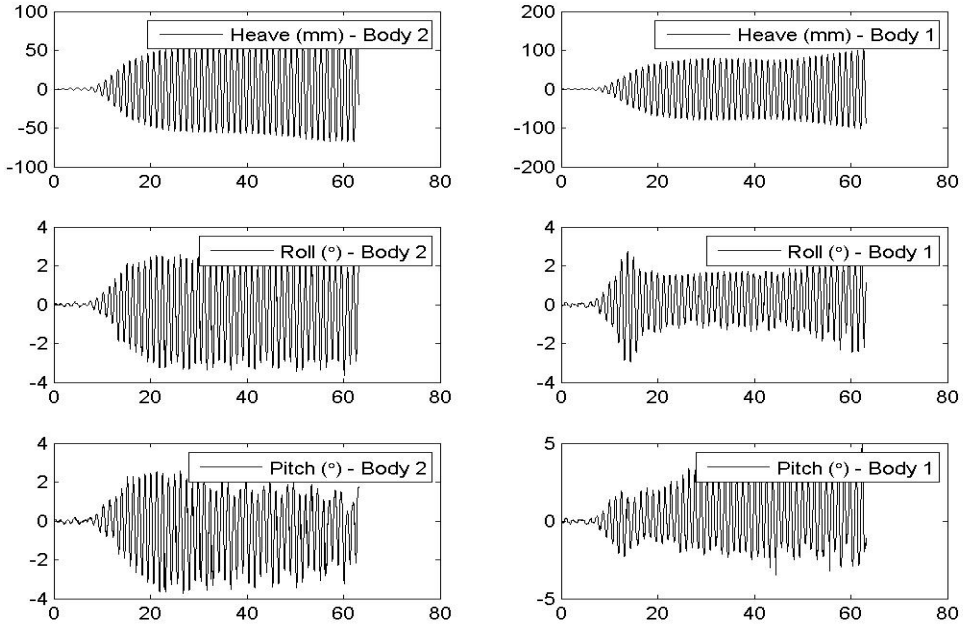

Vessel Motions, 60° Heading, 450 mm Gap and kL= 3.2165

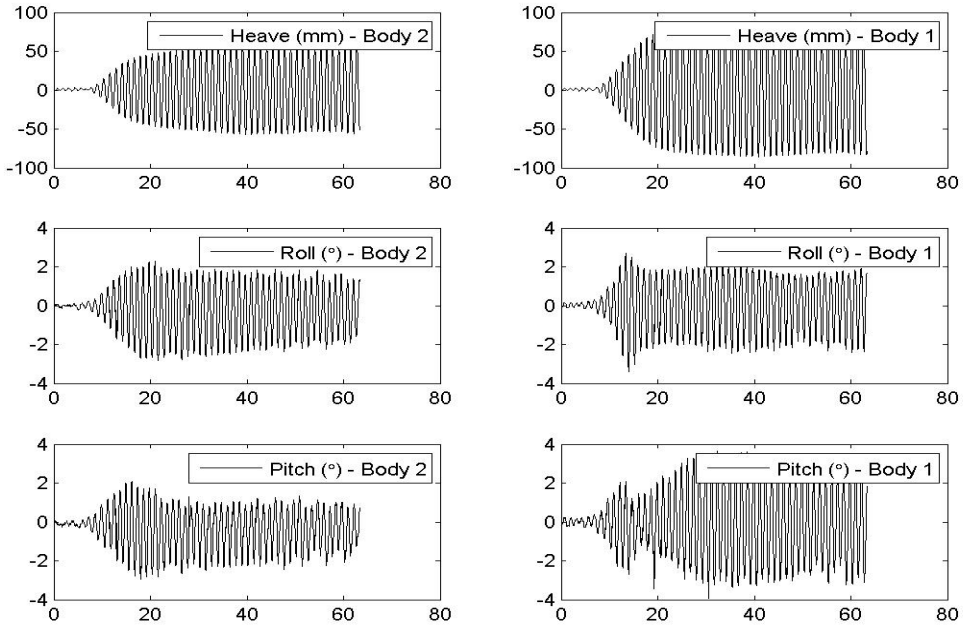

Vessel Motions, 60° Heading, 450 mm Gap and kL= 3.0278

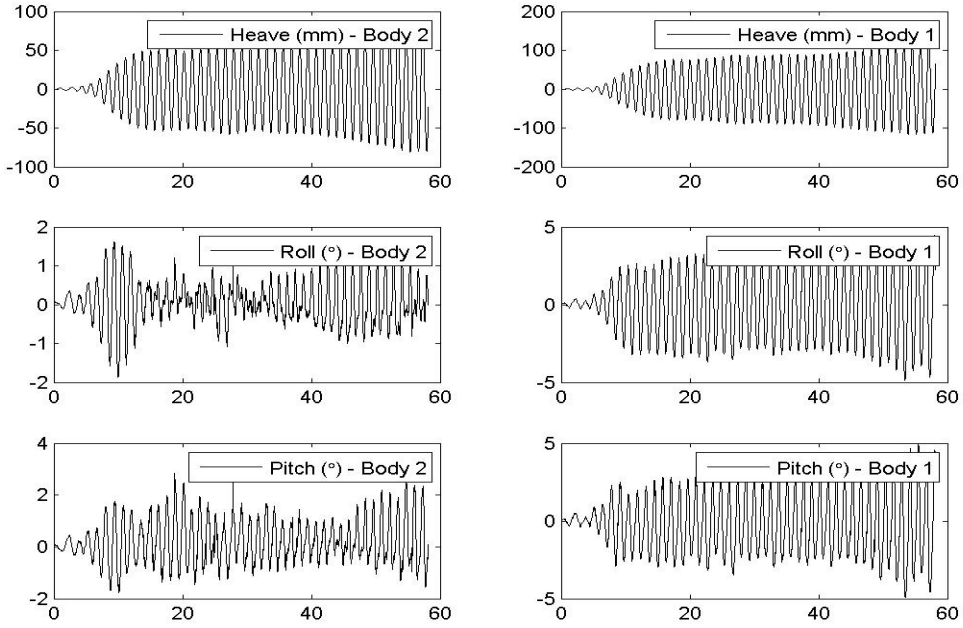

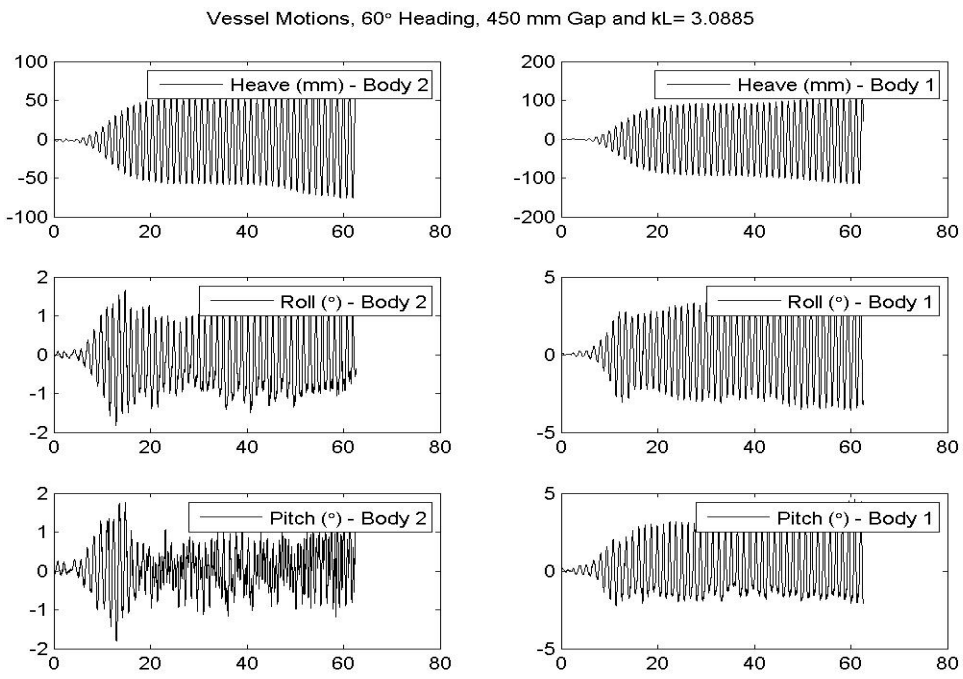
Vessel Motions, 60° Heading, 450 mm Gap and kL= 3.0885
Heave (mm) - Body 2
Heave (mm) - Body 1
Roll (°) - Body 2
Roll (°) - Body 1
Pitch (°) - Body 2
Pitch (°) - Body 1

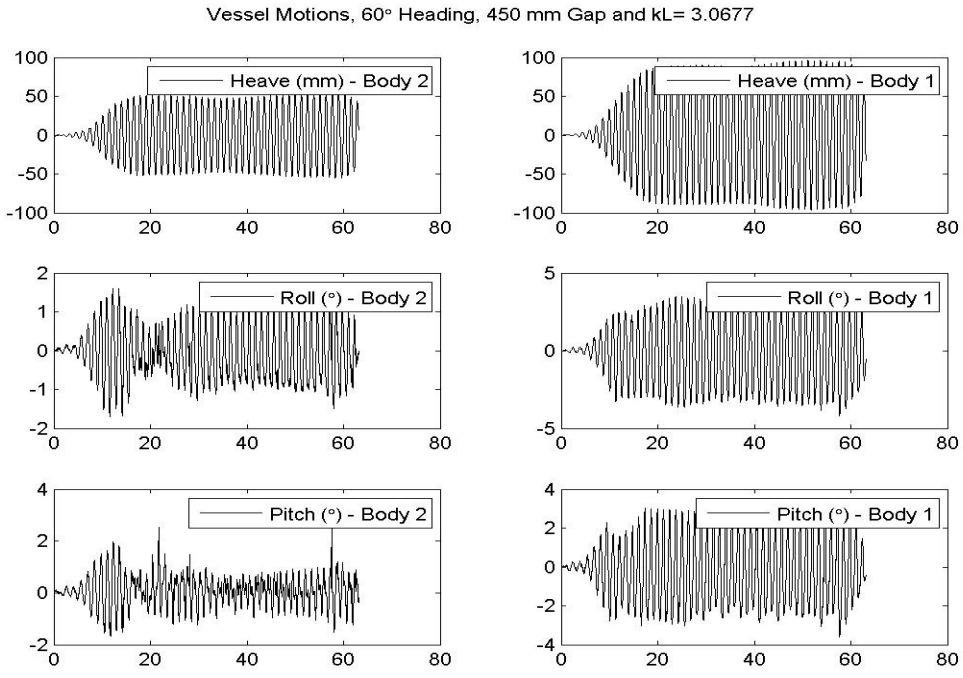
Vessel Motions, 60° Heading, 450 mm Gap and kL= 3.0677
Heave (mm) - Body 2
Heave (mm) - Body 1
Roll (°) - Body 2
Roll (°) - Body 1
Pitch (°) - Body 2
Pitch (°) - Body 1

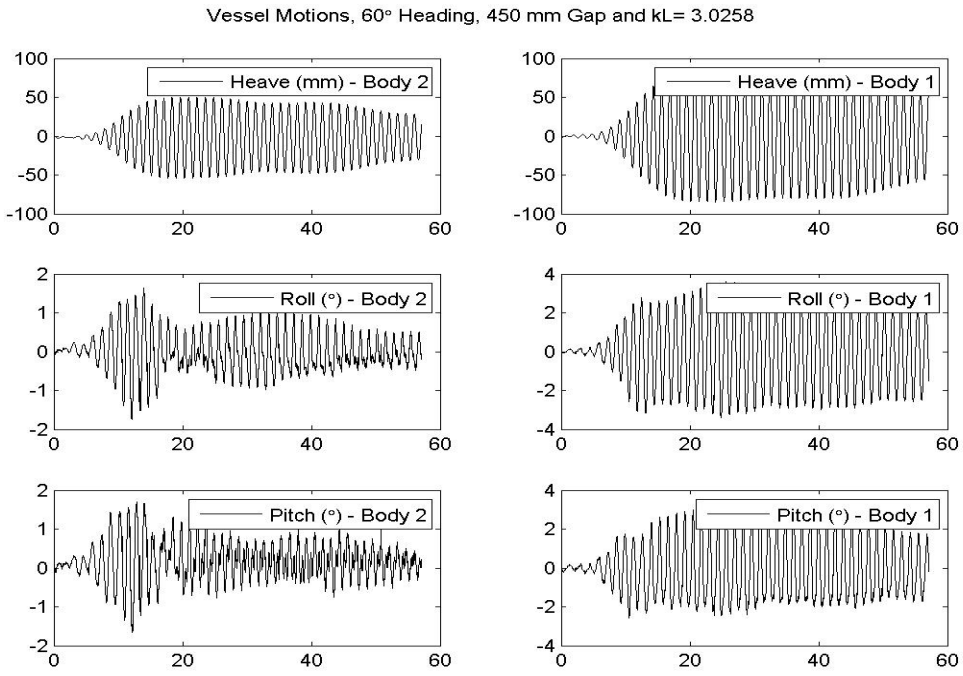
Vessel Motions, 60° Heading, 450 mm Gap and kL= 3.0258
Heave (mm) - Body 2
Heave (mm) - Body 1
Roll (°) - Body 2
Roll (°) - Body 1
Pitch (°) - Body 2
Pitch (°) - Body 1

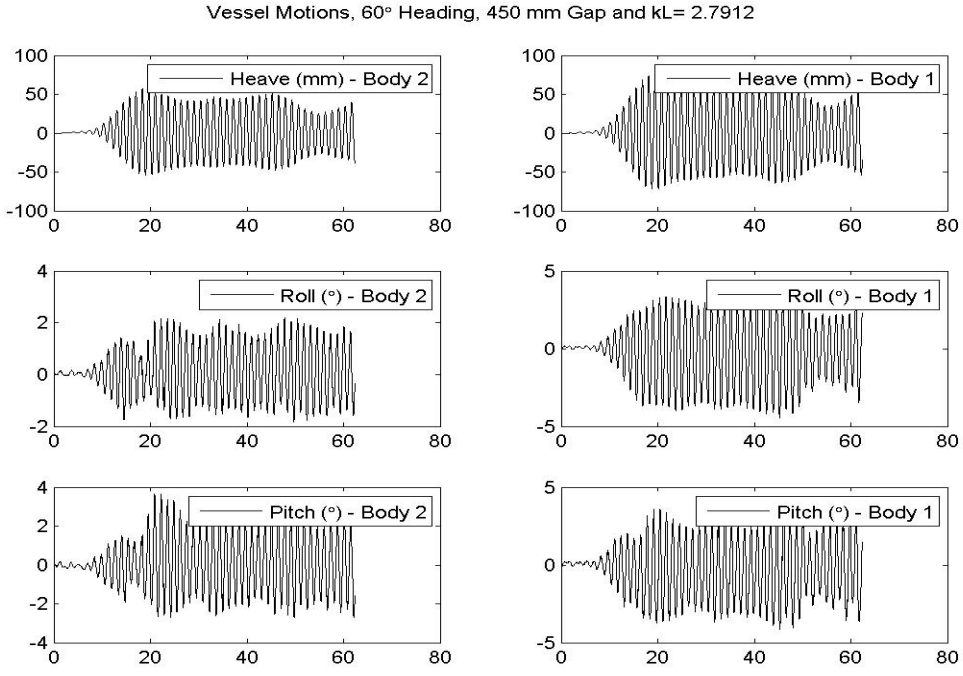
Vessel Motions, 60° Heading, 450 mm Gap and kL= 2.7912
Heave (mm) - Body 2
Heave (mm) - Body 1
Roll (°) - Body 2
Roll (°) - Body 1
Pitch (°) - Body 2
Pitch (°) - Body 1

Vessel Motions, 60° Heading, 450 mm Gap and kL= 2.8214

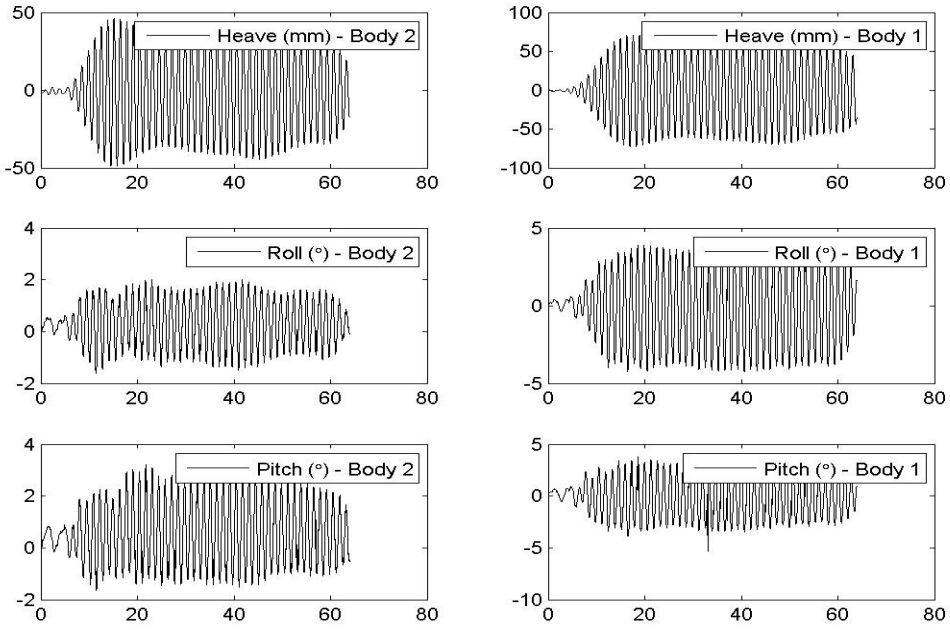

Vessel Motions, 60° Heading, 450 mm Gap and kL= 2.5889

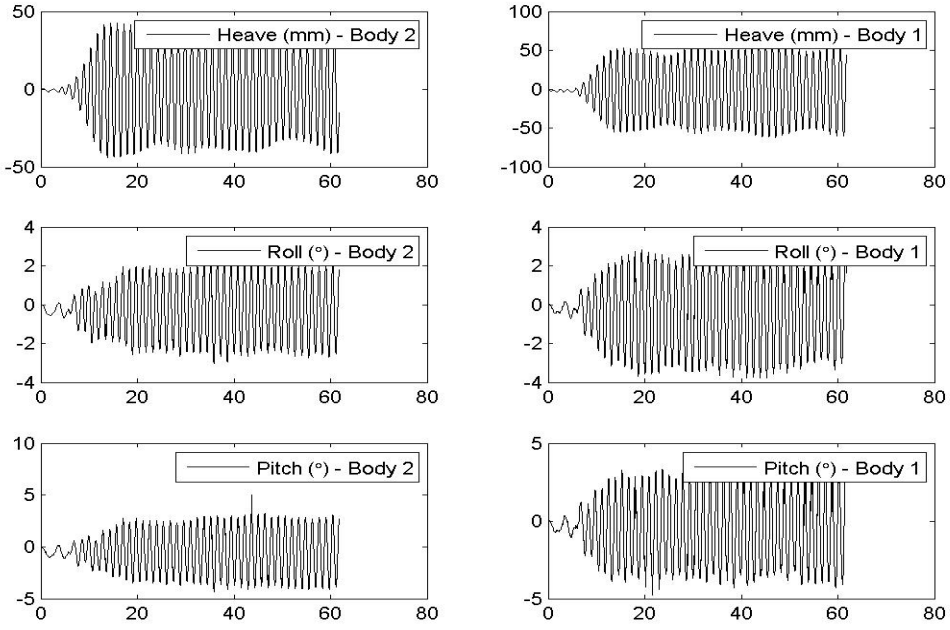

Vessel Motions, 60° Heading, 450 mm Gap and kL= 2.6291

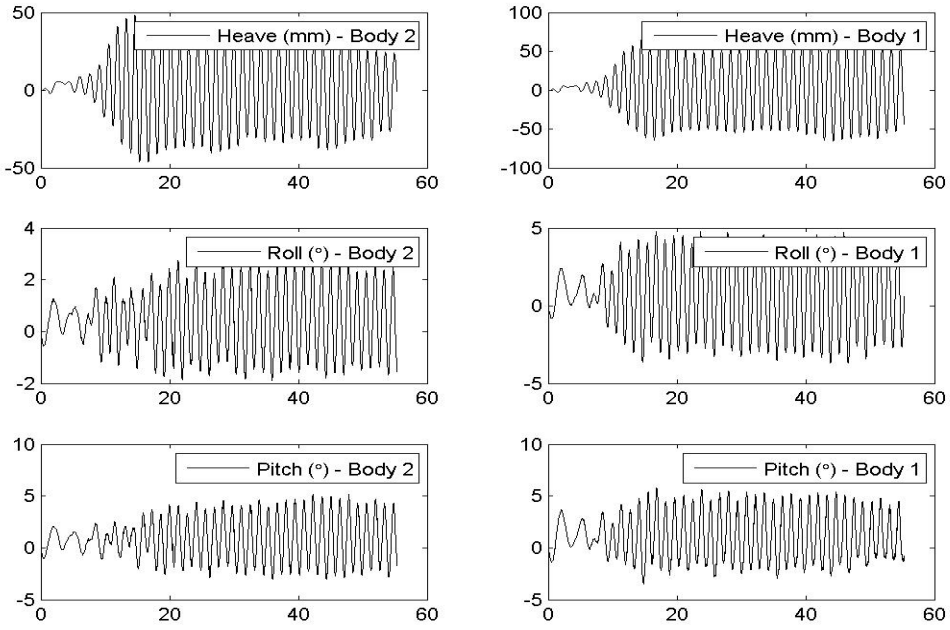

Vessel Motions, 60° Heading, 450 mm Gap and kL= 2.4816

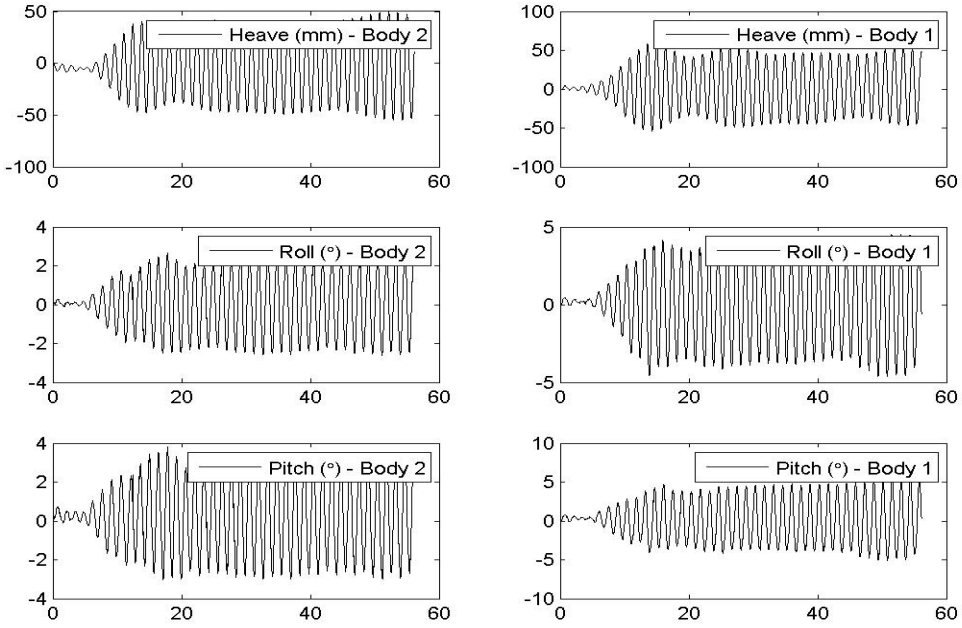

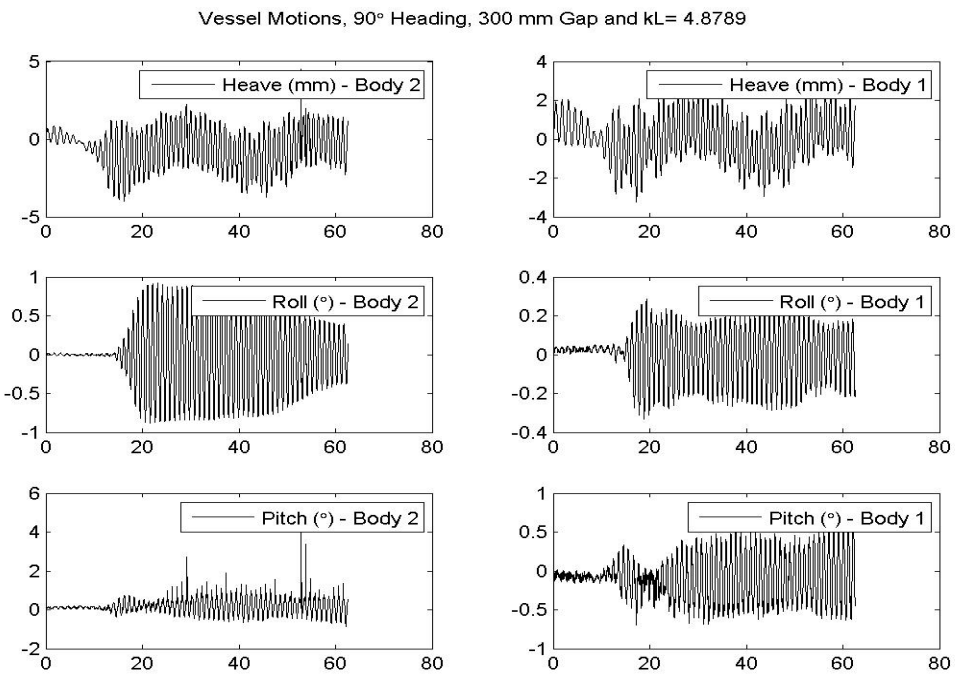
Vessel Motions, 90° Heading, 300 mm Gap and kL= 4.8789
Heave (mm) - Body 2
Heave (mm) - Body 1
Roll (°) - Body 2
Roll (°) - Body 1
Pitch (°) - Body 2
Pitch (°) - Body 1

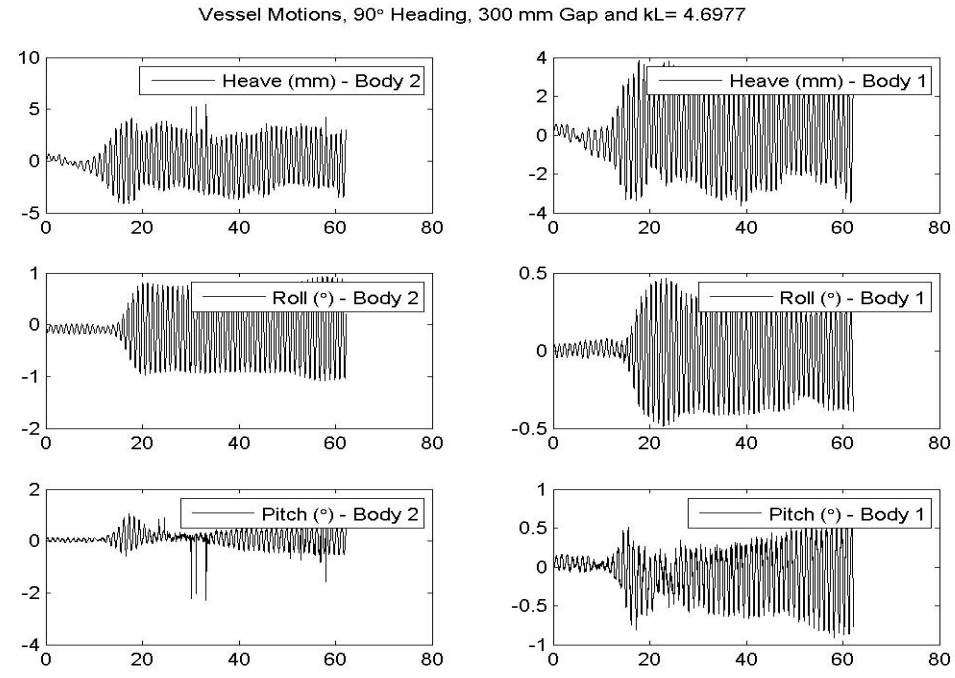
Vessel Motions, 90° Heading, 300 mm Gap and kL= 4.6977
Heave (mm) - Body 2
Heave (mm) - Body 1
Roll (°) - Body 2
Roll (°) - Body 1
Pitch (°) - Body 2
Pitch (°) - Body 1

Vessel Motions, 90° Heading, 300 mm Gap and kL= 4.2808

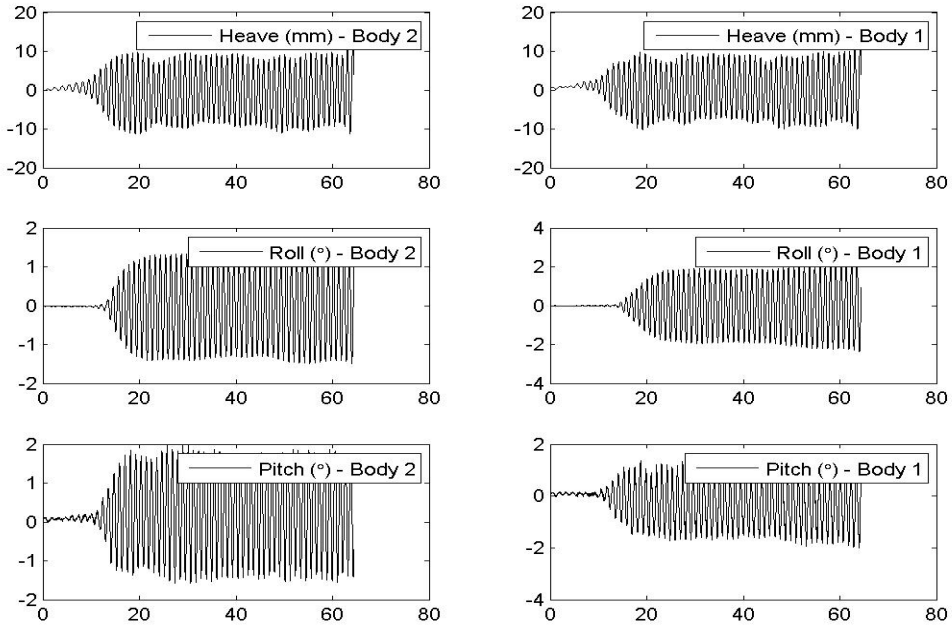

Vessel Motions, 90° Heading, 300 mm Gap and kL= 4.0206

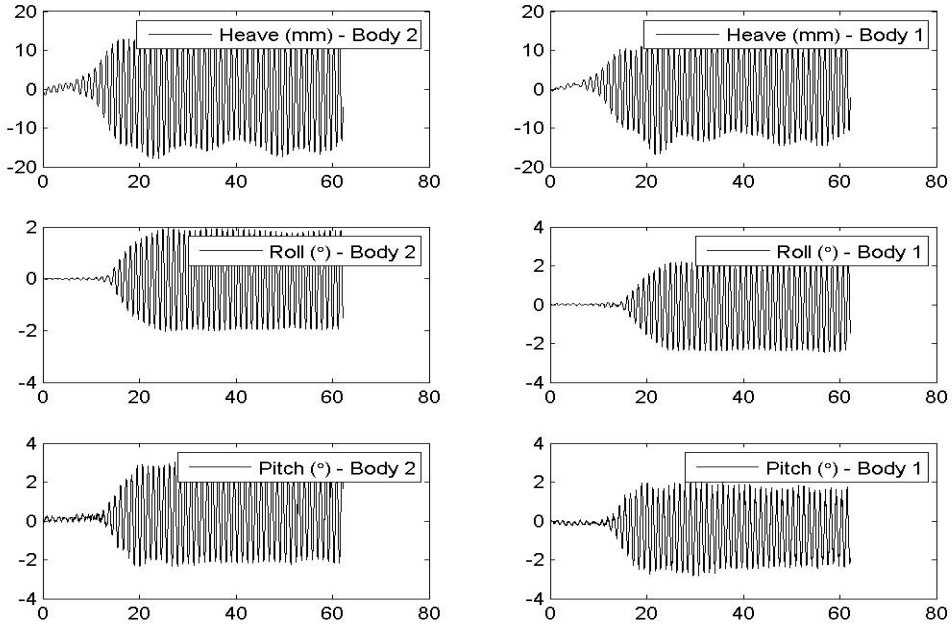

Vessel Motions, 90° Heading, 300 mm Gap and kL= 3.7926

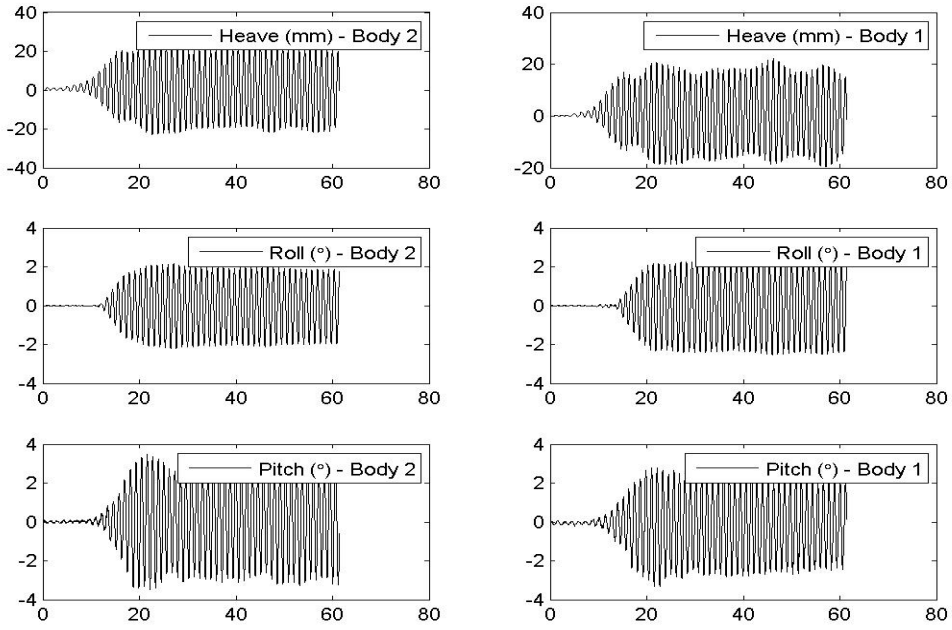

Vessel Motions, 90° Heading, 300 mm Gap and kL= 3.6835

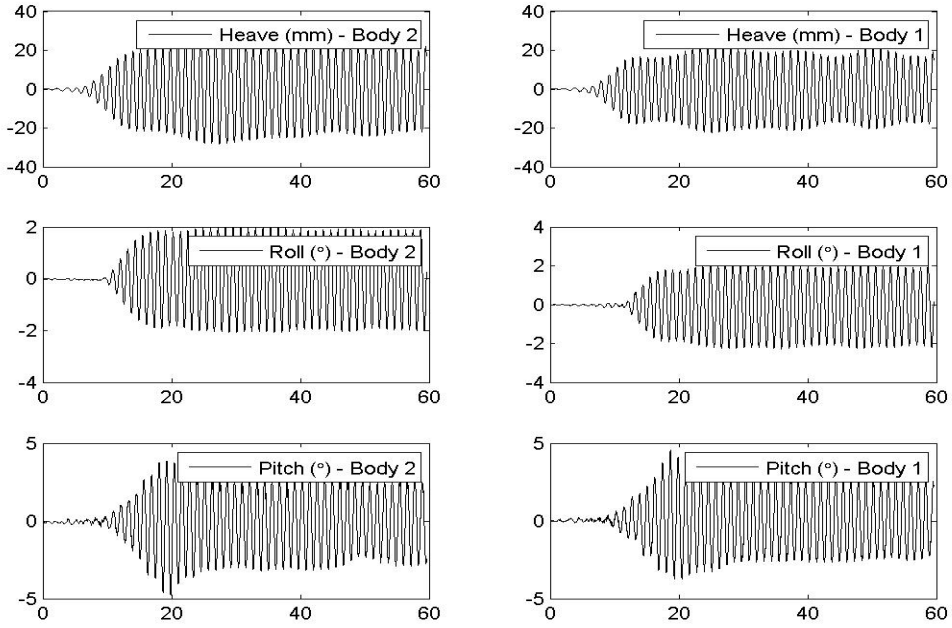

Vessel Motions, 90° Heading, 300 mm Gap and kL= 3.4876

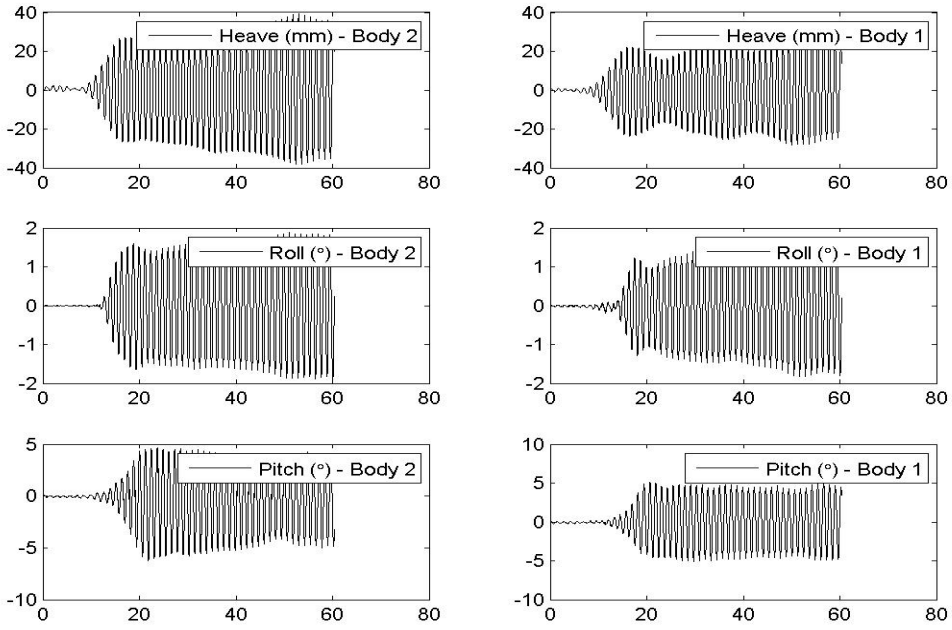

Vessel Motions, 90° Heading, 300 mm Gap and kL= 3.3935

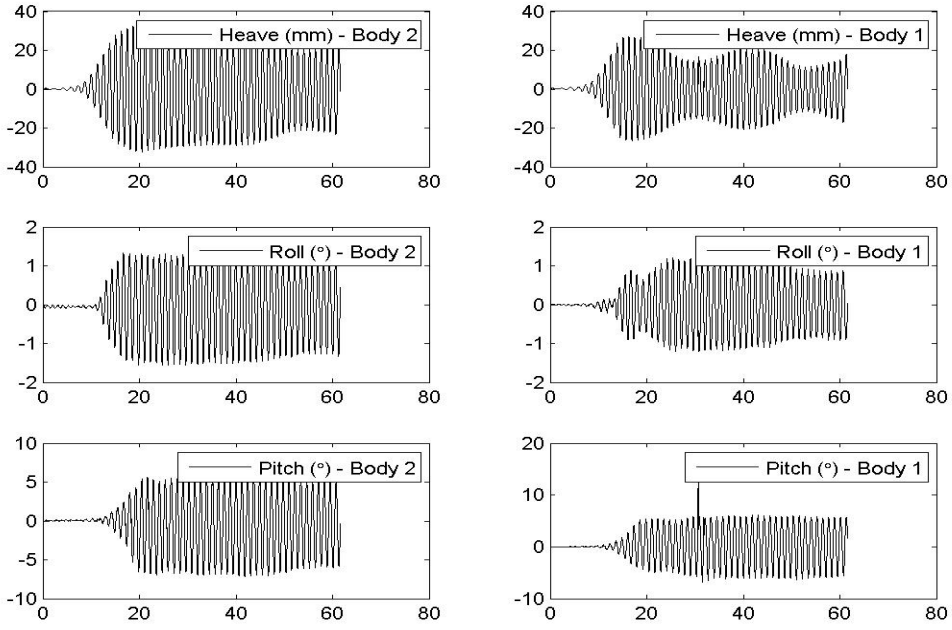

Vessel Motions, 90° Heading, 300 mm Gap and kL= 3.3587

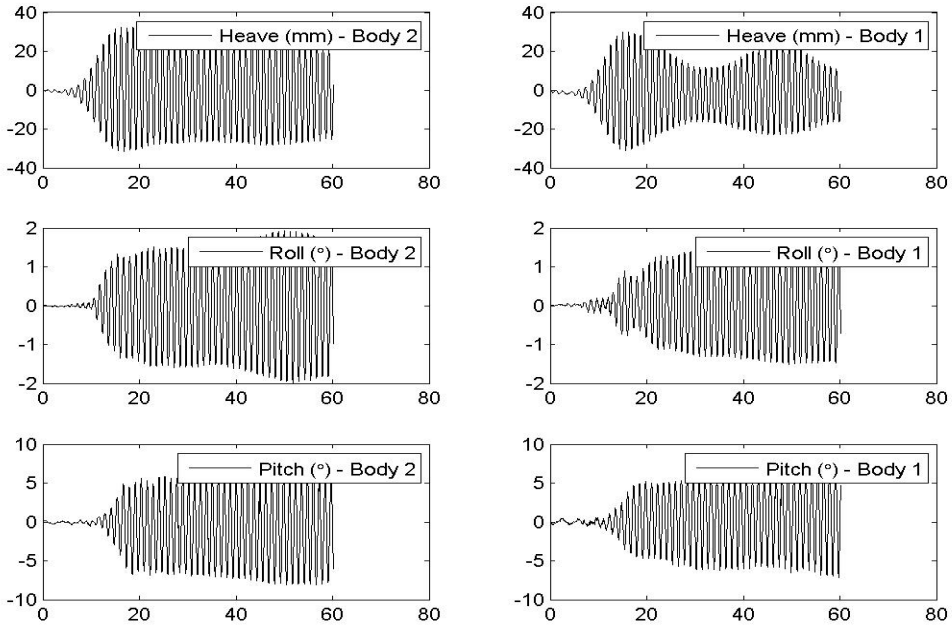

Vessel Motions, 90° Heading, 300 mm Gap and kL= 3.3008

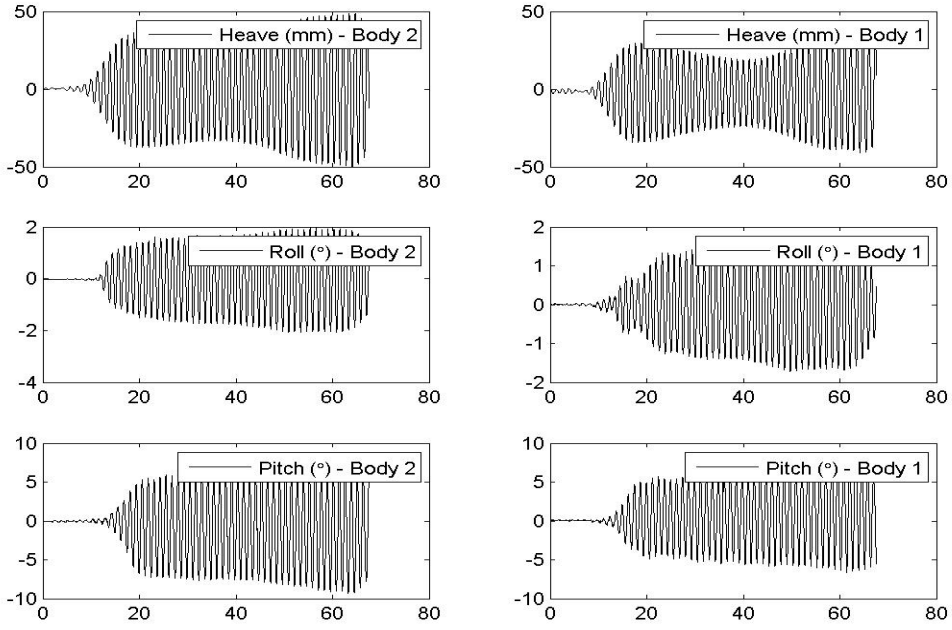

Vessel Motions, 90° Heading, 300 mm Gap and kL= 3.2389

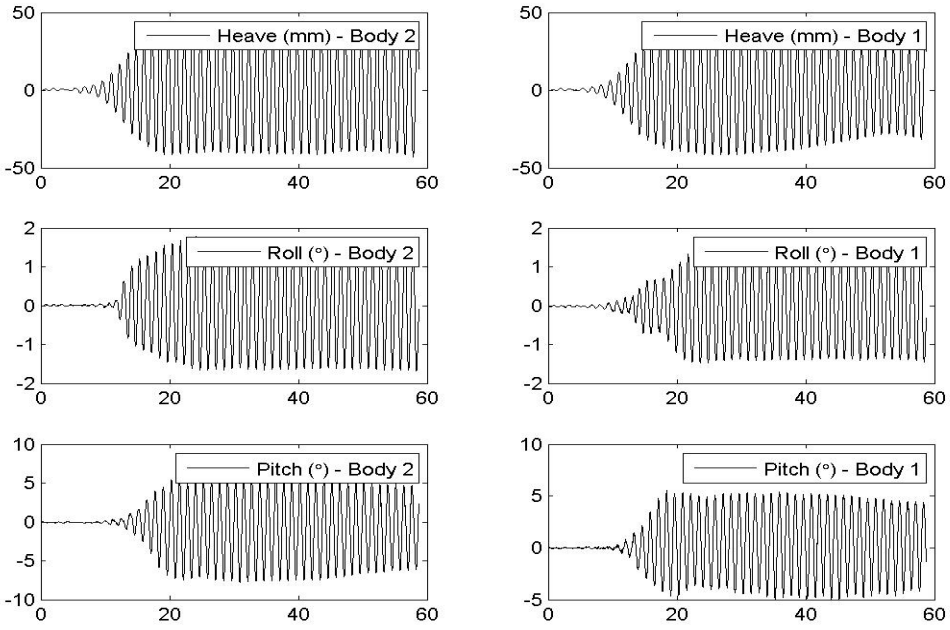

Vessel Motions, 90° Heading, 300 mm Gap and kL= 3.1247

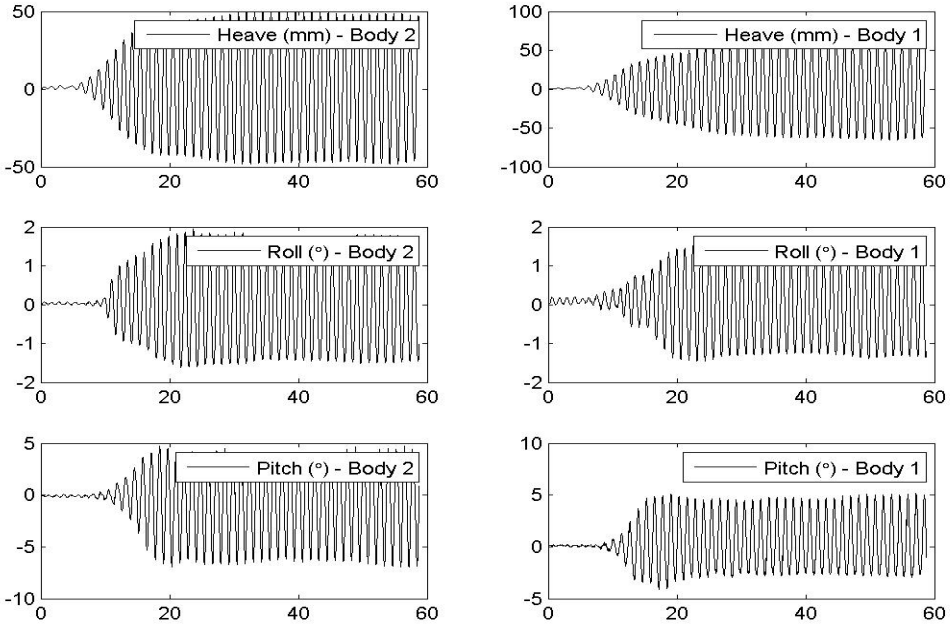

Vessel Motions, 90° Heading, 300 mm Gap and kL= 3.0466

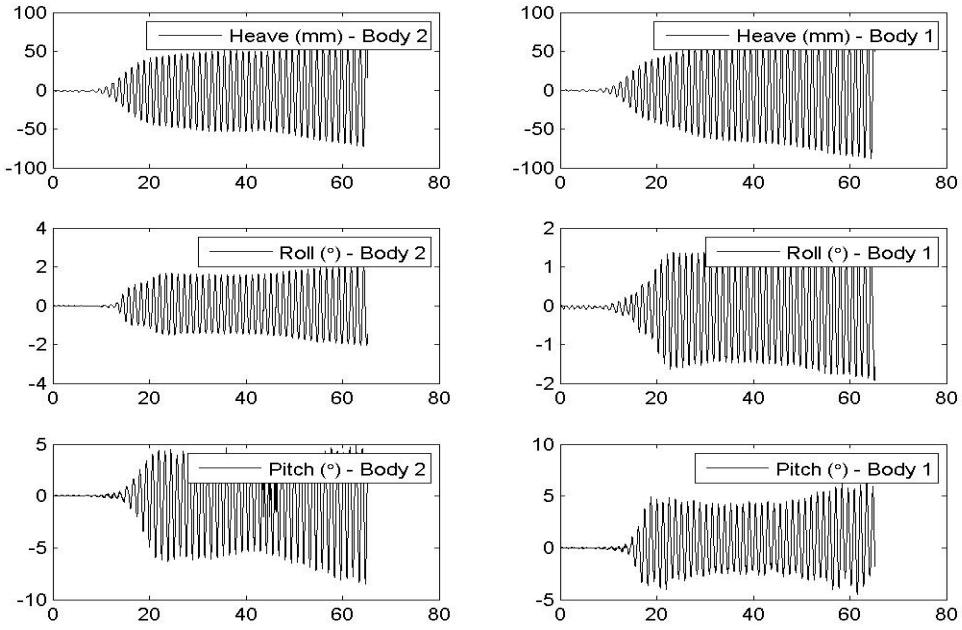

Vessel Motions, 90° Heading, 300 mm Gap and kL= 3.0302

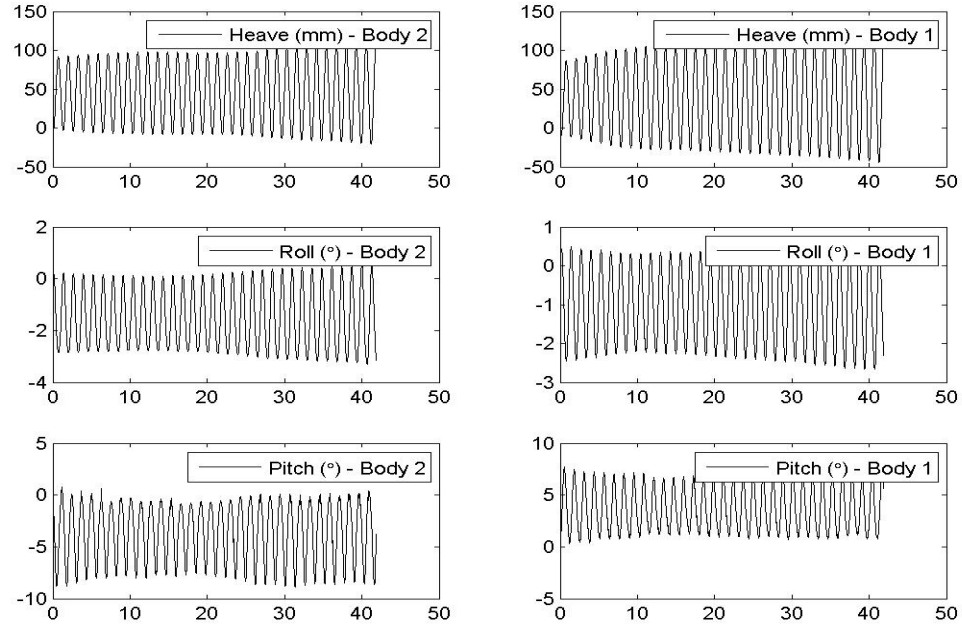

Vessel Motions, 90° Heading, 300 mm Gap and kL= 3.0065

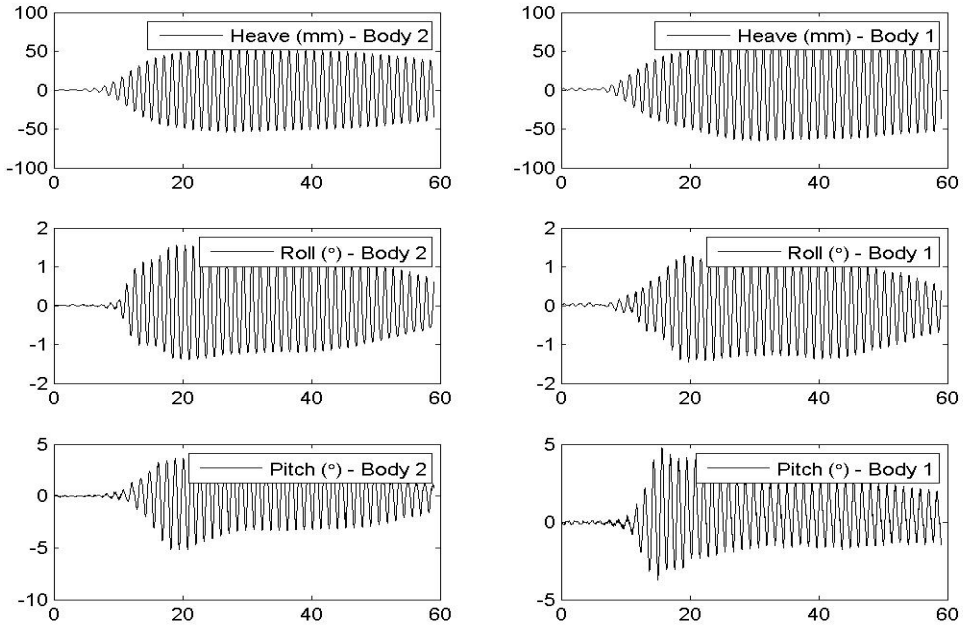

Vessel Motions, 90° Heading, 300 mm Gap and kL= 2.8598

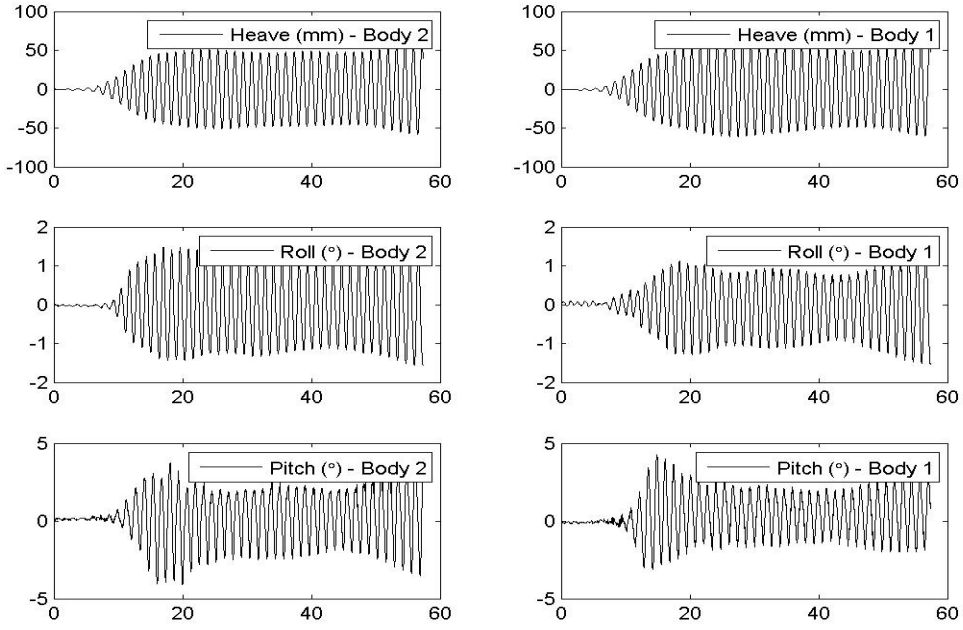

Vessel Motions, 90° Heading, 300 mm Gap and kL= 2.8398

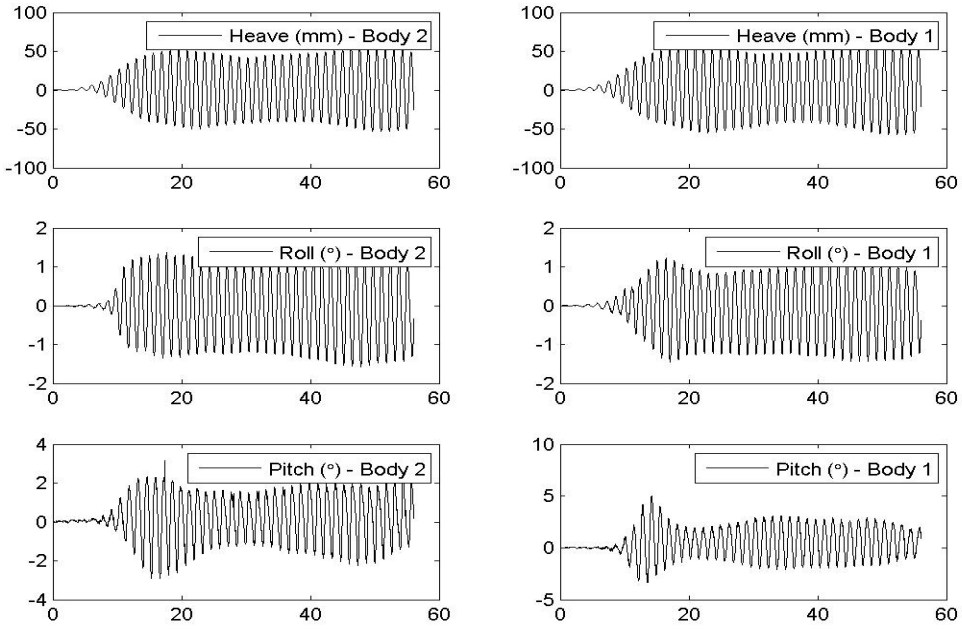

Vessel Motions, 90° Heading, 300 mm Gap and kL= 2.6697

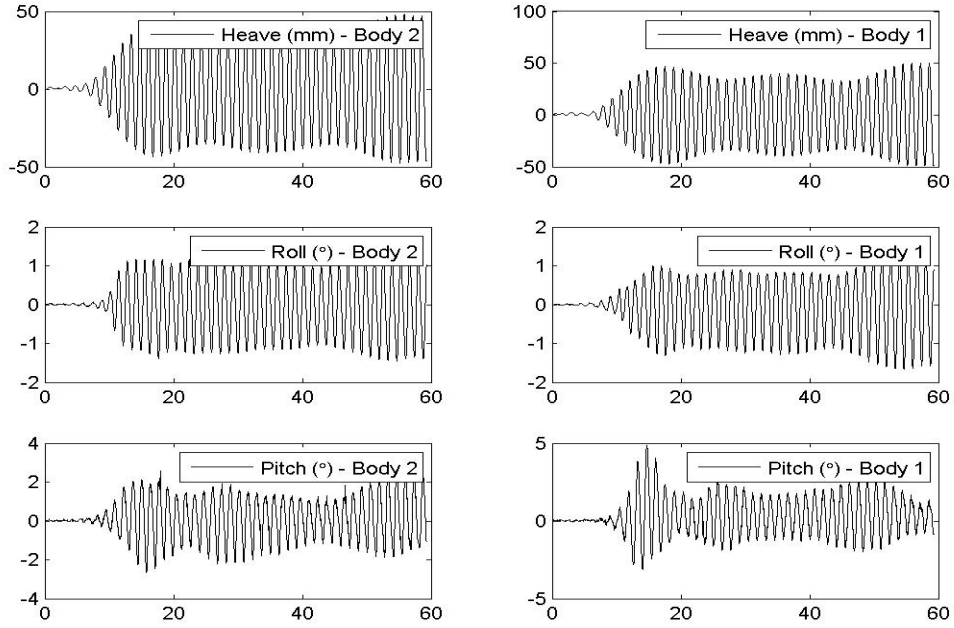

Vessel Motions, 90° Heading, 300 mm Gap and kL= 2.616

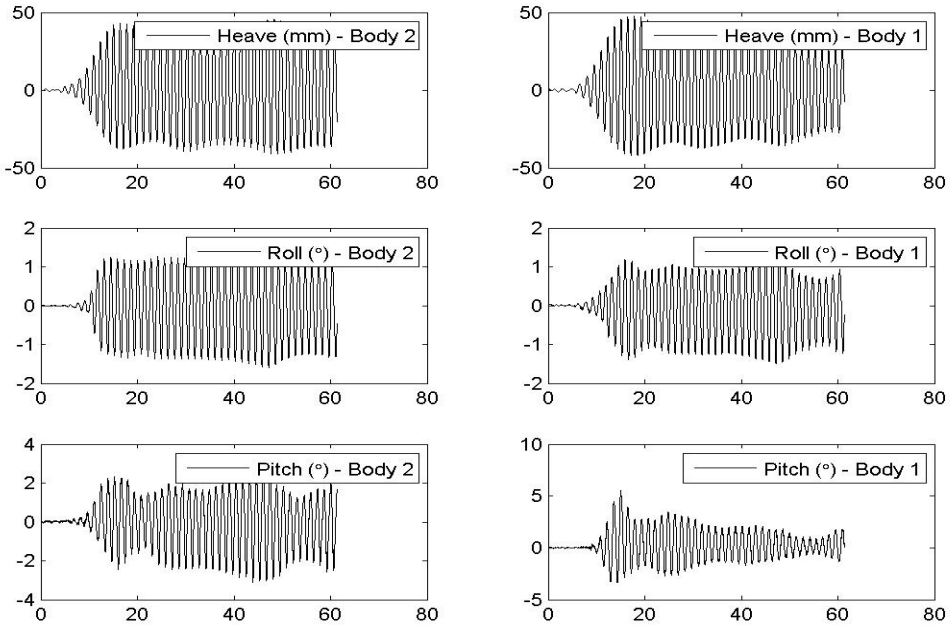

Vessel Motions, 90° Heading, 300 mm Gap and kL= 2.4933

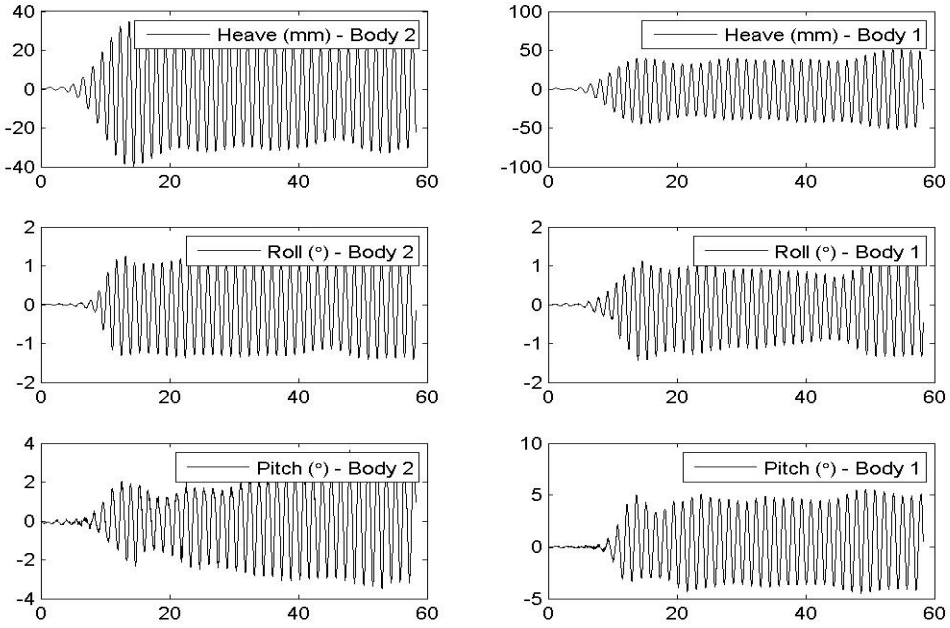

Vessel Motions, 90° Heading, 450 mm Gap and kL= 4.9091

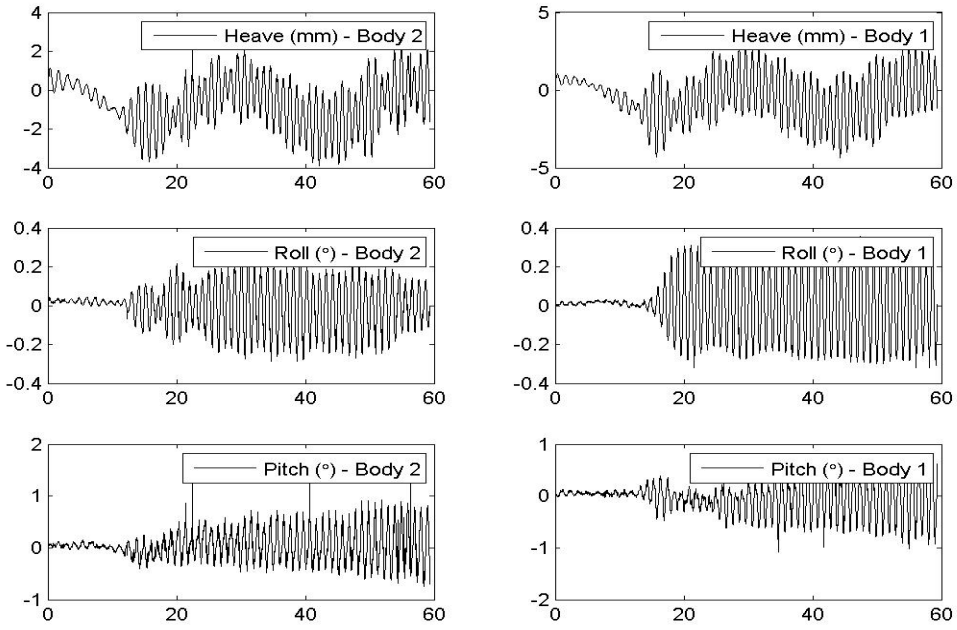

Vessel Motions, 90° Heading, 450 mm Gap and kL= 4.7336

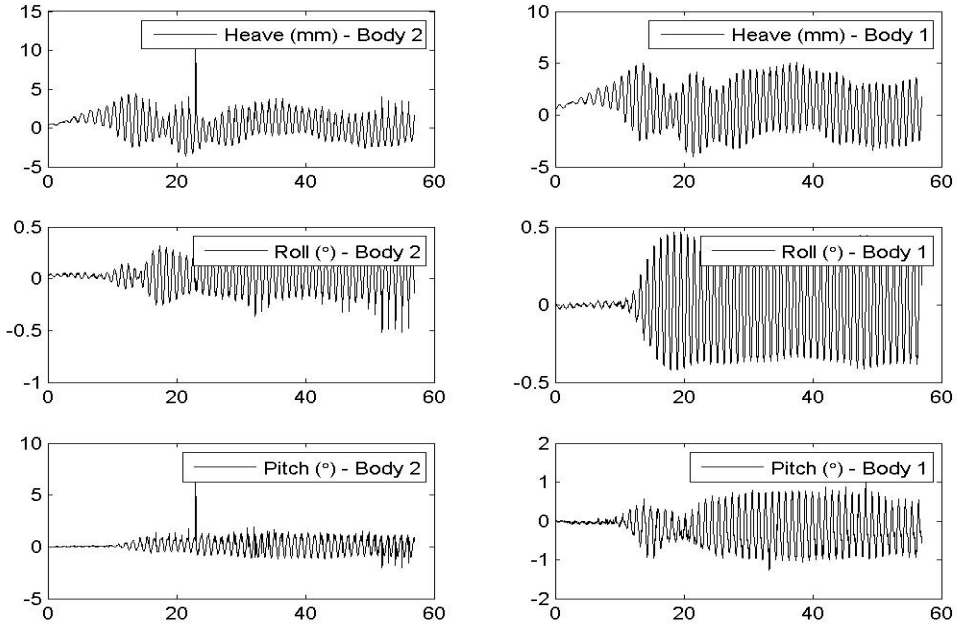

Vessel Motions, 90° Heading, 450 mm Gap and kL= 4.2984

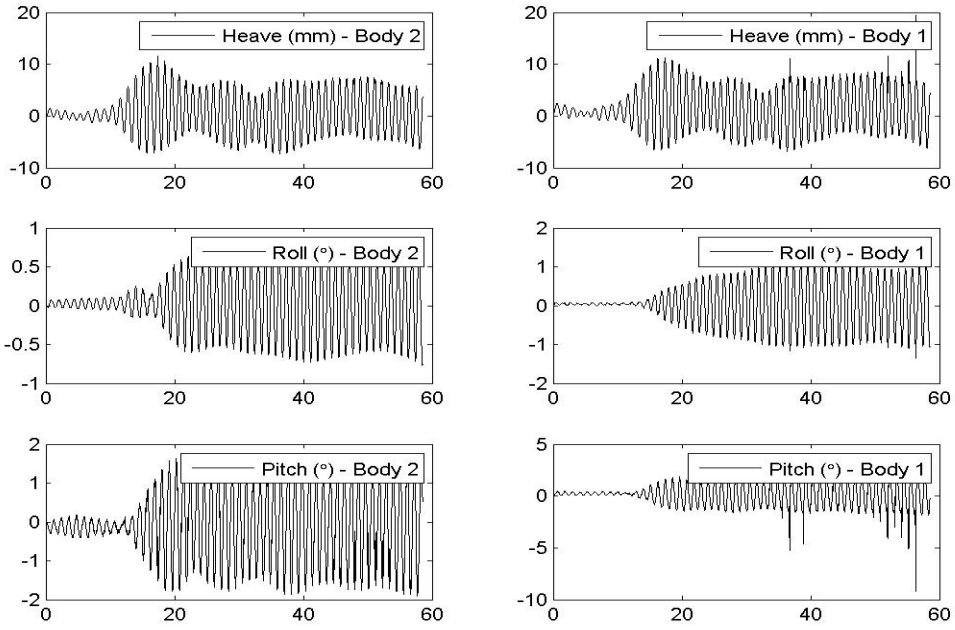

Vessel Motions, 90° Heading, 450 mm Gap and kL= 4.0576

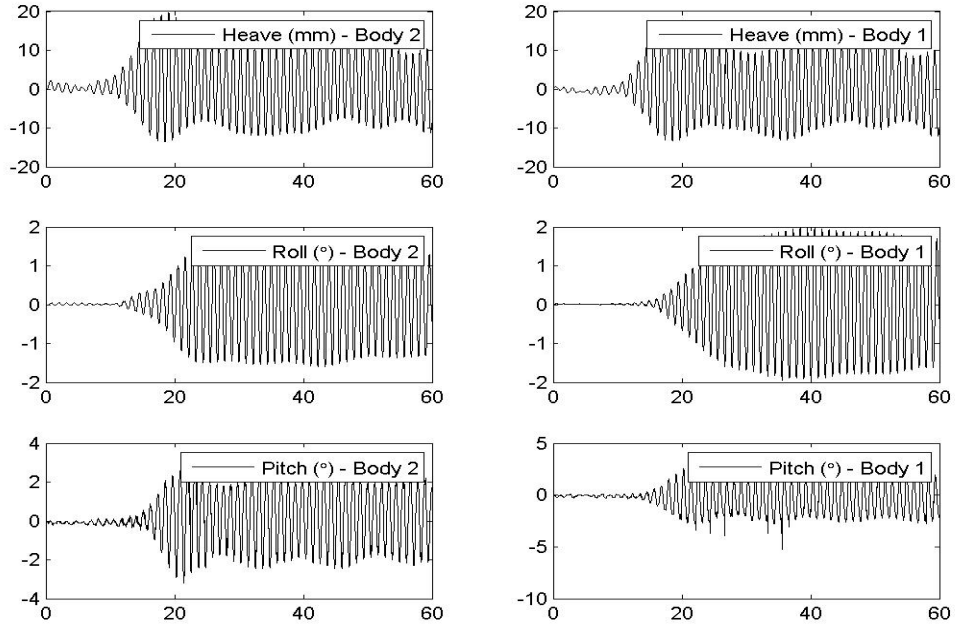

Vessel Motions, 90° Heading, 450 mm Gap and kL= 3.8168

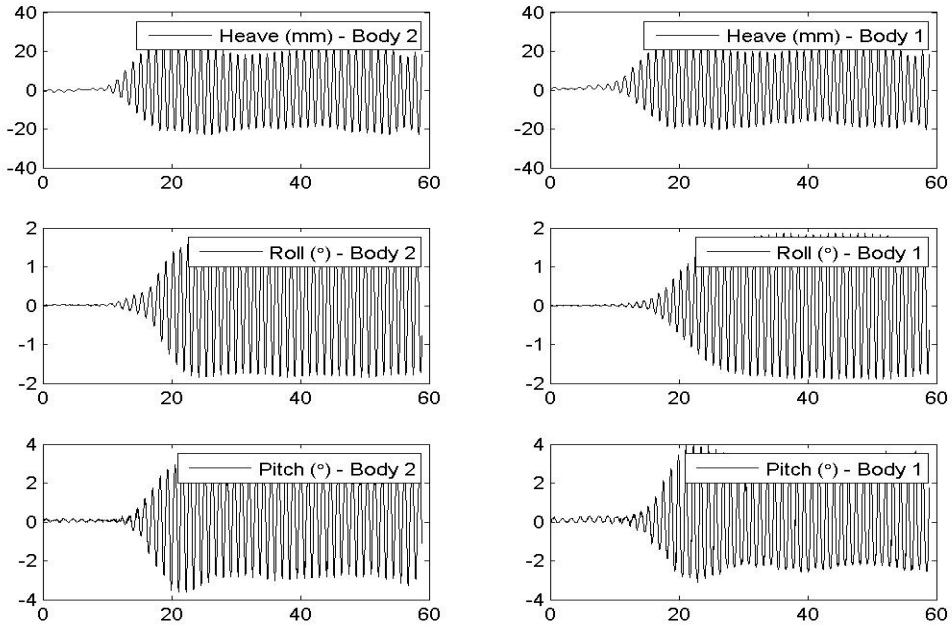

Vessel Motions, 90° Heading, 450 mm Gap and kL= 3.7012

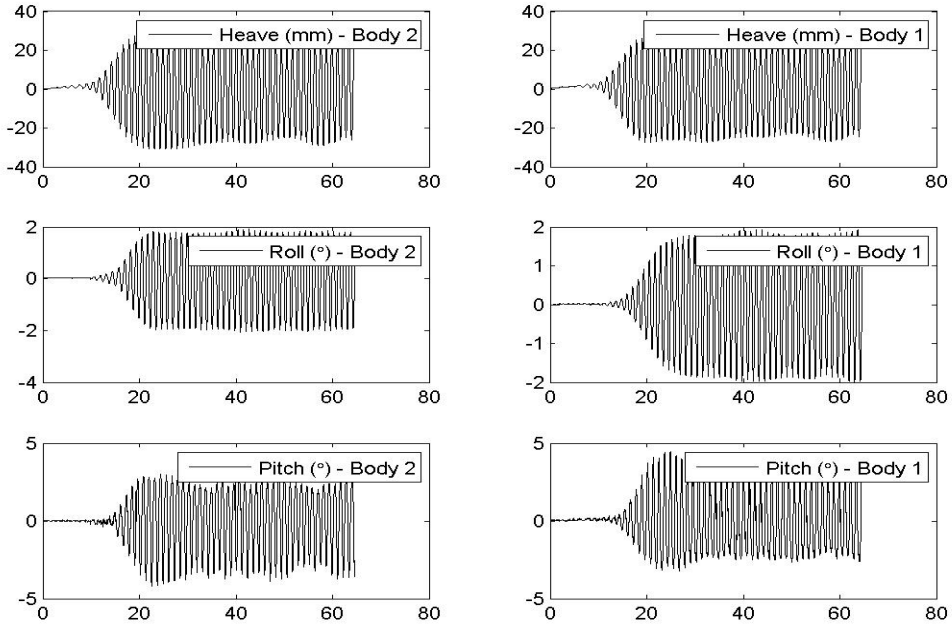

Vessel Motions, 90° Heading, 450 mm Gap and kL= 3.4675

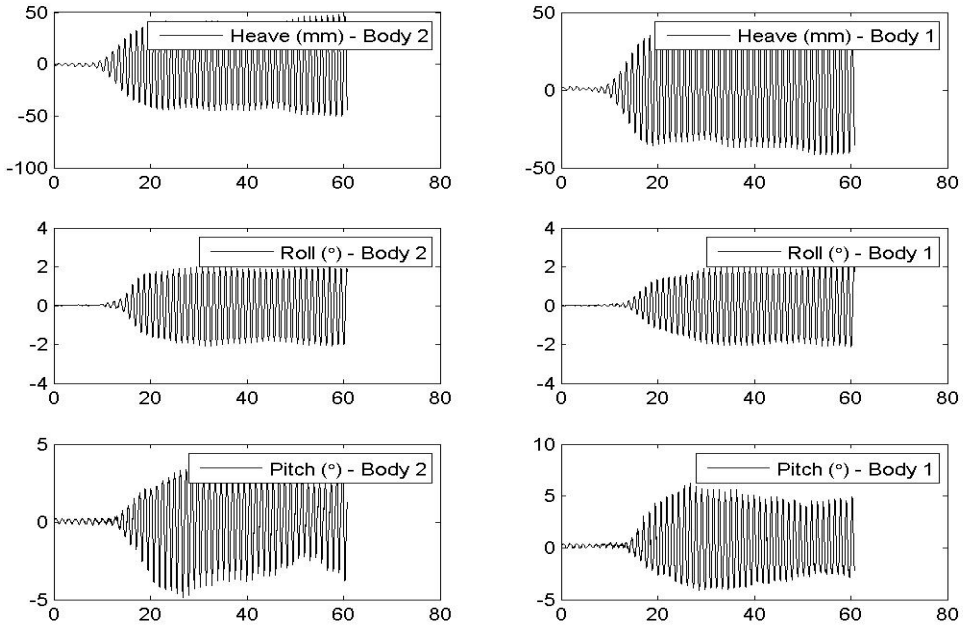

Vessel Motions, 90° Heading, 450 mm Gap and kL= 3.4082

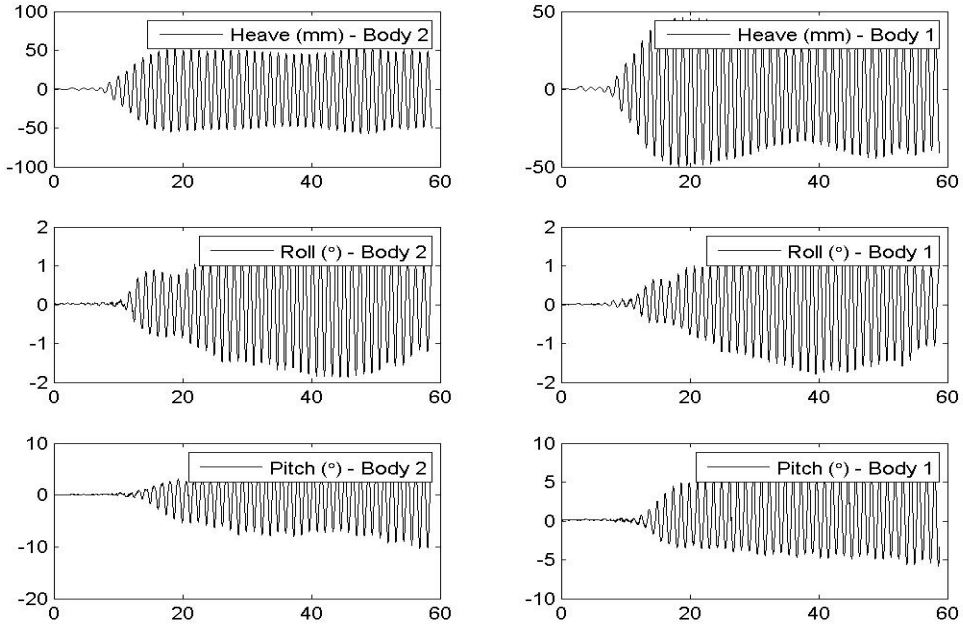

Vessel Motions, 90° Heading, 450 mm Gap and kL= 3.3193

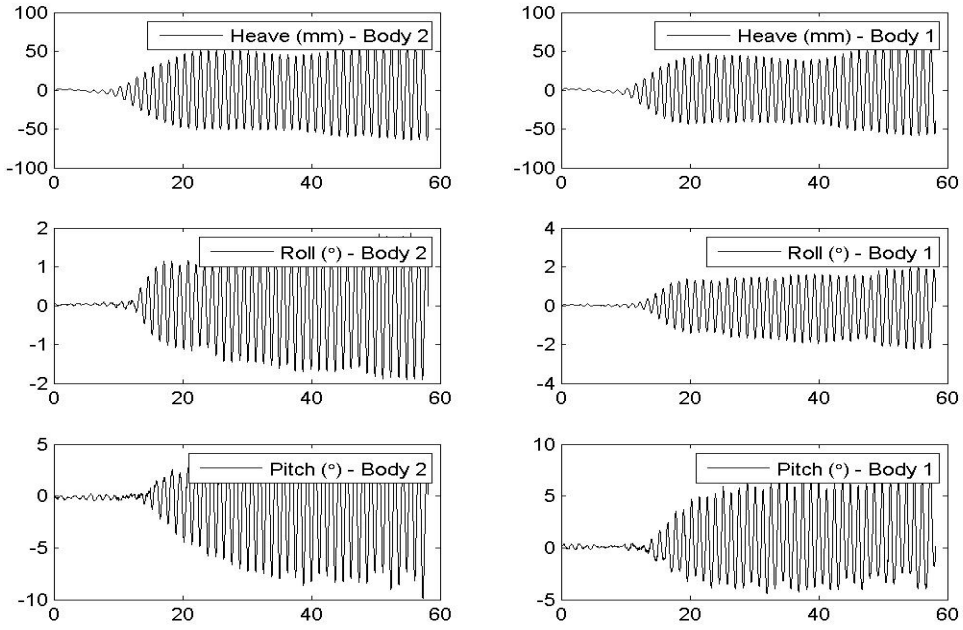

Vessel Motions, 90° Heading, 450 mm Gap and kL= 3.2967

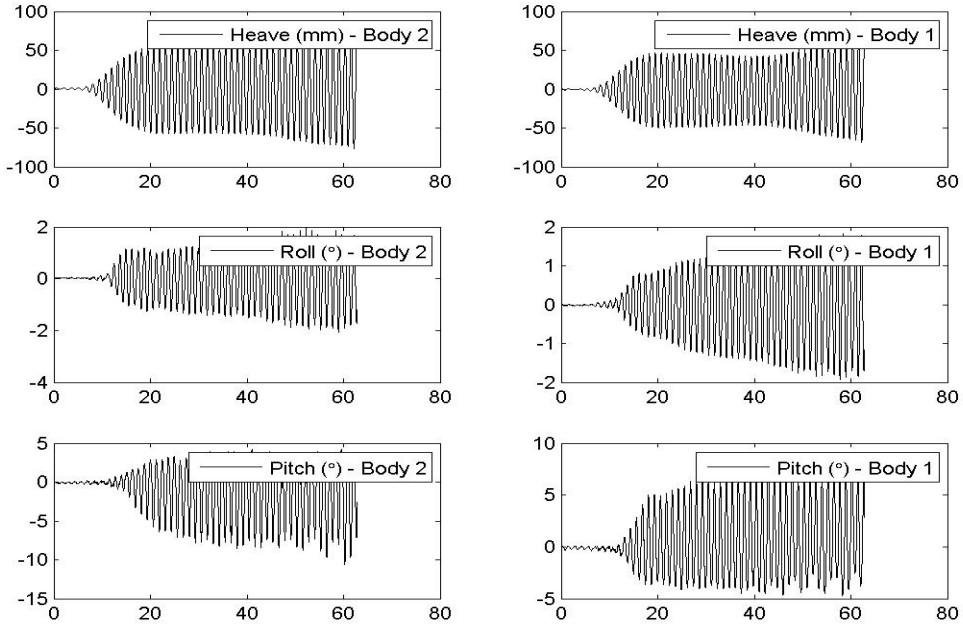

Vessel Motions, 90° Heading, 450 mm Gap and kL= 3.2331

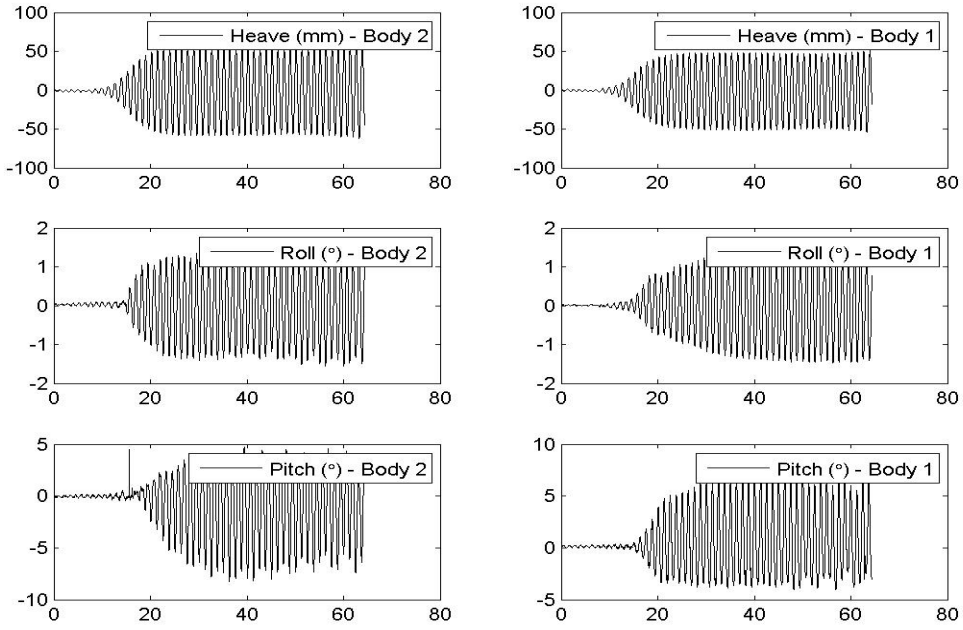

Vessel Motions, 90° Heading, 450 mm Gap and kL= 3.1126

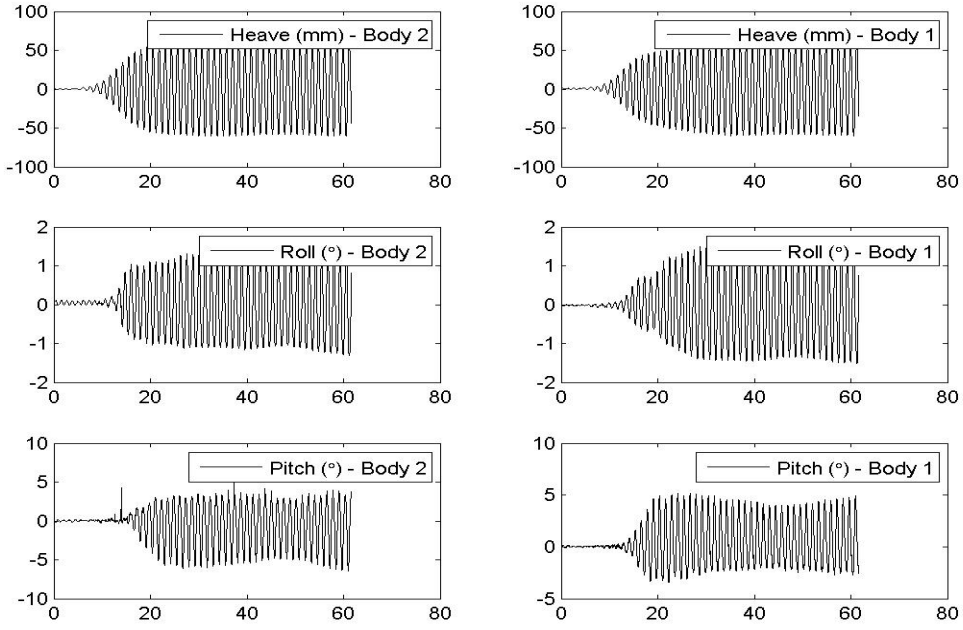

Vessel Motions, 90° Heading, 450 mm Gap and kL= 3.0352

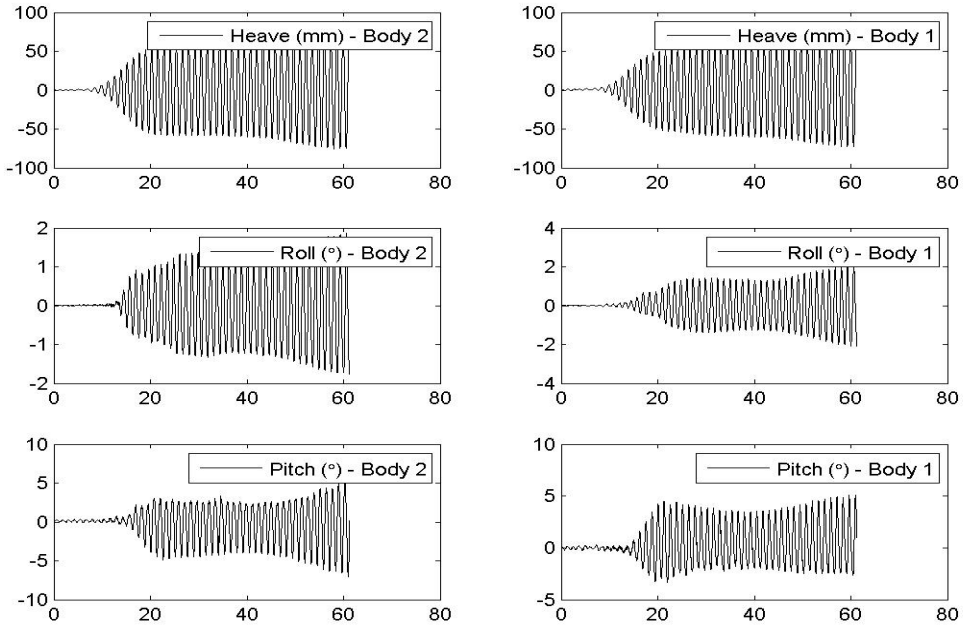

Vessel Motions, 90° Heading, 450 mm Gap and kL= 3.0295

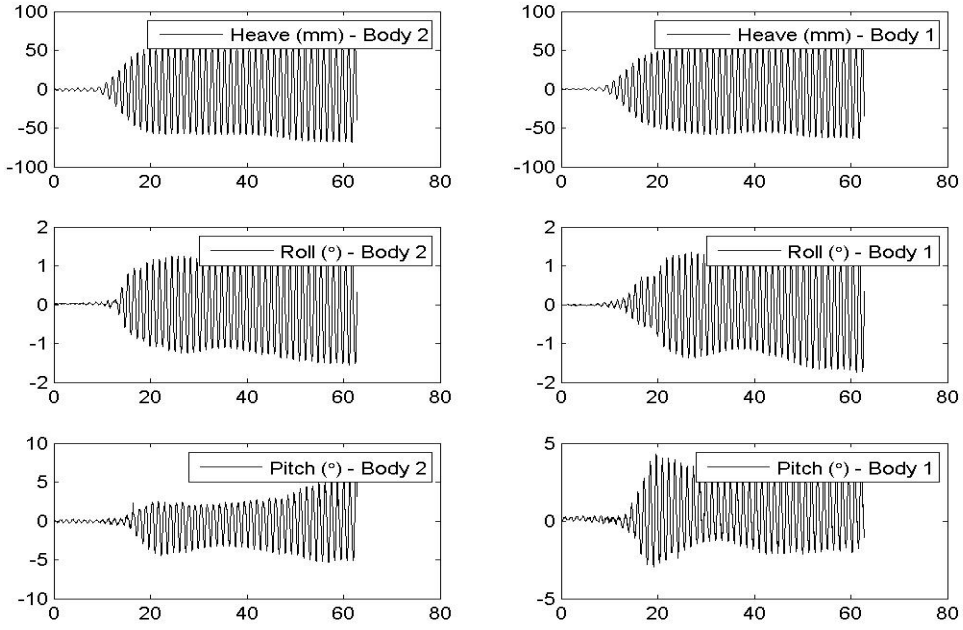

Vessel Motions, 90° Heading, 450 mm Gap and kL= 2.5822

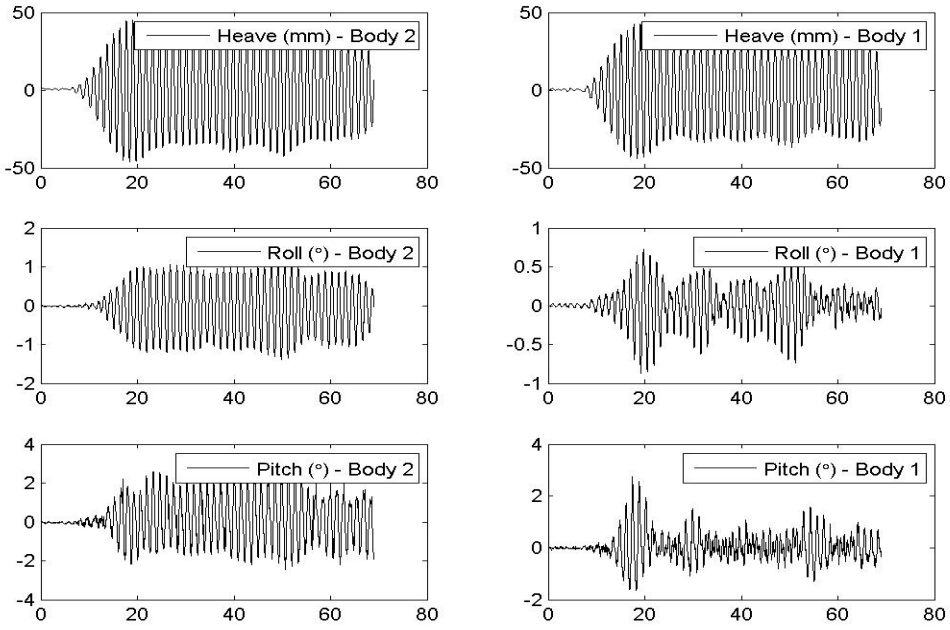

Vessel Motions, 90° Heading, 450 mm Gap and kL= 2.8472

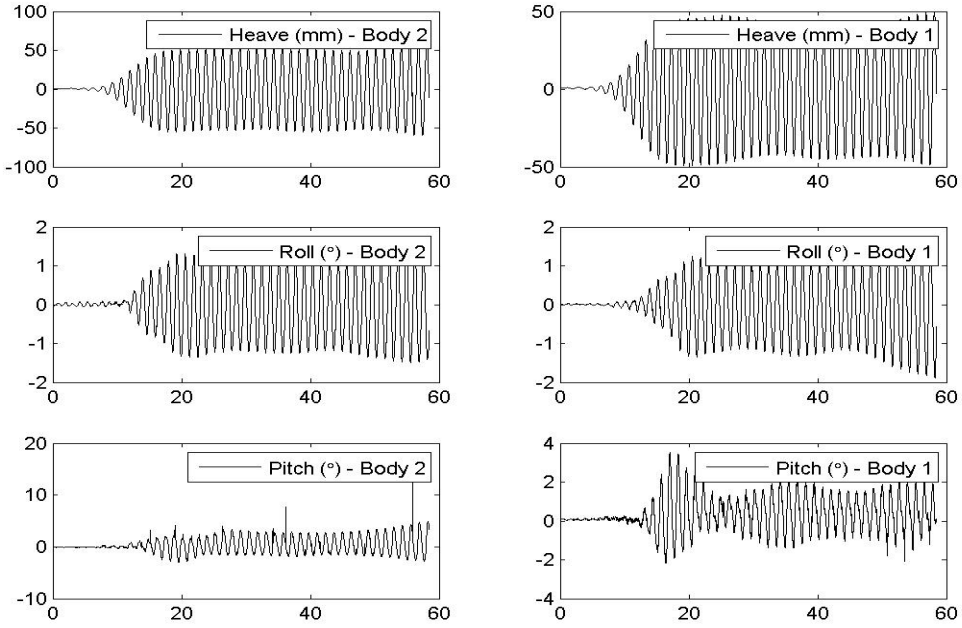

Vessel Motions, 90° Heading, 450 mm Gap and kL= 2.8195

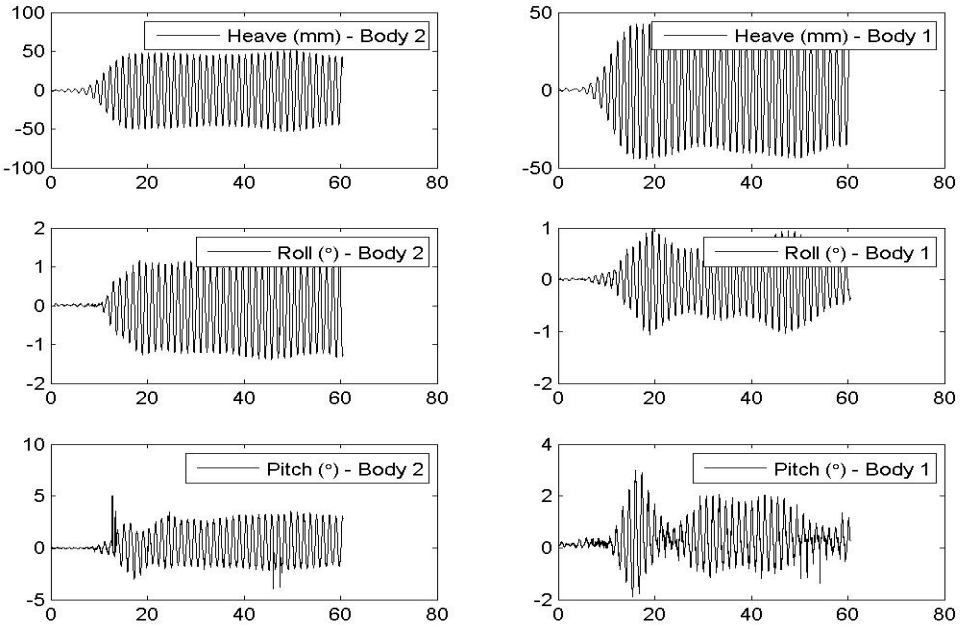

Vessel Motions, 90° Heading, 450 mm Gap and kL= 2.6674

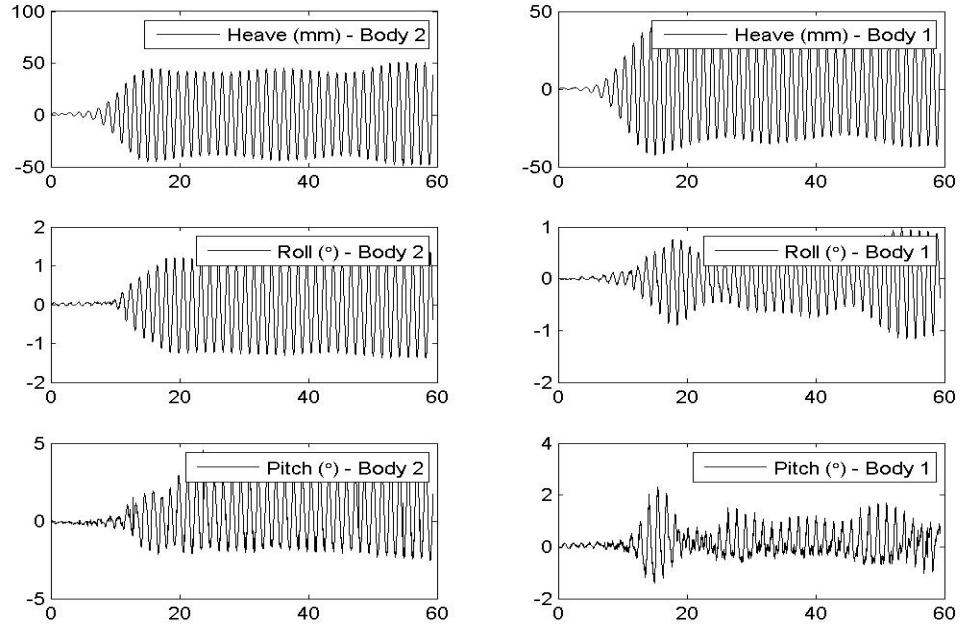

Vessel Motions, 90° Heading, 450 mm Gap and kL= 2.6519

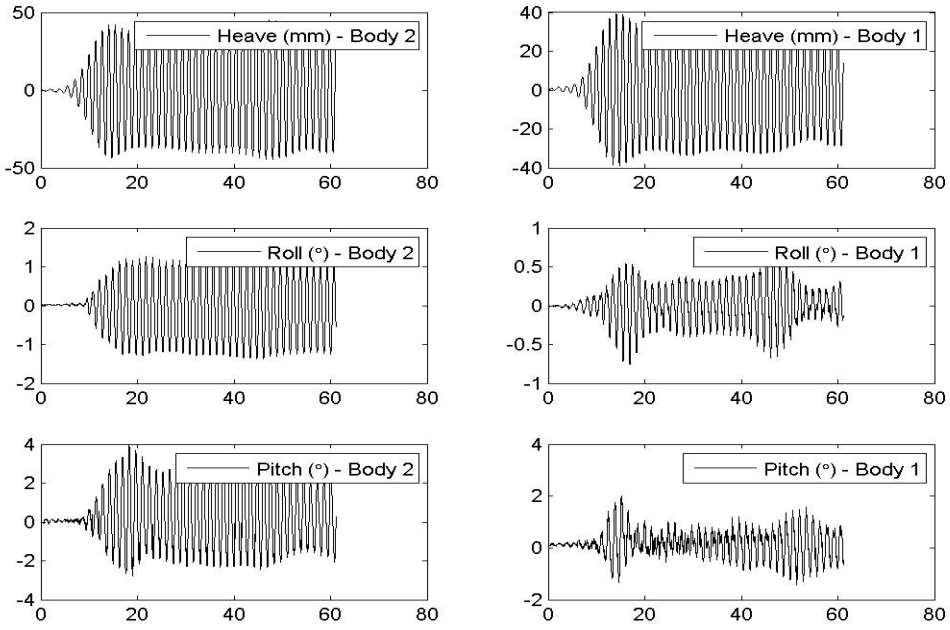

Vessel Motions, 90° Heading, 450 mm Gap and kL= 2.4668